ABSTRACT

CHENG, BIN. Dynamics of Rural and Urban Atmospheric Chemical Conditions and Inorganic Aerosols (Under the direction of Dr. Lingjuan Wang-Li).

Animal feeding operations (AFOs) are the largest ammonia (NH_3) emission sources in the United States (U.S.), the impacts of AFOs NH_3 emissions on the atmospheric chemical conditions and secondary inorganic $PM_{2.5}$ ($iPM_{2.5}$) formation are not well understood. While partitioning of $NH_3 - NH_4^+$ may be simulated by ISORROPIA II, disagreement between model predictions and measurements requires further study on applicability of ISORROPIA II for predicting $iPM_{2.5}$. Under the Southeastern Aerosol Research and Characterization (SEARCH) Network, concentrations of $iPM_{2.5}$ chemical compositions and precursor gases as well as meteorological data were measured at eight urban/nonurban sites labeled as JST/YRK, BHM/CTR, GFP/OAK, and PNS/OLF during 1998–2016. Using SEARCH data, this research investigated spatiotemporal variations of atmospheric chemical conditions, $PM_{2.5}$ mass closure, and $iPM_{2.5}$ in the Southeastern U.S. In addition, this research also assessed the performance of ISORROPIA II in simulating $iPM_{2.5}$ formation under different temperature (T), relative humidity (RH), and model setups in urban and rural locations. Upon model performance assessment, this research further studied the effects of changes in total NH_3 (gas + particle), total H_2SO_4, and total HNO_3 (gas + particle) on $iPM_{2.5}$ and partitioning of $NH_3 - NH_4^+$ in the Southeastern U.S. Results indicate that AFOs NH_3 emissions contributed to greater values of gas ratio (GR), gas-phase NH_3 molar fraction (NH_3/NH_x), and total available NH_3 (gaseous NH_3 + aerosol NH_4^+) to sulfate (SO_4^{2-}) molar ratio (TA/TS) in wind directions coming from AFO farms at YRK and OAK sites than other wind directions. The temporal upward trend in NH_3/NH_x and TA/TS indicates that partitioning of $NH_3 - NH_4^+$ shifted towards gas phase, while the temporal downward trend in mass

ratio of ammonium (NH_4^+) + nitrate (NO_3^-) to total $PM_{2.5}$ (AN/$PM_{2.5}$) may implicate that smaller fraction of $PM_{2.5}$ was directly NH_3 sensitive. The AFOs NH_3 emissions at YRK may facilitate reactions of NH_3 with acidic gases, leading to higher NH_4^+, SO_4^{2-} and NO_3^- concentrations at YRK agricultural site than other sites, except JST and BHM urban sites. The ISORROPIA II model assessment indicates that model predicts i$PM_{2.5}$ well due to dominance of SO_4^{2-}. The reduction of total H_2SO_4 was more effective than reducing total HNO_3 and total NH_3 to reduce i$PM_{2.5}$ especially when total available NH_3 was in excess to fully neutralize acidic gases. In addition, reduction of total H_2SO_4 may render partitioning of NH_3– NH_4^+ towards gas phase and led to NO_3^- increase when NH_3 was not in excess to fully neutralize acidic gases. Thus, future reduction of i$PM_{2.5}$ requires the coordinated reduction of both H_2SO_4 and HNO_3. Understanding of spatiotemporal variations of atmospheric chemical conditions, $PM_{2.5}$ mass closure and i$PM_{2.5}$ provides insights to improve our understanding of impacts of AFOs NH_3 emissions on the potential for i$PM_{2.5}$ formation under rural and urban conditions. The ISORROPIA II simulation provides projected prediction about i$PM_{2.5}$ formation, thus serves as a powerful tool to get an in-depth understanding of partitioning of NH_3– NH_4^+.

Dynamics of Rural and Urban Atmospheric Chemical Conditions and Inorganic Aerosols

by
Bin Cheng

A dissertation submitted to the Graduate Faculty of
North Carolina State University
in partial fulfillment of the
requirements for the degree of
Doctor of Philosophy

Biological and Agricultural Engineering

Raleigh, North Carolina

2018

APPROVED BY:

_____	_____
Dr. Lingjuan Wang-Li Committee Chair	Dr. Nicholas Meskhidze
_____	_____
Dr. John Classen	Dr. Peter Bloomfield

DEDICATION

To my grandmother, for her everlasting love.

BIOGRAPHY

Bin Cheng received his bachelor degree in agricultural structure environment and energy engineering from China Agricultural University in 2013. After that, he came to U.S. to continue and pursue the academic career. He joined the department of biological and agricultural engineering at North Carolina State University to pursue the Ph.D. degree in August 2013.

ACKNOWLEDGMENTS

At first, I would like to express my greatest appreciation to my advisor, Dr. Lingjuan Wang-Li. As a great mentor, she provided continuous guidance and encouragement for me to get over all the difficulties I've come across. For all the individual and group meeting time she has spent with me, I really enjoyed the in-depth discussion about this research with her. This work wouldn't have been accomplished without her advice and support.

All the committee members have been super supportive throughout my Ph.D. study period. I thank Dr. Nicholas Meskhidze for his face-to-face meeting with me; he always gave me very inspiring ideas and suggestions regarding my paper revisions. I sincerely thank Dr. Peter Bloomfield for helping me improve my data analysis skills. The support from Dr. John Classen is deeply appreciated; his great questions give me many inspirations to think and work on my dissertation. Great thanks to Eric Edgerton from ARA, Inc. for providing the SEARCH data.

Last but not the least, the gratitude goes to all the Wang-Li's group members, the BAE faculty and staff, my family members, and friends who have helped and supported me to get this work done. All your encouragements, supports, and assistance are sincerely appreciated and will be memorized in my heart forever.

TABLE OF CONTENTS

LIST OF TABLES

LIST OF FIGURES

CHAPTER 1: INTRODUCTION

1.1. Background

The rapidly growing world population has exerted a large burden on the environment and agricultural production systems (Gilland, 2002; Pimentel and Pimentel, 2006). To provide sufficient food, traditional livestock and poultry production was transformed to high density mode with larger and more specialized facilities (MacDonald and McBride, 2009). These industrialized food animal facilities where animals are raised and kept in confined conditions are referred to as animal feeding operations (AFOs) (USEPA, 2010). On the one hand, large amounts of food products (e.g., meat, milk, and eggs) are produced by AFOs; on the other hand, gaseous pollutants (e.g., ammonia (NH_3), hydrogen sulfide (H_2S)) and particulate matter (PM) emanated from AFOs contribute to ambient air pollution (NRC, 2003). The major sources of NH_3 in the United States (U.S.) includes AFOs, fertilizer application, fuel combustion, industrial processes etc. Based on U.S. Environmental Protection Agency (EPA)'s National Emission Inventory (NEI), AFOs contributed to more than 70% of the total NH_3 emissions across the U.S. (USEPA, 2004).

Air pollution is closely associated with people's daily life, it is crucial to regulate the emissions of air pollutants to protect the health and welfare of the public. The U.S. EPA has established National Ambient Air Quality Standards (NAAQS) to regulate six criteria pollutants: ozone (O_3), PM ($PM_{2.5}$ and PM_{10}), carbon monoxide (CO), nitrogen oxides (NO_x), sulfur dioxide (SO_2) and lead (Pb) (USEPA, 2013). Among these criteria air pollutants, $PM_{2.5}$ is PM with aerodynamic equivalent diameter (AED) less than or equal to 2.5 μm that may cause detrimental outcomes to the environment and human beings such as visibility degradation, and adverse health effects (Donham et al., 1995; Pope et al., 2009; Pui et al., 2014). The $PM_{2.5}$ can be inhaled

and deposited in the respiratory system. Furthermore, PM may absorb pollutant gases and irritating odors, carry harmful bio–aerosols, thus, it can cause premature mortality and morbidity from cardiovascular and respiratory diseases (Ma et al., 2011; Pope et al., 2009; Cambra–Lopez et al., 2010). Moreover, $PM_{2.5}$ can also cause visibility degradation due to its efficient light absorption and scattering ability in ambient air (Hinds, 1998).

Based upon different physical, chemical, biological characteristics and formation mechanisms, PM may be classified into different categories. At first, ambient PM is distributed in a wide range of sizes and consists of various chemical compositions. Thus, PM can be classified as fine and coarse PM, organic and inorganic PM. Secondly, PM may be formed through different processes, primary PM is directly emitted from sources, while secondary PM is formed through chemical reactions of various precursor gases, condensation and other atmospheric processes (Hinds, 1998). Particulate matter can be directly emitted from AFOs and many studies have shown that the majority of PM emitted from AFOs was primary, coarse and organic in nature (Cambra–Lopez et al., 2010, 2011a, 2011b, 2011c).

Recently, NH_3 emissions from AFOs have become more concern due to its potential contribution to the formation of secondary inorganic $PM_{2.5}$ ($iPM_{2.5}$) (Bittman & Mikkelsen, 2009; Li, 2012; Yang et al., 2011; Zhao, 2007). In addition, a significant increase trend in atmospheric NH_3 concentration has been observed in the eastern U.S. due to less chemical loss and higher soil temperature (Warner et al., 2017). Moreover, based on the modeling results, agricultural production activities were reported to play an important role in the formation of secondary $iPM_{2.5}$ in ambient air (Paulot and Jacob, 2014). Therefore, further research is needed to advance our understanding of the impact of AFOs NH_3 emissions on the formation of $iPM_{2.5}$ under different conditions.

1.2. Precursor gases of secondary inorganic $PM_{2.5}$

As a subset of total $PM_{2.5}$ mass, most of secondary $iPM_{2.5}$ is formed through the reactions of NH_3, H_2SO_4, and HNO_3. In ambient air, photochemical reactions readily convert SO_2 and NO_x to H_2SO_4 and HNO_3. Therefore, NH_3, SO_2, NO_x are crucial precursor gases to the formation of secondary $iPM_{2.5}$.

1.2.1. Precursor gases emissions

- *Ammonia emissions from AFOs*

Quantification of AFOs NH_3 emissions requires comprehensive investigation of the NH_3 production in different animal growth processes. Ammonia emission factors account for NH_3 emissions from housing, excreta storage, treatment and land application, thus serves as a good method to quantify AFOs NH_3 emissions (Arogo et al., 2006).

Ammonia volatilization from animal manure is affected by many factors such as nitrogen content in manure, pH, temperature (T), and wind speed. In addition, the housing types, excreta treatment techniques are different in different areas of U.S., the NH_3 emission factors may vary with various production management systems. Therefore, spatial and temporal variations of AFOs NH_3 emissions exist (Arogo et al., 2006). The studies regarding the NH_3 emissions from poultry AFOs houses are summarized in Table 1.1.

Table 1.1. Emission factors for poultries

Source	Emission Factor ($g\ NH_3\ bird^{-1}\ d^{-1}$)	Animal Species	Housing Type	Techniques	Geographic Region
Liang et al. (2005)	0.90 ± 0.027/ 0.81 ± 0.02[1]	Layers	Cross Ventilation + High–rise	Concentration + Ventilation	Iowa
	0.83 ± 0.070	Layers	Cross Ventilation + High–rise	Concentration + Ventilation	Pennsylvania
	0.054 ± 0.0035	Layers	Quasi Tunnel Ventilation + Manure–belt (daily removal)	Concentration + Ventilation	Iowa
	0.094 ± 0.006	Layers	Cross and Tunnel Ventilation + Manure–belt (twice a week)	Concentration + Ventilation	Pennsylvania
Lin et al. (2012a)	0.95 ± 0.67	Layers	Cross Ventilation + High–rise	Concentration + Ventilation	California
Wang-Li et al. (2013)	0.599 ± 0.200 /0.600 ± 0.250	Layers	Tunnel Ventilation + High–rise	Concentration + Ventilation	North Carolina
Wheeler et al. (2006)	0.031 ± 0.001	Broiler	Tunnel Ventilation	Concentration + Ventilation	Kentucky & Pennsylvania
Lin et al. (2012b)	0.503 ± 0.436	Broiler	Tunnel Ventilation	Concentration + Ventilation	California
Siefert and Scudlark (2008)	0.158	Broiler	Tunnel Ventilation	Inverse Gaussian plume model	Virginia
Lacey et al. (2003)	0.632	Broiler	Tunnel Ventilation	Concentration + Ventilation	Texas

[1] 0.90 ± 0.027 is for standard diet, 0.81 ± 0.02 is for 1% lower crude protein diet.

Liang et al. (2005) estimated the NH_3 emission rates from layer farms in Iowa and Pennsylvania using different dietary and manure handling systems. The emission rates for the

high–rise layer farms with standard diet were reported to be 0.90 ± 0.027 g NH_3 $bird^{-1}$ d^{-1}, while 1% lower crude protein diet can lead to emission rate of 0.81 ± 0.02 g NH_3 $bird^{-1}$ d^{-1} for high–rise layer farms. The emission rate for the manure–belt systems with daily removal was reported to be 0.054 ± 0.0035 g NH_3 $bird^{-1}$ d^{-1}, the different emission rates indicated that manure handling strategy can impact NH_3 emission in layer farms. Another finding from this research was that the emission rates exhibited a significant seasonal variation with higher emission rates in warmer seasons; a diurnal variation was also observed: the emission rates were higher in early afternoon in high–rise layer houses and higher when manure removal occurred. However, the opposite seasonal variation of NH_3 emissions was found by Lin et al. (2012a) in California, and the estimated NH_3 emissions from layer farms exhibited higher emissions in winter and lower in summer due to drier manure in summer. Another research performed by Wang–Li et al. (2013) measured the NH_3 emission rates from a high-rise layer farm in North Carolina (NC), the results indicated that the NH_3 emission rates from two high-rise layer houses were 0.599 ± 0.200 g d^{-1} hen^{-1} and 0.600 ± 0.250 g d^{-1} hen^{-1} exhibiting a slightly diurnal variation with higher rates in early afternoon but no significant seasonal variation; this research also determined that house exhaust temperature had the most significant impact on NH_3 emission rate.

Redwine et al. (2002) estimated summer NH_3 emission from the tunnel ventilated broiler houses in Texas. The NH_3 emission was reported to be 38–2105 g hr^{-1} with increasing trend as the birds grew up. Wheeler et al. (2006) monitored the NH_3 emissions from mechanically ventilated broiler chicken houses in Kentucky and Pennsylvania, emission factors were estimated to be 0.028 g $bird^{-1}d^{-1}$, 0.034 g $bird^{-1}d^{-1}$ and 0.038 g $bird^{-1}d^{-1}$ for three broiler farms with built–up litter and 0.024 g $bird^{-1}d^{-1}$ for broiler farm with new litter; the results indicated that no significant seasonal pattern for NH_3 emission rates was observed even exhaust NH_3

concentration was the highest in cold weather while ventilation rates were the highest in warm weather. Harper et al. (2010) estimated NH_3 emissions from broiler farms in California using backward Lagrangian stochastic (bLS) dispersion model approach. No significant variation was observed between summer and winter emissions, and the annual emissions were found to be 0.099 ± 0.010 kg NH_3 $bird^{-1}$ $year^{-1}$ with increasing trend as birds grew older.

For poultry production, many factors such as housing types, stocking density, bird age, waste treatment strategy, flocks number may affect the NH_3 emissions from production houses. Wheeler et al. (2006) and Gates et al. (2008) indicated that older bird may produce more manure, leading to more NH_3 gas and higher emissions rate. The waste treatment strategy may also affect NH_3 emissions from AFOs farms. In addition to raising time, the empty broiler houses with built-up litter were found to emit NH_3 during the downtime as well. Topper et al. (2008) observed that empty broiler houses with built–up litter emitted less NH_3 than regular raising time, and the reduced emission rates can be attributed to lower litter temperature, less litter accumulation, and lower house ventilation.

Cattle husbandry is another important NH_3 emission source, the quantifications of NH_3 emissions from cattle farms are summarized in Table 1.2.

Table 1.2. Emission factors for cattle

Source	Emission Factor ($kg\ NH_3\ animal^{-1}\ yr^{-1}$)	Animal Species	Housing Type	Techniques	Geographic Region
Flesch et al. (2007)	54.8[1]	Beef	Open lots	bLS[2] inverse dispersion model	Texas
Todd et al. (2008)	19.3/0.7[3]	Beef	Open lots	bLS[2] inverse dispersion model	Texas
Flesch et al. (2009)	19-20	Dairy	Natural ventilation + free–stall barns	bLS[2] inverse dispersion model	Wisconsin
Rumburg et al. (2006; 2008a; 2008b)	34/40/55[4]	Dairy	Free–stall barns	Field measurement	Washington
Mukhtar et al. (2008)	9.4 ± 5.6/11.6 ± 7.1/6.2 ± 3.7[5]	Dairy	Open lots	Flux chamber	Texas
Cassel et al. (2005b)	22.2[6]	Dairy	Free–stall	Micrometeorological mass balance	California
	45.6[6]	Dairy	Free–stall + open lots	Micrometeorological mass balance	California

[1] 54.8 is for feedlots emissions.

[2] Backward Lagrangian stochastic.

[3] 19.3 is for feed yard emissions, 0.7 is for retention pond emissions.

[4] 34 is for land application emissions, 40 is for barn emissions, and 55 is for lagoon emission.

[5] 9.4 ± 5.6 is for annual emissions, 11.6 ± 7.1 is for summer emissions, and 6.2 ± 3.7 is for winter emissions.

[6] 22.2 and 45.6 are both for winter emissions.

Pinder et al. (2004) calculated the NH_3 emission factors for dairy cow in spatial and temporal scales across the U.S. based on process–based model under various farming practices, climate conditions and animal population data. A seasonal variation was observed with the highest emission factors in spring and fall, and the lowest emission factors in winter due to intensive manure application in spring and fall. Moreover, higher housing and storage emissions were also observed under high temperature conditions in summer. This research also discovered that higher emission factors were observed in the South and West of the U.S. due to high temperature conditions and manure management favoring the volatilization of NH_3 in these areas.

Cassel et al. (2005a) estimated NH_3 emissions from an open–lot dairy farm using the micrometeorological flux measurement technique. NH_3 emission factors were found to be in the range of 19–143 g $head^{-1}day^{-1}$, for which high temperature and low RH favored the emissions of NH_3. Cassel et al. (2005b) estimated winter NH_3 emissions from two dairy farms in California, one confined dairy cattle in free–stall farms, the other confined dairy cattle in the combination of free–stall farms and open lots based on micrometeorological flux measurement technique. A diurnal pattern was observed for emission factor with a peak in late afternoon from 1:00 pm to 6:00 pm; the measured NH_3 emissions for the two dairy farms were 22.2 and 45.6 kg NH_3 $animal^{-1}$ yr^{-1}.

Todd et al. (2008) estimated the NH_3 emission factor for an open lot beef cattle feed yard in Texas based on bLS dispersion model. The annual emission factor was 19.3 kg NH_3 $animal^{-1}$ yr^{-1}. The NH_3 emissions in winter were less than half of that in summer. Harper et al. (2009) also employed bLS dispersion model to estimate the NH_3 emissions from natural ventilation and free–stall housing dairy farms in Wisconsin. A significant seasonal and diurnal trend were

observed for NH_3 emissions pattern, higher in summer and later afternoon. Winter emissions were 0.014–0.023 g NH_3/kg of body weight/d, and the summer emissions were 0.137–0.171 g NH_3/kg of body weight/d. Most of the NH_3 was emitted from lagoons and sand separators but not from barns.

In some areas of the U.S., swine husbandry may be a major NH_3 emission source due to intensive swine productions. The swine feeding operations were classified into three categories bases on different growth stages of swine: farrowing, nursery and finishing (Faulkner and Shaw, 2008). The studies regarding the NH_3 emissions from swine production are summarized in Table 1.3.

Table 1.3. Emission factors for swine

Source	Emission Factor (kg NH_3 $animal^{-1}$ yr^{-1})	Animal stage	Techniques	Geographic Region
Doorn et al. (2002)	7 ± 2 [1]	Composite	Mass balance	North Carolina
	3.7 ± 1.0 [1]	Finishing	Mass balance	North Carolina
	2.4[1]	Composite	Mass balance	North Carolina
Flesch et al. (2005)	2.37/5.84[2]	Nursery	bLS[3] dispersion model	Western U.S.
Harper et al. (2006)	3.13[4]	Sow	Process model	Utah
	0.38[4]	Nursery	Process model	Utah
	2.22[4]	Finishing	Process model	Utah

[1] 7 ± 2 is generic emission factor, 3.7 ± 1.0 is house emission factor, and 2.4 is lagoon emission factor.

[2] 2.37 is emission factor in March and 5.84 is emission factor in May.

[3] bLS: backward Lagrangian stochastic.

[4] 3.13, 0.38, and 2.22 are all lagoon emission factors.

Aneja et al. (2000) measured the NH_3 emissions from a swine lagoon in NC, the results indicated that there was a significant seasonal variation in NH_3–N flux with the highest value in summer (4017 ± 987 μg N m^{-2} min^{-1}) and the lowest value in winter (305 ± 154 μg N m^{-2} min^{-}

[1]). Doorn et al., (2002) developed farm level NH_3 emission factor for swine production in NC to be 7 ± 2 kg NH_3 $animal^{-1}year^{-1}$. This estimation used mass balance method and considered NH_3 emissions from swine houses, lagoons and field application, thus providing a good reference to calculate NH_3 emissions from swine farms. Harper et al. (2006) estimated the NH_3 emissions from swine lagoon in the Utah Great Basin, using the process based method and the measurements of physical and chemical parameters on lagoons. The calculated NH_3 emission factors for hogs in different growth stages were 3.13, 0.38, and 2.22 kg NH_3 $animal^{-1}$ yr^{-1}, for sow, nursery, and finishing, respectively. The results indicated that temperature and wind speed were two important factors affecting NH_3 emissions.

The aforementioned studies monitored the NH_3 emissions from AFOs farms with different animal species in different areas of U.S. under unique climate conditions, therefore, different seasonal or diurnal pattern were observed. The temporal pattern of AFOs NH_3 emissions may affect ambient NH_3 concentrations in the vicinity of AFOs farms, thus affecting possible reaction of NH_3 with acidic gases in ambient air.

- *Temporal variations of NO_x and SO_2 emissions*

In ambient air, SO_2 and NO_x are mainly produced from fossil fuel combustions. SO_2 mainly comes from coal–burning power plants, where the sulfur in the fuel is converted into sulfur oxides during the combustion processes. NO_x is mainly attributed to exhausted gases emitted from motor vehicles, in which the nitrogen reacted with oxygen under high temperature condition to form nitrogen oxides. Moreover, the nitrogenous compound in the fuel can be converted into nitrogen oxides as well (USEPA, 2016a, 2016b).

As vehicle emissions are the major sources of NO_x, NO_x emissions pattern may follow the diurnal variation of traffic volumes on the highways. Batterman et al. (2015) estimated

temporal variation of traffic volumes in highways, and reported that a significant diurnal and weekday versus weekend pattern of traffic volumes was observed. In weekdays, there was a bimodal pattern with higher traffic volumes in morning and afternoon; while in weekend, only unimodal pattern was observed with peak traffic volumes in early afternoon.

For coal–burning power plants, the plumes emitted from power plants may exhibit a constant pattern under the steady operation of the electricity generating facilities. Therefore, there might not be temporal variations in SO_2 emission from the plants.

The emission patterns of major NO_x and SO_2 sources may affect the ambient concentrations of NO_x and SO_2, thus affecting the fate and transport of NO_x and SO_2.

1.2.2. Fate and transport of AFOs NH_3 emissions

Ammonia has a short lifetime (0.5 h to 5 d) in ambient air (Seinfeld and Pandis, 2006), the contribution of AFOs NH_3 emissions to the formation of secondary $iPM_{2.5}$ may be limited by the fast removal of NH_3 through its dry and wet depositions. Research regarding the fate and transport of NH_3 indicates that NH_4^+ salts can be transported in a long distance while NH_3 could be removed from air in a short distance (Aneja et al., 2003, Duyzer, 1994, Lefer et al., 1999). High spatial variability has been observed in NH_3 dry deposition, caused by the spatial inhomogeneity of emission sources and differences in land uses and management practices (Duyzer, 1994; Sutton et al., 1994). Fate and transport of NH_3 gas in the atmosphere is illustrated in Figure 1.1.

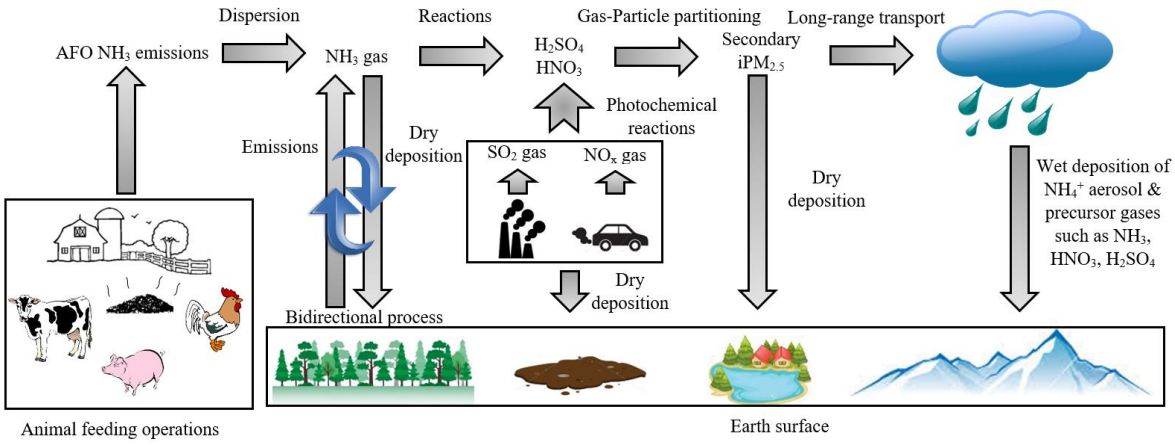

Figure 1.1. Fate and transport of NH_3 emitted from AFOs in the atmosphere

The closer to AFOs farms, the higher the NH_3 concentration can reach. After emissions from AFOs farms, NH_3 concentration may be gradually reduced due to dry and wet depositions. Allen et al. (1988) measured the NH_3 and NH_4^+ concentrations at 19 sites affected by various NH_3 emission sources such as livestock farms, landfill sites, sewage treatment plants, an arable farm, busy road, and marine sources. The study discovered that the NH_3 emissions from livestock farms led to significant increase in local NH_3 concentration and a slight increase in local NH_4^+ concentration. Seasonal variation of local NH_3 concentration in locations close to livestock farms was observed with higher concentration in summer. Diurnal variation of ambient NH_3 concentrations exhibited a higher concentration in the afternoon, which may be complicated by both NH_3 emission pattern from AFOs facilities and meteorological conditions. Fowler et al. (1998) investigated the gradients of NH_3 concentration and deposition in woodland surrounding a poultry farm with approximate 4800 kg annual NH_3 emission. It was reported that only a small fraction (3–6%) of NH_3 was dry deposited within 300 m of the woodland surrounding the poultry farm, a horizontal spatial gradient of NH_3 concentration was observed in the vicinity of poultry farms. Asman and van Jaarsveld (1992) studied the dry and wet depositions of NH_3 and NH_4^+

derived from a 1 m height point source under Dutch climatic condition through model simulation. Their results indicated that NH_3 dry deposition dominated in the proximity of emission source while NH_4^+ wet deposition served as the main pathway depleting NH_3 in the long distance. Specifically, 10% and 20% of NH_3 emissions was dry deposited within 100 m and 1000 m, respectively, while within 400 m from emission source, wet deposition of NH_3 together with dry and wet deposition of NH_4^+ didn't start to have impacts. The acidic gases (NO_x and SO_2) have low concentrations in agricultural intensive areas due to limited emission sources but high concentrations in urban areas, therefore, removal of NH_3 from rural ambient air may limit its interactions with the acidic precursor gases in urban areas.

1.3. Formation of secondary $iPM_{2.5}$

Different chemical compositions of $PM_{2.5}$ can be linked to the different emission sources and the formation processes of secondary $PM_{2.5}$ (Abdeen et al., 2014). The investigation of secondary $iPM_{2.5}$ formation requires detailed information of $PM_{2.5}$ chemical compositions, including ions (e.g., ammonium (NH_4^+), sulfate (SO_4^{2-}), nitrate (NO_3^-)), organic carbon (OC), elemental carbon (EC), various elements (e.g., crustal materials), and other unknown components (Frank, 2006; Malm et al., 1994). The formation of secondary $iPM_{2.5}$ may be characterized by the thermodynamic equilibrium of gas-phase NH_3 and particle-phase NH_4^+ partitioning.

1.3.1. Thermodynamic equilibrium

In the atmosphere, NH_3 may react with acidic gases to produce NH_4NO_3, $(NH_4)_2SO_4$ and NH_4Cl, which are the major compositions of $iPM_{2.5}$ (Zhang et al., 2012). A thermodynamic equilibrium may exist between $iPM_{2.5}$ and its precursor gases (Seinfeld and Pandis, 2006; Wang–Li, 2015). When NH_3 reacts with acidic gases, it is converted from gas phase to particle phase in

the form of NH_4^+ salts. There are two steps involving in the chemical reaction processes for the formation of $iPM_{2.5}$. The first step is so-called the oxidation process, in which NO_x and SO_2 are transformed into HNO_3 and H_2SO_4 through photochemical reactions. In the second step, acidic gases, HNO_3 and H_2SO_4, may then react with NH_3 to form NH_4^+ salts. This step is also known as partitioning between gas and particle phases. Partitioning of gas–NH_3 and particle–NH_4^+ is highly dependent upon T, relative humidity (RH), and molar concentrations of total H_2SO_4 (gas + particle), total HNO_3 (gas + particle) and total NH_3 (gas + particle) (Pay et al., 2012). These two steps can be expressed in the following equations (Zhang et al., 2008; Ansari and Pandis, 1998; Wang–Li, 2015):

$$SO_2 + 2OH \rightarrow H_2SO_4\,(g) \qquad (1\text{-}1)$$

$$2NH_3 + H_2SO_4 \leftrightarrow (NH_4)_2SO_4\,(particle) \qquad (1\text{-}2)$$

$$NO_2 + OH \rightarrow HNO_3\,(g) \qquad (1\text{-}3)$$

$$NH_3\,(g) + HNO_3\,(g) \leftrightarrow NH_4NO_3\,(particle) \qquad (1\text{-}4)$$

$$NH_3\,(g) + HCl\,(g) \leftrightarrow NH_4Cl\,(particle) \qquad (1\text{-}5)$$

Another pathway to form HNO_3 at night is the heterogeneous hydrolysis of N_2O_5, the key reactions of this process are shown in the following equations (Nenes et al., 1998; Blanchard et al., 2000; Seinfeld and Pandis, 2006).

$$O_3 + NO_2 \rightarrow NO_3 + O_2 \qquad (1\text{-}6)$$

$$NO_2 + NO_3 \leftrightarrow N_2O_5 \qquad (1\text{-}7)$$

$$N_2O_5 + H_2O \rightarrow 2HNO_3\,(aq) \qquad (1\text{-}8)$$

Gas-phase SO_2 may be oxidized by oxidants such as O_3 and OH into H_2SO_4 gas or SO_4^{2-} ions (Makar et al., 2009). Aqueous phase SO_2 may also be oxidized by O_3, hydrogen peroxide (H_2O_2), or oxygen (O_2) with or without the catalyst of metals. As SO_4^{2-} owns very low vapor

pressure, nearly all gas-phase SO_4^{2-} can partition to the particle phase SO_4^{2-} (Seinfeld and Pandis, 2006).

As it has been reported, concentration of $iPM_{2.5}$ may respond to the changes of precursor gas concentrations nonlinearly (Ansari and Pandis, 1998). The NH_3 gas preferentially reacts with H_2SO_4 to form $(NH_4)_2SO_4$ and ammonium bisulfate (NH_4HSO_4), the NH_3 in excess may react with HNO_3 to form NH_4NO_3, a semi–volatile compound (Nenes et al., 1998; Huntzicker et al., 1980). The SO_4^{2-} salts and NO_3^- salts have different levels of thermal stability characteristic. As NH_4NO_3 is not thermally stable enough, it may decompose back to HNO_3 and NH_3 under environmental conditions with high T and low RH that does not favor the particle phase, or vice versa, condenses back onto particles. On the contrary, SO_4^{2-} salts are thermally stable as compared with NO_3^- salts (Olszyna et al., 2005).

1.3.2. Atmospheric chemical conditions

In the literature, atmospheric chemical reaction potential and chemical conditions may be examined by six parameters. Among these six parameters, two parameters are used to assess the neutralization potentials of NH_3 (Ansari and Pandis, 1998), and the other four parameters are used to evaluate the responses of $iPM_{2.5}$ to the changes of NH_3 concentrations and atmospheric chemical conditions (Makar et al., 2009). These six parameters are as following:

- Gas ratio (GR): this ratio is to assess the neutralization degree of NH_3 (Ansari and Pandis, 1998) and it is defined by:

$$GR = \frac{[TA] - 2[TS]}{[TN]} \qquad (1\text{-}9)$$

Where TA is total ammonia including NH_3 and NH_4^+, TS is total sulfate including SO_4^{2-}, HSO_4^-

, and H_2SO_4, TN is total amount of NO_3^- and HNO_3:

When GR>1, the amount of TA is enough to neutralize both TS and TN, under this condition, the changes of TA concentration isn't a key factor to affect the concentration of secondary $iPM_{2.5}$.

When 0<GR<1, the amount of TA is enough to neutralize all TS but not TN, therefore, only NH_4NO_3 formation is limited by TA, under this condition, the decrease of NH_3 leads to corresponding decrease of NH_4NO_3.

When GR<0, the amount of TA is not enough to neutralize either TS or TN, therefore, both $(NH_4)_2SO_4$ and NH_4HSO_4 formation are limited by TA.

- Molar ratio (R) of $(NH_4^+ - NO_3^- - Cl^-)/SO_4^{2-}$. This ratio is to assess neutralization degree of NH_3 (Walker et al., 2006; Liu et al., 2009; Li et al., 2014). The R is defined by:

$$R = \frac{[NH_4^+] - [NO_3^-] - [Cl^-]}{[SO_4^{2-}]} \qquad (1\text{-}10)$$

When R is less than 0.5, H_2SO_4 and NH_4HSO_4 both exist in the particle;

When R lies between 0.25 and 0.5, the secondary $iPM_{2.5}$ is dominated by NH_4HSO_4;

When R is equal to 1.25, the secondary $iPM_{2.5}$ is dominated by $(NH_4)_3H(SO_4)_2$;

When R is equal to 1.5, the secondary $iPM_{2.5}$ consists of $(NH_4)_3H(SO_4)_2$;

When R is larger than 1.5, $(NH_4)_2SO_4$ is formed;

When R is equal to 2, the secondary $iPM_{2.5}$ is dominated by $(NH_4)_2SO_4$.

- Particle neutralization ratio (PNR):

$$PNR = \frac{[NH_4^+]}{2[SO_4^{2-}] + [NO_3^-]} \qquad (1\text{-}11)$$

When the ratio is equal to 1, the $iPM_{2.5}$ is NH_3-saturated, significant NH_3 reductions is needed to reduce $iPM_{2.5}$.

When the ratio is less than 1, the $iPM_{2.5}$ is NH_3-limited, small NH_3 reductions may lead to significant reduction of $iPM_{2.5}$.

- Total ammonia to sulfate molar ratio (TA/TS):

$$TA/TS = \frac{[NH_3]+[NH_4^+]}{[SO_4^{2-}]} \qquad (1\text{-}12)$$

When the ratio is less than 1, indicating acidic conditions, both NH_4HSO_4 and H_2SO_4 exist in the particle phase.

When the ratio is between 1 and 2, indicating intermediate acidity, NH_4HSO_4, $(NH_4)_3H(SO_4)_2$, and $(NH_4)_2SO_4$ all exist in the particles.

When the ratio is greater than 2, indicating less acidic conditions, both $(NH_4)_2SO_4$ and NH_4NO_3 may exist in the particles.

- Gas-phase ammonia molar fraction (NH_3/NH_x):

$$NH_3/NH_x = \frac{[NH_3]}{[NH_3]+[NH_4^+]} \qquad (1\text{-}13)$$

Any changes in this ratio indicate the change in the partitioning of gas–phase ambient NH_3 and particle–phase NH_4^+ .

- $PM_{2.5}$ Ammonium + Nitrate to total $PM_{2.5}$ mass ratio: $AN/PM_{2.5}$

$$AN/PM_{2.5} = \frac{NH_4^+ + NO_3^-}{PM_{2.5}} \qquad (1\text{-}14)$$

The changes of NH_3 emissions is apt to directly affect NH_4^+ & NO_3^- at first, this ratio indicates the fraction of $PM_{2.5}$ mass that is directly NH_3 sensitive.

In addition to the reactions with HNO_3 and H_2SO_4, NH_3 can react with HCl as well. According to the study by Walker et al. (2006), NH_4Cl may also be the important component of $iPM_{2.5}$ in coastal regions; however, Cl^- only accounted for minor part of the total $iPM_{2.5}$ in agricultural environments in the southeastern U.S.

Extensive field research has been done to study the mechanisms of the thermodynamic reactions between NH_3 and acidic precursor gases (Saylor et al., 2010, 2015; Walker et al., 2006; Mwankiki et al., 2014; Robarge et al., 2002; Gong et al., 2013; Li et al., 2014). Saylor et al. (2015) analyzed the temporal change trend of total NH_3 concentrations from 2004 to 2014 in the southeastern U.S., the results showed a decreased trend in total NH_3 concentrations but an increased trend in the gas-phase NH_3 molar fraction (NH_3/NH_x). These change trends were attributed to the recent NH_3, SO_2 and NO_x emissions change; less acidic precursor gases were available to react with NH_3 leading to the partitioning of $NH_3 – NH_4^+$ towards gas-phase NH_3.

Li et al. (2014) measured the 24–hr average concentrations of NH_3, HNO_3, NH_4^+, NO_3^- and SO_4^{2-} for five years in a rural natural gas production area in Wyoming, the sampling site was impacted by the NO_x emissions from gas extraction operations and transportation as well as NH_3 emissions from agricultural sources. The results indicated that NH_3 and SO_4^{2-} exhibited seasonal variation with higher concentrations in summer and lower concentration in winter. On the contrary, NO_3^- concentration was higher in winter and lower in summer. Furthermore, both gas-phase NH_3 molar fraction (NH_3/NH_x) and gas-phase HNO_3 molar fraction ($[HNO_3]/([NO_3^-] + [HNO_3])$) exhibited higher values in summer and lower values in winter. The seasonal variation of these gas and particle phase compositions as well as gas-phase NH_3 and HNO_3 molar fractions

revealed the impact of T and RH on the thermodynamic equilibrium existing in gas–particle system.

1.3.3. Thermodynamic equilibrium model–ISORROPIA II

The partitioning of gas-phase NH_3 and particle–phase NH_4^+ may be assumed in the thermodynamic equilibrium state, thus thermodynamic equilibrium model can be utilized to simulate the reactions of various precursor gases of secondary $iPM_{2.5}$. In addition to the equilibrium models, dynamic and hybrid aerosol models have been developed to simulate the aerosol dynamics in ambient air. Dynamic model resolves the particle size change in the gas-particle partitioning process (Meng et al., 1998), while hybrid model simulates particulate matter with aerodynamic diameter less than 1 μm (PM_1) using equilibrium approach and larger particles using dynamic approaches (Capaldo et al., 2000). Koo et al. (2003) assessed the performance of these three types of models (equilibrium, dynamic, and hybrid models) in simulating the concentrations of $iPM_{2.5}$ and iPM_{10} chemical compositions. The comparison between model simulations and field measurements indicated that both dynamic and hybrid models performed better than equilibrium model with dynamic model having the best agreement with field measurements. However, dynamic models are not computationally efficient, at least 10 times slower than equilibrium model (Koo et al., 2003), thus it's not appropriate to be combined with large-scale chemical transport model (CTM). As a widely used thermodynamic equilibrium model, ISORROPIA II has been coupled to large-scale CTMs to predict the concentrations of secondary $iPM_{2.5}$ at equilibrium state.

The default assumption made in the thermodynamic equilibrium model is that the gas and particle system is in a chemical equilibrium state, namely, the total free energy of the system is minimized and equal to zero (Seinfeld and Pandis, 2006). The ISORROPIA II (Fountoukis and

Nenes, 2007) is one of the commonly used thermodynamic models, in which gas–particle partitioning phenomenon and the impacts of temperature (T) and relative humidity (RH) are incorporated. Mutual deliquescence region (MDR) and hysteresis phenomenon are both resolved in the model. In addition, compared with other thermodynamic models, ISORROPIA II is more computationally efficient with stable performance (Ansari and Pandis, 1999b; Nenes et al., 1998, 1999; Fountoukis and Nenes, 2007). Input data required by the ISORROPIA II include the concentrations of NH_3, HNO_3, H_2SO_4, and hydrochloric acid (HCl) both in gas and particle phases, T and RH. Two types of problems (forward and backward) can be solved by ISORROPIA II (Fountoukis et al., 2009). The input data for forward problem include total concentrations of precursor gases existing both in gas and particle phases. The input data for backward problem include the concentrations of precursor gases exclusively in particle phase. In addition, thermodynamically stable and metastable states can be set by user to adapt to different application scenarios. The difference between these two states reflects if the salts in the solution will precipitate when super saturation state is achieved. For thermodynamically stable state, the salts will precipitate when super saturation is achieved, while for metastable state, the salts remain in the aqueous phase. The outputs of the model include the concentrations of precursor gases, i$PM_{2.5}$ chemical compositions, hydrogen ion, and water content at chemical equilibrium state for both forward and backward problems.

The ISORROPIA II model assumes that the thermodynamic equilibrium is established instantaneously. In order to prove the validity of this assumption, the timescale to reach thermodynamic equilibrium state were assessed by Meng and Seinfeld (1996), and Fountoukis et al. (2009). The theoretical calculations revealed that it takes around 5-30 min for submicron (PM_1) and more than 1-hr for super-micron ($PM_{1-2.5}$) aerosols to reach equilibrium state.

Therefore, the application of equilibrium models (e.g., ISORROPIA II) using field measurements with long integration time (e.g., 24-hr) is questionable. The field sampling with long integration time may not be able to detect the variation of gas- and particle-phase pollutants caused by dramatic changes of ambient conditions. Zhang et al. (2003) indicated that the filter-based measurements with low time resolution (12 hr to 24 hr) may be problematic to assess the performance of thermodynamic equilibrium models.

Time resolution of the concentrations of $iPM_{2.5}$ and its precursor gases varied in different field studies from several minutes to 24 hr due to the differences in the measurement instruments and techniques. Zhang et al. (2003), Yu et al. (2005) and Fountoukis et al. (2009) used 5-6 min measurements to assess the performance of ISORROPIA II; Yu et al. (2005) and Takahama et al. (2004) used 1-3 hr measurements to check the prediction skill of ISORROPIA II; Moya et al. (2001), Yu et al. (2005) and Goetz et al. (2008) used 6-24 hr measurements to investigate the performance of ISORROPIA II. The measurements with 6 to 24 hr time resolution may not be suitable to assess the model prediction skill because the greater time scale loses resolution to detect the impact of ambient condition changes on the $NH_3 - NH_4^+$ partitioning process.

Factors influencing the gas-particle system equilibrium state include ambient meteorological condition (Walker et al., 2006), surface heterogeneity and multiphase chemistry (Ravishankara, 1997), and organic aerosols coating inorganic aerosols (Silvern et al., 2017; Gill et al., 1983). Thus the application of thermodynamic model such as ISORROPIA II may also be affected by those factors (Wexler & Seinfeld, 1992). The departures from equilibrium assumption may cause disagreement between model simulations and field measurements. Thermodynamic equilibrium models predict the molar ratio R ($R = ([NH_4^+] - [NO_3^-] - [Cl^-])/[SO_4^{2-}]$) to be 2 when NH_3 is in excess to neutralize acidic gases, corresponding to the

stoichiometry of $(NH_4)_2SO_4$. Research conducted by Li et al. (2014a, b) detected the high concentration of NH_3 gas near the source region. It was observed that the mean R was 1.75, which is less than 2, although this ratio should be close to 2 under high NH_3 concentration environment. Further investigation of Li et al. (2014a, b) suggested that wind speed might affect the local thermodynamic equilibrium status as the time for establishing such equilibrium may exceed the time needed for transporting NH_3-ladend air parcel from layer farm under high wind speed. In another research by Walker et al. (2006), the concentrations of $iPM_{2.5}$ chemical compositions and precursor gases were measured at an agricultural site located in an area impacted by the NH_3 emissions from intensive animal production activities and fertilizer application. It was also discovered that the mean R was approximately 1.43. The high NH_3 concentrations at the site was in excess to neutralize acidic gases, and the excessive NH_3 should render molar ratio R close to 2. Walker et al. (2006) noted that the possible reason to the low molar ratio R may be due to the non-equilibrium state of the $NH_4^+ - NO_3^- - SO_4^{2-}$ system, the mass transport between gaseous NH_3 and particles may limit sufficient NH_3 to fully neutralize SO_4^{2-}. Although the applicability of ISORROPIA II in rural area with high NH_3 concentrations was not fully assessed in the research, ISORROPIA II model was utilized to investigate the responses of secondary $iPM_{2.5}$ to the changes of precursor gases. Further investigation should be conducted to advance our understanding on the thermodynamic equilibrium assumption.

The impact of organic matter on the chemistry of NH_3 and acidic gas H_2SO_4 involves complex processes, and in the literature, there are two contradictory explanations. Liggio et al. (2011) investigated the time to achieve equilibrium state in the system of NH_3-H_2SO_4-organics. In a closed chamber, particle-free ambient air was exposed to H_2SO_4 aerosols. The initial molar ratio of total NH_3/total H_2SO_4 was set at various values and the steady $[NH_4^+]/[SO_4^{2-}]$ molar

ratio was treated as the equilibrium indicator. The comparison of equilibrium time between organic-free system and organic-rich system indicated the delay effect of organics on the NH_3 uptake to H_2SO_4 particles. The inorganic particles may be coated by organic materials, leading to a long equilibrium time in as long as hours instead of minutes. Silvern et al. (2017) compared the $[NH_4^+]/[SO_4^{2-}]$ in the air with the values in rainwater in the eastern U.S. The results indicated that SO_4^{2-} was not fully neutralized even with excessive NH_3 in ambient air. The possible reason to the incomplete neutralization of SO_4^{2-} may be the organic aerosol (OA) coating on the inorganic particles. On the other hand, Guo et al. (2017) challenged the ability of organic film to retard NH_3 uptake. In this newer research, the $OA/PM_{2.5}$ mass fraction was utilized to represent the thickness of organic film. No significant relationship between the measured molar ratio of $[NH_4^+]/[SO_4^{2-}]$ and $OA/PM_{2.5}$ mass fraction was observed. This finding may challenge the ability of organic film to retard NH_3 uptake.

The ISORROPIA II model simulates the K^+–Ca^{2+}–Mg^{2+}–NH_4^+–Na^+–SO_4^{2-}–NO_3^-–Cl^-–H_2O system, however, often times, the nonvolatile cations (NVCs) such as potassium (K^+), calcium (Ca^{2+}), magnesium (Mg^{2+}), and sodium (Na^+) may not be monitored due to the limitation of measurement instruments and techniques. Fountoukis et al. (2009) and Guo et al. (2017) observed that the inlusion of measured Na^+ to the model input significantly improved the performance of ISORROPIA II in reproducing the gas-phase and particle-phase pollutants.

Based on the above literature review, further research is needed to assess the performance of the ISORROPIA II model, especially model performance assessment with high time resolution onsite measurements.

1.4. The impact of AFOs NH_3 emissions on the formation of secondary $iPM_{2.5}$

While AFOs emit insignificant amount of primary $PM_{2.5}$ to ambient PM, potential of their significant amount of NH_3 emissions to the formation of secondary $iPM_{2.5}$ in atmosphere has become an increasing concern. The fundamental knowledge regarding the chemical reactions between different precursors to form $iPM_{2.5}$ has been intensively studied; however, the contributions of AFOs NH_3 emissions to the formation of ambient secondary $iPM_{2.5}$ are not well understood and experimentally quantified.

Researchers have reported that agricultural NH_3 sources can influence local concentrations of NH_4^+ salts in the atmosphere and precipitation both in the U. S. and Europe (Asman et al., 1998). Aneja et al. (2003) investigated the relationship between NH_3 emissions from agricultural sources and ambient NH_4^+ concentrations in the southeastern U.S. with spatiotemporally varied NH_3 emissions and NH_4^+ concentrations data. This research indicated that the higher NH_3 emissions led to the higher NH_4^+. Furthermore, the research discovered that in the coastal plain region of NC, ambient NH_3 concentration was high, sometime reaching up to 34.80 μg m^{-3}; ambient air was dominated by NH_3–rich conditions due to high NH_3 emissions from AFOs (Robarge et al., 2002; Walker et al., 2000a). Walker et al. (2004) compared the $iPM_{2.5}$ concentrations at three sites in NC coastal plain region with different NH_3 emission densities. The results indicated that NH_3 emitted from agricultural sources such as AFOs and fertilizer posed large influences on ambient $iPM_{2.5}$ concentrations. Ambient concentrations of NH_3 and $iPM_{2.5}$ exhibited a positive correlation with local agricultural NH_3 emission density such that the higher total NH_3 emissions led to the higher $iPM_{2.5}$ concentrations in rural areas being investigated. Goetz et al. (2008) analyzed the major chemical compositions of $PM_{2.5}$ in Eastern North Carolina (NC) from 2001 to 2004 at sites representing urban and rural

environment. Their analysis of wind direction and $PM_{2.5}$ concentration indicated the potential impact of NH_3 emissions from swine farms on the increase in ambient $PM_{2.5}$. Saylor et al. (2010) compared the total NH_3 ($NH_3 + NH_4^+$) concentrations and NH_3 gas concentration at two sites representing urban and agricultural rural environment in Georgia. The data analysis showed that both total NH_3 concentration and NH_3 gas concentration at agricultural rural site were higher than the urban site, especially in the wind direction blown from broiler farms. This research indicated the potential local impact of AFOs NH_3 emissions, which may increase the NH_3 concentration in the proximity of AFOs farms and contribute to the formation of secondary $iPM_{2.5}$.

While the above investigations only suggested the qualitative implication that the NH_3 emissions from AFOs may pose impact on the formation of secondary $iPM_{2.5}$, no quantification efforts have been done to corroborate the potential contribution of AFOs NH_3 emissions to ambient $iPM_{2.5}$.

A more recent study conducted by Paulot and Jacob (2014) estimated the health impacts of $PM_{2.5}$ attributable to agricultural export through model simulation. In this research, several models and databases were employed to simulate (1) NH_3 emission inventory from agriculture export sources by Magnitude and Seasonality of Agricultural Emissions (MASAGE), (2) ambient NH_3 concentrations in response to the simulated NH_3 emission inventory from agricultural exports by GEOS–Chem global CTM (v9.1.3), (3) formation of ambient $iPM_{2.5}$ in responses to the simulated ambient NH_3 concentrations by ISORROPIA II, and (4) mortality attributed to the simulated $iPM_{2.5}$ caused by NH_3 emissions from agricultural exports by the USEPA BenMAP version 4.0. The research concluded that 5100 premature deaths can be attributed to food export–related $PM_{2.5}$ and this was much larger than the 460 premature deaths

reduction that can be achieved by a reduction in $PM_{2.5}$ NAAQS from 15μg m^{-3} to 12 μg m^{-3}. The simulation of $PM_{2.5}$ concentration change attributed to agricultural export is illustrated in the following flow chart:

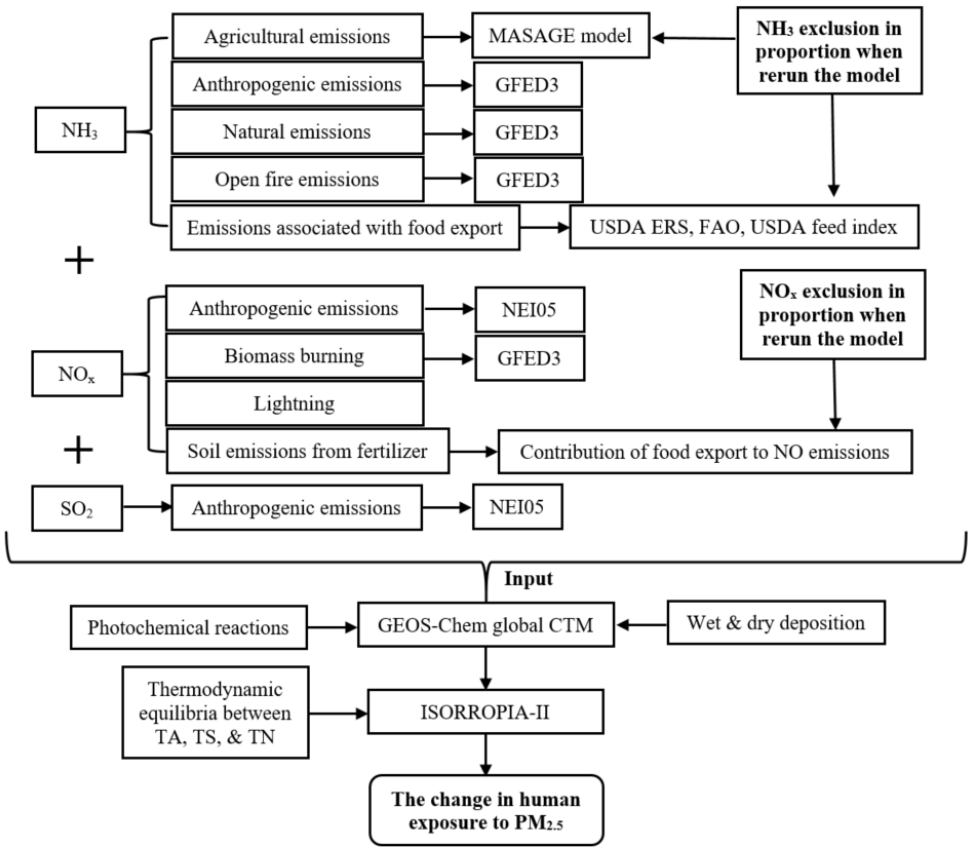

Figure 1.2. Flow chart summary for agricultural NH_3 impact simulation by Paulot and Jacob (2014)

While Paulot and Jacob (2014) provided one approach to estimate the contribution of AFO NH_3 emissions to the formation of secondary $iPM_{2.5}$, some limitations exist along every step of the model simulations in this research. Figure 1.3 summarizes these limitations that may challenge the major findings of the research.

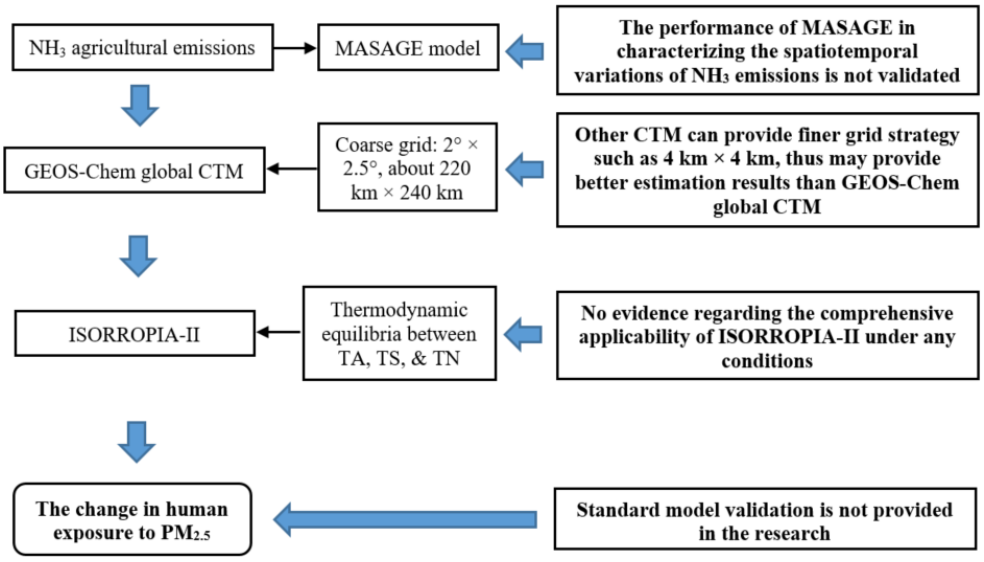

Figure 1.3. Limitation summary for agricultural NH_3 impact simulation by Paulot and Jacob (2014)

At first, the critical input data into GEOS–Chem model, agricultural NH_3 emissions were calculated by MASAGE model to account for the spatiotemporal variations of agricultural NH_3 emissions, however, the accuracy of MASAGE model was not validated. Paulot and Jacob (2014) also noted that there was discrepancy between the data generated by MASAGE model and data from U.S. EPA National Emission Inventory (NEI), therefore, the bias in NH_3 emissions data may lead to greater biases in $PM_{2.5}$ concentration change. Secondly, the coarse–grid strategy employed in the GEOS–Chem simulation (2° × 2.5°, about 220 km × 240 km) may not be appropriate to simulate the population exposure, finer–grid strategy (36 km × 36 km to 4 km × 4 km) may be required to simulate and assess the population exposure due to large spatial heterogeneity in pollutant concentrations. The closer to the pollutant emission sources, the higher pollutants may be observed. Thirdly, ISORROPIA II model was employed to study the thermodynamic equilibrium of secondary $iPM_{2.5}$ and its precursor gases, however, there was no evidence corroborating the comprehensive applicability of ISORROPIA II under different conditions such as high humidity, NH_3–rich conditions, therefore, there was a lack of reliability for the final simulation results. At last, there was a lack of model validation for the models from

NH_3 emission assessment all the way to the prediction of the secondary $iPM_{2.5}$ formation, therefore, there was no determination if the change in human exposure to $PM_{2.5}$ was accurate either qualitatively or quantitatively.

As NH_3 can be removed from the air through dry and wet depositions very efficiently and the formation of secondary $iPM_{2.5}$ can be limited by the availability of acidic gases under rural condition. Therefore, more efforts including field measurements and assessment of exiting thermodynamic equilibrium model should be taken to develop systematic understanding of the impact of AFO NH_3 emissions on the formation of $iPM_{2.5}$.

1.5. SEARCH Network

The Southeastern Aerosol Research and Characterization (SEARCH) Network is a long-term air quality monitoring network established in the Southeastern U.S. (AL, FL, GA, and MS) (EPRI, 2008). The SEARCH Network aimed to address questions regarding tropospheric ozone formation, PM ($PM_{2.5}$ and PM_{10}) mass and chemical compositions, mercury issues, and visibility degradation. The network provided high-quality field measurements of $PM_{2.5}$ mass and chemical compositions. The continuous measurements of $iPM_{2.5}$ chemical compositions and its precursor gases provide more information with high time-resolution to investigate the impact of different emissions sources on the atmospheric pollutants. The comprehensive measurements of gas-phase and particle-phase pollutants at eight sites cover agricultural rural areas and urban areas. The hourly measurements in this network serve as a good data source to investigate the spatial and temporal variations of atmospheric chemical conditions as well as thermodynamic equilibrium of $iPM_{2.5}$ and its precursor gases.

Under the SEARCH, the concentrations of $iPM_{2.5}$ chemical compositions and its precursor gases were measured at four paired urban/nonurban sites. The measurements of

SEARCH Network started from 1998/1999 and ended in 2016. The eight monitoring sites are illustrated in Figure 1.4.

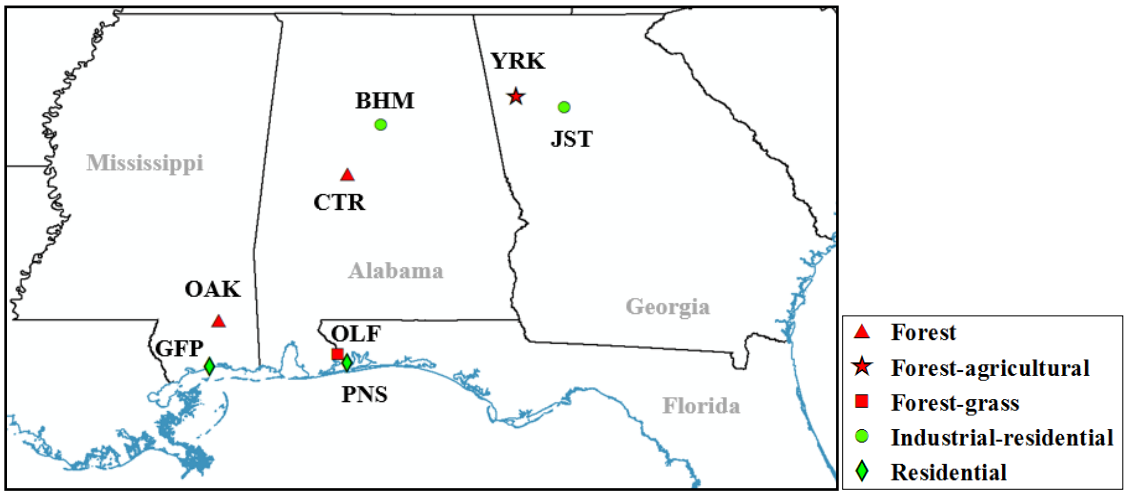

Figure 1.4. The geographical locations of the eight monitoring sites under the SEARCH (Hansen et al., 2003)

Under the SEARCH, meteorological parameters and the concentrations of precursor gases, $PM_{2.5}$ mass and compositions at each of the monitoring sites were measured. The onsite measurements were started in 1998/1999, providing processed 1–hr average concentrations of precursor gases, $iPM_{2.5}$ chemical compositions, and meteorological condition measurements. In addition, the 24-hr average measurements of $iPM_{2.5}$ chemical compositions were also performed. The details of the measurements made at the eight sites were introduced by Hansen et al. (2003), shown in Table 1.4.

Table 1.4. Continuous and discrete field measurements at the eight sites (Adapted from Hansen et al., 2003)

Observable	Technique	Max Resolution	Detection Limit (ppb or $\mu g/m^3$)
Gases			
NO	CL	1–min	0.05
NO_2	Photolysis/CL	1–min	0.1
HNO_3	Denuder/Mo reduction/CL	1–min	0.1
NO_y	Mo reduction/CL	1–min	0.1
SO_2	UV–fluorescence	1–min	0.2
NH_3	Denuder/Pt oxidation/CL	5–min	0.2
$iPM_{2.5}$ chemical compositions			
SO_4^{2-}	Fe reduction/UV–fluorescence	5–min	0.4
NO_3^-	Filter/Mo reduction/CL	5–min	0.2
NH_4^+	Filter/Pt oxidation/CL	5–min	0.1
Meteorological conditions			
T/RH/SR/BP	Various	1–min	N/A
WS/WD/Precipitation	Various	1–min	N/A
Discrete $iPM_{2.5}$ chemical compositions			
NO_3^-	Teflon filer + IC	24–hr	0.01
Volatile NO_3^-	Nylon filer + IC	24–hr	0.02
NH_4^+	Teflon filer + AC	24–hr	0.03
Volatile NH_4^+	Citric acid annular denuder + AC	24–hr	0.04
SO_4^{2-}	Teflon filter + IC	24–hr	0.05
K^+-Ca^{2+}-Mg^{2+}-Na^+	Teflon filter + ICP-MS	24–hr	N/A

CL: chemiluminescence; SR: solar radiation; BP: barometric pressure; WS: wind speed; WD: wind direction; IC: ion chromatography; AC: automated colorimetry; ICP-MS: inductively coupled plasma mass spectrometry; N/A: not applicable.

1.5.1. Spatial and temporal variations of iPM$_{2.5}$ and its precursor gases

Hansen et al. (2003) analyzed the $PM_{2.5}$ chemical compositions measured at the eight sites of SEARCH Network from 1999 to 2001, and reported that the concentrations of SO_4^{2-}, NO_3^-, NH_4^+, NH_3, black carbon and organic materials exhibited an increasing trend from the coastal sites (OLF, PNS, OAK, GFP) to the northward sites (YRK, JST, BHM, CTR). The spatial variation of $PM_{2.5}$ chemical compositions may be attributed to the clean marine air blowing from offshore, various $PM_{2.5}$ chemical compositions were gradually accumulated in the air mass during the mixing progress towards inland. Edgerton et al. (2005) examined the seasonal variations of 5 years (1999-2003) $PM_{2.5}$ mass and chemical composition concentrations at the eight sites, and discovered that higher $PM_{2.5}$ mass concentration occurred in summer, and the seasonality was primarily attributed to the seasonal variation of SO_4^{2-}. It was believed that more intense photochemical activities and more SO_2 emissions in summer due to peak electricity generation led to more SO_4^{2-} production. While analyzing the NH_4^+ concentrations at the eight sites, Edgerton et al. (2006) found that NH_4^+ concentration at the YRK (agricultural-forest) site was slightly higher than the paired urban site named JST (industrial-residential) in Atlanta, and significantly higher than all the other rural sites (see Figure 1.4, the monitoring site map). Higher NH_4^+ concentration at the YRK site was partially due to the NH_3 emissions from poultry farms to the southeast of the site. In addition, the Metropolitan Atlanta, GA was also located 50-55 km to the southeast of the YRK site, the air mass rich with NO_y gas blowing from the Atlanta (southeast wind direction) may explain the concurrent high NH_4^+ and NO_3^- concentrations at the YRK site.

In 2007, Edgerton et al. further investigated the 24-h average NH_3 and $iPM_{2.5}$ concentrations at the eight sites and found that the NH_3 concentrations were higher at urban sites than the paired rural sites except the YRK site, which was exposed to the NH_3 emissions from nearby poultry farms. The NH_3 gas fraction of NH_x ($NH_3 + NH_4^+$) was larger at the JST, YRK, and BHM sites, which indicated the significant influence by local NH_3 emission sources. The NH_3 gas fraction as a function of SO_4^{2-} at the CTR, OAK, PNS, and OLF sites indicated that the formation of $iPM_{2.5}$ was limited by the NH_3 availability at these sites.

In another research, Saylor et al. (2010) studied the NH_3 and NH_x change trend at the YRK agricultural-rural site and the JST industrial-residential site in 2007, and discovered that both NH_3 and NH_x were higher in hotter months and lower in colder months. The concentrations of NH_3 and NH_x correlated with wind direction, and the NH_3 and NH_x concentrations were higher in wind direction blown from broiler farm to the southeast of the YRK site, which indicated the significant impact of NH_3 emissions from poultry farms to the southeast of the YRK site. Saylor et al. (2015) analyzed the temporal variations of NH_3 and NH_4^+ from 2004 to 2012 at the eight sites, and reported that the NH_3 gas fraction in total NH_x exhibited a significant increasing trend. The partitioning of $NH_3 – NH_4^+$ towards gas phase may lead to the deposition pattern change of NH_3 so that more NH_3 may be dry deposited in the proximity of the emission sources instead of being transported in a long distance through $iPM_{2.5}$.

In a study by Blanchard et al. (2013a, 2013b) on the spatial and temporal variations of gas and particle phase pollutants measured from 1999 to 2010, it was discovered that pollutants concentrations at the eight sites were affected by source proximity, topography, and local meteorological conditions. The OAK site was the least affected by any nearby anthropogenic sources. The CTR site may be impacted by nearby urban air mass. The YRK site was influenced

by the Atlanta plumes and poultry NH_3 emissions. The JST site was affected by the pollutants emissions from local traffic and industrial sources. The BHM site may be affected by the nearby industrial sources. The PNS and GFP sites were located in the coastal areas, which may be influenced by local traffic emissions. The analysis of temporal variation may provide some insights to evaluate the effectiveness of emission controls. The concentrations of CO, SO_2, NO_y, SO_4^{2-} all exhibited reduction trend, which was consistent with the reduction in CO, SO_2 and NO_x emissions in the SEARCH region (Xing et al., 2013).

1.5.2. Thermodynamic equilibrium model assessment

The high temporal resolution measurements of $iPM_{2.5}$ and its precursor gases under the SEARCH Network provide a good data set to check the performance of the thermodynamic model such as ISORROPIA II. To assess the ability of ISORROPIA II to reproduce the gas-phase and particle-phase pollutants, the model predictions should be compared with field measurements.

Using 5-min average measurements, Zhang et al. (2003) evaluated the performance of ISORROPIA model in predicting the partitioning of $NH_3 – NH_4^+$. The total NH_3-total HNO_3-total H_2SO_4 together with temperature and RH were used as the model inputs, the comparison between model prediction and measurements in $NH_3 – NH_4^+ – HNO_3 – NO_3^-$ indicated that there was a discrepancy between prediction and measurements. Zhang et al. (2003) noted that the existence of both submicron and super–micron particles in $PM_{2.5}$ may challenge thermodynamic equilibrium assumption due to the possible non–equilibrium state of super–micron particles. Only the assumption of thermodynamic equilibrium between secondary $iPM_{2.5}$ and its precursor gases was corroborated to be reasonable, can the thermodynamic model be employed to predict the partitioning of $NH_3 – NH_4^+$ as well as be utilized to investigate the responses of secondary

$iPM_{2.5}$ to the changes of precursor gases. Therefore, more efforts are required to check and verify the applicability of thermodynamic model under different conditions.

The prediction of the partitioning of $NH_3 – NH_4^+$ may be complicated by the semi–volatile characteristic of NH_4NO_3. Yu et al. (2005) utilized three datasets covering various ambient conditions to test the performance of ISORROPIA in predicting the partitioning of $NH_3 – NH_4^+$. They are 5-min average data at Atlanta in the summer of 1999, 2-hr average data at the Pittsburgh in the winter of 2002, and 12-hr average data at the Clinton Horticultural crop research station in NC for the whole year of 1999. Large discrepancies were observed between model predictions and measurements. Four possible reasons were suggested in an attempt to understand the cause of the discrepancy, including (1) the uncertainties in SO_4^{2-} and NH_x measurements, (2) invalid assumption of the thermodynamic equilibrium assumption, (3) deficiencies of the metastable state and internally mixing assumptions, and (4) other pathways to produce NO_3^-. As the accuracy of the measurement data itself is critical to the model performance assessment, the uncertainties in SO_4^{2-} and NH_x may lead to large discrepancy; therefore, the high-quality data is required for ISORROPIA model assessment. Moreover, the $iPM_{2.5}$ measurements include both submicron and super micron particles, thermodynamic equilibrium may not apply for super micron particle in terms of the low time resolution measurement (2-hr to 12-hr). Furthermore, the applicability of stable and metastable model setups was not assessed individually, thus the third reason may be challenged and need further assessment. In addition, the effect of other pathways to produce NO_3^- on the ISORROPIA model performance was not investigated, thus the fourth reason is questionable. At last, this research didn't check the impact of other factors such as ambient T/RH and organic aerosol on the

performance of ISORROPIA. The ambient T/RH are critical to the partitioning of NH_3– NH_4^+, and the aforementioned organic film effect may cause longer equilibrium time for $iPM_{2.5}$ and its precursor gases, thus this research wasn't a comprehensive ISORROPIA model performance assessment.

1.5.3. Effects of changes in precursor gases on $iPM_{2.5}$

More than ten years' measurement dataset of SEARCH Network was used by various research to examine the effects of changes in precursor gases on $iPM_{2.5}$ mass concentration. Findings of such examinations are summarized in the following.

Blanchard and Hidy (2003) used the thermodynamic equilibrium mode-Simulating Composition of Atmospheric Particles at Equilibrium (SCAPE2) to study the responses of NO_3^- to the changes in the precursor gases. In this study, the model input included 24-hr average data of NH_3, NH_4^+, HNO_3, NO_3^-, and SO_4^{2-} along with T and RH measured at eight sites of SEARCH Network in 1998-1999. It also applied the different strategies of precursor gases reduction to examine the responses. These strategies include 20% reduction in total NH_3, 20% reduction in total HNO_3, 20–40% reduction in total H_2SO_4, and 20% reduction in total HNO_3 + 20–40% reduction in total H_2SO_4. The model simulation results suggested that the reduction in total HNO_3 and total NH_3 may be more effective to decrease NO_3^- concentration and the formation of NO_3^- was constrained by the availability of NH_3 at all eight sites of SEARCH Network. The model assessment in this research indicated that SCAPE2 model tends to over predict NO_3^- concentration, however, this model was still used to investigate the responses of NO_3^- to different precursor gases reduction strategies, thus the conclusions may be challenged.

Blanchard and Hidy (2005) also used SCAPE2 model to investigate the responses of $PM_{2.5}$ mass concentrations to the changes in precursor gases reductions, the reductions in the sum of SO_4^{2-}, NO_3^-, and NH_4^+ concentrations was treated as the predicted changes in $PM_{2.5}$ mass. The model input included 24-hr average data of NH_3, NH_4^+, HNO_3, NO_3^-, and SO_4^{2-} along with T and RH measured at eight sites of SEARCH Network in 1998-2001. Different precursor gases reduction strategies were used in this research including 46-63% reduction in total H_2SO_4, 40% reduction in total HNO_3, 55% reduction in total HNO_3, and 55% reduction in total HNO_3 and total NH_3. Several conclusions were made from the isopleth plot analysis: (1) the reduction in total H_2SO_4 led to 1.8-3.9 μg m^{-3} reduction in $PM_{2.5}$ mass; (2) Combining the reduction in total H_2SO_4 and 40% reduction in HNO_3 led to more reduction in $PM_{2.5}$ mass concentration; (3) 55% reduction in HNO_3 led additional 0-0.4 μg m^{-3} reduction in $PM_{2.5}$ mass. However, this research didn't assess the applicability of thermodynamic model-SCAPE2 under the conditions that the sensitivity test was performed.

Blanchard et al. (2007) used three datasets to study the effects of precursor gases reductions on $PM_{2.5}$ mass concentrations. The three datasets included 24-hr average measurements of NH_3, NH_4^+, HNO_3, NO_3^-, and SO_4^{2-} in 2004 of SEARCH Network, 24-hr average measurements of NH_3, NH_4^+, HNO_3, NO_3^-, and SO_4^{2-} in 2003-2004 in the Midwestern U.S., and multi-hour resolution measurements of NH_3, NH_4^+, HNO_3, NO_3^-, and SO_4^{2-} in 2000 winter, California. The thermodynamic model-SCAPE2 was employed to perform the sensitivity analysis; the results from isopleth plot analysis suggested four conclusions: (1) the responses of $iPM_{2.5}$ to the changes of precursor gases varied in different geographic regions; (2) The southeastern sites exhibited the lowest concentration of NO_3^- and least sensitivity of $iPM_{2.5}$ to

reduction in total HNO_3; (3) The Midwestern sites exhibited higher NO_3^- concentration and the reductions in total HNO_3 and H_2SO_4 led to reduction in $PM_{2.5}$ mass; (4) In California, both NO_3^- and $PM_{2.5}$ concentrations exhibited reduction trend in response to the reduction in total HNO_3. This research assessed the model performance of SCAPE2 in reproducing the concentrations of NH_3, NH_4^+, HNO_3, and NO_3^-, however, the statistical analysis didn't show the conditions under which the SCAPE2 performed better, therefore, more comprehensive assessment is required to assess the thermodynamic model in reproducing the gas phase and particle phase pollutants.

1.5.4. Source apportionment studies

Using different methods such as positive matrix factorization (PMF) and chemical mass balance (CMB), source apportionment studies were performed to investigate the quantitative contributions of various emission sources to the $PM_{2.5}$ chemical compositions.

Kim et al. (2003) used PMF model to apportion the contributions of different emission sources to the various compositions of $PM_{2.5}$ at the JST site, one of the eight sites of SEARCH Network. Based upon the 24-hr average data of $PM_{2.5}$ mass and chemical compositions measured in 1998-2000, this research identified eight sources for $PM_{2.5}$ and their quantitative contributions to $PM_{2.5}$ concentrations varied. The results indicated that 56%, 22%, 11%, and 7% of $PM_{2.5}$ concentration was attributed to SO_4^{2-} rich secondary aerosol, motor vehicle, wood smoke, NO_3^- rich secondary aerosol, respectively. The other $PM_{2.5}$ concentration can be attributed to mixed source of cement kiln and organic carbon, airborne soil, metal recycling facility, bus station and metal processing.

Blanchard et al. (2012) used the CMB method and U.S. EPA's NEI to estimate the contributions of various emission sources to the gas phase and particle phase pollutants at the SEARCH sites. It was discovered that at the JST urban site, vehicle gas emissions contributed to

the largest portion of NH_x ($NH_3 + NH_4^+$), whereas agricultural NH_3 emissions contributed to the most of the NH_x concentration at the YRK agricultural site. In summary, area sources, point sources, and mobile sources contributed 2.0-3.7 μg m^{-3}, 3.0-4.6 μg m^{-3}, 1.0-6.0 μg m^{-3}, respectively to the mean $PM_{2.5}$ mass concentrations at the eight sites. The CMB method requires the information of emission sources and $PM_{2.5}$ chemical compositions, thus NEI and $PM_{2.5}$ chemical composition measurements may both add uncertainties to the source apportionment analysis. In addition, the source apportionment method such as CMB itself may be subject to the influence of emission sources close to the monitoring site, thus over or under estimation of emission source contribution may occur. As suggested by Blanchard et al. (2012), the agricultural NH_3 contribution at the BHM site may be inappropriately estimated because of the industrial emission sources within 10 km of the site. Therefore, more source apportionment studies are required to investigate the contribution of agricultural NH_3 emissions especially AFOs NH_3 emissions to the formation of $iPM_{2.5}$.

The $PM_{2.5}$ mass and chemical composition measurements at the SEARCH Network in the past 20 years have fostered hundreds of studies regarding spatial and temporal trend of $PM_{2.5}$ (Blanchard et al., 2013a, 2013b; Hidy et al., 2014), validation of CTM simulation (Yu et al., 2005), and source apportionment (Blanchard et al., 2012). However, very few studies were performed to investigate the contributions of AFOs NH_3 emissions to the differences in atmospheric chemical conditions, $iPM_{2.5}$ formation, and partitioning of NH_3–NH_4^+ under urban and rural environments (Saylor et al., 2010). Therefore, this research was performed to assess the impact of AFOs NH_3 emissions on atmospheric chemical condition and to evaluate the applicability of the thermodynamic equilibrium model such as ISORROPIA II under different conditions.

1.6. Hypotheses and Objectives

Based upon the literature review, the following research questions and hypotheses were formed to address the knowledge gaps.

1.6.1. Key research questions

1. How would the NH_3 emissions from AFOs affect the difference of the atmospheric chemical condition, $iPM_{2.5}$ formation, and partitioning of $NH_3 – NH_4^+$ in the urban and rural areas?

2. Which factors would affect the performance of thermodynamic equilibrium model-ISORROPIA II for predicting inorganic aerosols?

1.6.2. Research hypotheses

1. Atmospheric chemical conditions and $iPM_{2.5}$ formation are affected by AFOs NH_3 emissions, leading to the difference between urban and rural areas.

2. The performance of ISORROPIA II for predicting inorganic aerosols is affected by ambient conditions and model input.

3. Partitioning of $NH_3 – NH_4^+$ is different under urban and rural conditions due to NH_3 emissions from AFOs.

1.6.3. Research objectives

1. Investigate the spatial and temporal variations of atmospheric chemical conditions, $PM_{2.5}$ mass closure, and $iPM_{2.5}$ in the Southeastern U.S.

2. Investigate the applicability of ISORROPIA II for predicting inorganic aerosols under different T & RH, model setups, locations & with/without nonvolatile cations in model input.

3. Advance our understanding about dynamics of the partitioning of $NH_3 – NH_4^+$ using ISORROPIA II under urban and rural conditions.

CHAPTER 2: SPATIAL AND TEMPORAL VARIATIONS OF ATMOSPHERIC CHEMICAL CONDITIONS IN THE SOUTHEASTERN U.S.

Abstract

Animal feeding operations (AFOs) are the largest ammonia (NH_3) emission sources in the United States (U.S.). However, the impact of NH_3 emissions from AFOs on the atmospheric chemical conditions has not been systematically assessed. Under the Southeastern Aerosol Research and Characterization (SEARCH) Network, the hourly concentrations of $iPM_{2.5}$ chemical compositions and its precursor gases as well as meteorological data were measured at eight urban/nonurban sites labeled as JST/YRK, BHM/CTR, GFP/OAK, and PNS/OLF during 1998–2016. Using the SEARCH data, this research investigated the spatiotemporal variations of atmospheric chemical conditions in those rural and urban areas. The spatiotemporal variations of atmospheric chemical conditions at the eight sites are characterized by four parameters, including (1) gas ratio (GR), (2) gas-phase NH_3 molar fraction (NH_3/NH_x), (3) total available NH_3 (gaseous ammonia + aerosol ammonium) to sulfate (SO_4^{2-}) molar ratio (TA/TS), and (4) $PM_{2.5}$ ammonium + nitrate to total $PM_{2.5}$ mass ratio ($AN/PM_{2.5}$). Results indicate that the NH_3 emissions from AFOs may explain the greater values of GR, NH_3/NH_x, and TA/TS in the wind directions coming from AFOs at two rural sites, i.e., YRK & OAK, than the other wind directions. In the wind directions coming from AFOs at YRK and OAK, NH_3 was in excess of fully neutralizing acidic gases, more NH_3 stayed in gas phase than those in other wind directions, and both ammonium sulfate and ammonium nitrate existed in $iPM_{2.5}$. The upward trend in NH_3/NH_x and TA/TS indicates that gas–particle partitioning of $NH_3 - NH_4^+$ changed towards gas phase, while the downward trend in $AN/PM_{2.5}$ may implicate that smaller fraction of $PM_{2.5}$ was directly NH_3 sensitive. Understanding of the spatiotemporal variations of atmospheric chemical

conditions provides insights to improve our understanding of the impact of AFOs NH_3 emissions on the potential for $iPM_{2.5}$ formation under rural and urban conditions.

2.1. Introduction

Particulate matter with aerodynamic equivalent diameter less than or equal to 2.5 μm (i.e., $PM_{2.5}$) has gained intensive attention due to its adverse health and visibility degradation effects (Cambra–Lopez et al., 2010; Hinds, 1998; Ma et al., 2011; Pope et al., 2009; Pui et al., 2014). $PM_{2.5}$ may be formed through different processes. Primary $PM_{2.5}$ is directly emitted from sources, while secondary $PM_{2.5}$ is formed through chemical reactions of various precursor gases in homogeneous and/or heterogeneous processes (Hinds, 1998). In ambient air, ammonia (NH_3) as the major alkaline gas, may react with acidic gases, i.e., nitric acid (HNO_3) and sulfuric acid (H_2SO_4), to form secondary inorganic $PM_{2.5}$ ($iPM_{2.5}$) in a process called thermodynamic equilibrium gas-particle partitioning of $NH_3 - NH_4^+$ (Seinfeld and Pandis, 2006; Zhang et al., 2008). Secondary $iPM_{2.5}$ constitutes a significant fraction of atmospheric $PM_{2.5}$ (Tolocka et al., 2001; Walker et al., 2004). In the troposphere, NH_3 gas preferentially reacts with H_2SO_4 to form ammonium sulfate ($(NH_4)_2SO_4$) and ammonium bisulfate (NH_4HSO_4) (Seinfeld and Pandis, 2006). If excessive NH_3 is available, ammonium nitrate (NH_4NO_3) salt is expected to exist in $iPM_{2.5}$; however, the fractional contribution of NH_4NO_3 to $iPM_{2.5}$ depends on environmental conditions (Nenes et al., 1998; Huntzicker et al., 1980). Due to its lack of thermal stability, NH_4NO_3 may decompose to the gaseous forms of HNO_3 and NH_3 under high temperature (T) and low relative humidity (RH), the environmental conditions that do not favor the particle phase. On the other hand, SO_4^{2-} salts are thermally stable compared with NO_3^- salts, thus, almost all the NH_3 that reacted with SO_4^{2-} stays in the particle phase (Olszyna et al., 2005).

In the atmosphere, the gas-phase NH_3 is directly emitted from emission sources, while

HNO_3 and H_2SO_4 are largely formed from gaseous pollutants such as nitrogen oxides (NO_x) ($NO_x = NO + NO_2$) and sulfur dioxide (SO_2) through (photo)chemical reactions. Ammonia emissions from agricultural sources such as animal feeding operations (AFOs) are the largest sources of atmospheric NH_3 in the United States (U.S.) (USEPA, 2004). Thus, the AFOs NH_3 emissions may have important impact on the atmospheric chemistry of secondary $iPM_{2.5}$. Once emitted, NH_3 will experience complex transport and transformation processes prior to its removal (see Figure 1.1).

Tropospheric lifetime of NH_3 is from 0.5 h to 5 d (Seinfeld and Pandis, 2006) with dry deposition being the major removal process. Due to short lifetime, the spatial variation of atmospheric concentration of NH_3 can be caused by both the variabilities in the emission sources associated with agricultural activities and presence of AFOs as well as dry deposition rates associated with the land use practices (Duyzer, 1994; Sutton et al., 1994). Due to relatively short lifetime of NH_3 and spatial separation of emission sources of NH_3 and acidic precursor gases (transportation and industrial activities), NH_3 emissions from AFOs may have variable potential for the formation of $iPM_{2.5}$ in rural and urban environments.

In the literature, four chemical parameters have been proposed to evaluate the potential effects of NH_3 emissions on $iPM_{2.5}$ formation (Makar et al., 2009; Ansari and Pandis, 1998).

First is the gas ratio (GR) that depicts the relative abundance of the precursor gases of $iPM_{2.5}$ and can be used to characterize the neutralization degree of NH_3 (Ansari and Pandis, 1998):

$$GR = \frac{[TA] - 2[TS]}{[TN]} \qquad (2\text{-}1)$$

where TA (in units of μmole m^{-3}) equals to the sum of gas-phase NH_3 and aerosol-phase

ammonium (NH_4^+), TS (in units of μmole m^{-3}) stands for the total sulfate including SO_4^{2-}, bisulfate (HSO_4^-) and H_2SO_4, and TN (in units of μmole m^{-3}) stands for total amount of NO_3^- and HNO_3. The GR represents the potential for neutralization. If one assumes uniform mixing conditions, GR = 1 would be indicative of full neutralization; GR > 1 would indicate the NH_3-rich condition when all acidic species are fully neutralized and there is excessive NH_3, while GR < 1 would reveal the NH_3-poor condition when acidic species are not fully neutralized. More specifically, atmospheric conditions when 0 < GR < 1 would indicate that the amount of total available NH_3 (gaseous NH_3 + aerosol NH_4^+) is enough to react with all H_2SO_4, but not total available HNO_3 (gaseous HNO_3 + aerosol NO_3^-). While conditions with GR < 0 would reveal that the amount of total available NH_3 is not enough to react with either total available H_2SO_4 or total available HNO_3.

Second, gas-phase NH_3 to NH_x (=NH_3+ NH_4^+) molar fraction can be used to assess the changes of $NH_3 - NH_4^+$ partitioning:

$$NH_3/NH_x = \frac{[NH_3]}{[NH_3]+[NH_4^+]} \qquad (2\text{-}2)$$

Third, the total available NH_3 to SO_4^{2-} molar ratio (TA/TS) can be used to assess the atmospheric acidic conditions and the possible chemical composition of $iPM_{2.5}$. When TA/TS < 1, the NH_4^+ salts in inorganic aerosols may consist of both NH_4HSO_4 and H_2SO_4. When 1 < TA/TS < 2, the NH_4^+ salts in inorganic aerosols may consist of NH_4HSO_4, letovicite ($(NH_4)_3H(SO_4)_2$), and $(NH_4)_2SO_4$. When TA/TS > 2, the NH_4^+ salts in inorganic aerosols may consist of both $(NH_4)_2SO_4$ and NH_4NO_3 (Makar et al., 2009).

$$TA/TS = \frac{[NH_3]+[NH_4^+]}{[SO_4^{2-}]} \qquad (2\text{-}3)$$

Fourth, the mass ratio of $NH_4^+ + NO_3^-$ to total $PM_{2.5}$ ($AN/PM_{2.5}$) characterizes the fraction of $PM_{2.5}$ mass that is directly sensitive to the changes in NH_3 emissions. The change of NH_3 emissions is apt to directly affect the concentrations of NH_4^+ and NO_3^- at first, and then SO_4^{2-} concentration may be affected depending the magnitude in the change of NH_3 emissions.

$$AN/PM_{2.5} = \frac{NH_4^+ + NO_3^-}{PM_{2.5}} \qquad (2\text{-}4)$$

The objective of this study was to investigate the spatial and temporal variations of GR, NH_3/NH_x, TA/TS, and $AN/PM_{2.5}$ in urban and rural areas of Southeastern U.S.

2.2. Methodology

2.2.1. Data collection sites description

The data collected at eight Southeastern Aerosol Research and Characterization Network (SEARCH) sites from 2004 to 2016 were used in this study. The SEARCH network was established in the early 90s to (1) help states monitor $PM_{2.5}$ for regulatory purposes, (2) to collect long-term data for air quality model evaluation, and (3) to identify the long-term spatial and temporal trends of $PM_{2.5}$, mercury (Hg) and ozone (O_3) (USGS, 2016).

As shown in Figure 1.4, the SEARCH Network monitored air quality data at eight sites representing urban and rural environments. The details regarding the site description can be found in Hansen et al. (2003) and Blanchard et al. (2013). Briefly, the JST site is an urban site in the midtown of Atlanta. The site is affected by the emissions from local traffic and industrial sources. The YRK site represents a rural site located in a forest and agricultural area of Georgia and is influenced by the emissions from a cattle pasture as well as animal production house

emissions nearby. The BHM site is in the city of Birmingham and is impacted by the emissions from traffic and industrial sources. The CTR site is in a forest area approximately 85 km to the southwest of Birmingham and 50 km to the south of Tuscaloosa, and is impacted by air masses coming from these two urban areas. The GFP site is an urban site located in coastal area, 1.5 km from the Gulf of Mexico. The atmospheric chemical condition at the GFP site is influenced by residential emission sources, local roads and highways. The OAK site is a rural site located in a forest area, away from industrial emission sources. The PNS site is an urban site located in the coastal area, 5 km from the Gulf of Mexico, and is impacted by emission sources coming from industrial activities and major highways. The OLF site is a suburban site, impacted by the nearby residential emissions and local roads. Measurements at all onsite monitoring stations started in 1998/1999. Measurement details at the eight sites are summarized in Table 1.4.

Concentrations of gas-phase pollutants (e.g., NH_3, HNO_3, SO_2) and $iPM_{2.5}$ chemical compositions (e.g., NO_3^-, NH_4^+ and SO_4^{2-}) were simultaneously measured using continuous/semi-continuous methods (averaged over 1 hr) and filter–based method (averaged over 24 hrs). Measurement method, duration, frequency, quality control (QC), and quality assurance (QA) were reported by Edgerton et al. (2005, 2006, 2007).

2.2.2. Data analysis

The following steps were taken to pre-process the 1 hr average and 24-hr average filter-based data for analysis of temporal variations of GR, NH_3/NH_x, TA/TS, and $AN/PM_{2.5}$:

- Some measurement values were reported to be either negative or below the detection limit (DL) of the instruments. The negative values less than (–DL) were considered questionable and excluded from the dataset, while the other values below the DL were replaced with half of the DL (USEPA 2000; Cohen and Ryan 1989);

- Following the method by Blandchard et al. (2012), the days at each site with more than 3-hr precipitation were labeled as wet days and were excluded from the data analysis.
- Following the method by Saylor et al. (2010), the values of each parameter within 10° wind direction bin were grouped together. Average values and 95% confidence intervals of the hourly data in each 10° wind direction were calculated for each wind sector.

The hourly data of NH_3 gas concentration are only available at six out of eight sites and only during specific years: YRK (2008-2016), JST (2010-2016), CTR (2012-2016), BHM (2011-2016), OLF (2013-2016), and OAK (2010). Therefore, the parameters requiring hourly NH_3 gas concentration measurements (i.e., GR, NH_3/NH_x, and TA/TS) were only analyzed at the YRK, JST, CTR, BHM, and OLF sites in 2013 and at the OAK site in 2010. The temporal variation of NH_3/NH_x, TA/TS, $AN/PM_{2.5}$ at eight sites was based on 24-hr average filter-based data in 2004-2016. Diurnal and seasonal variations of $AN/PM_{2.5}$ at six sites were based on 1-hr average data. As for YRK, JST, CTR, BHM, and OLF sites, the completeness of hourly $AN/PM_{2.5}$ data is better in 2013, therefore, the data in 2013 at these sites were chosen for diurnal and seasonal analysis. While as for OAK sites, the hourly $AN/PM_{2.5}$ data were only available in 2010, thus, the diurnal and seasonal analysis of $AN/PM_{2.5}$ was only performed in 2010 at the OAK site. Tukey honest significant difference (HSD) test was utilized to check the year-to-year temporal variation of NH_3/NH_x, TA/TS, $AN/PM_{2.5}$.

To obtain thorough information of AFOs farms distribution, visually check of the zoom-in Google map approach was used to identify the dry-based poultry farms and wet-based swine farms locations. Spatial distributions of the poultry and swine farms within 100 km (radius) of the eight sites were utilized to assist in wind sector analysis.

2.3. Results and Discussion

2.3.1. Spatial variation of the GRs

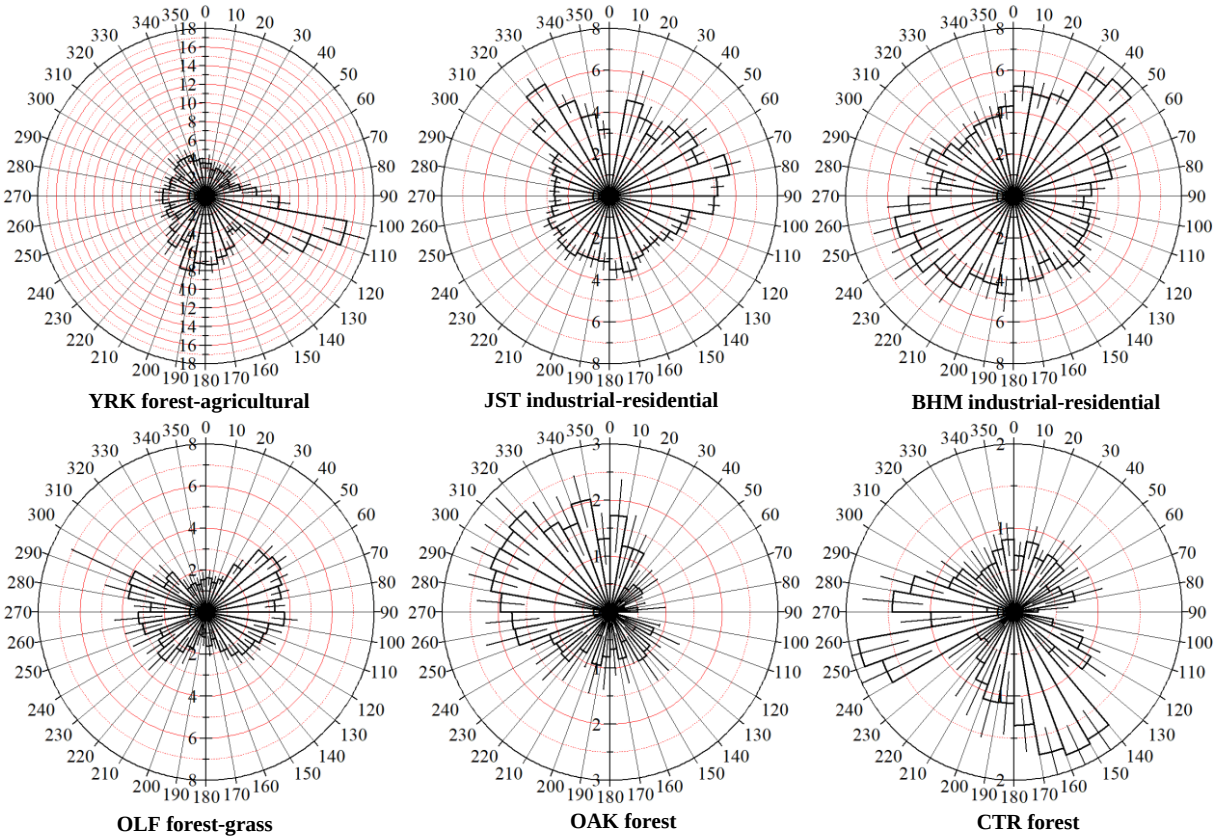

Figure 2.1. The gas ratios at the YRK, JST, CTR, BHM, and OLF sites in 2013 and OAK site in 2010. Note different scales in the figures.

Figure 2.1 shows the wind sector analysis of GR values at the six sites with available hourly data. According to Figure 2.1, as for both YRK and JST sites, GR values were greater than one, suggesting NH_3-rich conditions at these two sites for all wind directions. For the BHM and CTR sites, the BHM site exhibited NH_3-rich conditions with the GRs greater than one for all wind directions. As for the CTR site, GR values varied in different wind directions with GR values greater than one for the southeast and north wind directions. The OLF site was in NH_3-rich area with GRs greater than one, while the GRs at the OAK site exhibited variations in different wind directions with GR values greater than one for the westerly-northwesterly wind

directions.

Out of all the sites examined, Figure 2.1 shows the largest GR values for the YRK site in the wind sector of 100°-130°. The YRK site also exhibited large variations in GRs for different wind directions, suggesting the possibility of significant NH_3 emission sources at the proximity of the site. The Google map (see Figure 2.2) shows three poultry farms located at 1.5 km, 1.5km, and 3.1 km southeast (100°-130°) of the YRK site. This result is consistent with the findings of Saylor et al. (2010) who analyzed the NH_3 gas and NH_x concentrations for different wind directions at the YRK site in 2007 and reported significantly higher NH_3 gas and NH_x concentrations in the wind direction of 100°-140°.

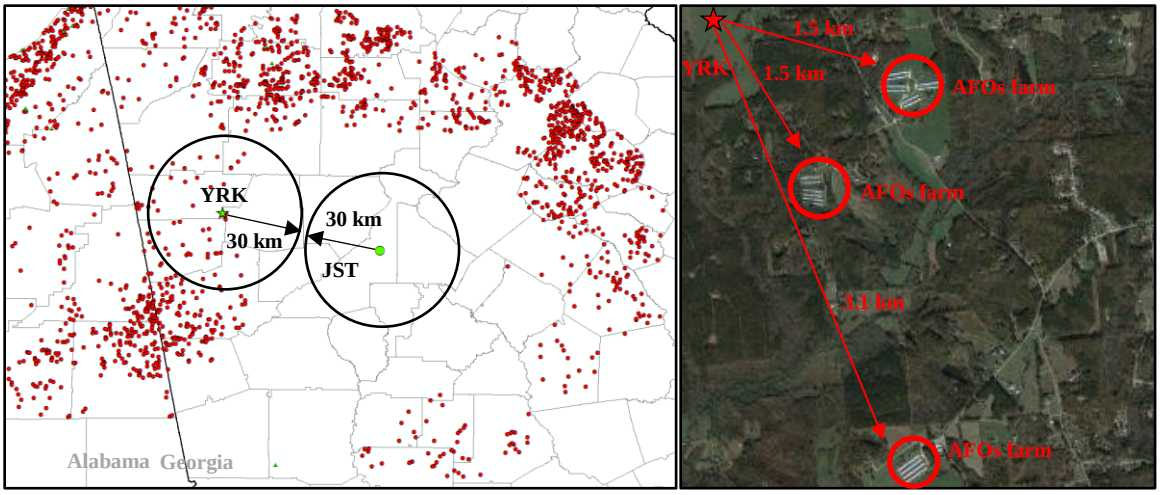

Figure 2.2. AFOs farm distribution within 100 km of the YRK and JST sites (left) and in the proximity of the YRK site (right)

The wind direction-based analysis of GRs reveals that AFOs farms, located in the distance of 1.5-3.1 km upwind, can significantly affect the GR values at the YRK site. In addition, Figure 2.1 shows some dependence of GRs on the wind direction at JST site. Blanchard et al. (2012) used chemical mass balance (CMB) method and U.S. EPA's National Emission Inventory (NEI) to estimate the contributions of various emission sources to the gas-phase and particle-phase pollutants in the Southeastern U.S. Their results indicated that at the JST site,

vehicle emissions accounted for the largest portion of NH_x concentration. Google map showed that NH_x emissions from a trucking facility (located within 100 m to the north of the JST site) and a parking lot (located within 150 m to the east of the JST site) may be responsible for higher GR values in 10°-20° and 70°-100° sectors, respectively. Moreover, a rail yard, a wastewater treatment facility, and a power plant located within 3.6 km to 7.5 km to the northwest of the JST site could be responsible for NH_3 emissions, causing higher values of GRs in 310°-340° wind directions.

Figure 2.1 shows that the GRs exhibited higher values in the wind direction of 30°-50° at the BHM site. Three large industrial emissions sources were located to the northeast of the BHM site (USEPA, 2011); the google map in 2016 also confirmed the existence of these three large industrial emissions sources.

To the northeast of the BHM site, one steel mills as well as ferroalloy manufacturing plant are 4.6 km away from the BHM site, the coke battery plants in these facilities are important emission sources of NH_3, SO_2, and NO_x. In addition, one construction material company is 3.4 km away from the BHM site; crushed limestone mining and quarrying emitted both SO_2 and NO_x. The closest industrial source to the northeast of the BHM site is an iron foundry company, the coke battery in the company emitted NH_3, SO_2, and NO_x. At the CTR site, the NH_3-poor conditions dominated in 2013; while in the wind direction of 140°-170°, the GRs were greater than two. The NH_x concentration *vs.* wind direction at the CTR site didn't exhibit the higher NH_x concentration to the southeast of the CTR site, therefore, the higher GRs in the wind direction of 140°-170° may be due to the lack of acidic gases, the lower acidic gases (HNO_3 and H_2SO_4) concentrations in the wind direction of 140°-170° still made higher GRs.

The GRs exhibits higher values to the west and northeast of the OLF site. The NH_x

concentration *vs.* wind direction analysis indicates that the higher NH_x concentration appeared to the west and northeast of the OLF site as well. The geographic location of the OLF site may explain the variations of NH_x concentration and GRs in different wind directions. The forest and grassland were located to the north and south of the OLF site, therefore, lack of NH_3 emission sources in these two wind directions led to lower NH_x concentration and GRs.

As for the OAK site, high GRs appear in the wind direction of 250°-350°, this may be explained by the AFOs NH_3 emissions surrounding the OAK site. The AFOs farms distribution within 100 km of the paired sites-OAK and PNS sites is in Figure 2.3.

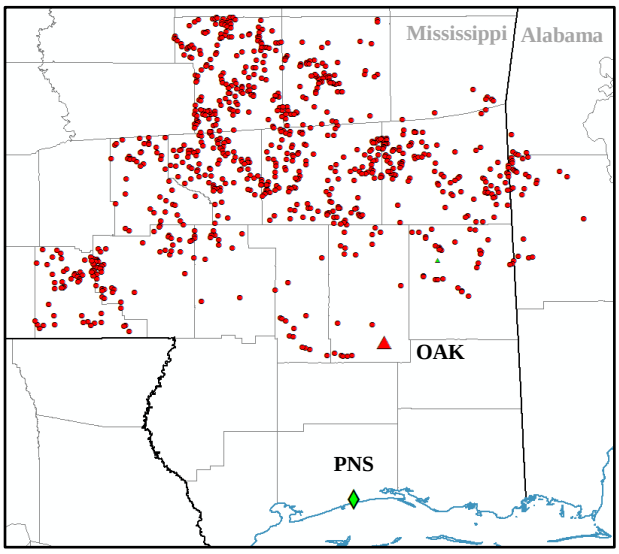

Figure 2.3. AFOs farm distribution within 100 km of the OAK and PNS sites

The OAK site is about 67 km to the Gulf of Mexico in the coastal area. Moreover, the OAK site is in the forest area with a large number of AFOs farms located to the north and west of the site. The source apportionment analysis by Blanchard et al. (2012) showed that agricultural NH_3 contributed more than half of the NH_x concentration at the OAK site. The forest may inhibit the transport of NH_3, SO_2, and NO_x to the OAK site from the southern and eastern wind directions. While the significant NH_3 emissions from AFOs farms to the north and west of the OAK site may pose great impact on the GR, thus making the GRs higher in north and west wind

directions at the OAK site.

2.3.2. Spatial and temporal variations of NH_3/NH_x

The change of $NH_3 - NH_4^+$ partitioning can be characterized by gas-phase NH_3 molar fraction (i.e. NH_3/NH_x). Out of all the sites examined in this study, NH_3/NH_x exhibited a significant upward trend over the past 13 years, with the exception of BHM and PNS sites (see Table 2.1). This upward trend is consistent with the analysis of Saylor et al. (2015). The observed increase in NH_3/NH_x indicates that the partitioning of $NH_3 - NH_4^+$ changed toward gas phase, thus, the formation of $iPM_{2.5}$ tended to be limited by the availability of acidic gases instead of NH_3. Xing et al. (2013) noted the decreasing trend in NO_x and SO_2 emissions due to the implementation of various regulations in the past decade.

Table 2.1. Yearly averaged values of NH_3/NH_x at the eight sites[a]

Year	YRK	JST	BHM	CTR	GFP	OAK	PNS	OLF
2004	0.45±0.21	0.40±0.19	0.54±0.20	0.17±0.13	0.36±0.21	0.18±0.13	0.41±0.21	0.27±0.16
2005	0.49±0.19	0.42±0.18	0.57±0.19	0.19±0.15	0.38±0.20	0.22±0.15	0.39±0.18	0.28±0.17
2006	0.53±0.18	0.39±0.17	0.55±0.17	0.18±0.12	0.42±0.20	0.23±0.16	0.39±0.18	0.27±0.15
2007	0.61±0.17	0.48±0.17	0.58±0.17	0.29±0.21	0.44±0.18	0.25±0.18	0.44±0.19	0.31±0.16
2008	0.53±0.20	0.44±0.15	0.61±0.15	0.18±0.12	0.40±0.18	0.19±0.15	0.38±0.19	0.26±0.16
2009	0.61±0.18	0.53±0.16	0.60±0.16	0.24±0.15	0.45±0.17	0.25±0.14	0.42±0.17	0.31±0.15
2010	0.59±0.19	0.51±0.15	0.60±0.13	0.23±0.14	0.45±0.18	0.26±0.16	N/A	0.30±0.20
2011	0.58±0.17	0.56±0.16	0.57±0.17	0.26±0.16	0.43±0.17	N/A	N/A	0.31±0.15
2012	0.69±0.14	0.62±0.14	0.62±0.15	0.28±0.13	0.48±0.17	N/A	N/A	0.35±0.15
2013	0.59±0.18	0.62±0.16	0.57±0.17	0.28±0.15	N/A	N/A	N/A	0.36±0.14
2014	0.58±0.14	0.63±0.14	0.56±0.15	0.32±0.13	N/A	N/A	N/A	0.37±0.14
2015	0.62±0.17	0.66±0.16	0.48±0.17	0.35±0.17	N/A	N/A	N/A	0.44±0.13
2016	N/A	0.66±0.14	N/A	0.34±0.15	N/A	N/A	N/A	N/A

[a] N/A: Not available

Figure S1 in Appendix A shows the NH_3/NH_x ratios under different wind directions at the six sites. The NH_3/NH_x ratios close to zero would correspond to the conditions when all NH_3 is neutralized by acidic trace gases, while values greater than 0 would describe chemical conditions with excess unneutralized NH_3 in the gas phase, e.g., the ratio NH_3/NH_x=0.5, would indicate equal amounts of NH_3 in the gas phase and NH_4^+ in the particle phase. According to Figure S1 an excessive amount of NH_3 in the gas phase was measured at all the sites, suggesting that the formation of $iPM_{2.5}$ was limited by the availability of acidic gases. The NH_3/NH_x ratio was higher (more than 60% of NH_x was in the gas phase) at YRK, JST, and BHM sites compared to OAK, OLF, and CTR sites (where ~ 40% of the NH_x resided in the gas phase). The variation of the NH_3/NH_x in different wind directions can be explained by the spatial heterogeneity of NH_3, SO_2, and NO_x emission sources as well as the fate and transport of these three gases. At the YRK site, the NH_3/NH_x was higher in the wind sector of 100°-120°, which can be attributed to NH_3 emissions from the AFOs located southeast of the YRK site (see Figure 2.2). At the OAK site, the NH_3/NH_x ratios are generally higher for the air masses coming from the westerly-northwesterly directions, which may also be explained by the locations of AFO farms. Finally, OLF, CTR, JST and BHM sites do not exhibit considerable wind-direction dependence as the NH_3/NH_x ratios are likely be controlled by spatial distribution of NH_3, SO_2, and NO_x emissions sources as well as the fate and transport of these three gases.

2.3.3. Spatial and temporal variations of TA/TS

The yearly averaged values of TA/TS for 2004-2016 are summarized in Table 2.2. According to this table, the TA/TS exhibits a significant positive trend at the eight sites. The positive trend in TA/TS is likely associated with the reduction in SO_2 emission in the Southeastern U.S. Less SO_2 available to be transformed into H_2SO_4 through (photo)chemical

reactions, leading to lower concentration of SO_4^{2-} in the particle phase. Overall, Table 2.2 shows that the annual average values of TA/TS at the eight sites (except OAK site in 2004) were always greater than 2 in the past 13 years, indicating that ammonium salts in inorganic aerosols may consist of both $(NH_4)_2SO_4$ and NH_4NO_3.

Table 2.2. Yearly averaged values of the TA/TS at the eight sites[a]

Year	YRK	JST	BHM	CTR	GFP	OAK	PNS	OLF
2004	4.32±3.00	3.53±1.60	4.53±2.44	2.09±0.62	2.72±1.25	1.92±0.71	3.09±1.51	2.26±0.74
2005	4.70±3.00	3.77±1.75	4.78±2.74	2.17±0.99	3.01±2.05	2.12±1.12	2.97±1.15	2.52±1.42
2006	5.20±4.50	3.49±1.44	4.52±1.97	2.05±0.60	3.05±1.50	2.18±1.24	2.91±1.11	2.28±0.68
2007	7.85±9.39	4.34±1.92	5.27±3.22	3.00±2.87	3.21±1.93	2.29±1.28	3.48±2.00	2.66±0.88
2008	6.08±4.26	3.95±1.76	5.62±3.74	2.44±1.24	3.11±1.40	2.29±0.93	3.00±1.20	2.51±1.17
2009	6.94±4.45	4.86±2.00	5.91±6.67	2.66±1.04	3.75±2.18	2.41±0.98	3.54±1.56	2.64±0.94
2010	6.30±3.62	4.62±1.61	5.31±1.85	2.47±0.74	3.74±2.14	2.60±0.94	N/A	2.98±1.46
2011	6.16±4.08	5.30±2.58	5.51±2.78	2.66±0.97	3.55±1.49	N/A	N/A	2.96±0.92
2012	7.94±4.37	5.95±2.71	5.81±2.54	2.55±0.86	3.78±2.34	N/A	N/A	3.11±1.62
2013	6.20±3.58	6.52±3.64	5.50±2.71	2.61±0.72	N/A	N/A	N/A	2.98±0.76
2014	9.30±7.52	8.00±4.42	7.76±5.28	5.06±6.96	N/A	N/A	N/A	4.09±2.39
2015	18.59±15.73	12.13±10.11	13.32±10.81	11.51±13.90	N/A	N/A	N/A	9.26±7.82
2016	N/A	14.91±8.72	N/A	9.89±9.94	N/A	N/A	N/A	N/A

[a] N/A: Not available

The TA/TS under different wind directions at the six sites are shown in Figure S2 in Appendix A. For the spatial variation, TA/TS exhibited lower values at the OLF, OAK, and CTR sites, higher values at the YRK, JST and BHM sites. The OAK and CTR sites are away from NH_3, NO_x, and SO_2 emission sources, the relatively clean air made the TA/TS lower. The agricultural NH_3 emission sources at the YRK site, NH_3 emissions from vehicles at the JST and BHM sites made the TA/TS higher. Especially in the wind direction of 100°-130° at the YRK site, the values of TA/TS were significantly higher than the other wind directions, which indicates the impact of poultry farm NH_3 emissions to the southeast of the YRK site.

2.3.4. Spatial and temproal variations of AN/$PM_{2.5}$

The temporal variation of AN/$PM_{2.5}$ at the eight sites in 2004-2016 is shown in Table 2.3. In general, AN/$PM_{2.5}$ exhibited a significant decrease trend over the past 13 years except BHM, GFP, OAK, and PNS sites. Saylor et al. (2015) analyzed the temporal variation of NH_4^+ and NO_3^- in the Southeastern U.S. in 2004-2012 and discovered a significant reduction trend at the eight sites. The reduction in the concentrations of NH_4^+ and NO_3^- may result in the reduction of AN/$PM_{2.5}$. Thus, smaller fraction of $PM_{2.5}$ mass was directly NH_3 sensitive.

Table 2.3. Temporal variation of AN/$PM_{2.5}$ at the eight sites[a]

Year	YRK	JST	BHM	CTR	GFP	OAK	PNS	OLF
2004	0.16±0.06	0.15±0.06	0.14±0.07	0.13±0.06	0.12±0.04	0.11±0.04	0.11±0.03	0.12±0.03
2005	0.17±0.06	0.16±0.06	0.13±0.06	0.12±0.04	0.13±0.09	0.11±0.04	0.12±0.03	0.13±0.04
2006	0.17±0.08	0.14±0.06	0.13±0.06	0.12±0.06	0.12±0.04	0.11±0.05	0.12±0.04	0.13±0.06
2007	0.19±0.08	0.16±0.07	0.14±0.08	0.12±0.05	0.13±0.05	0.12±0.04	0.12±0.03	0.12±0.03
2008	0.18±0.07	0.17±0.08	0.14±0.07	0.13±0.06	0.13±0.06	0.12±0.04	0.12±0.03	0.13±0.04
2009	0.17±0.08	0.15±0.08	0.14±0.08	0.12±0.06	0.13±0.08	0.11±0.05	0.12±0.04	0.12±0.04
2010	0.17±0.11	0.15±0.08	0.13±0.08	0.12±0.06	0.12±0.04	0.13±0.07	N/A	0.12±0.04
2011	0.15±0.08	0.14±0.08	0.14±0.07	0.13±0.07	0.13±0.06	N/A	N/A	0.13±0.05
2012	0.12±0.06	0.13±0.07	0.11±0.05	0.11±0.04	0.12±0.04	N/A	N/A	0.11±0.03
2013	0.14±0.07	0.14±0.07	0.13±0.08	0.10±0.05	N/A	N/A	N/A	0.11±0.03
2014	0.11±0.08	0.14±0.11	0.13±0.09	0.09± 0.05	N/A	N/A	N/A	0.09±0.03
2015	0.13±0.10	0.19±0.14	0.14±0.10	0.08± 0.06	N/A	N/A	N/A	0.10±0.04
2016	N/A	0.14±0.11	N/A	0.08±0.04	N/A	N/A	N/A	N/A

[a] N/A: Not available

The diurnal and seasonal variations of AN/$PM_{2.5}$ at six sites were analyzed and are shown

in Figure 2.4. As it can be seen, AN/$PM_{2.5}$ exhibited a significantly seasonal and diurnal pattern at six sites. For seasonal variation, the values of AN/$PM_{2.5}$ were higher in colder seasons and lower in hotter seasons. The semi-volatile characteristic of NH_4NO_3 can explain the observation of this seasonal variation (Olszyna et al., 2005). The NH_4NO_3 aerosol was not thermally stable under high T such as summer condition, therefore, NH_4NO_3 decomposes into gas–phase NH_3 and HNO_3; while under low T such as winter condition, NH_4NO_3 tends to stay in particle phase. For diurnal variation, the values of AN/$PM_{2.5}$ were higher at noon. This may be explained by the diurnal variation of $PM_{2.5}$ mass, NH_4^+ and NO_3^- concentrations. Edgerton et al. (2006) analyzed the diurnal variation of $PM_{2.5}$ mass concentration and its chemical compositions at the SEARCH eight sites, the results indicated that the $PM_{2.5}$ mass and NO_3^- concentrations exhibited higher values in the early morning and at night and lower values in the daytime. While NH_4^+ concentration exhibited no specific diurnal pattern, the combined effects of the diurnal variation of $PM_{2.5}$ mass, NH_4^+ and NO_3^- concentrations led to the higher AN/$PM_{2.5}$ at noon.

The values of AN/$PM_{2.5}$ were higher at the JST and BHM sites than the YRK and CTR sites at noon. This can be explained by the abundance of the NO_x and SO_2 gas in the urban areas. The NO_x gas emitted from vehicles and SO_2 gas emitted from electricity generating unit (EGU) can be transformed by the more intense solar radiation into HNO_3 and H_2SO_4 at noon at the JST and BHM sites. The NH_3-rich condition at the JST and BHM sites facilitated the reaction of NH_3 with HNO_3 and H_2SO_4.

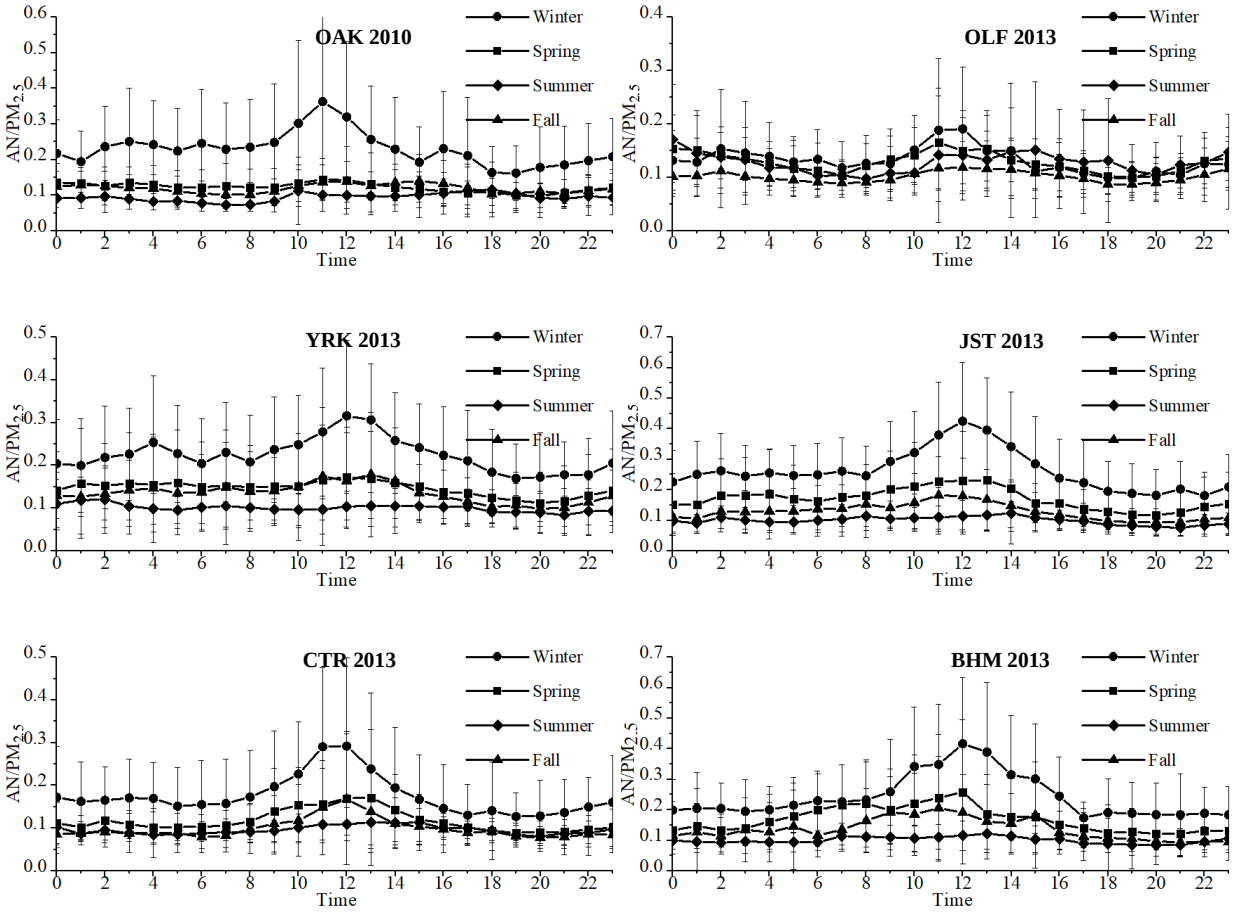

Figure 2.4. Diurnal and seasonal variations of the AN/$PM_{2.5}$ at six sites. Note the different scales on figures.

2.4. Conclusions

Spatial and temporal variations of atmospheric chemical conditions at eight urban/nonurban sites under SEARCH Network were investigated based on the analysis of four parameters, i.e., GR, NH_3/NH_x, TA/TS, and AN/$PM_{2.5}$. It is discovered that from 2004 to 2016, NH_4^+ salts in $iPM_{2.5}$ may consist of both $(NH_4)_2SO_4$ and NH_4NO_3 at the eight sites. The GRs analysis reveals that AFOs NH_3 emissions contributed to the higher GRs at two rural monitoring sites coded as YRK and OAK sites in the wind direction coming from AFOs farms. The NH_3/NH_x ratio exhibited similar variations in different wind directions as the GRs. An increase in the temporal trend NH_3/NH_x ratio was observed, indicating more NH_3 stayed in gas phase over the past 13 years. The TA/TS also exhibited an increase trend in 2004-2016 in response to the reduction

in SO_2 emissions in the Southeastern U.S. over the past 13 years. The AN/$PM_{2.5}$ analysis indicates that smaller fraction of $PM_{2.5}$ mass was directly NH_3 sensitive. Understanding of the spatial and temporal variations of atmospheric chemical conditions may provide insights to improve our understanding of the impact of AFOs NH_3 emissions on the potential for i$PM_{2.5}$ formation under rural and urban conditions.

CHAPTER 3: SPATIAL AND TEMPORAL VARIATIONS OF $PM_{2.5}$ MASS CLOSURE AND $IPM_{2.5}$ IN THE SOUTHEASTERN U.S.

Abstract

As a criteria pollutant regulated under National Ambient Air Quality Standards (NAAQS), fine particulate matter (i.e., $PM_{2.5}$) has gained intensive attention due to its adverse health and visibility degradation effects. The impact of $PM_{2.5}$ on the human health and visibility may vary due to the spatiotemporal heterogeneity of the contributions of different chemical compositions to $PM_{2.5}$. Thus, it is important to quantify the spatiotemporal variations of $PM_{2.5}$ and its chemical compositions in order to provide more information for $PM_{2.5}$ regulation. The gas– and particle–phase pollutants measured at the eight sites of Southeastern Aerosol Research and Characterization (SEARCH) Network from 2001 to 2016 were used to analyze the spatial and temporal variations of $PM_{2.5}$ mass closure and inorganic $PM_{2.5}$ ($iPM_{2.5}$) in the Southeastern U.S. The $PM_{2.5}$ concentrations exhibited a significant reduction trend from 2001 to 2016 at all eight sites. In general, $PM_{2.5}$ concentrations were higher in urban sites than nonurban sites, and higher in inland sites than coastal sites. The spatial heterogeneity of $PM_{2.5}$ may be caused by the atmospheric transport and spatial distribution of primary and secondary $PM_{2.5}$ emissions sources. The concentrations of $PM_{2.5}$, SO_4^{2-} and NH_4^+ exhibited the same seasonal variation, higher in summer and lower in winter. While NO_3^- concentration exhibited an inverse seasonal variation, higher in winter and lower in summer. The seasonal variation of $PM_{2.5}$ became less significant in later years (2012-2016). The concentrations of NH_4^+, SO_4^{2-} and NO_3^- were higher at four inland sites than coastal sites and higher in urban sites than the nonurban sites. Specifically, the concentrations of NH_4^+, SO_4^{2-} and NO_3^- at the agricultural rural site coded asYRK were higher than the other sites, except two urban sites coded asJST and BHM. The significant NH_3

emissions from AFOs at the YRK site may explain the higher $iPM_{2.5}$ concentrations; the abundant NH_3 facilitates the reaction of NH_3 with acidic gases. Furthermore, the strong correlation between NH_4^+, SO_4^{2-} and $PM_{2.5}$ indicated the day-to-day covariation. At four inland sites, the $iPM_{2.5}$ was the dominant composition of $PM_{2.5}$ before 2011, while OCM was the dominant composition of $PM_{2.5}$ after 2011. At four coastal sites, the $iPM_{2.5}$ was the dominant composition of $PM_{2.5}$ over the past 16 years. Moreover, the reduction in peak concentrations of $PM_{2.5}$ can be observed as well. The Bayesian Information Criteria (BIC) step-wise model selection determined the best fitting Multiple Linear Regression (MLR) model to predict NH_4^+ at six sites, there is a strong positive correlation between cation- NH_4^+ and anions- SO_4^{2-} & NO_3^-. The NH_3 is excluded from the regression model at the YRK site due to the abundant NH_3 emitted from AFOs. The nonvolatile cations (NVCs) and chloride (Cl^-) are the significant impact factors for the NH_4^+ salts formation. The spatial variations of $PM_{2.5}$ mass closure and $iPM_{2.5}$ indicate the spatial heterogeneity of various emission sources and local meteorology. In addition, the temporal variations of $PM_{2.5}$ mass closure and $iPM_{2.5}$ are the important evidence of air quality improvement in the Southeastern U.S. over the past 16 years.

3.1. Introduction

Fine particulate matter ($PM_{2.5}$) causes hazardous health problems such as adverse cardiovascular and respiratory effects (Pope and Dockery, 2006; Kampa and Castanas, 2008; Xing et al., 2016). Research has indicated that there's a positive correlation between daily morality and $PM_{2.5}$ concentration, especially for sensitive populations such as the elderly (Schwartz et al., 1996). In addition to the adverse health effect, $PM_{2.5}$ can also affect the radiative forcing on earth, and thus contribute to climate change (Haywood and Boucher, 2000; IPCC, 2013). The direct radiative forcing is caused by the scattering and absorption of solar radiation

(Ramanathan et al., 2001). Moreover, inorganic aerosols such as ammonium sulfate ($(NH_4)_2SO_4$) can facilitate the cirrus cloud formation by acting as ice nuclei, which may have potential impact on the climate, and this is referred as indirective radiative forcing (Abbatt et al., 2006). Furthermore, Malm et al. (1994) noted that $PM_{2.5}$ contributed to the visibility degradation, especially sulfate (SO_4^{2-}) and organic materials, which are the main contributors to the light extinction in the eastern United States (U.S.). Based on collaborated research of scientists and latest scientific observations on the adverse effects of $PM_{2.5}$, the $PM_{2.5}$ national ambient air quality standards (NAAQS) have been revised twice over the past two decades. The $PM_{2.5}$ 24-hour average concentration standard was reduced from 65 μg m^{-3} to 35 μg m^{-3} in 2006 and the primary $PM_{2.5}$ annual average concentration threshold was strengthened from 15 μg m^{-3} to 12 μg m^{-3} in 2012 (USEPA, 2018a).

Research has indicated that the vigorous explanation of the impact of $PM_{2.5}$ on human health and visibility required the detailed measurements of $PM_{2.5}$ chemical compositions including ions, carbonaceous materials, and various elements (Franklin et al., 2008; Hand et al., 2014). The major chemical compositions of $PM_{2.5}$ can be classified as inorganic and organic chemical species. Ammonium (NH_4^+), SO_4^{2-}, nitrate (NO_3^-), and chloride (Cl^-) are the major components of inorganic $PM_{2.5}$ ($iPM_{2.5}$), in addition, nonvolatile cations (NVCs) such as magnesium (Mg^{2+}), potassium (K^+), sodium (Na^+), calcium (Ca^{2+}) may also contribute to $iPM_{2.5}$ (Snider et al., 2016). Other chemical components of $PM_{2.5}$ include organic carbon (OC), elemental carbon (EC), crustal elements, particle-bound water and unknown substances (Frank, 2006). The $iPM_{2.5}$ is usually formed through the reactions of precursor gases (NH_3, H_2SO_4, HCl, and HNO_3). Thus, ammonium salts such as $(NH_4)_2SO_4$, ammonium nitrate (NH_4NO_3), and ammonium chloride (NH_4Cl) contribute to the majority of $iPM_{2.5}$ (Walker et al., 2006). The

reactions of NH_3 and acidic gases may be in a thermodynamic equilibrium state (Seinfeld and Pandis, 2006). The formation of $iPM_{2.5}$ may be impacted by the availability of precursor gases and meteorological conditions (Ansari and Pandis, 1998; Hidy et al., 2014). Different chemical compositions of $PM_{2.5}$ can be attributed to various emission sources and formation processes, the spatial and temporal variations of emissions sources and local meteorology can thus lead to the variable contributions of different chemical compositions to $PM_{2.5}$ concentration (Abdeen et al., 2014).

Ramanathan et al. (2001) noted that the short lifetime of aerosols results in substantial variations of aerosol concentrations in spatiotemporal scales. Due to the important contribution of $iPM_{2.5}$ to $PM_{2.5}$ concentration, more research is required to advance our understanding on the spatial and temporal variations of $PM_{2.5}$ chemical compositions. This research investigated the spatial and temporal variations of $PM_{2.5}$ mass closures and $iPM_{2.5}$ in 2001-2016 in the Southeastern U.S., and quantitatively characterized the contributions of different chemical compositions to $PM_{2.5}$ in spatial and temporal scales.

3.2. Methodology

3.2.1. Data acquisition and adjustment

This research utilized the daily and hourly measurements of $PM_{2.5}$ mass and chemical compositions concentrations from Southeastern Aerosol Research and Characterization (SEARCH) Network in 2001-2016. The comprehensive measurements from 2001 to 2016 were available at the BHM, CTR, JST, OLF, and YRK sites, while GFP (2001-2014), OAK (2001-2012), PNS (2001-2009) sites only have certain periods of measurements.

Some measurement values were reported to be either negative or below the detection limit (DL) of the instruments. The negative values less than (–DL) were considered questionable

and excluded from the dataset, while the other values below the DL were replaced with half of the DL (USEPA 2000; Cohen and Ryan 1989). As for the seasonal variations, spring includes March, April, and May; summer includes June, July, and August; fall includes September, October, and November; and winter includes December, January, and February. The OC measurements under the SEARCH Network only accounted for the carbon fraction of the organic carbon matter (OCM), thus OC was adjusted to derive the mass concentration of OCM using Equation 3-1 (Hansen et al., 2003).

$$OCM = 1.4 \times OC \qquad (3\text{-}1)$$

where OCM = organic carbon matter; OC = measured organic carbon. In this research, OCM concentrations were used to construct the pie chart of $PM_{2.5}$ mass closure.

The SEARCH Network made a simple assumption on soil elements: six elements including aluminum (Al), calcium (Ca), iron (Fe), potassium (K), silicon (Si), and titanium (Ti) are in their oxide forms, and these soil materials are referred to as major metal oxides (MMO) (Hansen et al., 2003).

$$MMO = Al \times 1.89 + Ca \times 1.40 + Fe \times 1.43 + K \times 1.21 + Si \times 2.14 + Ti \times 1.67 \qquad (3\text{-}2)$$

The contributions of various chemical compositions to $PM_{2.5}$ were characterized using pie chart. Moreover, the $PM_{2.5}$ mass closure analysis was based on Equation 3-3:

$$P_i = (C_i/C_m) \times 100 \qquad (3\text{-}3)$$

where P_i = percentage of the chemical component i to the total $PM_{2.5}$ mass concentration, C_i = measured or adjusted concentration of the chemical composition i, C_m = measured $PM_{2.5}$ mass concentration using Federal Reference Method (FRM).

The percentiles of $PM_{2.5}$ mass concentration, SO_4^{2-}, NH_4^+, and NO_3^- were calculated to analyzed the trends in extrema in 2001-2016.

3.2.2. Multiple linear regression (MLR) model

The multiple linear regression **(**MLR) model was constructed to exam the response of NH_4^+ to various factors. Step-wise model selection method based on the Bayesian information criterion (BIC) was used to select best fitting model from Equation 4:

$$NH_4^+ = \beta_0 + \beta_i \times x_i + \text{interaction terms} + \text{quadratic terms} + \varepsilon_i \qquad (3\text{-}4)$$

where x_i are i$PM_{2.5}$ chemical compositions and acidic gases including SO_4^{2-}, NO_3^-, Ca^{2+}, Mg^{2+}, K^+, Na^+, Cl^-, NH_3, and HNO_3 and ambient temperature (T) and relative humidity (RH). Interaction terms include up to two factors. All the gas-phase and particle-phase pollutants are converted in the unit of μg m^{-3}, T is in ºC, RH is in %. The 24-hr average Cl^-, K^+, Na^+, Mg^{2+}, Ca^{2+}, NH_4^+, SO_4^{2-}, and NO_3^- data and 1-h average T, RH, NH_3, and HNO_3 data were available at the BHM site (2011-2016), CTR site (2012-2016), JST site (2010-2016), YRK site (2008-2016), OLF site (2013-2016), and OAK site (2010). The MLR model was built in two periods: 2008-2011, 2012-2016.

In this study, the step-wise model selection mothed identified the significant factors for the NH_4^+ formation at a particular location and for a particular span of years. The selected MLR model was not used to represent a variety of locations and time spans.

3.2.3. Statistical analysis and map development

The Tukey honest significant difference (HSD) test was used to check the spatial, temporal, and seasonal variations of $PM_{2.5}$ and its chemical compositions under 0.05 significance level. The statistical analysis was performed using R software and ArcMap 10.4 was used to develop $PM_{2.5}$ concentration map.

3.3. Results and discussion

Annual average $PM_{2.5}$ concentrations at eight sites of SEARCH Network in 2001-2016 are shown in Figure 3.1. The annual average $PM_{2.5}$ concentrations at each site for 2001, 2007, 2008, 2011, 2012, and 2016 are illustrated to reflect the $PM_{2.5}$ regulation changes in 2006 and 2012.

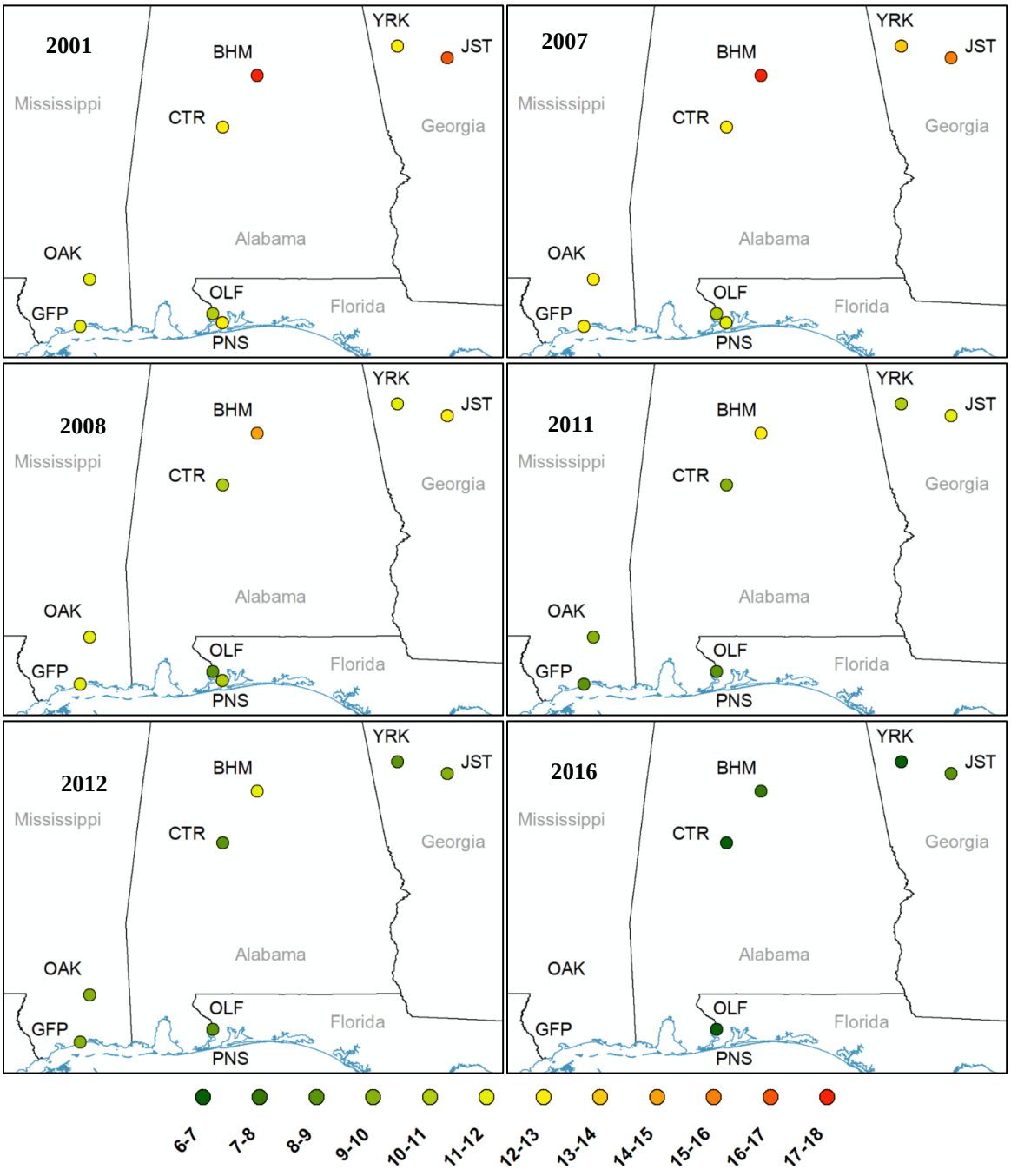

Figure 3.1 $PM_{2.5}$ annual average concentrations (μg m^{-3}) at eight sites

As it can be seen from Figure 3.1, there was a significant reduction in $PM_{2.5}$ concentrations at eight sites of SEARCH Network from 2001 to 2016. As for the spatial variation, in general, the annual average $PM_{2.5}$ concentrations were higher in inland sites (JST, YRK, BHM, and CTR) than coastal sites (OAK, GFP, OLF, and PNS). In addition, the annual average $PM_{2.5}$ concentrations were higher in urban sites (BHM, JST, and GFP) than the nonurban sites (CTR, YRK, and OLF) except two sites-PNS and OAK sites. The annual average $PM_{2.5}$ in rural site-OAK was higher than the urban site-PNS. The geographical locations of the eight sites and spatial heterogeneity of the emissions sources may explain the spatial pattern of $PM_{2.5}$ concentration. The coastal sites were closer to the Gulf of Mexico, the dilution effects of air mass blowing from ocean may lead to the lower $PM_{2.5}$ concentration at the coastal sites. On the other hand, more primary and secondary $PM_{2.5}$ emissions sources were located surrounding the urban sites. The interaction of atmospheric transport, various chemical reactions and spatial heterogeneity of emissions sources resulted in the spatial pattern of $PM_{2.5}$ concentrations at the eight sites of SEARCH Network.

The annual average $PM_{2.5}$ concentrations exhibited a significant reduction trend from 2001 to 2016 at all eight sites. In 2001, the annual average $PM_{2.5}$ concentrations were at least greater than 10 $\mu g\ m^{-3}$ at eight sites, moreover, the BHM and JST sites had annual average $PM_{2.5}$ concentrations 17.6 and 16.5 $\mu g\ m^{-3}$, respectively, which are greater than the annual concentration threshold (15 $\mu g\ m^{-3}$) under the NAAQS back then. In 2016, the annual average $PM_{2.5}$ concentrations at five sites were all below 12 $\mu g\ m^{-3}$, the latest NAAQS $PM_{2.5}$ mass concentration threshold. The reduction of $PM_{2.5}$ concentration resulted from the effective implementation of NAAQS and enactment of regulation laws such as Clean Air Act (CAA) and Clean Air Act Amendment (CAAA). In addition, EPA's Clean Air Interstate Rule (CAIR) in

2005 and Cross-State Air Pollution Rule (CSAPR) in 2011 guaranteed the continuous reduction of $PM_{2.5}$ in the past 16 years, both rules requested the reduction of emissions in SO_2 and NO_x, which led to the reduction in the formation of $iPM_{2.5}$ (USEPA, 2018b, c). The annual average $PM_{2.5}$ concentrations were all below 9.0 μg m^{-3} at five sites in 2016, even as low as 6.8 μg m^{-3} at the OLF site. The temporal reduction of $PM_{2.5}$ concentration indicated the significant improvement of air quality for $PM_{2.5}$ in the Southeastern U.S. over the past 16 years.

3.3.1. $PM_{2.5}$ mass concentration change trend

The monthly average of $PM_{2.5}$ mass and $iPM_{2.5}$ chemical compositions concentration change trends in the past 16 years from 2001 to 2016 at the eight sites of SEARCH Network are shown in Figures 3.2-3.9.

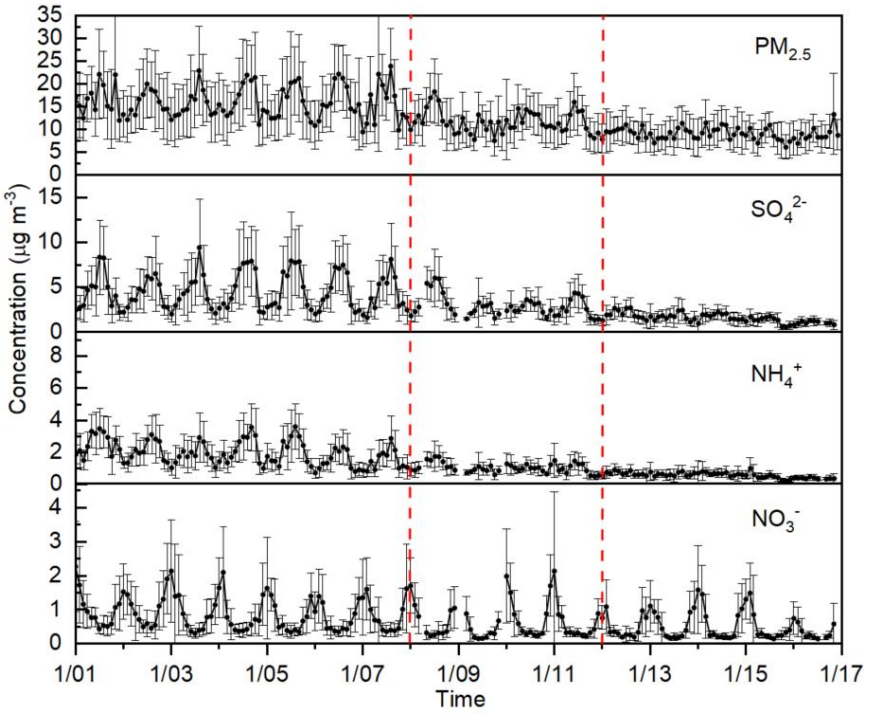

Figure 3.2. Monthly average of $PM_{2.5}$ mass and $iPM_{2.5}$ chemical compositions concentrations at the JST site (M/YY = month/year)

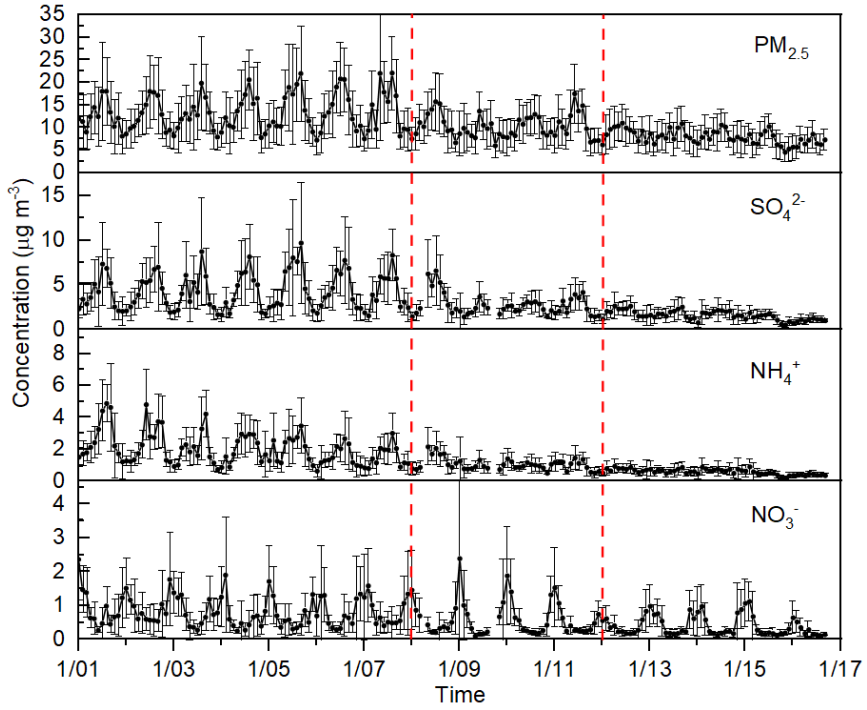

Figure 3.3. Monthly average of $PM_{2.5}$ and $iPM_{2.5}$ chemical compositions concentrations at the YRK site (M/YY = month/year)

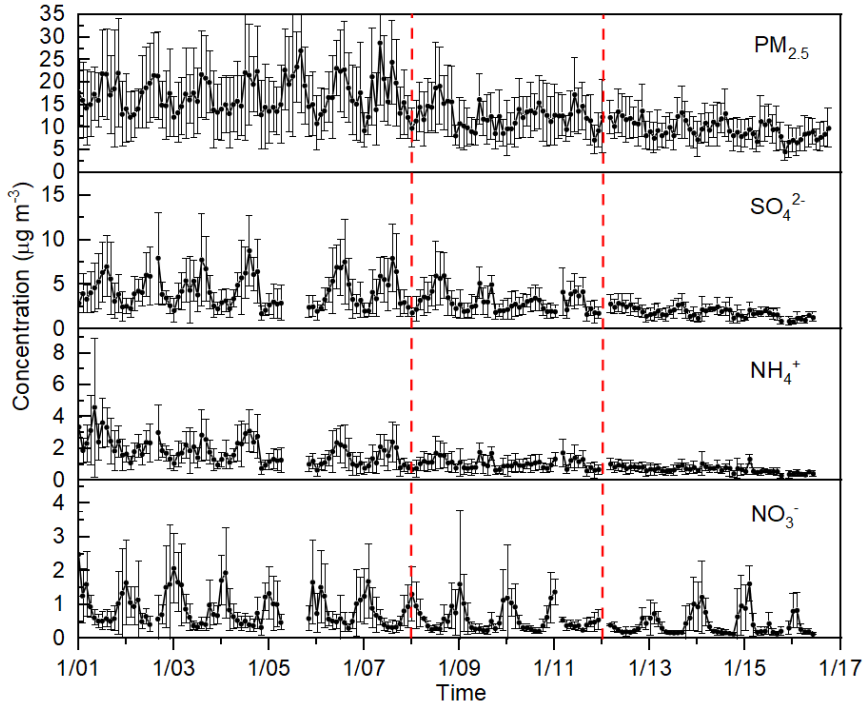

Figure 3.4. Monthly average of $PM_{2.5}$ mass and $iPM_{2.5}$ chemical compositions concentrations at the BHM site (M/YY = month/year)

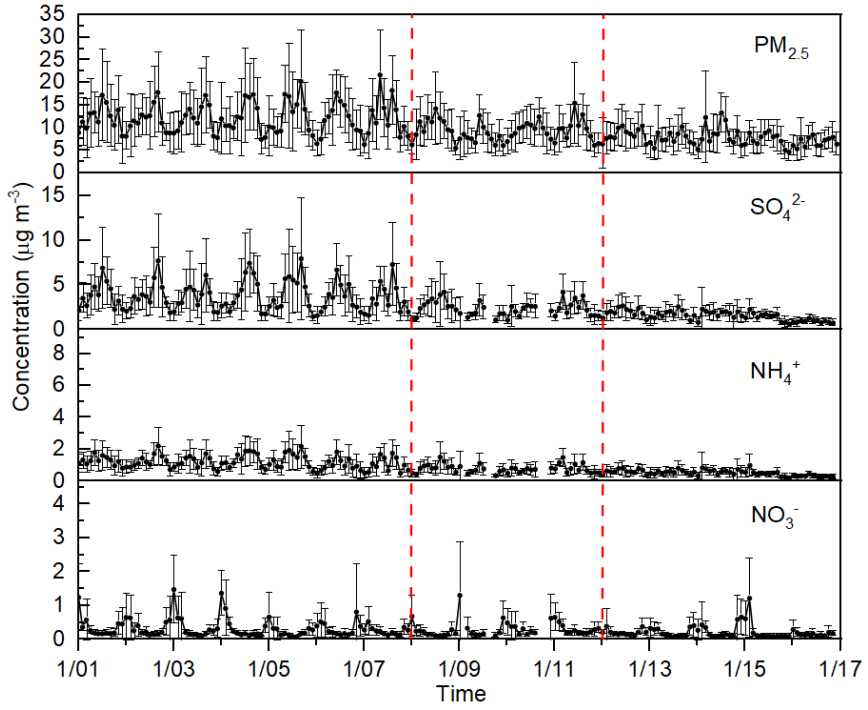

Figure 3.5. Monthly average of $PM_{2.5}$ mass and $iPM_{2.5}$ chemical compositions concentrations at the CTR site (M/YY = month/year)

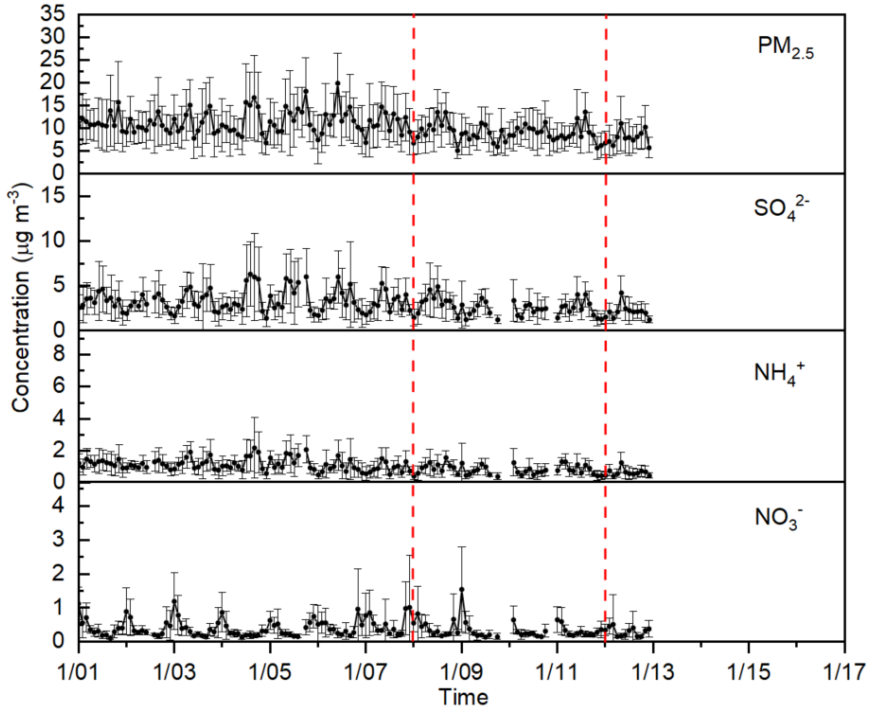

Figure 3.6. Monthly average of $PM_{2.5}$ mass and $iPM_{2.5}$ chemical compositions concentrations at the GFP site (M/YY = month/year)

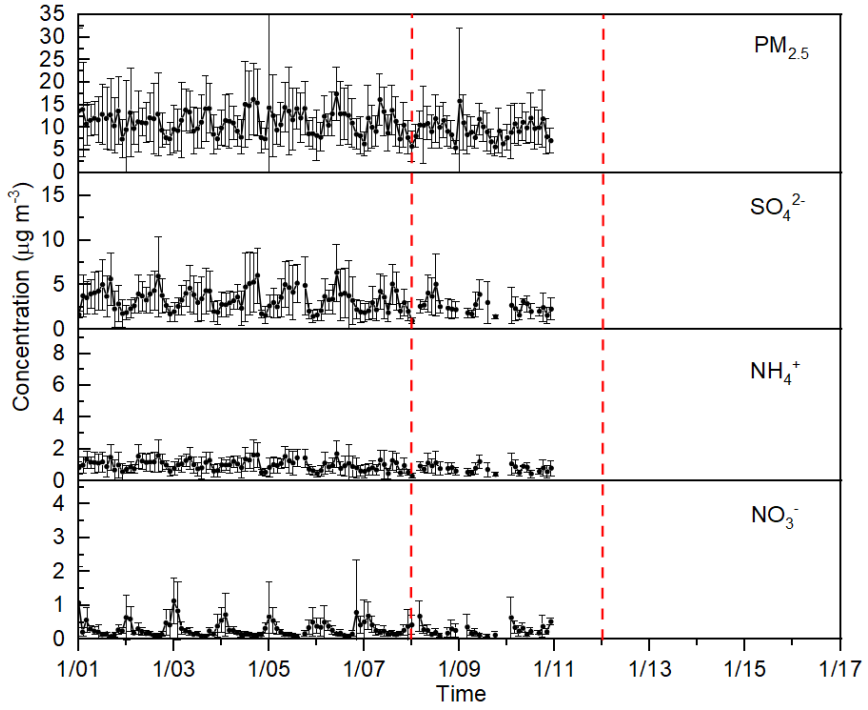

Figure 3.7. Monthly average of $PM_{2.5}$ mass and $iPM_{2.5}$ chemical compositions concentrations at the OAK site (M/YY = month/year)

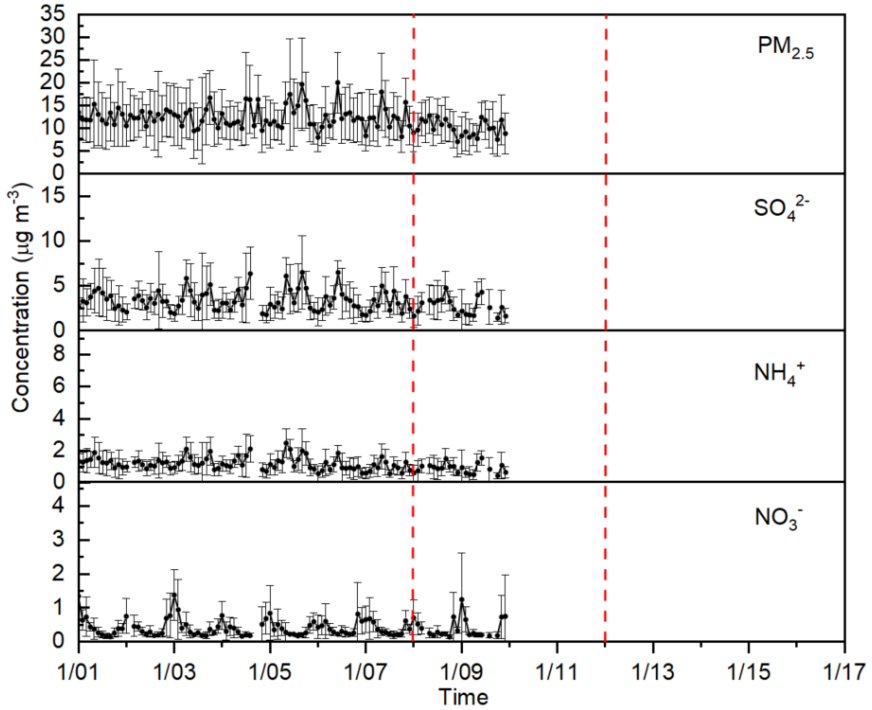

Figure 3.8. Monthly average of $PM_{2.5}$ mass and $iPM_{2.5}$ chemical compositions concentrations at the PNS site (M/YY = month/year)

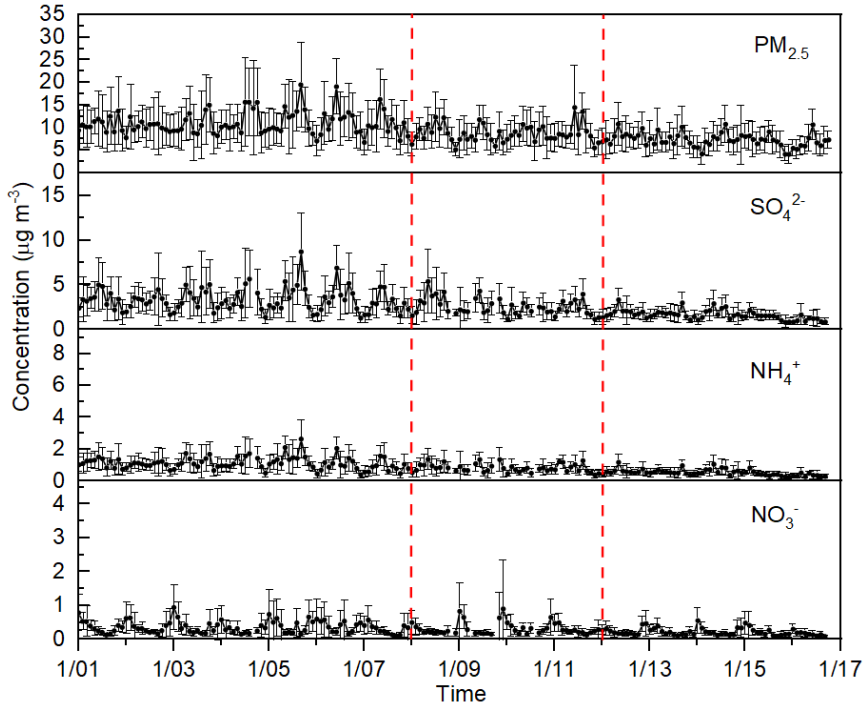

Figure 3.9. Monthly average of $PM_{2.5}$ mass and $iPM_{2.5}$ chemical compositions concentrations at the OLF site (M/YY = month/year)

As it can be seen from Figures 3.2-3.9, a reduction trend of monthly average $PM_{2.5}$ mass concentration occurred in the past 16 years. In addition, monthly average $PM_{2.5}$ concentration exhibited a significant seasonal variation before 2012; however, after 2012, the seasonal variation became less intense. In general, $PM_{2.5}$ concentrations were higher in summer and lower in winter at the eight sites of SEARCH Network. The seasonal variation of $PM_{2.5}$ concentration was attributed to the seasonal variation of different chemical compositions comprising $PM_{2.5}$, especially SO_4^{2-} & NH_4^+. As for the $iPM_{2.5}$ chemical compositions, the seasonal variation of SO_4^{2-} and NH_4^+ follow the seasonal variation of $PM_{2.5}$ mass concentration, higher in summer and lower in winter. However, NO_3^- exhibited an inverse seasonal variation, higher in winter and lower in summer.

Moreover, the past 16 years can be divided into 3 consecutive periods: 2001-2007, 2008-2011, and 2012-2016. To further illustrate the seasonal variations of $PM_{2.5}$ and $iPM_{2.5}$ chemical compositions concentrations, the seasonal pattern of $PM_{2.5}$ mass concentration, SO_4^{2-}, NH_4^+, and NO_3^- are summarized in Tables 3.1-3.4, the seasonal pattern of OCM, EC, and MMO is summarized in Appendix B, Tables 1S-3S.

Table 3.1. Seasonal variations of $PM_{2.5}$ concentration ($\mu g\ m^{-3}$) in 3 monitoring periods

Sites	Periods	Winter	Spring	Summer	Fall
JST	2001-2007	13.17 ± 6.30	15.07 ± 6.91	19.60 ± 8.15	16.13 ± 8.29
	2008-2011	10.44 ± 5.03	11.11 ± 4.55	14.29 ± 5.37	10.55 ± 4.79
	2012-2016	8.36 ± 3.75	8.76 ± 3.45	9.78 ± 3.58	9.21 ± 4.41
YRK	2001-2007	9.43 ± 4.29	12.82 ± 6.64	17.73 ± 8.13	13.21 ± 7.30
	2008-2011	8.44 ± 3.99	10.05 ± 4.35	13.45 ± 5.18	9.08 ± 4.29
	2012-2016	6.97 ± 3.25	8.16 ± 3.45	9.23 ± 3.62	7.63 ± 3.35
BHM	2001-2007	13.88 ± 7.18	16.51 ± 8.62	20.41 ± 9.80	18.04 ± 9.51
	2008-2011	10.38 ± 4.95	11.71 ± 5.20	14.87 ± 6.62	12.85 ± 6.50
	2012-2016	8.19 ± 3.78	9.67 ± 4.19	10.50 ± 4.22	10.16 ± 4.65
CTR	2001-2007	8.92 ± 4.82	12.58 ± 6.37	14.59 ± 7.77	12.53 ± 7.04
	2008-2011	7.29 ± 3.74	9.31 ± 4.06	11.59 ± 5.49	8.94 ± 4.26
	2012-2016	6.36 ± 3.15	7.93 ± 4.15	8.81 ± 3.88	7.92 ± 3.26
GFP	2001-2007	9.72 ± 4.85	11.07 ± 4.88	11.96 ± 6.43	12.43 ± 6.68
	2008-2011	7.56 ± 3.25	8.98 ± 3.29	10.58 ± 4.82	8.89 ± 4.24
	2012	6.43 ± 2.84	8.40 ± 4.74	7.70 ± 3.45	9.06 ± 3.85
OAK	2001-2007	9.80 ± 8.95	11.62 ± 4.99	12.38 ± 6.58	11.43 ± 6.29
	2008-2010	8.57 ± 7.38	9.85 ± 4.55	10.51 ± 4.41	9.10 ± 4.40
	2012-2016	N/A	N/A	N/A	N/A
PNS	2001-2007	11.48 ± 5.31	12.32 ± 5.55	12.80 ± 6.86	13.20 ± 6.71
	2008-2009	8.57 ± 4.08	10.03 ± 4.16	11.12 ± 4.04	10.21 ± 4.85
	2012-2016	N/A	N/A	N/A	N/A
OLF	2001-2007	9.21 ± 4.14	11.14 ± 4.80	11.90 ± 6.42	11.79 ± 6.50
	2008-2011	7.36 ± 3.14	8.70 ± 3.15	10.58 ± 5.20	8.42 ± 3.99
	2012-2016	6.45 ± 3.47	7.37 ± 3.32	8.14 ± 3.45	7.39 ± 3.15

Table 3.2. Seasonal variations of NH_4^+ concentration (μg m^{-3}) in 3 monitoring periods

Sites	Periods	Winter	Spring	Summer	Fall
JST	2001-2007	1.33 ± 0.76	1.87 ± 0.95	2.72 ± 1.26	2.18 ± 1.37
	2008-2011	0.93 ± 0.49	1.09 ± 0.49	1.50 ± 0.69	1.08 ± 0.56
	2012-2016	0.62 ± 0.41	0.62 ± 0.31	0.63 ± 0.31	0.53 ± 0.30
YRK	2001-2007	1.21 ± 0.74	1.73 ± 0.84	2.78 ± 1.42	2.17 ± 1.50
	2008-2011	1.02 ± 0.56	1.02 ± 0.55	1.39 ± 0.70	0.93 ± 0.55
	2012-2016	0.60 ± 0.37	0.62 ± 0.31	0.65 ± 0.31	0.56 ± 0.35
BHM	2001-2007	1.22 ± 0.69	1.62 ± 0.93	2.32 ± 1.20	1.48 ± 1.12
	2008-2011	0.82 ± 0.49	0.97 ± 0.50	1.30 ± 0.71	1.00 ± 0.54
	2012-2016	0.71 ± 0.44	0.67 ± 0.30	0.71 ± 0.29	0.69 ± 0.38
CTR	2001-2007	0.91 ± 0.46	1.25 ± 0.61	1.46 ± 0.82	1.34 ± 0.80
	2008-2011	0.72 ± 0.35	0.80 ± 0.40	1.01 ± 0.53	0.76 ± 0.43
	2012-2016	0.46 ± 0.28	0.57 ± 0.26	0.58 ± 0.28	0.48 ± 0.31
GFP	2001-2007	0.90 ± 0.46	1.22 ± 0.61	1.29 ± 0.77	1.31 ± 0.91
	2008-2011	0.73 ± 0.53	0.89 ± 0.46	0.86 ± 0.47	0.80 ± 0.46
	2012	0.53 ± 0.26	0.76 ± 0.52	0.59 ± 0.35	0.69 ± 0.31
OAK	2001-2007	0.77 ± 0.38	1.16 ± 0.55	1.15 ± 0.65	1.09 ± 0.71
	2008-2011	0.77 ± 0.61	0.80 ± 0.38	0.83 ± 0.45	0.75 ± 0.37
	2012-2016	N/A	N/A	N/A	N/A
PNS	2001-2007	0.95 ± 0.48	1.44 ± 0.73	1.30 ± 0.79	1.24 ± 0.79
	2008-2009	0.71 ± 0.56	0.94 ± 0.49	0.99 ± 0.62	0.99 ± 0.62
	2012-2016	N/A	N/A	N/A	N/A
OLF	2001-2007	0.84 ± 0.43	1.29 ± 0.64	1.32 ± 0.78	1.25 ± 0.78
	2008-2011	0.73 ± 0.42	0.89 ± 0.44	0.93 ± 0.51	0.77 ± 0.49
	2012-2016	0.50 ± 0.25	0.65 ± 0.35	0.53 ± 0.33	0.52 ± 0.33

Table 3.3. Seasonal variations of SO_4^{2-} concentration (μg m^{-3}) in 3 monitoring periods

Sites	Periods	Winter	Spring	Summer	Fall
JST	2001-2007	2.58 ± 1.36	4.59 ± 2.34	7.43 ± 3.70	5.21 ± 3.38
	2008-2011	2.07 ± 0.95	3.27 ± 1.79	5.00 ± 2.41	2.96 ± 1.75
	2012-2016	1.39 ± 0.87	1.74 ± 0.77	1.96 ± 0.90	1.40 ± 0.78
YRK	2001-2007	2.37 ± 1.24	4.29 ± 2.29	6.99 ± 3.70	4.82 ± 3.58
	2008-2011	2.06 ± 0.98	2.83 ± 1.71	4.16 ± 2.29	2.41 ± 1.41
	2012-2016	1.33 ± 0.82	1.72 ± 0.82	2.01 ± 0.88	1.47 ± 0.86
BHM	2001-2007	2.70 ± 1.21	4.38 ± 2.37	6.71 ± 3.52	4.22 ± 3.00
	2008-2011	2.07 ± 1.04	2.81 ± 1.36	4.19 ± 2.31	2.88 ± 1.61
	2012-2016	1.49 ± 0.87	1.90 ± 0.83	2.21 ± 0.82	1.82 ±0.95
CTR	2001-2007	2.36 ± 1.20	3.71 ± 2.09	5.23 ± 3.44	4.22 ± 3.20
	2008-2011	1.84 ± 0.95	2.45 ± 1.33	3.30 ± 1.71	2.35 ± 1.51
	2012-2016	1.28 ± 0.78	1.79 ± 0.84	1.91 ± 0.87	1.42 ± 0.88
GFP	2001-2007	2.30 ± 1.22	3.55 ± 1.82	4.25 ± 2.72	3.78 ± 2.69
	2008-2011	1.81 ± 1.21	2.73 ± 1.39	3.25 ± 1.67	2.39 ± 1.31
	2012	1.54 ± 0.73	2.60 ± 1.67	2.19 ± 1.15	2.12 ± 0.91
OAK	2001-2007	2.21 ± 1.19	3.67 ± 1.82	4.37 ± 2.64	3.67 ± 2.62
	2008-2011	2.17 ± 1.53	2.62 ± 1.32	3.05 ± 1.72	2.22 ± 1.14
	2012-2016	N/A	N/A	N/A	N/A
PNS	2001-2007	2.43 ± 1.31	3.78 ± 1.89	4.08 ± 2.59	3.50 ± 2.31
	2008-2009	1.90 ± 1.32	2.91 ± 1.39	3.35 ± 1.79	2.93 ± 1.75
	2012-2016	N/A	N/A	N/A	N/A
OLF	2001-2007	2.24 ± 1.27	3.59 ± 1.78	4.28 ± 2.65	3.71 ± 2.64
	2008-2011	1.83 ± 1.06	2.82 ± 1.71	3.25 ± 1.82	2.31 ± 1.49
	2012-2016	1.38 ± 0.68	1.94 ± 0.95	1.76 ± 0.97	1.51 ± 0.88

Table 3.4. Seasonal variations of NO_3^- concentration (μg m^{-3}) in 3 monitoring periods

Sites	Periods	Winter	Spring	Summer	Fall
JST	2001-2007	1.76 ± 1.20	0.73 ± 0.59	0.42 ± 0.21	0.72 ± 0.56
	2008-2011	1.24 ± 0.87	0.50 ± 0.37	0.27 ± 0.17	0.44 ± 0.38
	2012-2016	1.00 ± 0.73	0.40 ± 0.45	0.20 ± 0.09	0.43 ± 0.45
YRK	2001-2007	1.52 ± 1.02	0.65 ± 0.53	0.46 ± 0.37	0.71 ± 0.61
	2008-2011	1.25 ± 1.11	0.47 ± 0.29	0.24 ± 0.17	0.38 ± 0.24
	2012-2016	0.74 ± 0.55	0.36 ± 0.36	0.18 ± 0.10	0.36 ± 0.42
BHM	2001-2007	1.41 ± 1.00	0.73 ± 0.53	0.45 ± 0.22	0.56 ± 0.40
	2008-2011	0.98 ± 0.94	0.50 ± 0.39	0.29 ± 0.12	0.48 ± 0.34
	2012-2016	0.86 ± 0.70	0.33 ± 0.24	0.20 ± 0.12	0.34 ± 0.36
CTR	2001-2007	0.62 ± 0.64	0.28 ± 0.27	0.16 ± 0.06	0.27 ± 0.40
	2008-2011	0.51 ± 0.44	0.25 ± 0.19	0.18 ± 0.09	0.21 ± 0.14
	2012-2016	0.35 ± 0.35	0.17 ± 0.10	0.12 ± 0.06	0.19 ± 0.23
GFP	2001-2007	0.67 ± 0.55	0.37 ± 0.24	0.22 ± 0.11	0.34 ± 0.39
	2008-2011	0.64 ± 0.61	0.32 ± 0.22	0.23 ± 0.10	0.27 ± 0.24
	2012	0.38 ± 0.21	0.18 ± 0.10	0.33 ± 0.34	0.21 ± 0.11
OAK	2001-2007	0.53 ± 0.47	0.31 ± 0.20	0.16 ± 0.08	0.23 ± 0.41
	2008-2011	0.60 ± 0.58	0.32 ± 0.25	0.17 ± 0.08	0.22 ± 0.15
	2012-2016	N/A	N/A	N/A	N/A
PNS	2001-2007	0.68 ± 0.54	0.42 ± 0.30	0.23 ± 0.10	0.35 ± 0.36
	2008-2009	0.67 ± 0.73	0.30 ± 0.15	0.23 ± 0.10	0.35 ± 0.40
	2012-2016	N/A	N/A	N/A	N/A
OLF	2001-2007	0.56 ± 0.45	0.37 ± 0.29	0.25 ± 0.20	0.30 ± 0.24
	2008-2011	0.49 ± 0.48	0.26 ± 0.12	0.23 ± 0.09	0.24 ± 0.20
	2012-2016	0.33 ± 0.25	0.23 ± 0.13	0.17 ± 0.09	0.20 ± 0.15

Tukey test indicated that the seasonal variation of $PM_{2.5}$ exhibited higher values in summer and lower values in winter in all three periods. As for the seasonal variations of NH_4^+, SO_4^{2-} & NO_3^-, both NH_4^+ and SO_4^{2-} exhibited the same seasonal variation as $PM_{2.5}$ mass concentration, higher in summer and lower in winter. However, the Tukey test indicated that the there's no significant seasonal variation of NH_4^+ at five out of six sites of SEARCH Network, except the OLF site in 2012-2016. The NO_3^- concentration at the eight sites exhibited inverse seasonal variation, higher in winter, and lower in summer. The inverse seasonal variation of NH_4^+, SO_4^{2-} & NO_3^- can be attributed to the different formation processes of $iPM_{2.5}$ and thermal characteristics of SO_4^{2-} salts and NO_3^- salts. The more intense solar radiation in summer may convert more sulfur dioxide (SO_2) into H_2SO_4, thus leading to more $(NH_4)_2SO_4$ formation in summer (Seinfeld and Pandis, 2006). Moreover, the lower vapor pressure of H_2SO_4 resulted in the dominance of particle phase of SO_4^{2-} salts; on the contrary, NH_4NO_3 was semi-volatile compound, the higher T did not favor the formation of NH_4NO_3 in summer, thus NO_3^- concentration was lower in summer (Hildemann et al., 1984).

As for the spatial variations of $iPM_{2.5}$ chemical compositions, in general, the concentrations of NH_4^+, SO_4^{2-} and NO_3^- were higher at four inland sites (JST, YRK, BHM, and CTR) than coastal sites (OAK, GFP, OLF, and PNS). In addition, the concentrations of NH_4^+, SO_4^{2-} & NO_3^- were higher in urban sites (BHM, JST, PNS, and GFP) than the nonurban sites (CTR, YRK, OAK, and OLF). The spatial variations of $iPM_{2.5}$ and $PM_{2.5}$ exhibited the similar trend. Moreover, the concentrations of NH_4^+, SO_4^{2-} and NO_3^- at the agricultural rural site-YRK were higher than the other sites in the three periods, except two urban sites-JST and BHM. The

spatial heterogeneity of $iPM_{2.5}$ may be attributed to the geographical locations of the eight sites. The dilution effects of air parcel blowing from the ocean may result in the lower concentrations of $iPM_{2.5}$ at the coastal sites, pollutants may be accumulated during the movement of air parcel toward inland (Blanchard et al., 2013). The NH_3 and NO_x emissions from vehicles and industrial sources, SO_2 emissions from power plants and industrial sources at the urban sites (JST, BHM, and GFP) may facilitate the formation of $iPM_{2.5}$. As for the YRK site, the NH_3 emissions from AFOs farms lead to the abundant NH_3 existing in the air at the YRK site, the abundant NH_3 may facilitate the reaction of NH_3 with acidic gases (Blanchard et al., 2012). Thus, the $iPM_{2.5}$ concentrations at the YRK site were significantly higher than the other sites except for JST and BHM sites.

As for the temporal variation of $iPM_{2.5}$, a reduction trend can be observed for NH_4^+, SO_4^{2-} and NO_3^- at the eight sites in four seasons of the three monitoring periods. The reduction trend of $iPM_{2.5}$ was consistent with the temporal reduction trend in $PM_{2.5}$ mass concentration in the past 16 years. The concurrent variations of $PM_{2.5}$ mass and $iPM_{2.5}$ concentrations indicated the important contribution of $iPM_{2.5}$ to the reduction of $PM_{2.5}$ level in the Southeastern U.S.

3.3.2. Correlations between $PM_{2.5}$ and $iPM_{2.5}$ compositions concentration

The correlations between $PM_{2.5}$ mass concentration and $iPM_{2.5}$ chemical compositions are shown in Table 3.5.

Table 3.5. Correlation of $iPM_{2.5}$ chemical compositions with $PM_{2.5}$ mass concentration

Sites	Chemical species	Yearly	Winter	Spring	Summer	Fall
JST	SO_4^{2-}	0.82	0.56	0.76	0.93	0.80
	NH_4^+	0.82	0.63	0.73	0.89	0.81
	NO_3^-	**0.18**	0.59	**0.32**	**0.44**	**0.40**
YRK	SO_4^{2-}	0.89	0.75	0.76	0.93	0.92
	NH_4^+	0.84	0.81	0.73	0.87	0.87
	NO_3^-	**0.17**	0.69	**0.28**	**0.46**	**0.37**
BHM	SO_4^{2-}	0.78	0.55	0.75	0.90	0.76
	NH_4^+	0.78	0.63	0.72	0.86	0.75
	NO_3^-	**0.20**	**0.48**	**0.32**	0.54	**0.40**
CTR	SO_4^{2-}	0.84	0.59	0.77	0.90	0.90
	NH_4^+	0.84	0.66	0.78	0.89	0.88
	NO_3^-	**0.11**	**0.42**	**0.24**	**0.40**	**0.14**
GFP	SO_4^{2-}	0.86	0.63	0.84	0.91	0.88
	NH_4^+	0.87	0.71	0.85	0.90	0.91
	NO_3^-	**0.21**	0.64	**0.40**	**0.00**	**0.27**
OAK	SO_4^{2-}	0.81	0.51	0.75	0.91	0.92
	NH_4^+	0.82	0.60	0.82	0.87	0.93
	NO_3^-	**0.11**	**0.42**	**0.25**	**0.11**	**0.06**
PNS	SO_4^{2-}	0.77	0.46	0.79	0.90	0.87
	NH_4^+	0.80	0.64	0.80	0.85	0.90
	NO_3^-	**0.38**	0.70	0.50	**0.32**	**0.35**
OLF	SO_4^{2-}	0.85	0.66	0.79	0.89	0.91
	NH_4^+	0.86	0.71	0.81	0.90	0.92
	NO_3^-	**0.27**	0.60	**0.44**	**0.21**	**0.33**

All the values were Spearman correlation coefficient (R), $R < 0.5$ were marked bold.

As illustrated in Table 3.5, in general, both NH_4^+ and SO_4^{2-} concentrations were strongly correlated with $PM_{2.5}$ mass concentration ($R \geq 0.51$) in four seasons with stronger correlation in summer than in fall, spring, and winter. The strong correlation between NH_4^+, SO_4^{2-} and $PM_{2.5}$ indicated the day-to-day covariation. As for the correlation between NO_3^- and $PM_{2.5}$ mass concentration, an inverse seasonal variation of correlation can be observed with stronger correlation in winter than in spring, fall, and summer. The seasonal variation of correlation between NO_3^- and $PM_{2.5}$ was attributed to the semi–volatile NH_4NO_3, higher T in summer favored the gas–phase HNO_3 and NH_3 instead of particle-phase NH_4NO_3 salts (Hildemann et al., 1984).

3.3.3. $PM_{2.5}$ mass closure analysis

The spatiotemporal variations of the $PM_{2.5}$ concentrations were attributed to the spatiotemporal variations in $PM_{2.5}$ chemical compositions, thus, the contributions of various compositions to the $PM_{2.5}$ mass concentration were investigated as well. To get an in-depth understanding about the reduction trend of $PM_{2.5}$ concentration, the $PM_{2.5}$ mass closure analysis was constructed and results were shown in Figure 3.10 and Figure 3.11.

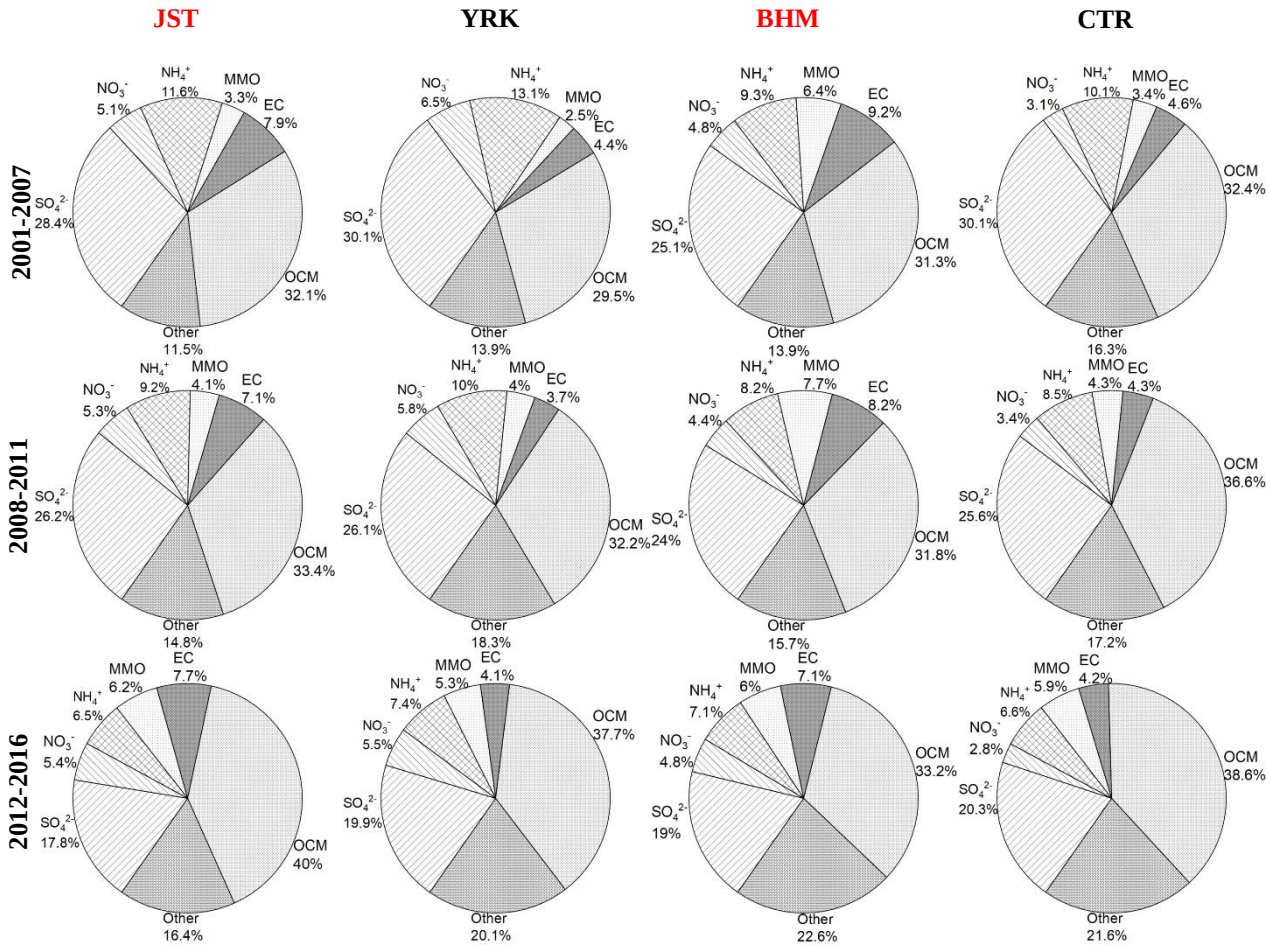

Figure 3.10. Mass distributions of $PM_{2.5}$ chemical compositions at the four inland SEARCH sites (Red label indicates urban sites; black label indicates rural sites)

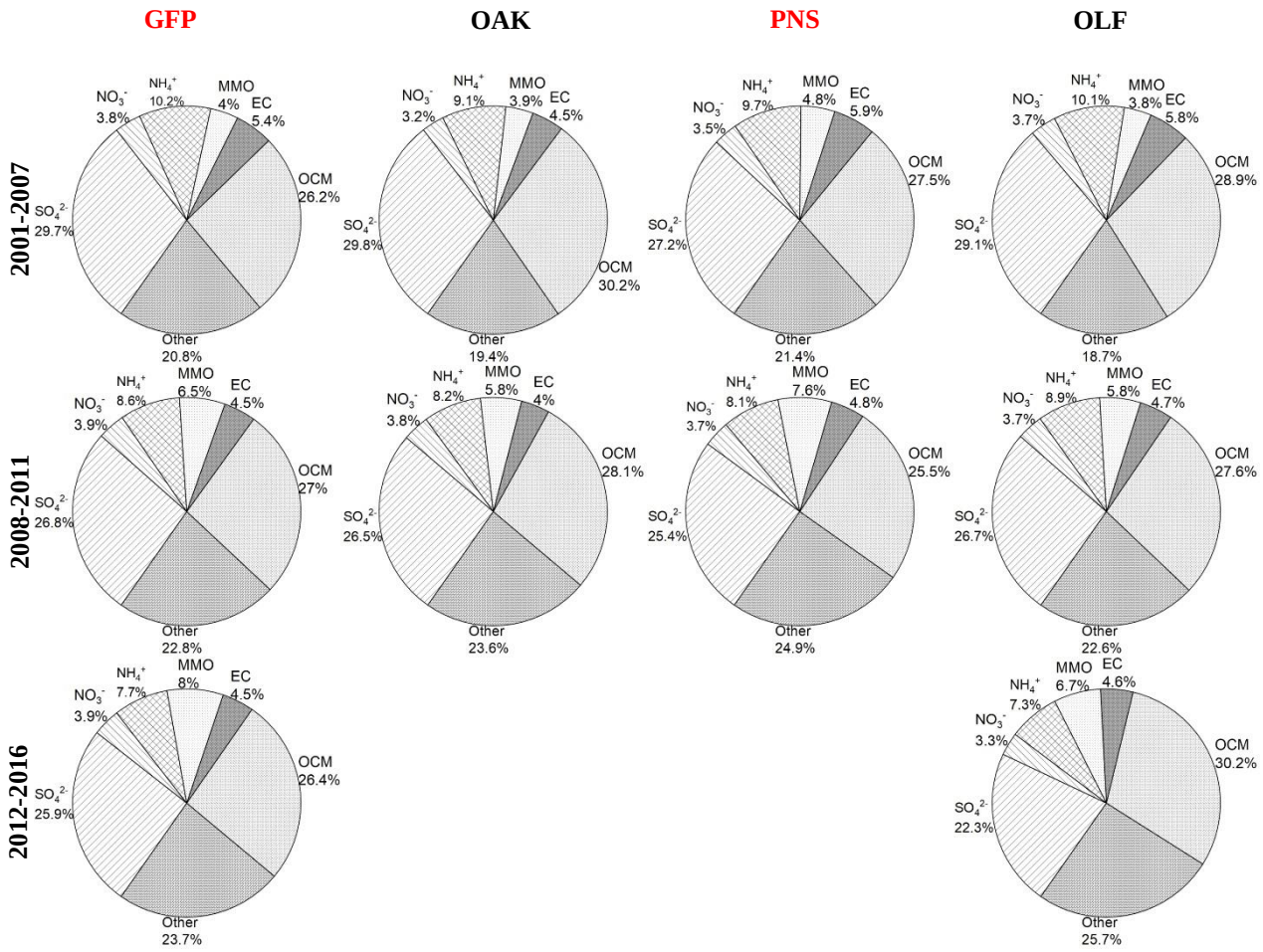

Figure 3.11. Mass distributions of $PM_{2.5}$ chemical compositions at the four coastal SEARCH sites (Red label indicates urban sites, black label indicates nonurban sites)

As it can be seen from Figures 3.10 and 3.11, at four inland sites, the sum of SO_4^{2-}, NO_3^- and NH_4^+ was the dominant composition of $PM_{2.5}$ before 2011, accounting for 39.2 % to 49.7 % of $PM_{2.5}$ in 2001-2007; 36.6 % to 41.9% of $PM_{2.5}$ in 2008-2011; 29.4% to 30.9% of $PM_{2.5}$ in 2012-2016. The OCM was the dominant composition of $PM_{2.5}$ after 2011 at four inland sites, accounting for 29.5% to 32.4% of $PM_{2.5}$ in 2001-2007; 31.8% to 36.6% of $PM_{2.5}$ in 2008-2011; 33.2% to 40% of $PM_{2.5}$ in 2012-2016. Among the 3 chemical compositions of $iPM_{2.5}$, SO_4^{2-} contributed the most to $PM_{2.5}$ concentration. The mass fractions of both SO_4^{2-} and NH_4^+ exhibited

a significant reduction trend in the 3 periods. While no significant reduction trend can be observed for the mass fraction of NO_3^-. Compared with four inland sites, the sum of SO_4^{2-}, NO_3^- and NH_4^+ was the dominant composition of $PM_{2.5}$ for the past 16 years and the OCM accounted for a smaller fraction of $PM_{2.5}$ mass at four coastal sites. In addition, the mass fractions of both SO_4^{2-} and NH_4^+ exhibited a reduction trend in the 3 periods at four coastal sites as well. The reduction of contributions of SO_4^{2-} and NH_4^+ in the past 16 years was indicative of the effective implementation of CAIR and CSAPR.

As for the seasonal variations of mass fractions of various chemical compositions of $PM_{2.5}$ (see Appendix B, Figures S3-S10), the mass fractions of SO_4^{2-} and NO_3^- exhibited an inverse seasonal variations at the eight sites. Following the seasonal variations of concentrations of SO_4^{2-} and NO_3^-, the mass fraction of SO_4^{2-} was higher in summer and lower in winter, while the mass fraction of NO_3^- was lower in summer and higher in winter. In contrast to the mass fractions of SO_4^{2-} and NO_3^-, no significant seasonal variation of mass fraction of NH_4^+ can be observed. The seasonal variations of mass fractions of SO_4^{2-} and NO_3^- was attributed to the difference in thermal characteristics of SO_4^{2-} and NO_3^- salts. The SO_4^{2-} salts were thermal stable compared with NO_3^- salts and more intense solar radiation in summer converted more SO_2 to H_2SO_4 (Seinfeld and Pandis, 2006).

3.3.4. Trends in extrema

The changes in the distributions of 24-hr average $PM_{2.5}$, SO_4^{2-}, NH_4^+ and NO_3^- in three periods are shown in Figures 3.12-3.15.

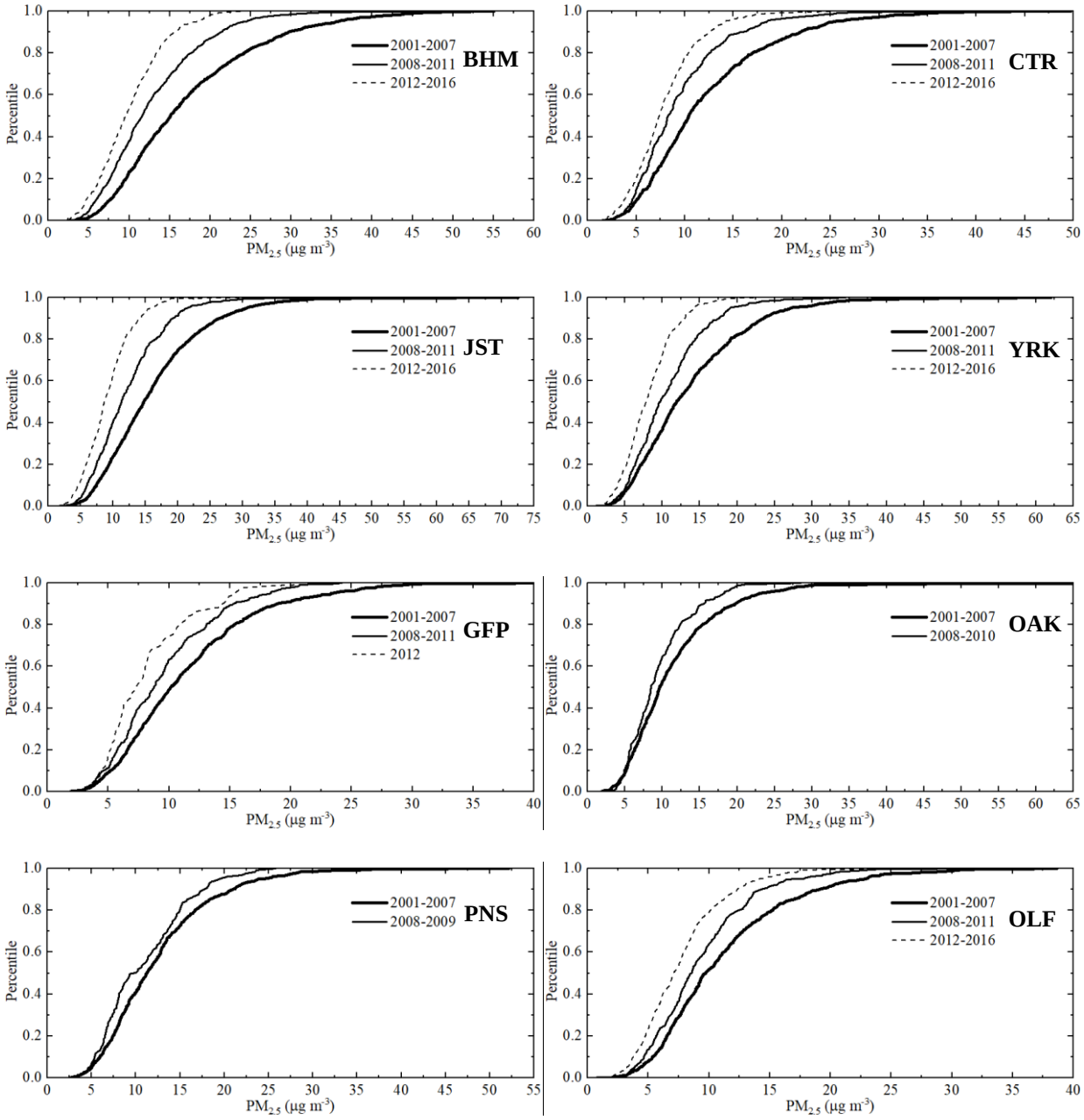

Figure 3.12. Statistical distributions of 24-hr average concentrations of $PM_{2.5}$ from 2001 to 2016

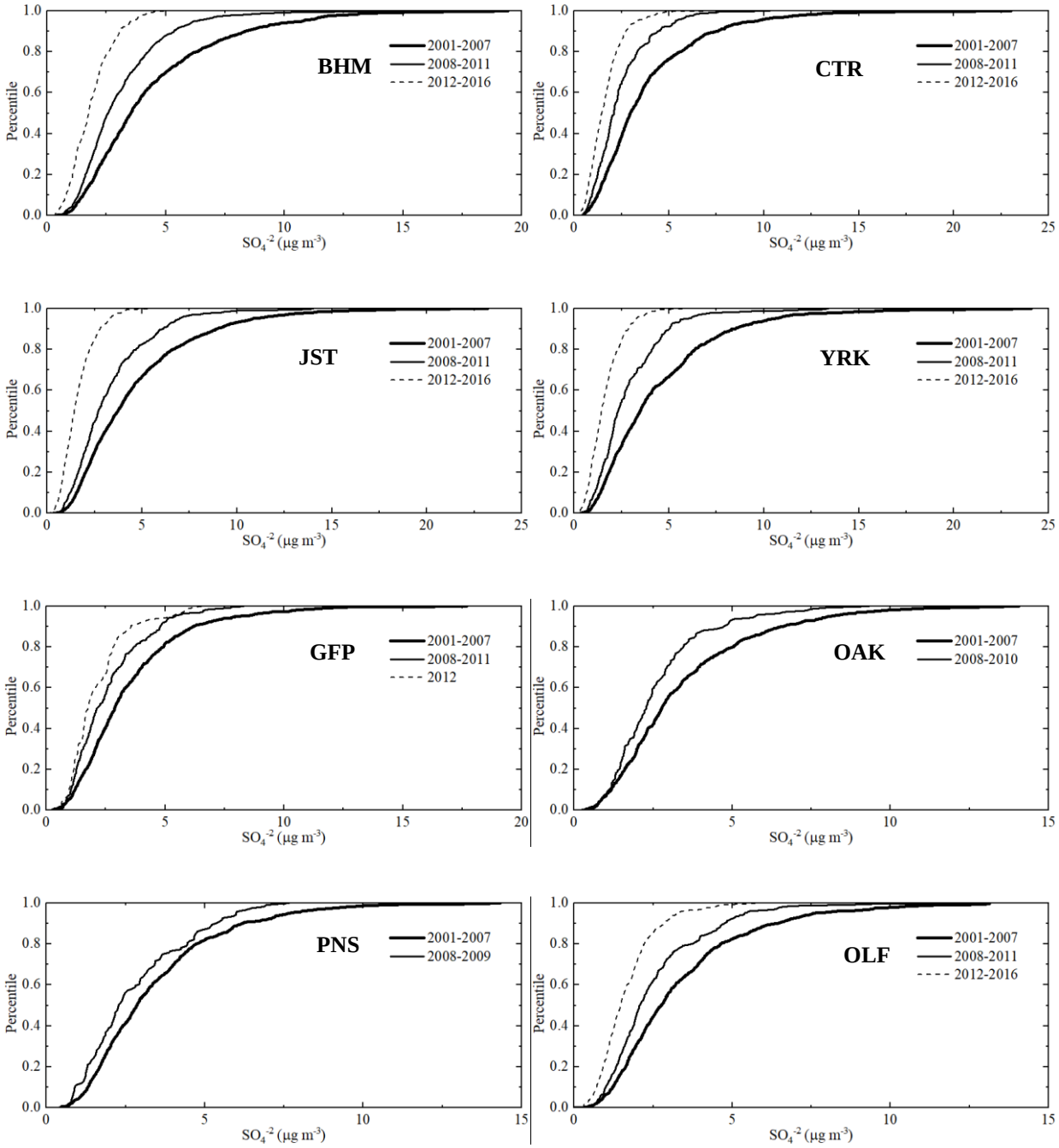

Figure 3.13. Statistical distributions of 24-hr average concentrations of SO_4^{2-} from 2001 to 2016

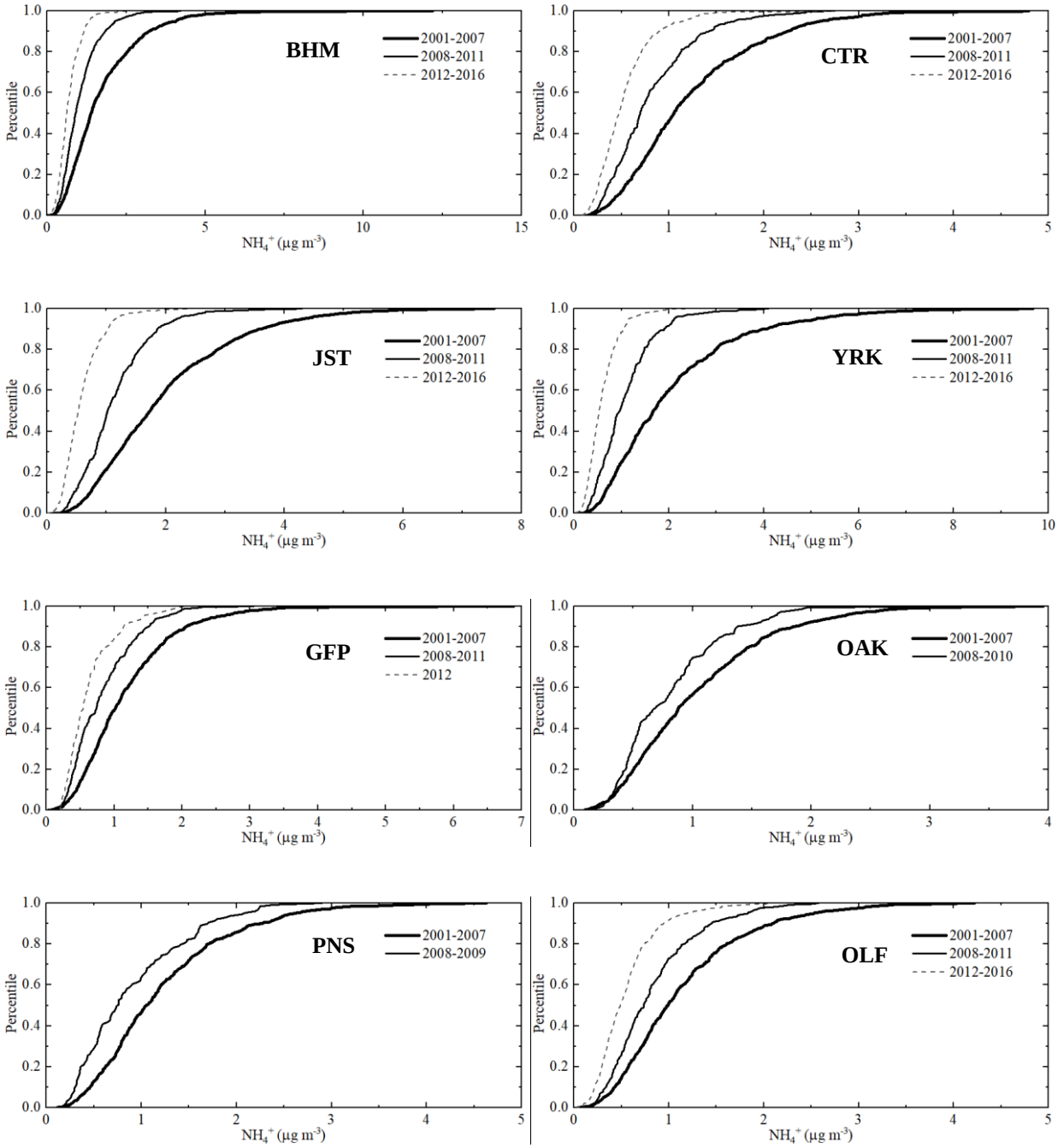

Figure 3.14. Statistical distributions of 24-hr average concentrations of NH_4^+ from 2001 to 2016

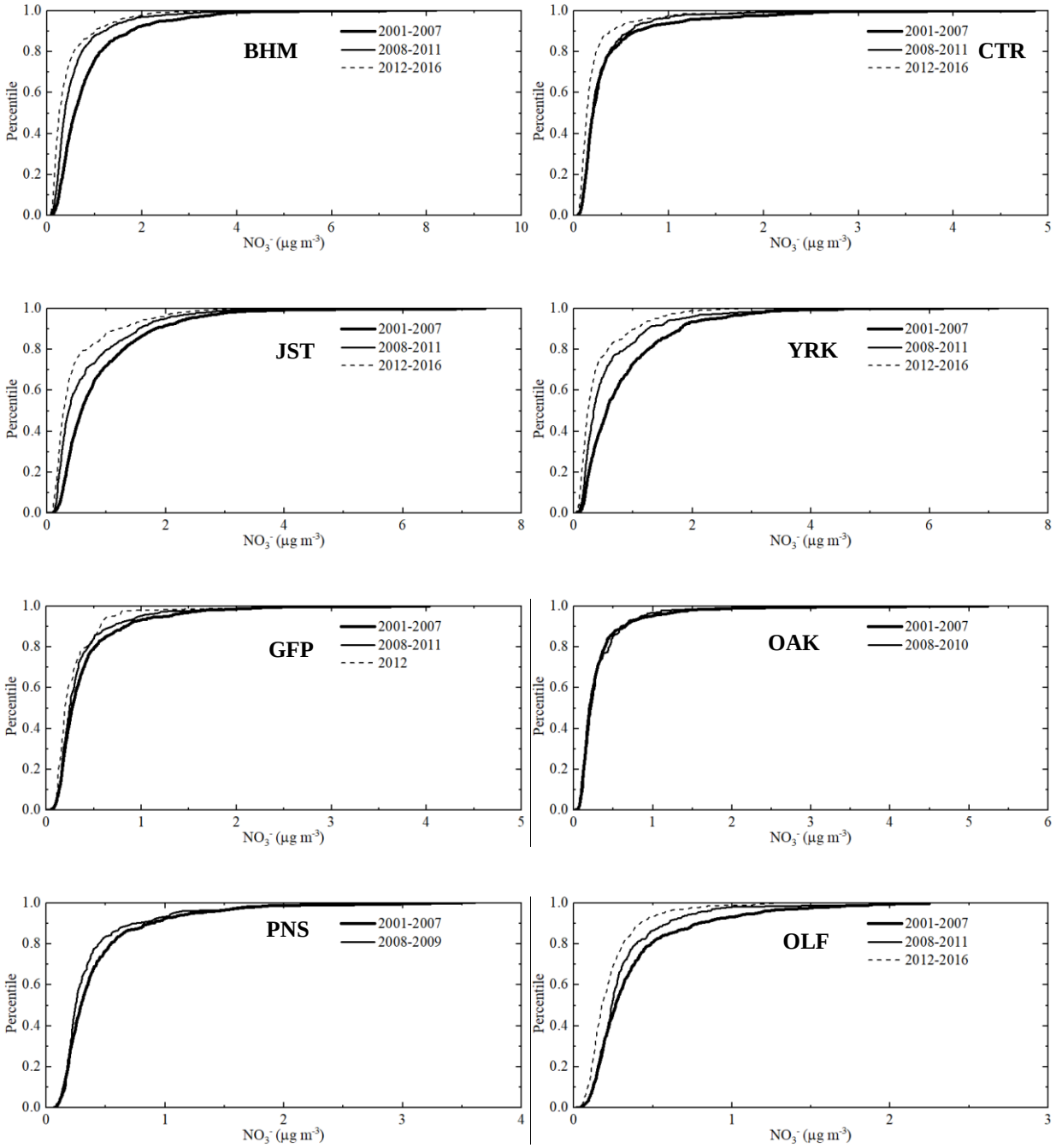

Figure 3.15. Statistical distributions of 24-hr average concentrations of NO_3^- from 2001 to 2016

As it can be seen from Figures 3.12-3.15, the comparisons among eight sites for the high concentrations of $PM_{2.5}$, SO_4^{2-}, NH_4^+ and NO_3^- indicates the spatial variation. The high concentrations of $PM_{2.5}$, SO_4^{2-}, NH_4^+ and NO_3^- occurred more frequently at the urban sites than the nonurban sites, and more frequently at the inland sites than the coastal sites. The spatial

variation of high concentrations was consistent with the spatial variation of annual average concentrations (Figure 3.1), which may also be explained by the atmospheric transport and spatial heterogeneity of emissions sources. Moreover, not only the monthly average or annual average concentrations of $PM_{2.5}$, SO_4^{2-}, NH_4^+ and NO_3^- were decreased in the past 16 years, fewer high concentrations of $PM_{2.5}$, SO_4^{2-}, NH_4^+, and NO_3^- at the eight sites occurred over time. The primary and secondary 24-hr average $PM_{2.5}$ NAAQS standard are 35 μg m^{-3} (98^{th} percentile, averaged over 3 years), Figure 3.12 indicates that 24-hr average $PM_{2.5}$ concentrations were all below the latest NAAQS standard in 2012-2016 at the eight sites. The reduction in the high concentrations was the important evidence of air quality improvement in the Southeastern U.S. over the past 16 years.

3.3.5. Multiple Linear Regression model

The effects of the various predictor variables on the response variable (NH_4^+) were estimated using regression analysis. The MLR models for the response of NH_4^+ to various factors in two periods (2008-2011 and 2012-2016) at six sites are shown in Tables 3.6-3.14.

Table 3.6. The summary of final MLR model coefficients at the JST site from 2010 to 2011

Predictors	Coefficients	SE	t value	Pr > |t|
Intercept (β_0)	0.08	0.04	1.97	0.054
SO_4^{2-} (β_1)	0.31	0.01	32.79	$< 2 * 10^{-16}$
NO_3^- (β_2)	0.25	0.03	7.91	$5.57 * 10^{-11}$
$(NO_3^- - 0.66)^2$ (β_3)	0.02	0.01	3.43	0.001
Mg^{2+} (β_4)	-6.69	2.95	-2.27	0.026

Residual standard error: 0.1104 on 62 degrees of freedom. Multiple R-squared: 0.9625. Adjusted R-squared: 0.96. F-statistic: 397.4 on 4 and 62 DF, p-value: $< 2.2 * 10^{-16}$.

Table 3.7. The summary of final MLR model coefficients at the JST site from 2012 to 2016

Predictors	Coefficients	SE	t value	Pr > |t|
Intercept (β_0)	0.1967	0.041	4.78	$5.64 * 10^{-6}$
SO_4^{2-} (β_1)	0.35	0.0074	46.74	$< 2 * 10^{-16}$
NO_3^- (β_2)	0.0052	0.0286	0.18	0.86
$(NO_3^- - 0.45)^2$ (β_3)	0.11	0.01	10.57	$< 2 * 10^{-16}$
T (β_4)	-0.013	0.0021	-6.08	$1.88 * 10^{-8}$
Mg^{2+} (β_5)	-1.15	1.68	-0.69	0.49
$(Mg^{2+} - 0.0077)^2$ (β_6)	-292.8	161.7	-1.81	0.07
NH_3 (β_7)	-0.06	0.027	-2.22	0.03
$(NH_3 – 1.31)^2$ (β_8)	-0.0297	0.014	-2.16	0.03
$T:NH_3$ (β_9)	0.0055	0.0013	4.20	$5.53 * 10^{-5}$

Residual standard error: 0.05489 on 107 degrees of freedom. Multiple R-squared: 0.9749. Adjusted R-squared: 0.9 7. F-statistic: 462 on 9 and 107 DF, p-value: $< 2.2 * 10^{-16}$.

Table 3.8. The summary of final MLR model coefficients at the YRK site from 2008 to 2011

Predictors	Coefficients	SE	t value	Pr > |t|
Intercept (β_0)	0.08	0.033	2.39	0.018
SO_4^{2-} (β_1)	0.33	0.009	37.11	$< 2 * 10^{-16}$
NO_3^- (β_2)	0.25	0.018	13.64	$< 2 * 10^{-16}$
$(SO_4^{2-} - 3.27)^2$ (β_3)	-0.008	0.001	-5.74	$4.5 * 10^{-8}$
Mg^{2+} (β_4)	-3.83	1.45	-2.65	0.0089

Residual standard error: 0.1672 on 161 degrees of freedom. Multiple R-squared: 0.9405. Adjusted R-squared: 0.94. F-statistic: 636.3 on 4 and 161 DF, p-value: $< 2.2 * 10^{-16}$.

Table 3.9. The summary of final MLR model coefficients at the YRK site from 2012 to 2016

Predictors	Coefficients	SE	t value	Pr > |t|
Intercept (β_0)	0.028	0.027	1.03	0.31
SO_4^{2-} (β_1)	0.38	0.013	29.58	$< 2 * 10^{-16}$
NO_3^- (β_2)	0.067	0.032	2.12	0.036
$(NO_3^- - 0.41)^2$ (β_3)	0.155	0.028	5.62	$1.23 * 10^{-7}$
Na^+ (β_4)	-0.54	0.132	-4.1	$7.48 * 10^{-5}$
T (β_5)	-0.0025	0.00149	-1.67	0.097
$(Na^+ - 0.04)^2$ (β_6)	0.71	0.29	2.43	0.0166
HNO_3 (β_7)	-0.045	0.027	-1.66	0.0995
K^+(β_8)	0.87	0.38	2.31	0.0226
SO_4^{2-}:T (β_9)	-0.0029	0.000684	-4.24	$4.39 * 10^{-5}$
T:HNO_3 (β_{10})	0.0045	0.0014	3.25	0.00149

Residual standard error: 0.05419 on 122 degrees of freedom. Multiple R-squared: 0.9732. Adjusted R-squared: 0.97. F-statistic: 443.7 on 10 and 122 DF, p-value: $< 2.2 * 10^{-16}$.

Table 3.10. The summary of final MLR model coefficients at the BHM site in 2011

Predictors	Coefficients	SE	t value	Pr > |t|
Intercept (β_0)	-0.0182	0.083	-0.219	0.83
SO_4^{2-} (β_1)	0.316	0.0132	23.95	$5.86 * 10^{-14}$
NO_3^- (β_2)	0.489	0.0659	7.42	$1.46 * 10^{-6}$
$(T - 18.23)^2$ (β_3)	0.00052	0.000196	2.64	0.018
$(Mg^{2+} - 0.014)^2$ (β_4)	-568.8	272.6	-2.09	0.053
$(NO_3^- - 0.68)^2$ (β_5)	-0.058	0.027	-2.15	0.047
Ca^{2+} (β_6)	3.85	0.904	-4.26	$5.96 * 10^{-4}$
NH_3 (β_7)	0.067	0.0345	1.95	0.07
$(NH_3 - 1.63)^2$ (β_8)	-0.063	0.0235	-2.69	0.016
$(Ca^{2+} - 0.052)^2$ (β_9)	37.05	8.998	4.12	0.00081
$(HNO_3 - 1.23)^2$ (β_{10})	0.110	0.041	2.60	0.019
$(Cl^- - 0.16)^2$ (β_{11})	0.287	0.766	0.374	0.71
T (β_{12})	-0.00353	0.00484	-0.729	0.48
Mg^{2+} (β_{13})	-0.0106	2.55	-0.004	0.997
HNO_3 (β_{14})	-0.0108	0.0458	-0.235	0.82
Cl^- (β_{15})	0.18	0.249	0.721	0.48

Residual standard error: 0.05312 on 16 degrees of freedom. Multiple R-squared: 0.9916. Adjusted R-squared: 0.98.

F-statistic: 126.5 on 15 and 16 DF, p-value: $1.008 * 10^{-13}$.

Table 3.11. The summary of final MLR model coefficients at the BHM site from 2012 to 2016

Predictors	Coefficients	SE	t value	Pr > |t|
Intercept (β_0)	0.248	0.044	5.68	$4.22 * 10^{-7}$
SO_4^{2-} (β_1)	0.292	0.024	12.09	$< 2 * 10^{-16}$
T (β_2)	-0.012	0.002	-6.17	$6.28 * 10^{-8}$
$(NO_3^- - 0.34)^2$ (β_3)	0.081	0.013	6.12	$7.81 * 10^{-8}$
$(Cl^- - 0.102)^2$ (β_4)	0.518	0.294	1.76	0.0833
Ca^{2+} (β_5)	-0.537	0.194	-2.77	0.0075
NO_3^- (β_6)	0.043	0.047	0.914	0.3642
Cl^- (β_7)	0.037	0.124	0.301	0.7645
SO_4^{2-}:T (β_8)	0.0023	0.001	2.43	0.0181

Residual standard error: 0.04904 on 60 degrees of freedom. Multiple R-squared: 0.9884. Adjusted R-squared: 0.99. F-statistic: 641.6 on 8 and 60 DF, p-value: $< 2.2 * 10^{-16}$.

Table 3.12. The summary of final MLR model coefficients at the CTR site from 2012 to 2016

Predictors	Coefficients	SE	t value	Pr > |t|
Intercept (β_0)	0.0049	0.012	0.403	0.687
SO_4^{2-} (β_1)	0.32	0.0057	55.84	$< 2 * 10^{-16}$
NO_3^- (β_2)	0.21	0.017	12.21	$< 2 * 10^{-16}$
Mg^{2+} (β_3)	-6.63	0.54	-12.26	$< 2 * 10^{-16}$
NH_3 (β_4)	0.14	0.028	5.12	$8.31 * 10^{-7}$
$(SO_4^{2-} - 1.59)^2$ (β_5)	-0.0169	0.0039	-4.36	$2.24 * 10^{-5}$

Residual standard error: 0.05129 on 168 degrees of freedom. Multiple R-squared: 0.9648. Adjusted R-squared: 0.96. F-statistic: 921.2 on 5 and 168 DF, p-value: $< 2.2 * 10^{-16}$.

Table 3.13. The summary of final MLR model coefficients at the OAK site in 2010

Predictors	Coefficients	SE	t value	Pr > |t|
Intercept (β_0)	0.103	0.054	1.89	0.068
SO_4^{2-} (β_1)	0.36	0.014	26.28	$< 2 * 10^{-16}$
T (β_2)	-0.0092	0.002	-4.45	0.0001
Mg^{2+} (β_3)	-5.41	1.04	-5.21	$1.19 * 10^{-5}$
$(SO_4^{2-} - 2.47)^2$ (β_4)	-0.02	0.0076	-2.62	0.013
NH_3 (β_5)	0.16	0.055	2.97	0.0056
NO_3^- (β_6)	0.19	0.054	3.52	0.0013
$(T - 17.46)^2$ (β_7)	-0.00028	0.00015	-1.86	0.073

Residual standard error: 0.06706 on 31 degrees of freedom. Multiple R-squared: 0.9739. Adjusted R-squared: 0.97. F-statistic: 165.5 on 7 and 31 DF, p-value: $< 2.2 * 10^{-16}$.

Table 3.14. The summary of final MLR model coefficients at the OLF site from 2013 to 2016

Predictors	Coefficients	SE	t value	Pr > |t|
Intercept (β_0)	-0.0013	0.024	-0.054	0.96
SO_4^{2-} (β_1)	0.33	0.0075	43.69	$< 2 * 10^{-16}$
NO_3^- (β_3)	0.35	0.061	5.74	$1.36 * 10^{-7}$
Mg^{2+} (β_2)	-4.69	0.88	-5.30	$8.78 * 10^{-7}$
$(Ca^{2+} - 0.03)^2$ (β_4)	-19.02	7.90	-2.41	0.0181
$(NO_3^- - 0.26)^2$ (β_5)	-0.283	0.0899	-3.16	0.0022
$(NH_3 - 0.45)^2$ (β_6)	0.13	0.0819	1.59	0.1153
Ca^{2+} (β_7)	-0.522	0.602	-0.868	0.3879
NH_3 (β_8)	0.0547	0.0425	1.288	0.2013

Residual standard error: 0.0681 on 87 degrees of freedom. Multiple R-squared: 0.9635. Adjusted R-squared: 0.96. F-statistic: 287.2 on 8 and 87 DF, p-value: $< 2.2 * 10^{-16}$.

The interaction terms may cause serious multi-collinearity problem, which provides redundant information (Montgomery et al., 2012), thus, the model diagnostics may exclude the

interaction terms when variance inflation factor (VIF) is greater than 10. The selection of predictor variables varied at different sites in different periods.

As it can be seen from Tables 3.6-3.14, in general, both SO_4^{2-} and NO_3^- are included in the regression models at six sites in two periods. The $iPM_{2.5}$ mainly consists of NH_4^+ salts, and most of the NH_4^+ cations are tied up with SO_4^{2-} and NO_3^- anions. The coefficients for both SO_4^{2-} and NO_3^- are positive, which indicates the positive correlation between cation-(NH_4^+) and anions-(SO_4^{2-} & NO_3^-). The positive regression coefficients (0.29-0.38) for SO_4^{2-} are greater than the coefficients for all the other predictor variables. The dominance of particle-phase SO_4^{2-} salts led to the significantly positive relationship between NH_4^+ and SO_4^{2-}, the changes in SO_4^{2-} can cause corresponding changes in NH_4^+. There are some centered quadratic terms included in the model as well, the quadratic terms indicate that the direction of relationship between NH_4^+ and SO_4^{2-}, NO_3^- may change as SO_4^{2-} and NO_3^- concentrations change. The complex relationship between NH_4^+ and SO_4^{2-}, NO_3^- may be caused by reactions between NH_3 and H_2SO_4, HNO_3, the dynamic changes of particle–phase SO_4^{2-}, NO_3^- may also change the dynamic reactions of NH_3 and various acidic gases. For example, the free NH_3 from the reduction of SO_4^{2-} may react with HNO_3 to form NH_4NO_3.

As for the gas-phase NH_3, the BIC step-wise model selection method doesn't include NH_3 in the MLR model at the JST site in 2010-2011, at the YRK site in 2008-2011 and 2012-2016, and at the BHM site in 2012-2016. The exclusion of NH_3 indicates that NH_3 may not be able to limit the formation of NH_4^+ salts at these three sites. Specifically, NH_3 is excluded from

the regression model from 2008 to 2016 at the YRK site. The NH_3 emissions from nearby AFOs contributed to the abundant NH_3 gas at the YRK site, the NH_3 was in excess of fully neutralizing acidic gases. While for CTR site in 2012-2016, OAK site in 2010, and OLF site in 2013-2016, the NH_3 is included in the regression model and the coefficients are positive. Especially, at the OAK site, coefficient of NH_3 is 0.16, which is higher than the other sites. The positive coefficients suggest that the higher NH_3 may lead to increased formation of NH_4^+ salts at these sites.

As for the gas-phase HNO_3, it's included in the regression model at the YRK site in 2012-2016, and at the BHM site in 2011, and the regression coefficients for HNO_3 in these two models are negative. The semi-volatile characteristic of NH_4NO_3 may explain the negative coefficient. Under certain ambient condition such as high T and low RH, the NH_4NO_3 may decompose into gas–phase NH_3 and HNO_3, the increase in gas–phase HNO_3 led to the decrease in NH_4^+. The interaction term-T:HNO_3 at the YRK site may indicate the dependence of the formation of NH_4NO_3 on ambient condition.

As for ambient meteorological condition, T and RH, only T is included in the regression models at the JST site in 2012-2016, at the YRK site in 2012-2016, at the BHM site in 2011 and 2012-2016, and at the OAK site in 2010. The RH is excluded from all the regression models. The coefficients for T are all negative, which indicates that the increase of T leads to the decrease of NH_4^+.

As for the NVCs and Cl^-, although the concentrations are lower compared with the other gas– and particle–phase species, either Mg^{2+}, Na^+ or Cl^- is included in the regression models, this indicates that the NVCs and Cl^- are important factors affecting the NH_4^+ concentration.

3.4. Conclusions

In this research, the spatial and temporal variations of $PM_{2.5}$ mass closure and $iPM_{2.5}$ concentrations were analyzed in the Southeastern U.S. using SEARCH Network data from 2001 to 2016. The results indicate that the $PM_{2.5}$ concentrations exhibited a significant reduction trend from 2001 to 2016 at the eight sites of SEARCH. In general, $PM_{2.5}$ concentrations were higher in urban sites than nonurban sites, and higher in inland sites than coastal sites. The spatial heterogeneity of $PM_{2.5}$ may be caused by the atmospheric transport, various chemical reactions and spatial distribution of primary and secondary $PM_{2.5}$ emissions sources at specific sites. The concentrations of $PM_{2.5}$, SO_4^{2-} and NH_4^+ exhibited the same seasonal variation, higher in summer and lower in winter, while NO_3^- concentration exhibited an inverse seasonal variation, higher in winter and lower in summer. The seasonal variation of $PM_{2.5}$ became less intense in later years (2012-2016). The concentrations of NH_4^+, SO_4^{2-} and NO_3^- were higher at four inland sites than coastal sites and higher in urban sites than the nonurban sites. Specifically, the concentrations of NH_4^+, SO_4^{2-} and NO_3^- at the agricultural rural site–YRK were higher than the other sites, except two urban sites–JST and BHM. The significant NH_3 emissions from AFOs at the YRK site may explain the higher $iPM_{2.5}$ concentrations because the abundant NH_3 facilitates the reaction of NH_3 with acidic gases. Furthermore, the strong correlation between NH_4^+, SO_4^{2-} and $PM_{2.5}$ indicated the day-to-day covariation. At four inland sites, the $iPM_{2.5}$ was the dominant composition of $PM_{2.5}$ before 2011, while OCM was the dominant composition of $PM_{2.5}$ after 2011. At four coastal sites, the $iPM_{2.5}$ was the dominant composition of $PM_{2.5}$ over the past 16 years. Moreover, the reduction in the high concentrations of $PM_{2.5}$ was observed as well. The BIC step-wise model selection determined the best fitting MLR model to predict NH_4^+ at six

sites, there is a strong positive correlation between cation- NH_4^+ and anions- SO_4^{2-} & NO_3^-. The NH_3 is excluded from the regression model at the YRK site due to the abundant NH_3 emitted from AFOs. The NVCs and Cl^- are the significant factors affecting NH_4^+ concentrations. The spatial variation of $PM_{2.5}$ mass closure and $iPM_{2.5}$ may be due to the spatial heterogeneity of various emission sources and fate and transport of various precursor gases. In addition, the temporal variation of $PM_{2.5}$ mass closure and $iPM_{2.5}$ is the important evidence of air quality improvement in the Southeastern U.S. over the past 16 years.

CHAPTER 4: PERFORMANCE OF ISORROPIA II FOR PREDICTING INORGANIC AEROSOLS IN THE SOUTHEASTERN U.S.

Abstract

As a significant fraction of atmospheric $PM_{2.5}$, secondary inorganic $PM_{2.5}$ ($iPM_{2.5}$) is formed through the gas–phase ammonia (NH_3) and particle–phase ammonium (NH_4^+) partitioning. While the partitioning of $NH_3 - NH_4^+$ may be simulated by thermodynamic equilibrium models, disagreement between models predictions and measurements have been realized and the applicability of the model in simulation $iPM_{2.5}$ formation under different conditions has not been well studied. This research was to investigate the applicability of one type of thermodynamic equilibrium models, named ISORROPIA II, under different atmospheric conditions and geographic locations. Based upon the field measurements at the Southeastern Aerosol Research and Characterization (SEARCH) Network, the performance of ISORROPIA II was assessed under different temperature-RH-model setups in urban and rural locations. The impact of organic aerosol (OA) on the partitioning of $NH_3 - NH_4^+$ was also evaluated. Results of this research indicate that the inclusion of nonvolatile cations (NVCs) in the model input is necessary to improve the model performance. Under high temperature (> 10 ºC) & low RH (< 60%) conditions, ISORROPIA II tends to over predict nitric acid (HNO_3) concentration and under predict nitrate (NO_3^-) concentration. The predominance of one phase (aerosol or gas) of semi-volatile compound can amplify the small errors in the model prediction of the other phase. The model with stable and metastable setups may also perform differently under different temperature-RH conditions. Metastable model setup performs better under high temperature (> 10 ºC) & low RH (< 60%) conditions, while stable model setup performs better under low temperature (< 5 ºC) condition. Furthermore, higher time resolution (e.g., 5-min) data may be

required to investigate the impact of OA on the thermodynamic equilibrium partitioning of NH_3–NH_4^+. This research provides systematic assessment of ISORROPIA II model under different conditions. Future studies using ISORROPIA II for the prediction of $NH_3 - NH_4^+$ partitioning should consider the inclusion of NVCs, the under/over predictions of NO_3^-/HNO_3, the selection of stable/metastable model setups under different temperature-RH conditions, spatiotemporal variations of $iPM_{2.5}$ chemical compositions.

4.1. Introduction

Fine particulate matter (i.e., $PM_{2.5}$) has gained attention due to its adverse health effects, visibility degradation, and the impacts on the Earth's ecosystems and radiative balance (USEPA, 2018d; Pui et al., 2014; Xing et al., 2016). Secondary inorganic $PM_{2.5}$ ($iPM_{2.5}$) constitutes a significant fraction of atmospheric $PM_{2.5}$ mass concentration (Bell et al., 2007; Hand et al., 2012) and the chemistry of secondary $iPM_{2.5}$ formation has been investigated for decades (Allen and Harrison, 1989; Hildemann et al., 1984; Stelson and Seinfeld, 1982; Shiraiwa et al., 2013). The formation of the secondary $iPM_{2.5}$ may be characterized by thermodynamic equilibrium of gas–phase ammonia (NH_3) and particle–phase ammonium (NH_4^+) partitioning (Seinfeld and Pandis, 2006). It is important to establish a holistic understanding of the formation of secondary $iPM_{2.5}$ such that the regional impact of $iPM_{2.5}$ may be fully understood. Secondary $iPM_{2.5}$ is usually formed through chemical reactions between different precursor gases such as NH_3, nitric acid (HNO_3) and sulfuric acid (H_2SO_4). In general, NH_3 gas is directly emitted, while HNO_3 and H_2SO_4 are mainly formed through (photo)chemical reactions during atmospheric transformation of sulfur dioxide (SO_2) and nitrogen oxides (NO_x) ($NO_x = NO + NO_2$). It was reported that $iPM_{2.5}$ mainly consists of ammonium nitrate (NH_4NO_3), ammonium sulfate ($(NH_4)_2SO_4$) and

ammonium chloride (NH_4Cl) (Saxena et al., 1986; Tanner et al., 1979; Tolocka et al., 2001; Walker et al., 2004). The partitioning of total available ammonia ($TA = NH_3 + NH_4^+$) into gas– and particle–phase is usually assumed to be in the thermodynamic equilibrium state such that thermodynamic model can be used to estimate the physical phases (gas, liquid, solid) and interactions of different precursor gases of $iPM_{2.5}$ (Ansari and Pandis, 1999a, Zhang et al., 2000). However, the non-equilibrium state may exist in ambient air due to surface heterogeneity (Ravishankara, 1997), the mass transport limitation between different sizes of particles (Wexler and Seinfeld, 1992) and the long timescale to reach equilibrium state for super-micron particles (Moya et al., 2002). Consequently, the applicability of thermodynamic equilibrium theory for modeling the $NH_3 - NH_4^+$ partitioning may be challenged under certain atmospheric condition, when nonequilibrium state exist.

In this study, we explore impacts of various factors, e.g., organic materials, ambient T and RH, model setups, and nonvolatile cations (NVCs) on the performance of ISORROPIA II model. This research aims to investigate the applicability of ISORROPIA II under different T–RH–model setup–locations for the prediction of inorganic aerosols.

4.2. Methodology

4.2.1. Monitoring network description

The Southeastern Aerosol Research and Characterization (SEARCH) Network is a long-term air quality monitoring network established in the Southeastern U.S. (AL, FL, GA, and MS) (EPRI, 2008). The SEARCH Network aimed to address questions regarding tropospheric ozone (O_3) formation, $PM_{2.5}$ and PM_{10} mass and chemical compositions, mercury (Hg) pollution, and visibility degradation. The network provides high-quality field measurements of $PM_{2.5}$ mass and chemical compositions. More specifically, the continuous measurements of $iPM_{2.5}$ chemical

compositions and its precursor gases provides information with high time resolution to investigate the partitioning of gas– and particle–phase pollutants at eight sites covering agricultural rural areas and urban regions.

Under the SEARCH, the concentrations of $iPM_{2.5}$ chemical compositions and its precursor gases were measured at four paired urban/nonurban sites, named as JST/YRK, BHM/CTR, GFP/OAK, and PNS/OLF. The measurements started from 1998/1999 and ended in 2016. These eight monitoring sites are shown in Figure 1.4.

The onsite measurements provided processed 1–hr average concentrations of precursor gases, $iPM_{2.5}$ chemical compositions, and meteorological conditions. In addition, the 24-hr average measurements of $iPM_{2.5}$ chemical compositions were also performed. The details of the measurements made at the eight sites are reported in Hansen et al. (2003) and summarized in Table 1.4.

4.2.2. Data cleaning and processing

Some of the reported gas– and particle–phase measurements were found to be negative or below the instrument's detection limit. As the model input can't be negative, all the negative values were excluded from the analysis. While those values below the detection limits were included in the data analysis (Cohen and Ryan, 1989).

During the SEARCH data collection period, rain events happened that led to pollutant wet depositions. The precipitation led to rapid decrease in the concentrations of gas– and particle–phase pollutants. Thus, the hourly and daily measurements in rain events are not suitable to assess the performance of the thermodynamic model. In data reduction process, the hours and days with precipitation were flagged and excluded from the analysis.

4.2.3. Thermodynamic model assessment

We explore the impact of factors including ambient T and RH, stable/metastable model setups, and NVCs on the performance of ISORROPIA II. Comparison of model predicted concentrations and measurements were performed to check the over or underestimations of ISORROPIA II under various conditions and to identify the possible reasons. In addition, the impact of OA on the thermodynamic equilibrium partitioning of $NH_3 - NH_4^+$ was evaluated as well. Model performance evaluation at eight sites exhibited the similar trend, thus, only the results at the YRK and JST sites are reported in this chapter.

The impacts of T and RH on the model performance were assessed using the following experimental design. The T and RH scenarios were broken down into various 5 °C T × 10% RH conditions, under each condition, the model–predicted concentrations of NH_3, NH_4^+, HNO_3, NO_3^-, and $iPM_{2.5}$ ($SO_4^{2-} + NH_4^+ + NO_3^-$) were assessed against hourly measurements of gas-phase and particle-phase pollutants.

The gas–phase NH_3 and HNO_3 molar fractions under different T–RH conditions were also analyzed. The gas–phase NH_3 molar fraction ($[NH_3]/[NH_x]$) and gas–phase HNO_3 molar fraction ($[HNO_3]/[TN]$) are defined in the following equations:

$$[NH_3]/[NH_x] = \frac{[NH_3]}{[NH_3]+[NH_4^+]} \quad (4\text{-}1)$$

$$[HNO_3]/[TN] = \frac{[HNO_3]}{[HNO_3]+[NO_3^-]} \quad (4\text{-}2)$$

where $[NH_x]$ is the sum of molar concentrations (μmol m^{-3}) of gas–phase NH_3 and particle–phase NH_4^+, [TN] is the sum of molar concentrations (μmol m^{-3}) of gas–phase HNO_3 and

particle–phase NO_3^-.

The ISORROPIA II is usually utilized to predict the gas–particle partitioning given the concentrations of precursor gases, thus forward mode was used as default in this study. The performance of ISORROPIA II with thermodynamically stable and metastable setups under different T and RH conditions was assessed by comparing forward model predictions with field measurements to check the applicability of the model under different conditions.

The hourly measurements only included the concentrations of NH_3, NH_4^+, HNO_3, NO_3^-, and SO_4^{2-}. The disagreement in the predictions of gas– and particle–phase pollutants may be due to the lack of other cations/anions measurements. Thus, the model performances of ISORROPIA II in simulating NH_3, HNO_3, NH_4^+ and NO_3^- under different gas ratios (GR) and measured charge balance (MCB) were analyzed. The GR characterizes the neutralization degree of NH_3 by acidic gases and MCB is the molar difference of cation (NH_4^+) and anions (SO_4^{2-} & NO_3^-). More specifically, GR and charge balance can be defined as:

$$GR = \frac{[TA] - 2[TS]}{[TN]} \qquad (4\text{-}3)$$

$$MCB = [NH_4^+] - 2\times[SO_4^{2-}] - [NO_3^-] \qquad (4\text{-}4)$$

where, TA is total available ammonia (= NH_3 + NH_4^+), TS is total sulfuric acid (= H_2SO_4 + HSO_4^- + SO_4^{2-}) and TN is total available nitric acid (= HNO_3 + NO_3^-).

In terms of the impact of NVCs inclusion on the model performance, only 24-hr average data of K^+, Ca^{2+}, Mg^{2+}, and Na^+ were available under SEARCH Network. Thus, 24-hr average data of $iPM_{2.5}$ chemical composition and its precursor gases were used to assess the impact of

NVCs inclusion/exclusion on the model performance. For each site, two datasets were used to run ISORROPIA II, one was NH_3–NH_4^+–HNO_3–NO_3^-–SO_4^{2-}–Cl^- system, the other one was Ca^{2+}–Mg^{2+}–K^+–Na^+–HCl–Cl^-–NH_3–NH_4^+–HNO_3–NO_3^-–SO_4^{2-} system.

If $iPM_{2.5}$ may be coated with organic film, which retards the uptake of NH_3 to react with H_2SO_4, the higher OA/SO_4^{2-} mass ratio may lead to lower probability of the reaction between NH_3 and H_2SO_4 (Liggio et al., 2011). The neutralization of H_2SO_4 by NH_3 was characterized by molar ratio R.

$$R = \frac{[NH_4^+]-[NO_3^-]-[Cl^-]}{[SO_4^{2-}]} \qquad (4\text{-}5)$$

The postulated organic film hypothesis was examined by testing if there was a significant correlation between molar ratio R and OA/SO_4^{2-} mass ratio. The negative correlation may indicate the organic film hypothesis, while no correlation may challenge the organic film hypothesis.

4.2.4. Statistical tests of the model performance assessment

Following the approaches by Chang and Hanna (2004), Kumar et al. (2006), and Fountoukis et al. (2009), fractional bias (FB) was used to evaluate the performance of the ISORROPIA II model, the criteria value for acceptable model performance and associated meanings are as follows: the bracket means averaging, C_o and C_p denote measured and predicted concentrations.

$$FB = \frac{2\times([C_p]-[C_o])}{[C_o]+[C_p]} \quad (-0.5 \le FB \le 0.5) \qquad (4\text{-}6)$$

Where FB is symmetrical and bounded between –2 and +2, FB = –2 indicates extreme under prediction and FB = 2 indicates extreme over prediction. The perfect model should have FB = 0.

The acceptable model performance should have FB in the range between –0.5 and 0.5. FB measures mean bias of the prediction and indicate systematic errors. FB can also be used to check the over or under prediction of the ISORROPIA II model: FB > 0 indicates over prediction and FB < 0 indicates under prediction.

4.3. Results and Discussion

The ISORROPIA II model performance evaluation at the YRK site (2007–2013), JST site (2010–2014), CTR site (2012–2013), BHM site (2011–2013), OAK site (2010), and OLF site (2013) are presented. The comparisons between model predictions and measurements at the YRK site are shown in Figure 4.1.

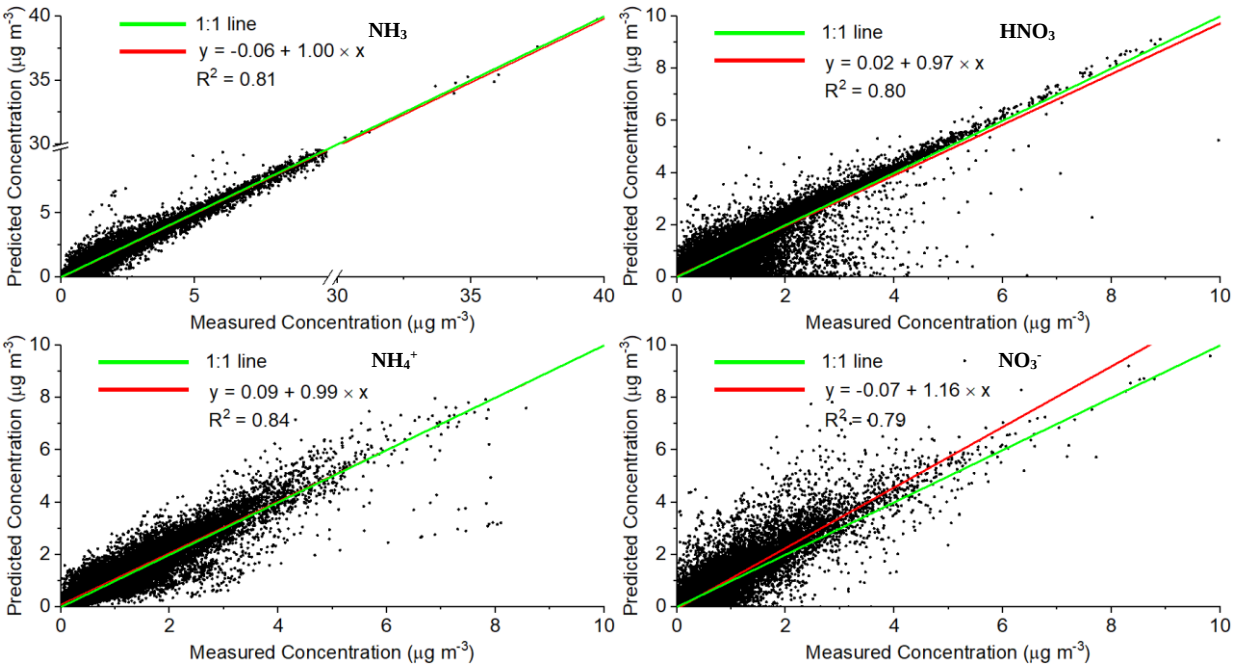

Figure 4.1. The comparisons of predictions and observations using stable setup at the YRK site

As it can be seen from Figure 4.1, in general, the ISORROPIA II model is able to reproduce NH_3, HNO_3, NH_4^+, and NO_3^- concentrations at the YRK site, with R^2 values above 0.79. As for NH_3 and NH_4^+, the slopes are 1.00 and 0.99, respectively, which indicate that the

ISORROPIA II model predicts NH_3 and NH_4^+ well. While for HNO_3 and NO_3^-, the ISORROPIA II model tends to under predict HNO_3 (slope is 0.97), and over predict NO_3^- (slope is 1.16). Especially when the measured concentrations of HNO_3 and NO_3^- are below 4 μg m^{-3}. Some disagreement between model prediction and measurements can be observed.

4.3.1. Ambient T-RH and ISORROPIA II stable & metastable setups

The impacts of T and RH on model performance exhibit the similar results at the six sites. Figures 4.2–4.4 show the ratios of prediction over observation (C_p/C_o) at the YRK site using stable and metastable model setups.

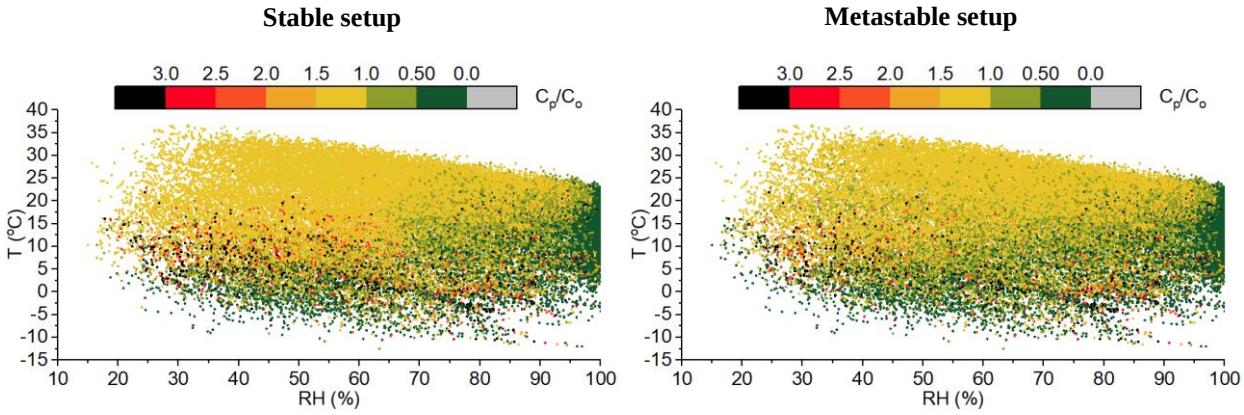

Figure 4.2. The ratios of C_p/C_o for HNO_3 using stable and metastable model setups

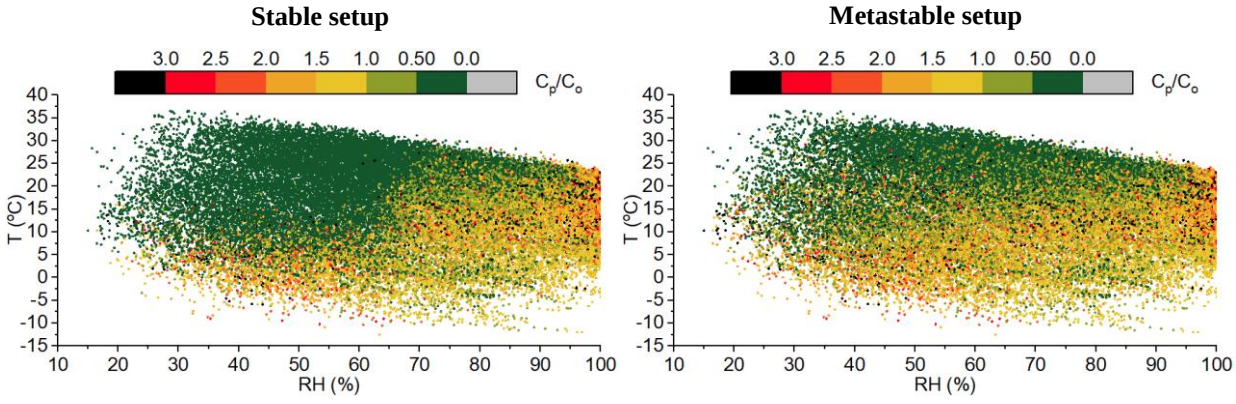

Figure 4.3. The ratios of C_p/C_o for NO_3^- using stable and metastable model setups

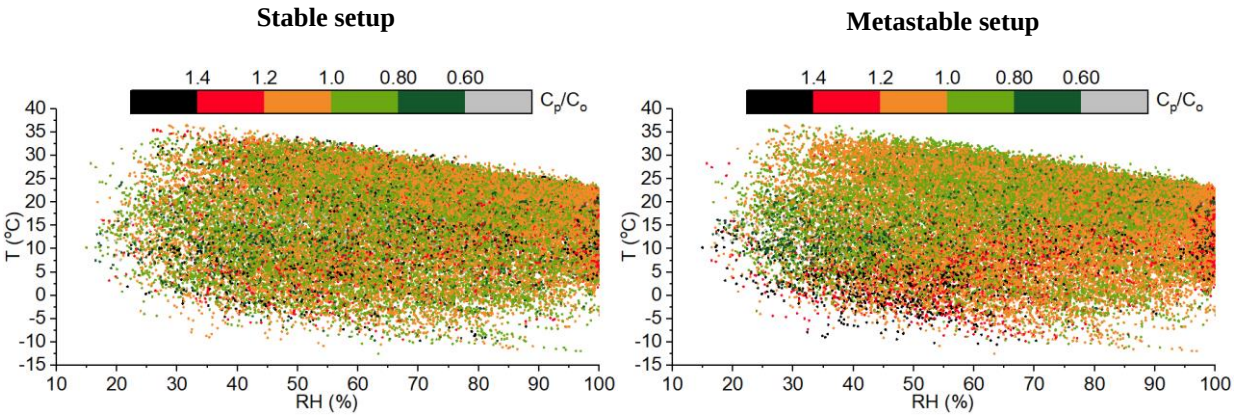

Figure 4.4. The ratios of C_p/C_o for $iPM_{2.5}$ (SO_4^{2-} + NH_4^+ + NO_3^-) using stable and metastable model setups

As it can be seen from Figures 4.2-4.4, under T > 10 °C & RH < 60% conditions, ISORROPIA II model tends to excessively partition N into a gas phase, i.e., over predict HNO_3 and under predict NO_3^-. As for the prediction of $iPM_{2.5}$ (SO_4^{2-} + NH_4^+ + NO_3^-), generally, ISORROPIA II model predicts the concentration of $iPM_{2.5}$ well, most of the C_p/C_o are within the range of 0.8 and 1.2. The accuracy of the prediction of $iPM_{2.5}$ is determined by three chemical compositions– SO_4^{2-}, NH_4^+ and NO_3^-. One of the assumptions made by ISORROPIA II model is that the vapor pressure of H_2SO_4 is low, thus, all the H_2SO_4 partitions into aerosol phase. The ISORROPIA II model always predicts SO_4^{2-} concentration well, if SO_4^{2-} accounts for the most of $iPM_{2.5}$ mass concentration, the prediction of $iPM_{2.5}$ is not sensitive to the disagreement between predictions and measurements for NO_3^- & NH_4^+. Among the three major chemical compositions of $iPM_{2.5}$, SO_4^{2-} accounted for greater than 59% of $iPM_{2.5}$ at the YRK site, which may explain the acceptable performance of ISORROPIA II in the prediction of $iPM_{2.5}$ concentration. The analyses of the mass closure of $PM_{2.5}$ in 2001-2016 at the agricultural rural site-YRK and industrial residential site-JST indicate that $iPM_{2.5}$ (SO_4^{2-} + NH_4^+ + NO_3^-) was the dominant

component of $PM_{2.5}$ mass concentration before 2011, while in 2012-2016, the mass fraction of $iPM_{2.5}$ was decreased and organic carbon matter (OCM) dominated in $PM_{2.5}$ mass concentration.

4.3.2. Statistical tests of model performance under different T-RH conditions

As for NH_3 and NH_4^+, the over prediction and under prediction both happened under all T–RH conditions. In order to quantitatively assess the performance of ISORROPIA II under different T–RH conditions, under each 5 °C T × 10% RH condition, the model performance for the prediction of NH_3, NH_4^+, HNO_3, NO_3^-, and $iPM_{2.5}$ at the YRK site was assessed. The data at the JST site exhibit the similar results, thus, the statistical analysis results at the JST site are not shown here. The values of FB for NO_3^- prediction with stable model setup at the YRK site are illustrated here; the results for the other gas– and particle–phase pollutants are in the Appendix C, Tables S4-S8.

Table 4.1. Model performance assessment for NO_3^- prediction with stable setup at the YRK site

	RH							
T	20-30%	30-40%	40-50%	50-60%	60-70%	70-80%	80-90%	90-100%
30-35 °C	**-2.00^{M}**	**-2.00^{M}**	**-2.00^{M}**	**-1.98^{M}**	**-1.81^{M}**	NA	NA	NA
25-30 °C	**-2.00^{M}**	**-2.00^{M}**	**-2.00^{M}**	**-1.99^{M}**	**-1.66^{M}**	**-0.71^{M}**	-0.48$^{S=M}$	NA
20-25 °C	**-2.00^{M}**	**-1.95^{M}**	**-1.84^{M}**	**-1.97^{M}**	**-1.10^{M}**	-0.27^{M}	-0.09^{M}	0.25$^{S=M}$
15-20 °C	**-0.78^{M}**	**-1.20^{M}**	**-1.33^{M}**	**-1.53^{M}**	-0.29^{M}	0.06^{S}	0.12^{S}	0.36$^{S=M}$
10-15 °C	**-0.65^{M}**	**-0.61^{M}**	-0.49^{S}	-0.47^{M}	-0.02^{S}	0.30^{S}	0.29^{S}	0.41$^{S=M}$
5-10 °C	-0.29^{M}	0.01^{S}	0.09^{S}	0.03^{S}	0.08^{S}	0.21^{S}	0.17^{S}	0.17$^{S=M}$
0-5 °C	0.18^{S}	0.30^{S}	0.29^{S}	0.25^{S}	0.12^{S}	0.09^{S}	0.07^{S}	0.17$^{S=M}$
-5-0 °C	NA	0.40^{S}	0.44^{S}	0.30^{S}	0.16^{S}	0.08^{S}	0.06^{S}	0.13$^{S=M}$
-10 - -5 °C	NA	NA	NA	0.37^{S}	0.20^{S}	0.05^{S}	0.02^{S}	NA

[1] The unacceptable FB values (< -0.5 or > 0.5) are labeled as bold values; NA: not applicable

[2] The FB values closer to 0 indicates the good model performance. The S superscript indicates the stable setup performs better, the M superscript indicates the metastable setup performs better, and the S=M superscript indicates the same model performance

As it can be seen from Tables S4 and S7, the performance of ISORROPIA II in the prediction of NH_3 and NH_4^+ is generally acceptable. While Table 4.1 indicates that the predictions of HNO_3 and NO_3^- are not satisfactory under certain T–RH conditions, especially under higher T and lower RH conditions, the ISORROPIA II model exhibits worse performance. The prediction of $iPM_{2.5}$ is acceptable under all T–RH conditions. The model performance in the prediction of HNO_3 and NO_3^- is sensitive to the dominant physical state (gas or aerosol) of HNO_3 in ambient air. Under high T (> 15 ^oC) and low RH (< 60%) conditions, the ammonium nitrate (NH_4NO_3) may decompose into gas–phase NH_3 and HNO_3 due to the semi–volatile characteristic of ammonium nitrate (NH_4NO_3), leading to the dominance of gas–phase HNO_3 (Dawson et al., 2007). Thus, most of the total available HNO_3 is in gas phase, the NO_3^- is more sensitive to the prediction uncertainties. The FB values for NO_3^- with T > 25 ^oC & RH < 70% are all negative, as small as –2, which indicates extreme under prediction. While under low T or high RH conditions, HNO_3 gas is under predicted, especially for T < –5 ^oC or RH > 90%. This can be explained that under low T and/or high RH conditions, most of the HNO_3 is in particle phase and the prediction of HNO_3 gas is more sensitive to prediction uncertainties.

To further investigate the partitioning of $NH_3 - NH_4^+$ and $HNO_3 - NO_3^-$, the measured gas–phase NH_3 and HNO_3 molar fractions under different T–RH conditions are shown in Figure 4.5.

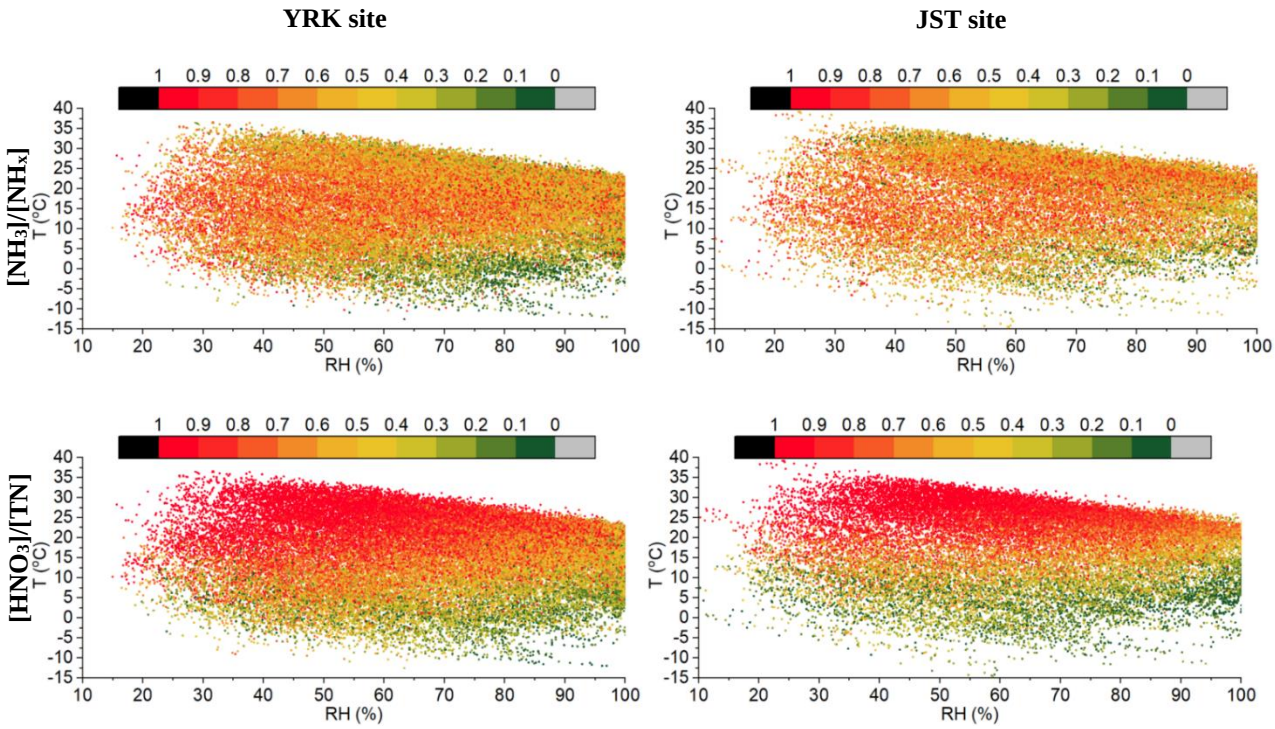

Figure 4.5. The measured gas-phase NH_3 and HNO_3 molar fractions under different T-RH conditions at the YRK and JST sites

As for NH_3, Table S4 shows that the values of FB are closer to 0 under T > 5 °C than under T < 5 °C , and this indicates that the model performance of ISORROPIA II is better under T > 5 °C than under T < 5 °C. The semi–volatile characteristic of NH_4NO_3 can lead to greater gas–phase NH_3 molar fraction under high T. When the gas–phase NH_3 dominates in the partitioning of $NH_3 - NH_4^+$, the particle–phase NH_4^+ is more sensitive to the prediction uncertainty and vice versa. The model performance in the prediction of NH_3 is better under T > 5 °C condition for both stable and metastable model setups. The predominance of one phase (aerosol or gas) of semi–volatile compound under certain T–RH conditions can amplify the small errors in the model prediction of the other phase. The variable sensitivities to the prediction errors for gas–phase and particle–phase pollutants are more apparent for the partitioning of $HNO_3 - NO_3^-$. As for HNO_3, Figure 4.5 indicates that under T > 15 °C & RH < 90% conditions, most of the

HNO_3 stays in the gas phase. The particle–phase NO_3^- only accounts for a small fraction of total HNO_3, the mass conservation of the HNO_3 renders the NO_3^- concentration more sensitive to the uncertainties in the prediction. On the contrary, under T < 5 ^oC condition, most of the HNO_3 stays in particle phase, the mass conservation of the HNO_3 renders the HNO_3 gas concentration more sensitive to the uncertainties in the prediction. The more sensitivity of the partitioning of HNO_3– NO_3^- to the T and RH makes the prediction of NO_3^- tougher than the other chemical compositions of $iPM_{2.5}$.

According to Ansari and Pandis (2000) and Fountoukis et al. (2009), under different T–RH conditions, the metastable and stable model setups may have different performances in the prediction of NH_3, HNO_3, NH_4^+, and NO_3^-, and $iPM_{2.5}$ ($SO_4^{2-} + NH_4^+ + NO_3^-$). The differences of predictions using stable and metastable model setups are shown in Figure 4.6.

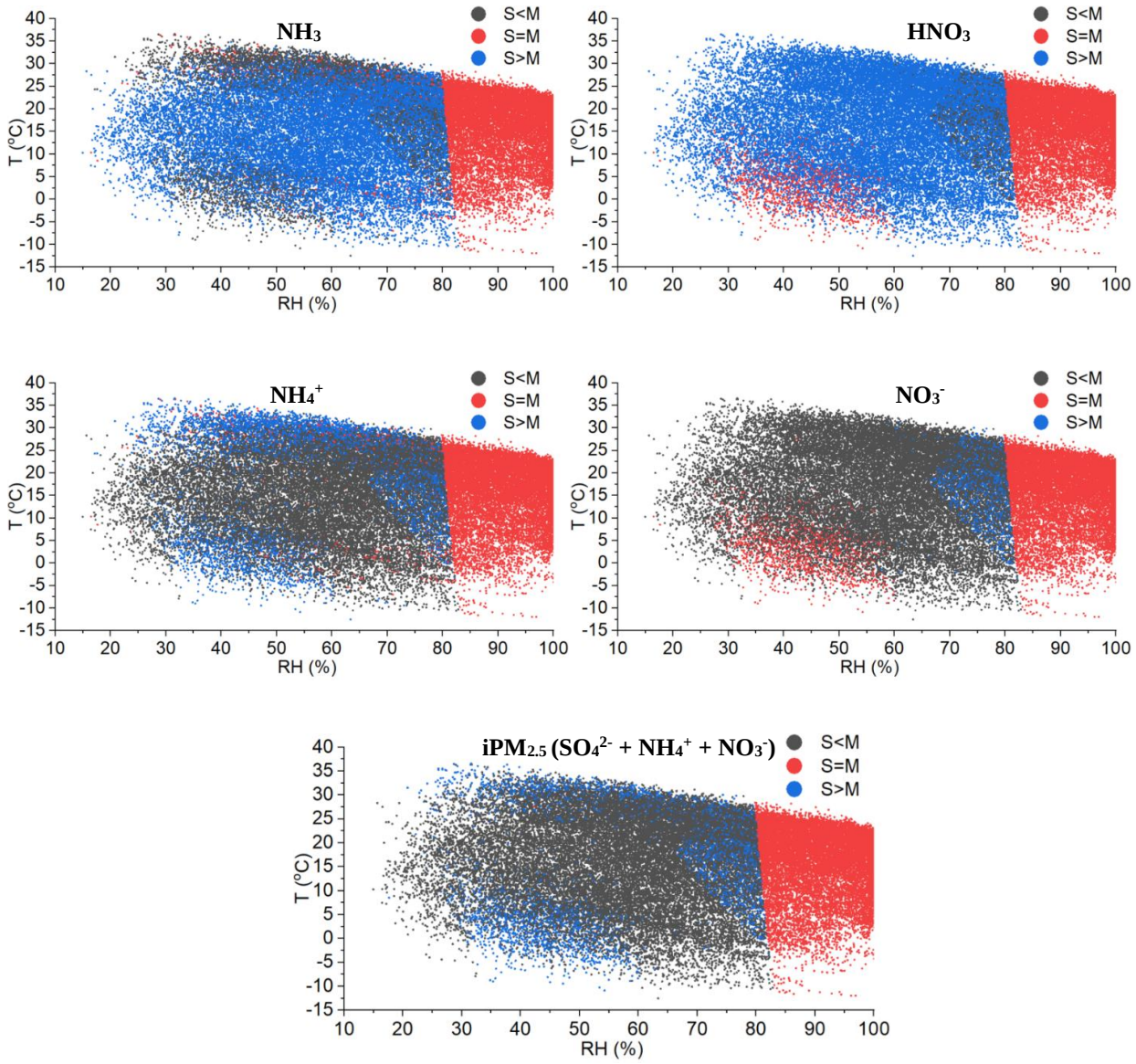

Figure 4.6. The difference of predictions using stable and metastable setups at the YRK site (S: stable; M: metastable)

As it can be seen from Figure 4.6, under high RH (RH>83%) condition, there's no difference for model prediction of NH_3, HNO_3, NH_4^+ and NO_3^-, and $iPM_{2.5}$ (SO_4^{2-} + NH_4^+ + NO_3^-) between the stable and metastable model setups. The high RH facilitates the absorption of water vapor to the $iPM_{2.5}$ particles, the particle always stays in the aqueous phase and there's no salts precipitation. Thus, the prediction of stable and metastable is the same. While Tables S4-S8

indicate that under certain T–RH conditions, stable and metastable model setups may have different performances in the prediction of NH_3, HNO_3, NH_4^+, NO_3^- and $iPM_{2.5}$. Under T > 10 °C & RH < 60% conditions, ISORROPIA II model with metastable setup tends to perform better in the prediction of NH_3, HNO_3, NH_4^+ and NO_3^-, and $iPM_{2.5}$. Under T < 5 °C & RH < 90% conditions, ISORROPIA II model with stable setup tends to perform better in the prediction of NH_3, HNO_3, NH_4^+, and NO_3^-, and $iPM_{2.5}$. This can be explained by the difference in the prediction of the partitioning of NH_3– NH_4^+ and HNO_3– NO_3^- by stable and metastable model setups.

As for NH_4^+, when RH < 80%, the prediction of NH_4^+ can be divided into four regions based on the difference between stable and metastable model setups. When T > 25 ^oC, 70% < RH < 80%, or T < 5 ^oC, the NH_4^+ prediction of stable setup tends to be either greater or smaller than the metastable setup. When 5 ^oC < T < 25 ^oC & RH < 70%, the NH_4^+ prediction of stable setup tends to be smaller than the metastable setup. As for NO_3^-, when RH < 80%, the prediction of NO_3^- can be divided into three regions based on the difference between stable and metastable model setups. When 70% < RH < 80%, the NO_3^- prediction of stable setup tends to be either greater or smaller than the metastable setup. When RH < 70%, the NO_3^- prediction of stable setup tends to be either equal to or smaller than the metastable setup.

Thus, the selection of stable and metastable model setups depends on ambient T and RH at the location.

The model performance of ISORROPIA II in simulating NH_3 and NH_4^+ under different GRs and measured charge balance is shown in the Figures 4.7 and 4.8.

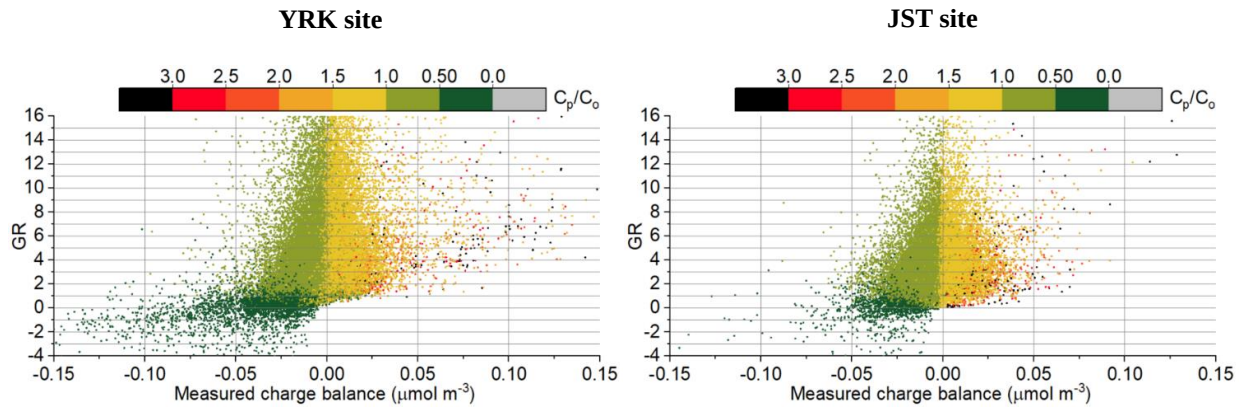

Figure 4.7. The ratios of prediction over observation for NH_3 using stable setup at the YRK and JST sites

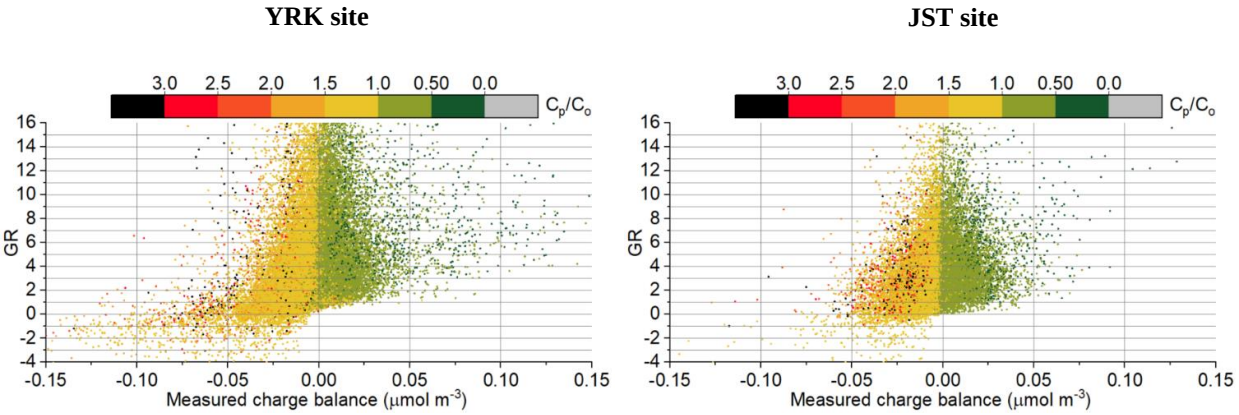

Figure 4.8. The ratios of prediction over observation for NH_4^+ using stable setup at the YRK and JST sites

As it can be seen from Figures 4.7 and 4.8, when the measured charge balance is negative, the NH_3 is under predicted and NH_4^+ is over predicted, especially when GR <1, the NH_3 is under predicted to a greater degree; when the measured charge balance is positive, the NH_3 is over predicted and NH_4^+ is under predicted. In ambient air, the charge balance $[NH_4^+] - 2\times[SO_4^{2-}] - [NO_3^-]$ is equal to $[OH^-] - [H^+]$ + [organic anion] + $[Cl^-] - [K^+] - [Na^+] - 2\times[Ca^{2+}] - 2\times[Mg^{2+}]$. However, only total NH_3, total HNO_3, and total H_2SO_4 are the input data for ISORROPIA II in this research. In the model, the charge balance $[NH_4^+] - 2\times[SO_4^{2-}] - [NO_3^-]$ is

equal to $[OH^-] - [H^+]$. Therefore, several possible reasons may explain the phenomena of over and under predictions of NH_3 & NH_4^+:

1. The measurement uncertainties in total H_2SO_4. Zhang et al. (2003) used 5-min measurements of $iPM_{2.5}$ chemical compositions and its precursor gases to test the validity of thermodynamic equilibrium assumption for the partitioning of NH_3– NH_4^+, the good agreement was found between filed measurements and ISORROPIA II predictions in NO_3^- and NH_4^+ when ~15% downward correction in SO_4^{2-} concentration was applied. Yu et al. (2005) used different time resolution (5-min, 2-hr, and 12 hr) measurements of NH_3, NH_4^+, HNO_3, NO_3^-, and SO_4^{2-} to assess the ability of ISORROPIA II in the prediction of HNO_3– NO_3^- partitioning. The sensitivity test indicated that the measurement uncertainties in SO_4^{2-} and total available NH_3 concentrations may explain the errors in the prediction of NO_3^-. The accurate prediction of NH_3 and NH_4^+ requires the accurate measurements of gas–phase and particle–phase pollutants as well as ambient T and RH, thus, the measurement uncertainty may explain part of the discrepancies between predictions and measurements.

2. The positive measured charge balance may be explained that part of the NH_4^+ cations are associated with organic anions, which ISORROPIA II model doesn't consider in the modeling system. In addition, NH_4^+ cations may also be associated with Cl^-, which is not incorporated in the model input; the negative measured charge balance may be explained by the exclusion of the NVCs in the modeling system. Metzger et al. (2006) investigated the partitioning of NH_3– NH_4^+ and HNO_3– NO_3^- using three thermodynamic models, the model performance was assessed with/without the inclusion of NVCs and organic acid (R-COOH) in the input data.

The comparison between model prediction and observations indicated that it is necessary to include NVCs and R-COOH in the model input of thermodynamic model to accurately predict the gas–particle partitioning of NH_3 and HNO_3.

To further investigate the over and under prediction of gas–phase and particle–phase pollutants, the impact of NVCs on the model performance of ISORROPIA II was assessed as following.

4.3.3. Nonvolatile cations (NVCs)

The comparisons between model predictions and measurements for particle-phase NH_4^+ and NO_3^- at the YRK site are shown in Figure 4.9, the data analysis at the JST site exhibits the similar result, thus is not shown here.

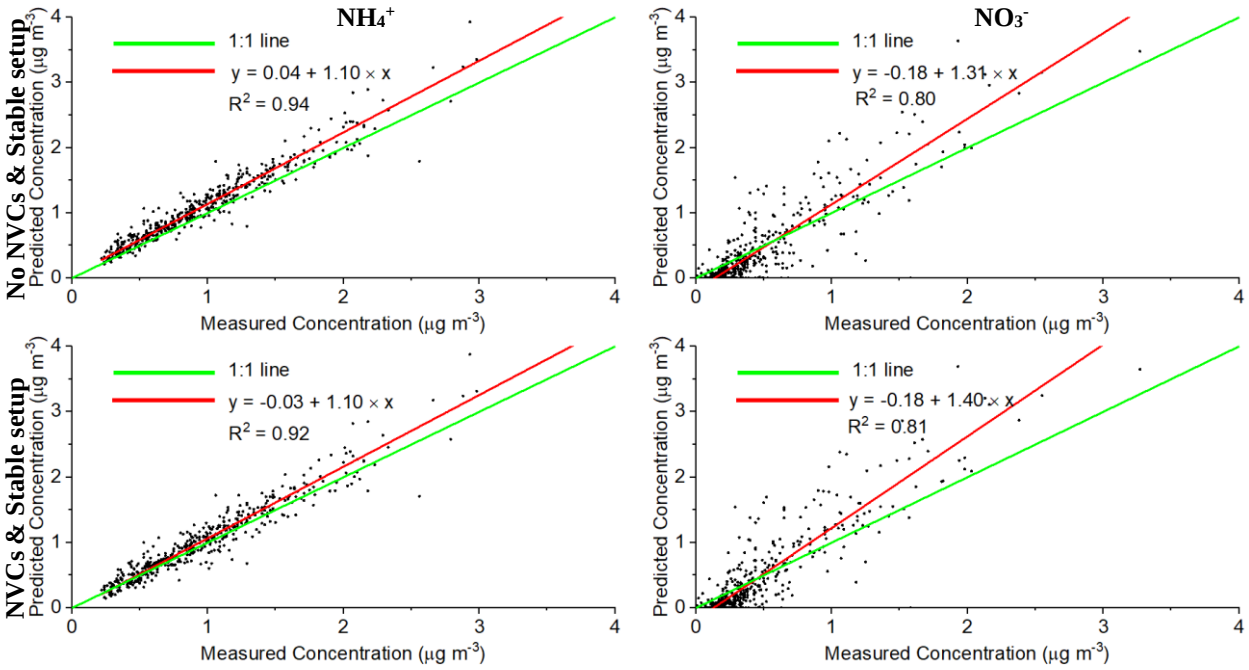

Figure 4.9. The comparisons of predictions and observations for NH_4^+ and NO_3^- at the YRK site

As it can be seen from Figure 4.9, as for daily measurements of gas–phase and particle–phase pollutants, in general, ISORROPIA II is able to reproduce the concentrations of NH_3,

HNO_3, NH_4^+, and NO_3^-. Factorial analysis of variance (ANOVA) statistical test is used to check if NVCs (with/without nonvolatile cations) and model setups (stable/metastable setups) have significant impact on the prediction of NH_3, HNO_3, NH_4^+, NO_3^-, and $iPM_{2.5}$. Only the data analysis results at the YRK site are shown in Table 4.2, the results at the JST site were similar, thus not shown here.

Table 4.2. Factorial ANOVA test results at the YRK site

Factors		NH_3 prediction		HNO_3 prediction		NH_4^+ prediction		NO_3^- prediction		$iPM_{2.5}$ prediction	
	DF	F-value	p-value	F-value	p-value	F-value	p-value	F-value	p-value	F-value	p-value
NVCs	1	59.26	**2.23×10^{-14}**	6.60	**0.01**	150.52	**$<2\times10^{-16}$**	2.71	0.10	4.56	**0.03**
Setup	1	2.42	0.12	15.54	**8.38×10^{-5}**	6.57	**0.01**	23.56	**1.3×10^{-6}**	15.51	**8.52×10^{-5}**
Both	1	0.7	0.80	0.34	0.56	0.23	0.63	0.08	0.77	0.55	0.46

[1] Significant p-values are labeled as bold.

Model setups and NVCs have varied impacts on the predictions of gas–phase and particle–phase pollutants. For NH_3 prediction, only NVCs has significant impact on the model performance. For NO_3^- prediction, only model setup has significant impact on the model performance. For HNO_3, NH_4^+ and $iPM_{2.5}$ predictions, both NVCs and model setups have significant impact on the model performance.

In order to quantitatively assess the impact of NVCs and model setups on the model performance. Fa_2 and FB values are calculated for model assessment at the YRK site.

Table 4.3. Model performance of ISORROPIA II at the YRK site

Species	NVCs + Stable		NVCs + Metastable		No NVCs + Stable		No NVCs + Metastable	
	Fa_2	FB	Fa_2	FB	Fa_2	FB	Fa_2	FB
NH_3	**0.97**	**-0.04**	0.97	-0.05	0.96	-0.09	0.95	-0.10
HNO_3	0.87	**-0.01**	0.89	-0.06	**0.91**	0.03	0.90	-0.04
NH_4^+	**1.00**	**0.06**	1.00	0.07	1.00	0.13	1.00	0.14
NO_3^-	0.51	**0.02**	**0.61**	0.12	0.50	-0.07	0.60	0.07
$iPM_{2.5}$	**1.00**	**0.02**	1.00	0.03	1.00	0.02	1.00	0.04

[1] The bold values indicate the better model performance

As it can be seen from Table 4.3, based upon the FB values, inclusion of NVCs into the modeling framework and stable model setup have a better performance in the prediction of NH_3, HNO_3, NH_4^+, NO_3^-, and $iPM_{2.5}$ concentrations at the YRK site. Statistical summary of T and RH data at the YRK site indicates that in the total 467 data points for the ISORROPIA II model assessment, 81 data points were under the T > 10 ^oC & RH < 60% conditions, under which metastable model setup is favored. In addition, 67 data points were under RH > 83% condition, under which the performance of the model with stable and metastable setups is the same. The other data points were under conditions that stable setup is favored. This may indicate the preference of stable model setup at the YRK site. This finding is consistent with the study performed by Moya et al. (2001), in which 6-hr measurements of NH_3, HNO_3, NH_4^+, NO_3^-, and SO_4^{2-} were used to assess the performance of ISORROPIA. Moya et al. (2001) noted that the inclusion of NVCs as equivalent Na^+ can improve the model performance in the prediction of NO_3^- concentration. Therefore, the inclusion of the NVCs into the model framework is necessary to accurately simulate the thermodynamic equilibrium partitioning of NH_3– NH_4^+.

4.3.4. Organic aerosol (OA)

The relationships between the molar ratio–(R) and (OA/SO_4^{2-}) mass ratio at the YRK and JST sites are shown in Figure 4.10.

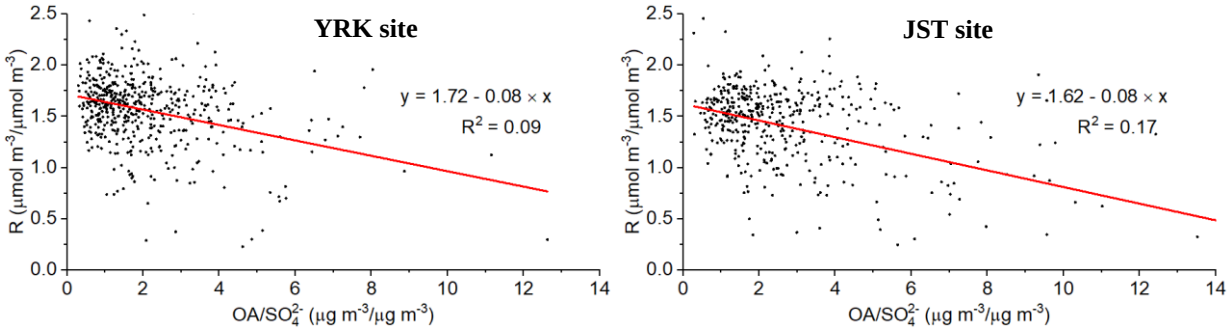

Figure 4.10. The relationships between molar ratio-R and OA/SO_4^{2-} mass ratio at the YRK and JST sites

There is a weak correlation between molar ratio-(R) and OA/SO_4^{2-} mass ratio, R^2= 0.09, 0.17 at the YRK and JST sites, respectively; the molar ratio-R slightly tends to decrease with OA/SO_4^{2-} mass ratio. As shown in Figure 4.10, no definite conclusion can be made about the impact of OA on the thermodynamic equilibrium partitioning of NH_3–NH_4^+. The higher OA/SO_4^{2-} mass ratio may indicate the lower probability for the uptake of NH_3 by H_2SO_4. However, in this research, only a weakly negative correlation between molar ratio-R and OA/SO_4^{2-} mass ratio can be observed. One explanation may be that the daily data itself can't adequately detect the impact of OA on the equilibrium process of NH_3–NH_4^+ partitioning. Other factors such as T and RH can also affect the equilibrium process, while the coarse resolution of daily measurement can't detect the variable sensitivities of the equilibrium process to the impact of different factors. Thus, higher time resolution data such as 5-min data may be required to detect the impact of OA on the formation of $iPM_{2.5}$.

4.3.5. Possible reasons for the disagreement between model predictions and measurements

In assessment of ISORROPIA II model performance under different T–RH–model setups conditions, it is discovered that ambient T & RH, model setups, NVCs have significant impacts on model prediction. The inclusion of NVCs in the ISORROPIA II input is necessary to improve the model performance. Under certain T & RH conditions, ISORROPIA II tends to over or under predict specific gas–phase or particle–phase pollutants. The stable and metastable model setups may also perform differently under different T–RH conditions. The impact of OA on the equilibrium assumption may not be detected by daily measurements, further research is needed to study the impact of OA on the equilibrium partitioning of NH_3–NH_4^+. The disagreement between model prediction and field measurements may be due to the following reasons:

1. The hourly and daily data were used in this research to assess the performance of ISORROPIA II model. The duration of the input data may not be adequate to detect the impact of atmospheric transport, ambient T and RH on the thermodynamic equilibrium partitioning of NH_3–NH_4^+. The hourly and daily data of NH_3, HNO_3, T and RH may not be able to represent the thermodynamic equilibrium state of gas–particle partitioning process. In addition, the thermodynamic equilibrium may not be established very rapidly, the hourly data may not be able to detect the dynamic changes of precursor gases of $iPM_{2.5}$ and meteorological conditions. Thus, the thermodynamic model–ISORROPIA II based on the hourly and daily average condition may not vigorously reproduce the gas–phase and particle–phase pollutants at the equilibrium state.

2. The gas–particle system was not in a chemical equilibrium state, which is assumed by ISORROPIA II model. The mixture of PM_1 and $PM_{1\text{-}2.5}$ in secondary $iPM_{2.5}$ may hinder

the applicability of ISORROPIA II model. Simple thermodynamic equilibrium assumption for $iPM_{2.5}$ may not adequately characterize the partitioning of NH_3–NH_4^+ in ambient air.

3. The inorganic $PM_{2.5}$ particles were assumed to be internally mixed; therefore, the particles were treated as an ensemble bulk. However, Koo et al. (2003) observed that dynamic model may perform better in the prediction of $iPM_{2.5}$ chemical compositions. The dynamic change of particle size distribution may require vigorous treatment of different physical processes such as condensation, evaporation and coagulation.

4. Field measurement uncertainty: the uncertainties can be divided into two aspects: the measurement uncertainties caused by instruments and techniques, and the uncertainties caused by the atmospheric transport of air mass. The values below the instrument's detection limit were included in the ISORROPIA II model assessment; this may cause some discrepancies between model predictions and measurements. Especially the small values are more sensitive to the prediction uncertainty. In addition, the ideal assessment of ISORROPIA II prediction skill should be based on the high time resolution measurements under controlled condition. In addition, the thermodynamic equilibrium models should simulate the equilibrium partitioning of NH_3–NH_4^+ and HNO_3–NO_3^- happening in the same air parcel. While in the field, air parcels laden with different concentrations of gas-phase and particle-phase pollutants may travel from and to any directions. Thus, the average measurements in one hour or day may not represent the thermodynamic equilibrium state of the same air parcel. Wind speed and wind direction may change rapidly in one hour/day. The air parcels from various directions may affect the monitoring

location. The air parcels may not only be laden with different concentrations of pollutants, the characteristics of T and RH may vary as well.

5. The history of RH experienced by air mass from different wind directions is not a priori, thus, the decision regarding the selection of stable and metastable setups is quite difficult, and this may also add some uncertainties to the model simulation.

Although the performance of ISORROPIA II in the prediction of $iPM_{2.5}$ concentration under all T–RH conditions is acceptable in Southeast U.S. due to the dominance of SO_4^{2-} in the $iPM_{2.5}$ concentration, it may perform differently in other regions where SO_4^{2-} is not dominant in the $iPM_{2.5}$ concentration. The $PM_{2.5}$ chemical compositions varied in spatial and temporal scales in the U.S. The $PM_{2.5}$ chemical compositions such as SO_4^{2-} and NO_3^- exhibited inverse seasonal variation patterns in eastern and western coast areas of U.S.; SO_4^{2-} exhibited a spatial heterogeneity with higher mass fraction in the eastern U.S. and lower mass fraction in the California (Bell et al., 2007). Thus, the model performance of ISORROPIA II in the prediction of $iPM_{2.5}$ may be different in spatial scale.

4.4. Conclusions

Based on the hourly and daily measurements of gas–phase and particle–phase pollutants at the SEARCH Network, the performance of ISORROPIA II was assessed under different T–RH–model setups–NVCs conditions. Impact of OA on the thermodynamic equilibrium partitioning of NH_3–NH_4^+ was also evaluated. Ambient T & RH, model setups, and NVCs have significant impact on model prediction. The inclusion of NVCs in the ISORROPIA II input is necessary to improve the model performance. Under high T (> 10 ^oC) & low RH (< 60%) conditions, ISORROPIA II tends to over predict HNO_3 concentration and under predict NO_3^-

concentration. The predominance of one phase (aerosol or gas) of semi–volatile compound can amplify the small errors in the model prediction of the other phase. The model with stable and metastable setups may also perform differently under different T–RH conditions. Metastable model setup performs better under high T (> 10 ^{o}C) & low RH (< 60%) conditions, while stable model setup performs better under low T (< 5 ^{o}C) condition. Under high RH (RH > 83%) condition, there's no difference in the model performance with stable and metastable setups. The dominance of SO_4^{2-} in the $iPM_{2.5}$ concentration may explain the acceptable model performance of ISORROPIA II in the prediction of $iPM_{2.5}$ under all T–RH conditions. Furthermore, higher resolution data may be required to investigate the impact of OA on the thermodynamic equilibrium partitioning of NH_3–NH_4^+. This research provides systematic assessment of ISORROPIA II model under different conditions. Future studies using ISORROPIA II for the prediction of NH_3–NH_4^+ and HNO_3–NO_3^- partitioning should consider the inclusion of NVCs, the under/over prediction of NO_3^-/HNO_3, the selection of stable/metastable model setups under different T–RH conditions, and spatiotemporal variations of $iPM_{2.5}$ chemical compositions.

CHAPTER 5: PARTITIONING OF $NH_3 - NH_4^+$ IN THE SOUTHEASTERN U.S.

Abstract

Inorganic fine particulate matter (i.e., $iPM_{2.5}$) constitutes a large portion of atmospheric $PM_{2.5}$. The formation of the $iPM_{2.5}$ can be characterized by thermodynamic equilibrium of $NH_3 - NH_4^+$ partitioning. To develop effective control of atmospheric $PM_{2.5}$, it is essential to understand the impact of the changes in different precursor gases on $iPM_{2.5}$ concentration and the partitioning of $NH_3 - NH_4^+$. In the Southeastern United States (U.S.), the atmospheric chemical condition varied in spatial and temporal scales. In order to gain some insights into the partitioning of $NH_3 - NH_4^+$ as impacted by various precursor gases in this region, responses of $iPM_{2.5}$ to precursor gases in four seasons were investigated based upon field measurements of $iPM_{2.5}$, precursor gases, and meteorological conditions. The ISORROPIA II model was used to examine the effects of the changes in total NH_3 (gas + particle), H_2SO_4, and total HNO_3 (gas + particle) on $iPM_{2.5}$ concentration and the partitioning of $NH_3 - NH_4^+$ in the Southeastern U.S. The results indicate that the reduction of total H_2SO_4 concentration is more effective than reducing total HNO_3 and total NH_3 concentrations to reduce $iPM_{2.5}$ concentrations especially when NH_3 is in excess of fully neutralizing acidic gases. In addition, the reduction of total H_2SO_4 may change the partitioning of $NH_3 - NH_4^+$ towards gas phase. Moreover, the reduction of total H_2SO_4 may lead to the increase of NO_3^- when NH_3 is not in excess of fully neutralizing the acidic gases. Thus, the future reduction of $iPM_{2.5}$ may necessitate the coordinated reduction of both H_2SO_4 and HNO_3 in the Southeastern U.S. It is discovered that the response of $iPM_{2.5}$ to the change of total H_2SO_4 is more sensitive in summer than winter. The dominance of SO_4^{2-} salts of $iPM_{2.5}$ and

high T in summer don't facilitate the formation of NH_4NO_3, the decrease in SO_4^{2-} salts caused by the reduction in total H_2SO_4 won't be offset by the increase in the NO_3^- salts. The significant NH_3 emissions from AFOs at the YRK agricultural rural site lead to the elevated NH_3 concentration, which is in excess of fully neutralizing acidic gases, thus have great impact on the partitioning of $NH_3 - NH_4^+$. The formation of NH_4NO_3 is not affected by the reduction of total H_2SO_4 at the YRK agricultural rural site. The ISORROPIA II model simulation provides projected prediction of $iPM_{2.5}$ formation, thus serves as a powerful tool to get an advanced understanding about the partitioning of $NH_3 - NH_4^+$. This research provides an insight into $iPM_{2.5}$ control and regulation in the Southeastern U.S.

5.1. Introduction

Particulate matter (PM) with aerodynamic equivalent diameter less than or equal to 2.5 μm (i.e., $PM_{2.5}$) is one of the six criteria air pollutants regulated under National Ambient Air Quality Standards (NAAQS) (USEPA, 2015a). In general, $PM_{2.5}$ consists of ions, organic carbon (OC), elemental carbon (EC), and various elements (Andrews et al., 2000). In addition, $PM_{2.5}$ can be classified as primary and secondary $PM_{2.5}$ based on formation processes. Primary $PM_{2.5}$ is directly emitted from emission sources and secondary inorganic $PM_{2.5}$ ($iPM_{2.5}$) is mainly formed through chemical reactions between basic (e.g., ammonia (NH_3)) and acidic precursor gases (e.g., nitric acid (HNO_3), sulfuric acid (H_2SO_4) and hydrochloric acid (HCl)) (Tolocka et al., 2001). Secondary $iPM_{2.5}$ is an important subset of $PM_{2.5}$ (Hinds, 1998). It has been reported that secondary $iPM_{2.5}$ may account for a large portion of total $PM_{2.5}$ in the atmosphere and secondary $iPM_{2.5}$ mainly consists of ammonium salts including ammonium nitrate (NH_4NO_3), ammonium sulfate ($(NH_4)_2SO_4$) and ammonium chloride (NH_4Cl) (Tanner et al., 1979; Walker et al., 2004; Li et al., 2009, 2012, 2014a). Ammonia is the major alkaline gas that may react with acidic gases

to form secondary $iPM_{2.5}$ in ambient air, and this process is called gas–particle partitioning of $NH_3 - NH_4^+$. Depending on the abundance of NH_3, H_2SO_4 may be partially or fully neutralized to form sulfate (SO_4^{2-}) salts. Moreover, if excessive NH_3 is available, NH_3 may also react with HNO_3 to form NH_4NO_3. As a semi–volatile compound, the formation of NH_4NO_3 also depends on ambient condition such as temperature (T) and relative humidity (RH), and low T and high RH tend to favor the formation of NH_4NO_3 (Hildemann et al., 1984).

Based on USEPA's National Emission Inventory (NEI), animal feeding operations (AFOs) contributed to more than 70% of the total NH_3 emissions in the United States (U.S.) (USEPA, 2015b). While the AFOs NH_3 emissions may present a great potential to the formation of $iPM_{2.5}$ in some regions, the dynamic contribution of such emissions to the ambient $iPM_{2.5}$ is not well understood. To gain holistic understanding of atmospheric $PM_{2.5}$, it is essential to understand the dynamic responses of atmospheric $iPM_{2.5}$ to the AFOs NH_3 emissions under different atmospheric chemical conditions and geographical locations (Wang-Li, 2015).

ISORROPIA is a commonly used thermodynamic equilibrium model developed to simulate the dynamics of phase changes (e.g., gas, liquid, and solid) and interaction of different chemical species (NH_4^+, NO_3^-, SO_4^{2-}, Cl^- and Na^+) in ambient air. In this model, gas–particle phase partitioning phenomenon and impacts of T and RH on such partitioning are quantified (Nenes et al., 1998, 1999; Fountoukis and Nenes, 2007; Fountoukis et al., 2009). In an application of ISORROPIA to assess the formation of $iPM_{2.5}$ at an agricultural site located in Eastern North Carolina (NC), Walker et al. (2006) studied the relationship of the atmospheric $iPM_{2.5}$ and its precursor gases through field data collection and model simulation. Moreover, the research examined the change of $iPM_{2.5}$ concentration in response to the half reduction of total NH_3 (gas + aerosol), total HNO_3 (gas + aerosol) and H_2SO_4 (aerosol) concentrations in winter

and summer. It was discovered that the half reduction of total NH_3 concentration had the least impact on the change of $iPM_{2.5}$ concentration as compared to the half reductions in total HNO_3 and total H_2SO_4. The research suggested that at agricultural sites with elevated atmospheric NH_3 concentration, the formation of $iPM_{2.5}$ is more sensitive to acidic gases rather than NH_3. In another $iPM_{2.5}$ study, Goetz et al. (2012) investigated the effect of NH_3 emissions from swine production facilities on the ambient $iPM_{2.5}$ concentration at three locations in Eastern NC. The $iPM_{2.5}$ chemical composition data obtained from ambient air quality monitoring database of NC Division of Air Quality and precursor gases measured or cited from literature were utilized to conduct $iPM_{2.5}$ simulation using ISORROPIA under three T and RH combinations. The results indicated that ISORROPIA simulation of $iPM_{2.5}$ agreed well with the observation. Furthermore, the research revealed that high precursor gas concentrations, low T, and high RH favored the formation of $iPM_{2.5}$. To gain advanced understanding of the formation of $iPM_{2.5}$ as impacted by AFOs NH_3 emissions, a study was performed to study the $iPM_{2.5}$ in response to NH_3 concentrations inside a production house and in the vicinity of an egg production farm in the Southeastern U.S. (Li et al., 2014b). Onsite measurements of NH_3 concentrations and $PM_{2.5}$ chemical speciation at in–house and ambient locations were used to conduct ISORROPIA II simulation to predict gas–particle partitioning of $NH_3 - NH_4^+$. The responses of $iPM_{2.5}$ to the concentrations of precursor gases, T, and RH confirmed that the most significant reduction of $iPM_{2.5}$ could be achieved by the reduction of total H_2SO_4 instead of NH_3. Li et al. (2014b) noted that this was because in NH_3–rich areas, NH_3 was in excess to fully neutralize all the acidic gases and the formation of the $iPM_{2.5}$ was limited by the availability of acidic gases. Responses of the partitioning of $NH_3 - NH_4^+$ to the changes of precursor gases may vary under different ambient conditions due to the unique atmospheric chemical conditions and local meteorology, thus, more

efforts are needed to investigate the partitioning of $NH_3 - NH_4^+$.

As the research gap exists in quantifying the formation of $iPM_{2.5}$ experimentally and/or through model simulation in AFOs region, the objective of this research was to investigate the partitioning of $NH_3 - NH_4^+$ in urban and rural areas under different meteorological conditions. The research findings may provide insights to address the impact of AFOs NH_3 emissions on the formation of $iPM_{2.5}$ that may lead to the development of reduction strategy for the control of ambient $PM_{2.5}$.

5.2. Methodology

5.2.1. Data processing

This research utilized the 24-hr and 1-hr average data of gas- and particle-phase measurements from Southeastern Aerosol Research and Characterization (SEARCH) Network (Hansen et al., 2003). The NH_3 gas concentration measurements were available at five sites coded asYRK, JST, CTR, BHM, and OLF in 2012-2016, thus, the responses of partitioning of $NH_3 - NH_4^+$ to the changes of precursor gases were investigate at these five sites.

Some measurement values are found to be either negative or below the detection limit. The negative values less than –DL were considered questionable and excluded from the dataset, while the other values below the DL were replaced with half of the DL (USEPA, 2000; Cohen and Ryan, 1989). As for the seasonal variations, spring includes March, April, and May; summer includes June, July, and August; fall includes September, October, and November; and winter includes December, January, and February.

5.2.2. Investigation of the partitioning of $NH_3 - NH_4^+$

The partitioning of $NH_3 - NH_4^+$ was investigated using ISORROPIA II. NH_3 measurements were available at five sites in 2012-2016. In this research, 10% to 80% reductions of total NH_3, total H_2SO_4, and total HNO_3 at five sites in four seasons were used to investigate the responses of $iPM_{2.5}$ to the changes of precursor gases in 2012–2016, only summer and winter results are reported, fall and spring results are in Appendix D. The examination of $iPM_{2.5}$ ($NH_4^+ + SO_4^{2-} + NO_3^-$) responses to the changes of precursor gases was conducted through sensitivity analysis using ISORROPIA II simulation results.

The concentrations of $iPM_{2.5}$, NH_4^+ under different total NH_3, total H_2SO_4 and total HNO_3 concentrations in four seasons were simulated using 24-hr average and 1-hr average data at five sites. In addition, the gas–phase NH_3 molar fraction (NH_3/NH_x) (Equation 5-1) was used to study the effects of changes of precursor gases on the partitioning of $NH_3 - NH_4^+$.

$$NH_3/NH_x = \frac{[NH_3]}{[NH_3]+[NH_4^+]} \qquad (5\text{-}1)$$

Gas ratio (GR) (Equation 2) was calculated to study the effects of changes of precursor gases concentrations on the atmospheric chemical condition and diurnal variation of $iPM_{2.5}$ and partitioning of $NH_3 - NH_4^+$.

$$GR = \frac{[TA]-2[TS]}{[TN]} \qquad (5\text{-}2)$$

where [TA] is the sum of molar concentrations of NH_3 and ammonium (NH_4^+) (in the unit of μmol m^{-3}); [TS] is the sum of molar concentrations of SO_4^{2-}, bisulfate (HSO_4^-), and H_2SO_4 (in the

unit of μmol m^{-3}); [TN] is the sum of molar concentrations of HNO_3 and nitrate (NO_3^-) (in the unit of μmol m^{-3}).

5.2.3. ISORROPIA II settings

For this study, the $iPM_{2.5}$ are assumed to be internally mixed, the thermodynamic equilibrium was also assumed to be established very rapidly. The ISORROPIA II allowed user to specify the problem type (forward or reverse) and thermodynamic state (stable or metastable), in this study, ISORROPIA II was set as forward type, and thermodynamic state was selected based on the findings of model performance assessment under different T–RH conditions in chapter 4.

5.3. Results and Discussion

5.3.1. Statistical characterization of the field measurement data

The statistical summary of $iPM_{2.5}$ precursor gases, nonvolatile cations (NVCs), T and RH at five sites in two periods (2008-2011 and 2012-2016) is presented in Appendix E, Tables S9 to S17. Tables S9 to S16 indicate the seasonal variatiosn of different precursor gases such as H_2SO_4, HNO_3, HCl, NH_3, and NVCs such as Na^+, K^+, Mg^{2+}, and Ca^{2+} as well as T and RH at five sites of the SEARCH Network. In general, T and RH were both lowest in winter, while highest T and RH happened in summer. The concentration of total H_2SO_4 was higher in summer than the other seasons at five sites. The concentrations of total NH_3 and total HNO_3 didn't exhibit certain seasonal pattern.

5.3.2. Seasonal simulation of partitioning of $NH_3 - NH_4^+$

The responses of $iPM_{2.5}$, NH_4^+ and NH_3/NH_x to the changes of total NH_3 and total HNO_3 in 2012-2016 are presented in Figures 5.1-5.5.

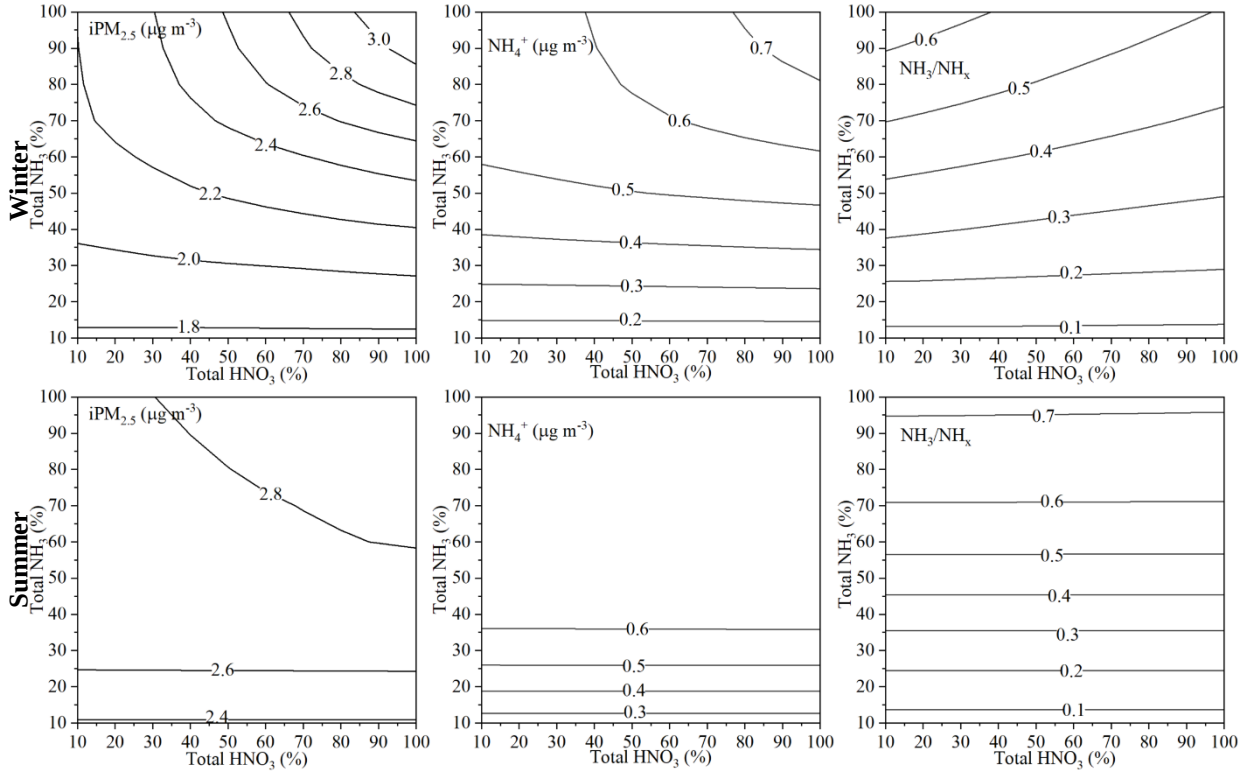

Figure 5.1. Responses of $iPM_{2.5}$ (left), NH_4^+ (middle), and NH_3/NH_x (right) to the changes of TNH_3 and $THNO_3$ at the YRK site in summer and winter of 2012-2016

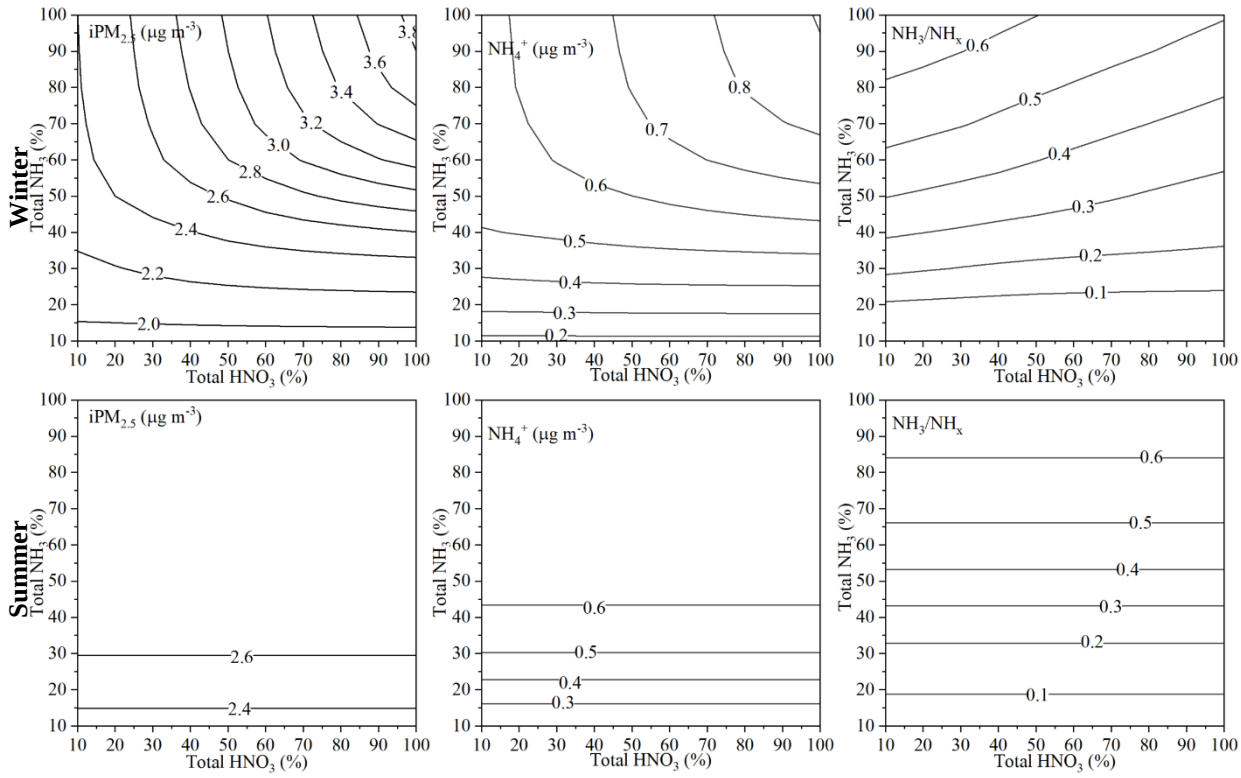

Figure 5.2. Responses of $iPM_{2.5}$ (left), NH_4^+ (middle), and NH_3/NH_x (right) to the changes of TNH_3 and $THNO_3$ at the JST site in summer and winter of 2012-2016

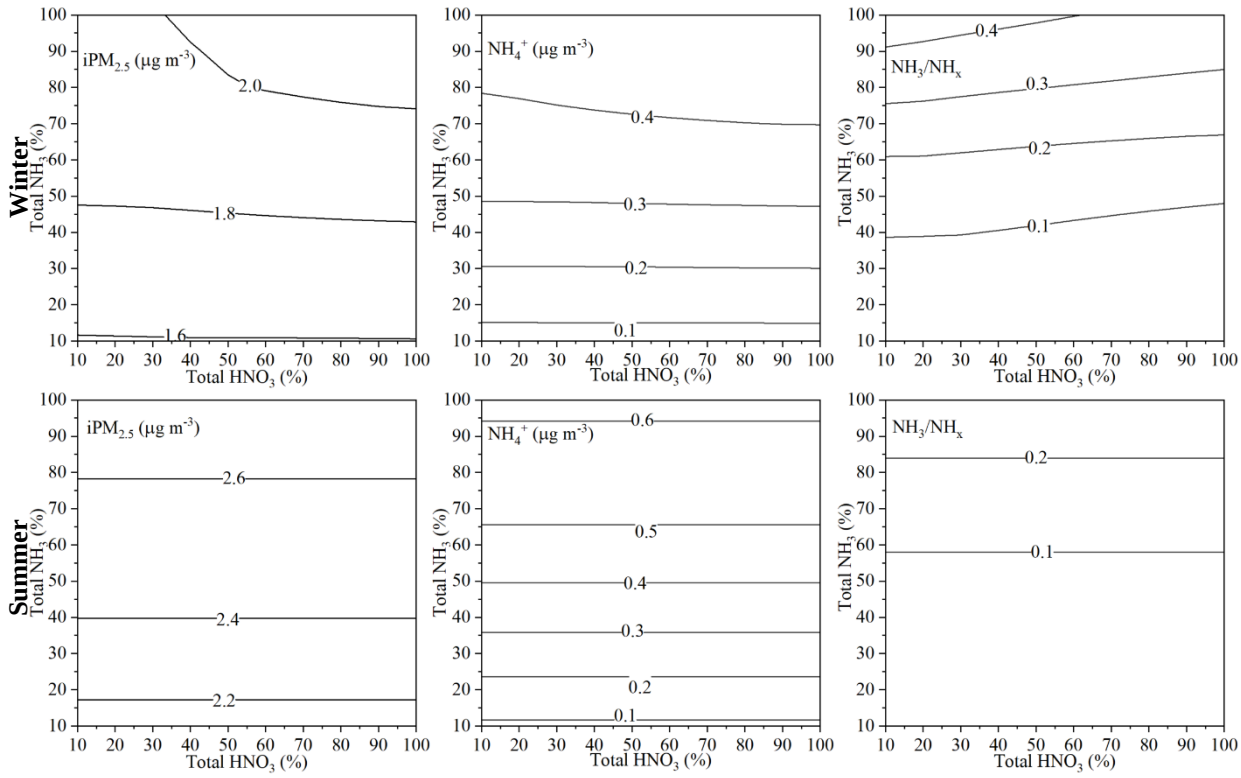

Figure 5.3. Responses of $iPM_{2.5}$ (left), NH_4^+ (middle), and NH_3/NH_x (right) to the changes of TNH_3 and $THNO_3$ at the CTR site in summer and winter of 2012-2016

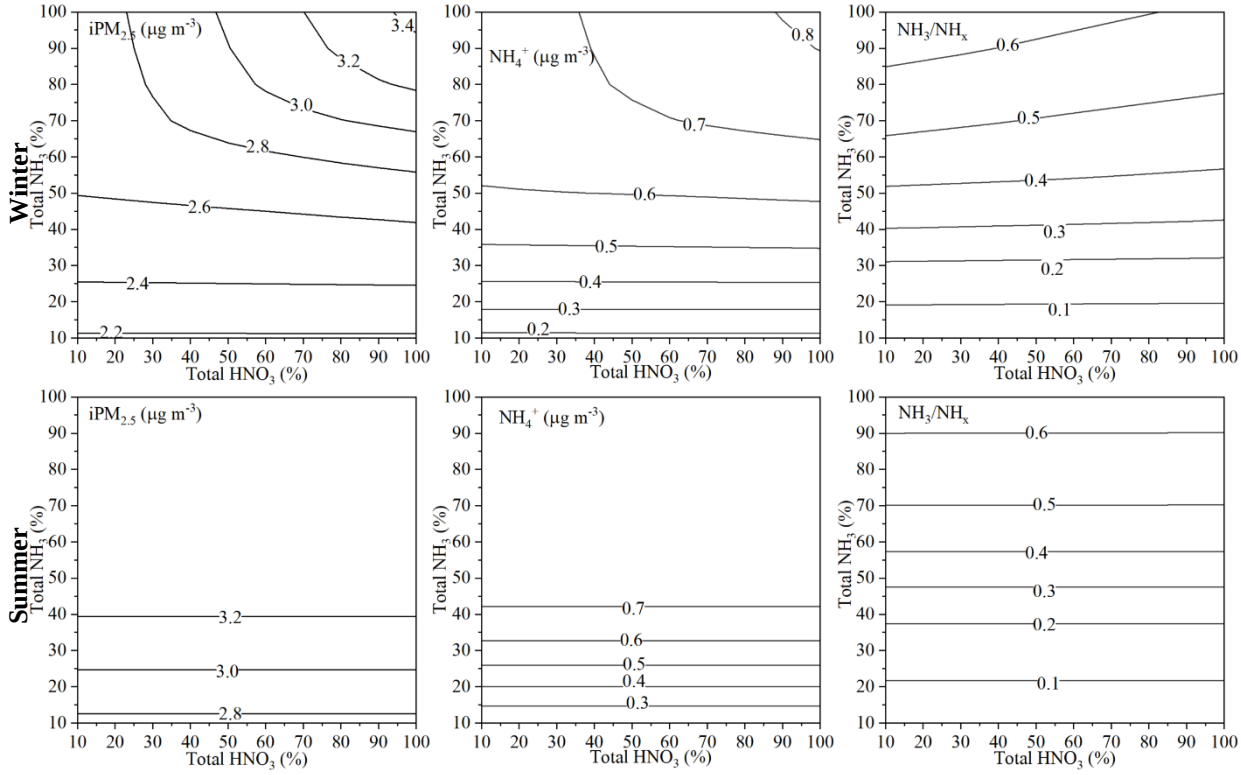

Figure 5.4. Responses of $iPM_{2.5}$ (left), NH_4^+ (middle), and NH_3/NH_x (right) to the changes of TNH_3 and $THNO_3$ at the BHM site in summer and winter of 2012-2016

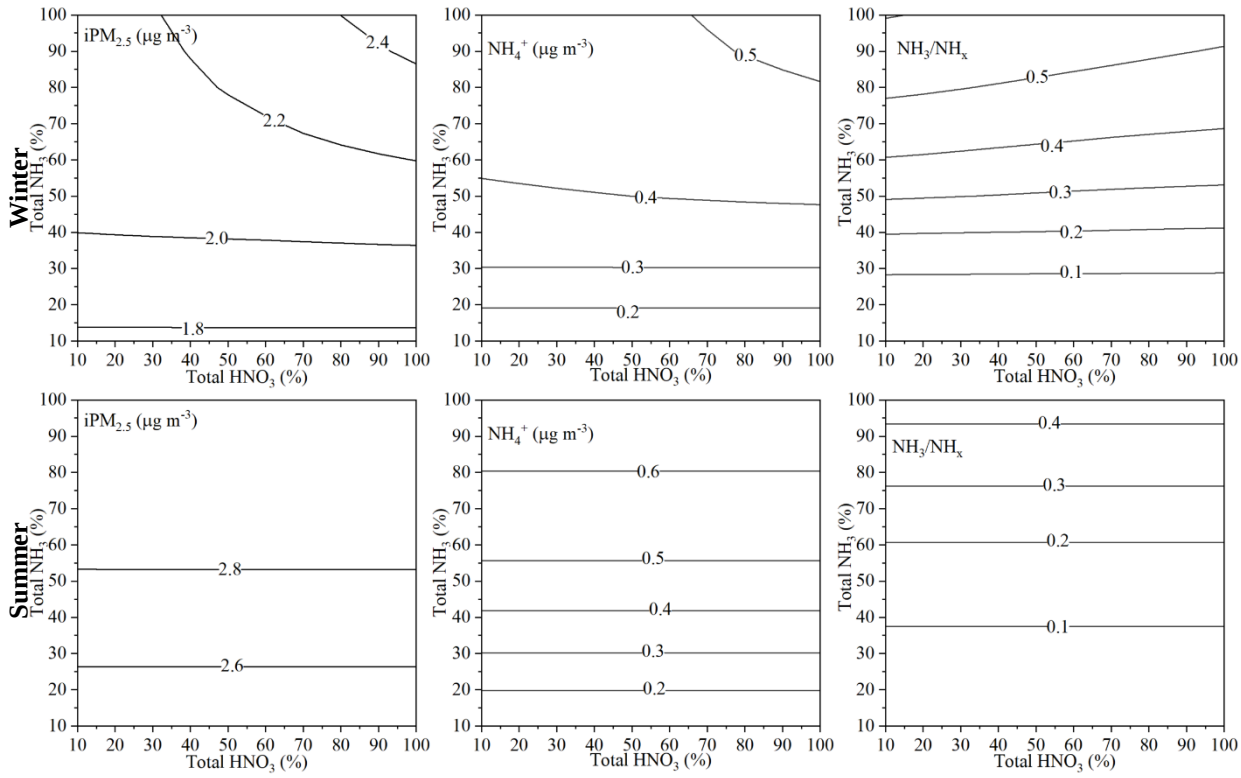

Figure 5.5. Responses of $iPM_{2.5}$ (left), NH_4^+ (middle), and NH_3/NH_x (right) to the changes of TNH_3 and $THNO_3$ at the OLF site in summer and winter of 2013-2016

As it can be seen in Figures 5.1-5.5, the formation of $iPM_{2.5}$ and the partitioning of $NH_3 - NH_4^+$ were not sensitive to the changes of total NH_3 concentration unless when total NH_3 concentration was reduced at least 20% or when total HNO_3 concentration remained at the approximately the same level in 2012-2016. The YRK, JST, BHM, OLF were all under NH_3–rich condition, thus, NH_3 was adequate to react with both H_2SO_4 and HNO_3 at these four sites. The reduction in total NH_3 concentration was able to decrease the gas–phase NH_3 concentration but not able to decrease the formation of $iPM_{2.5}$. When enough reduction in total NH_3 was achieved or acidic gases (total H_2SO_4 and total HNO_3) were in excess to react with NH_3 gas, the subsequent reduction in total NH_3 led to the decrease of $iPM_{2.5}$.

In addition, the formation of $iPM_{2.5}$ and the partitioning of $NH_3 - NH_4^+$ were more

sensitive to the changes of total NH_3 and total HNO_3 in winter than in the other seasons. The semi–volatile characteristics of NH_4NO_3 may explain the seasonal variation of the responses of $iPM_{2.5}$ to the change of total NH_3 and total HNO_3. The lower T in winter favored the formation of NH_4NO_3, if there was adequate NH_3 reacting with acidic gases, most of the HNO_3 staied in particle phase. Thus, as it can be observed from Figures 5.1-5.5, the formation of $iPM_{2.5}$ was sensitive to the change of total HNO_3 when total NH_3 was at approximately the same level in winter of 2012–2016.

The responses of $iPM_{2.5}$, NH_4^+ and NH_3/NH_x to the changes of total NH_3 and total H_2SO_4 are presented in Figures 5.6-5.10.

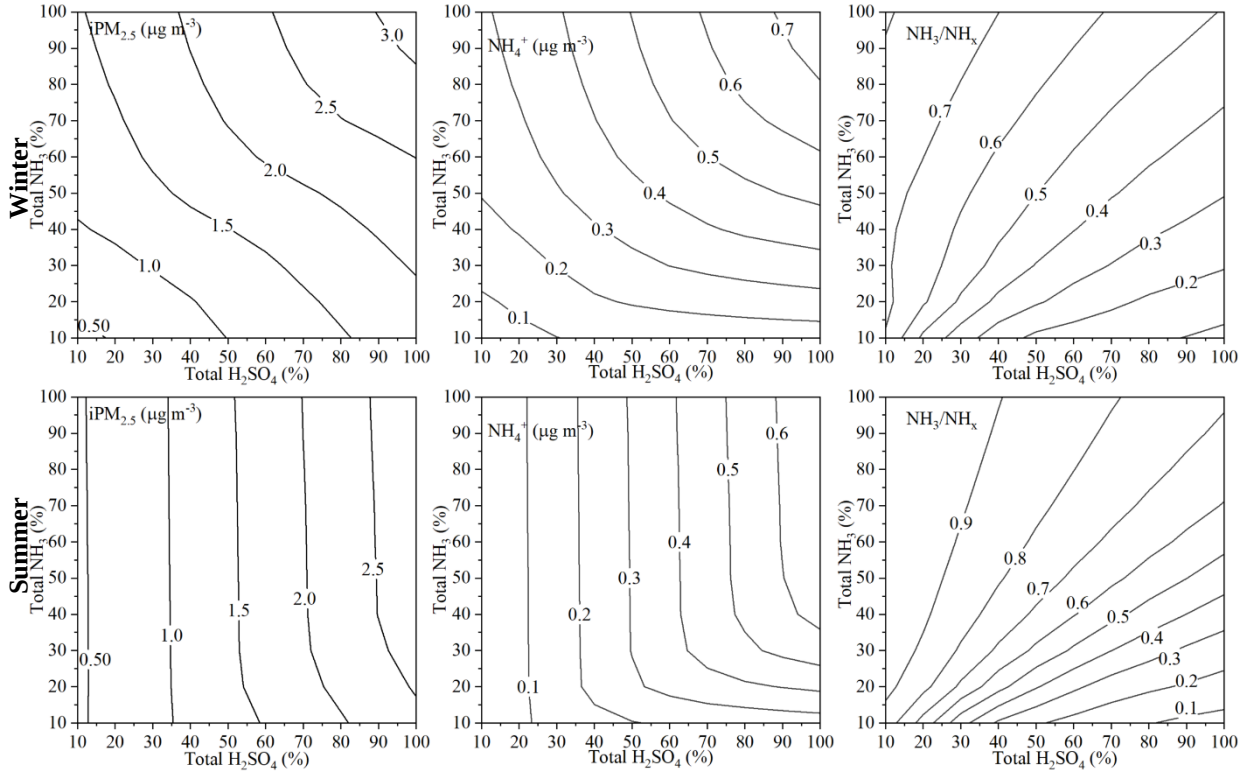

Figure 5.6. Responses of $iPM_{2.5}$ (left), NH_4^+ (middle), and NH_3/NH_x (right) to the changes of TNH_3 and TH_2SO_4 at the YRK site in summer and winter of 2012-2016

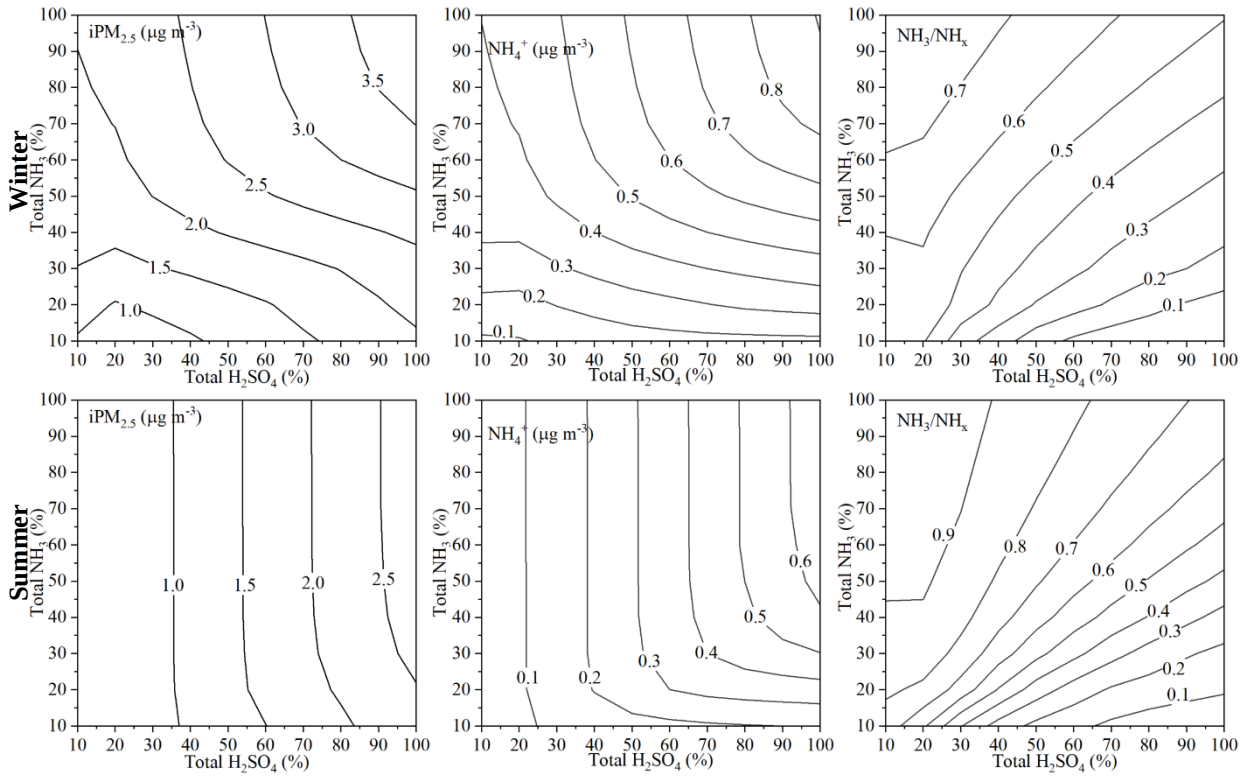

Figure 5.7. Responses of $iPM_{2.5}$ (left), NH_4^+ (middle), and NH_3/NH_x (right) to the changes of TNH_3 and TH_2SO_4 at the JST site in summer and winter of 2012-2016

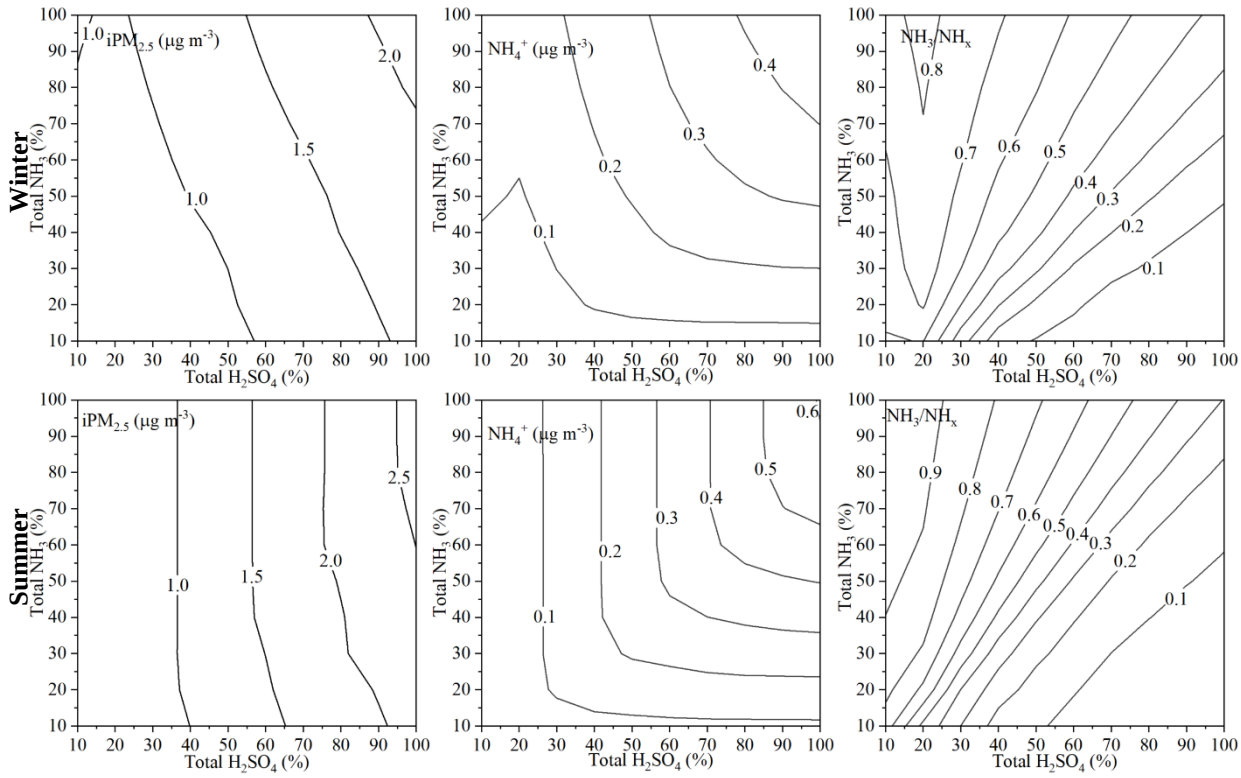

Figure 5.8. Responses of $iPM_{2.5}$ (left), NH_4^+ (middle), and NH_3/NH_x (right) to the changes of TNH_3 and TH_2SO_4 at the CTR site in summer and winter of 2012-2016

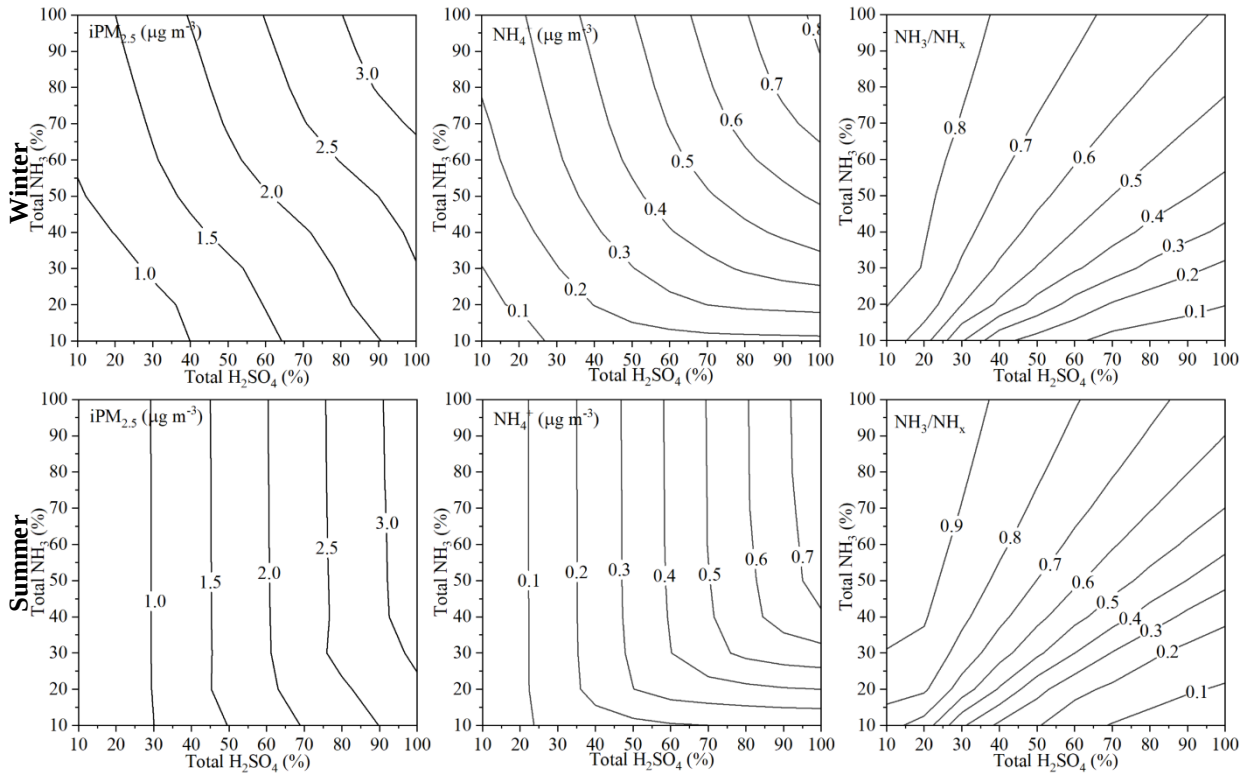

Figure 5.9. Responses of $iPM_{2.5}$ (left), NH_4^+ (middle), and NH_3/NH_x (right) to the changes of TNH_3 and TH_2SO_4 at the BHM site in summer and winter of 2012-2016

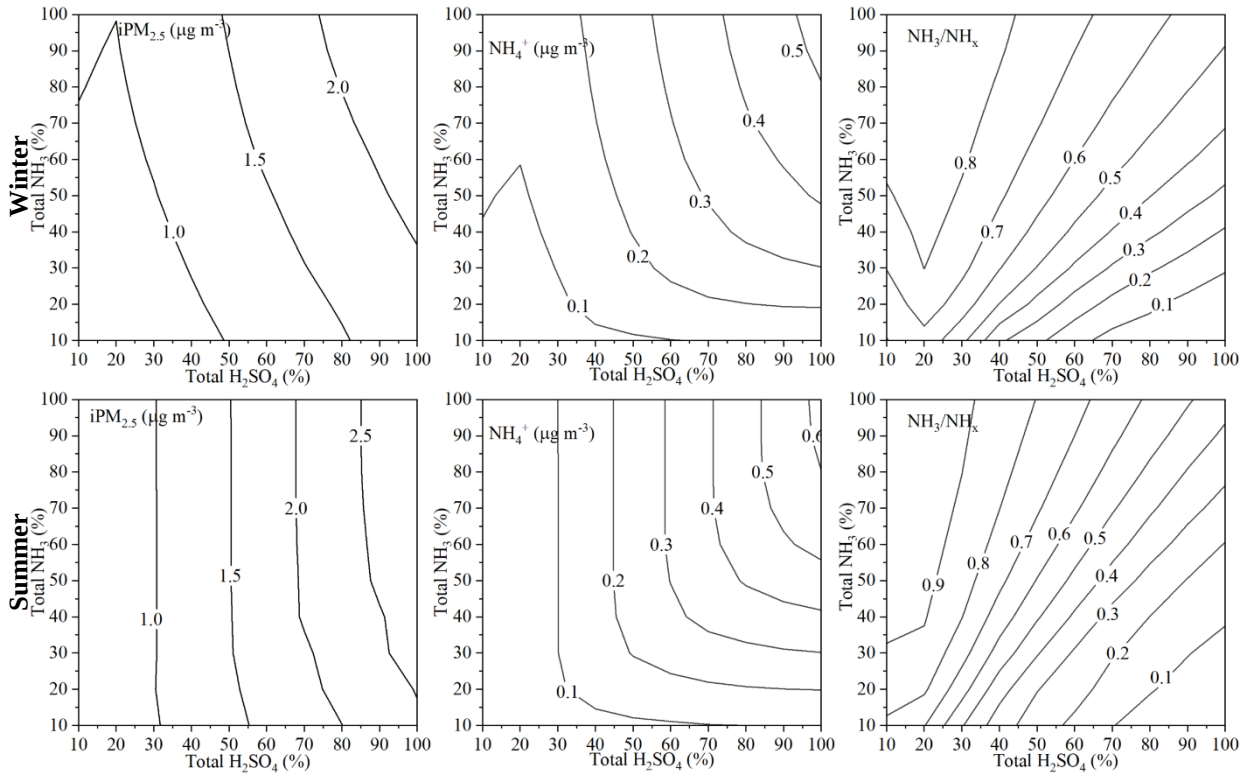

Figure 5.10. Responses of $iPM_{2.5}$ (left), NH_4^+ (middle), and NH_3/NH_x (right) to the changes of TNH_3 and TH_2SO_4 at the OLF site in summer and winter of 2013-2016

As it can be seen in Figures 5.6-5.10, the formation of $iPM_{2.5}$ was very sensitive to the change of total H_2SO_4 concentration in both summer and winter. The reduction of total H_2SO_4 effectively decreased the concentration of $iPM_{2.5}$, and more NH_3 stayed in gas phase in this process. The responses of NH_4^+ to the change of total H_2SO_4 may exhibit two different regions. The less reduction in total NH_3 and the more reduction in total H_2SO_4 were achieved, the more sensitive the NH_4^+ responded to the change of total H_2SO_4. This can be explained that when NH_3 was not adequate to react with both HNO_3 and H_2SO_4, the reduction of H_2SO_4 may free some NH_3 tied up with SO_4^{2-}, and the available NH_3 can react with HNO_3 to form NH_4NO_3, which lead to the decrease of SO_4^{2-} salts but increase of NO_3^- salts. Thus, NH_4^+ concentration may remain the approximately the same level. We can also observe that when greater than 80% reduction in

total H_2SO_4 is achieved, the reduction of total H_2SO_4 may lead to the increase of $iPM_{2.5}$ at the JST, CTR, and OLF sites in winter.

In addition, the formation of $iPM_{2.5}$ was more sensitive to the change of total H_2SO_4 in summer than in winter. This can be explained by the dominance of SO_4^{2-} salts of $iPM_{2.5}$ in summer. The more intense summer solar radiation enhances the transformation of SO_2 to SO_4^{2-} (Seinfeld and Pandis, 2006). Moreover, the high T in summer doesn't favor the formation of NH_4NO_3, the decrease in SO_4^{2-} salts caused by the reduction in total H_2SO_4 won't be offset by the increase in the NO_3^- salts.

5.3.3. Diurnal simulation of the partitioning of NH_3–NH_4^+

In addition to the investigation of partitioning of $NH_3 - NH_4^+$ in four seasons, the partitioning of $NH_3 - NH_4^+$ was also studied in different time of the day at five sites in 2012-2016.

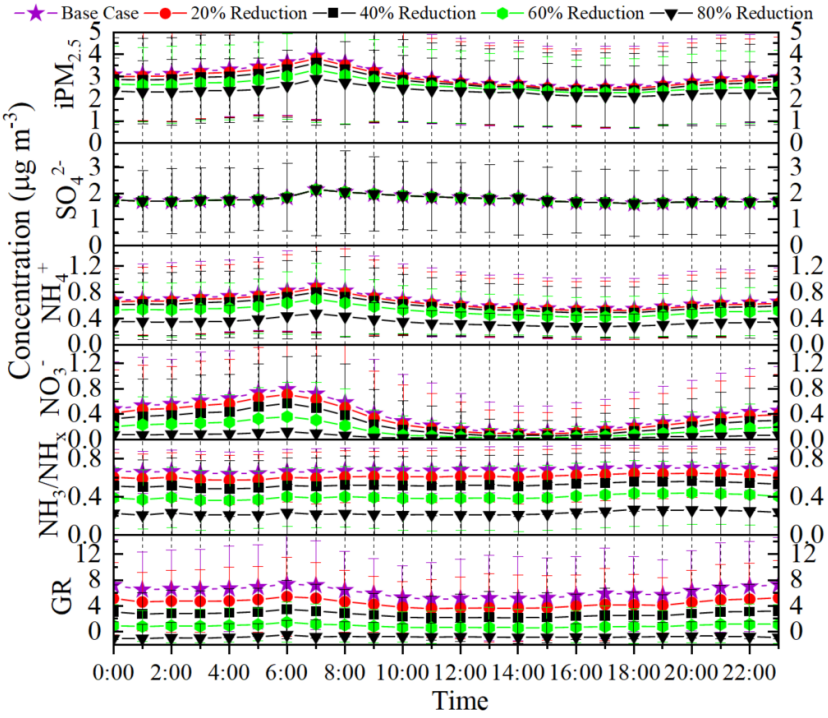

Figure 5.11. Responses of $iPM_{2.5}$, SO_4^{2-}, NH_4^+, NO_3^-, NH_3/NH_x, and GR to the reductions in TNH_3 at the BHM site in 2012-2016

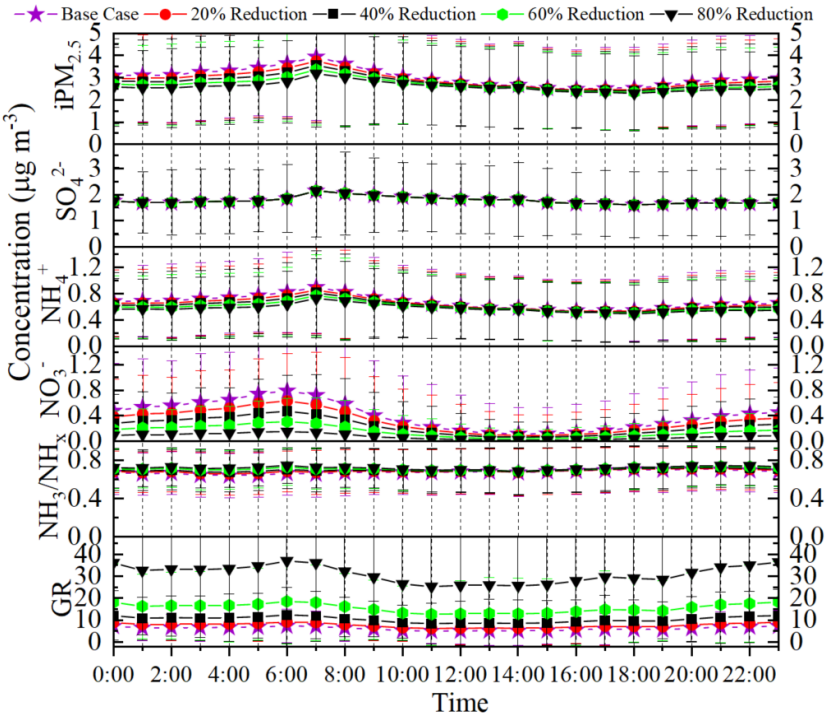

Figure 5.12. Responses of $iPM_{2.5}$, SO_4^{2-}, NH_4^+, NO_3^-, NH_3/NH_x, and GR to the reductions in $THNO_3$ at the BHM site in 2012-2016

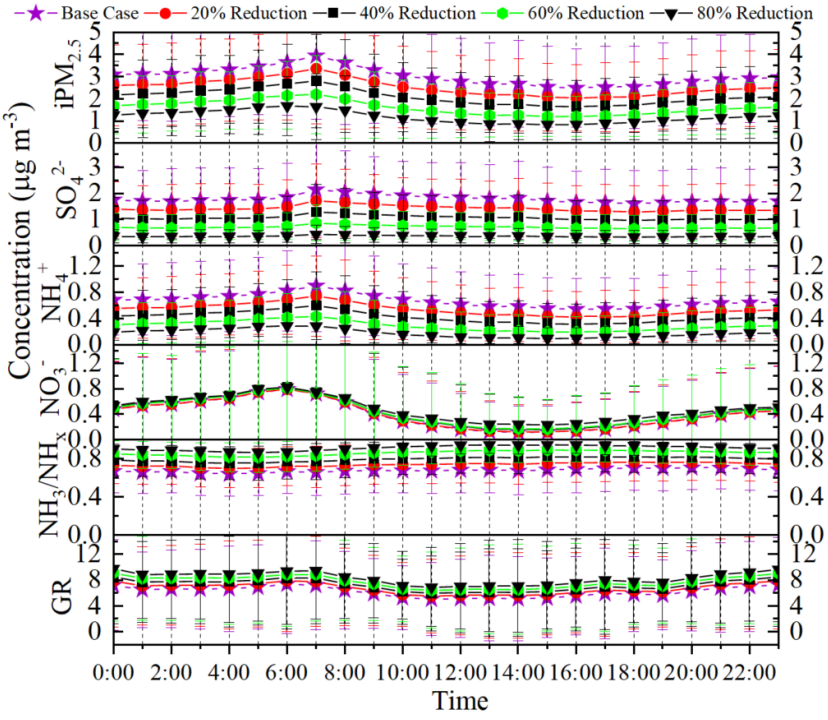

Figure 5.13. Responses of $iPM_{2.5}$, SO_4^{2-}, NH_4^+, NO_3^-, NH_3/NH_x, and GR to the reductions in TH_2SO_4 at the BHM site in 2012-2016

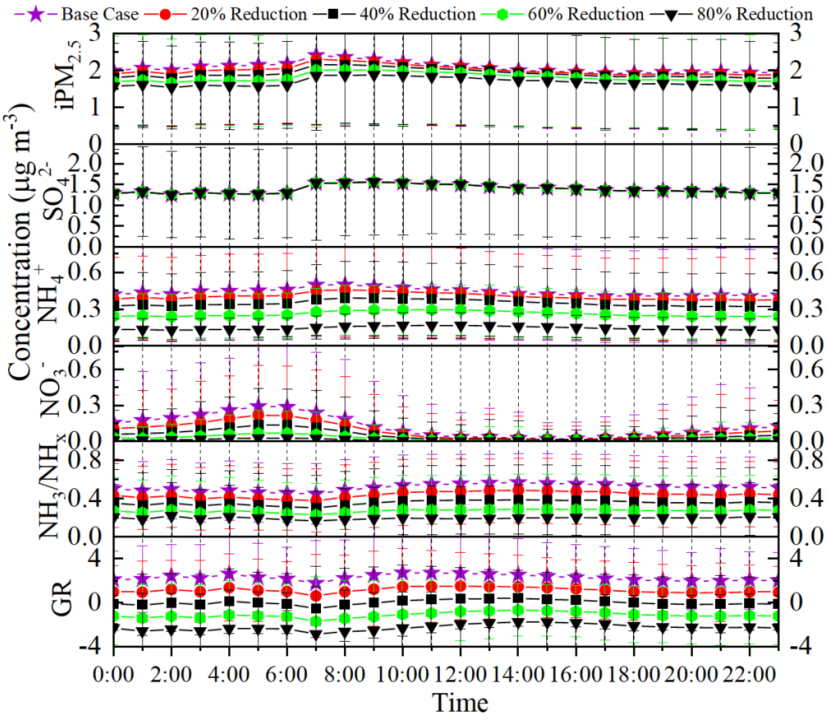

Figure 5.14. Responses of $iPM_{2.5}$, SO_4^{2-}, NH_4^+, NO_3^-, NH_3/NH_x, and GR to the reductions in TNH_3 at the CTR site in 2012-2016

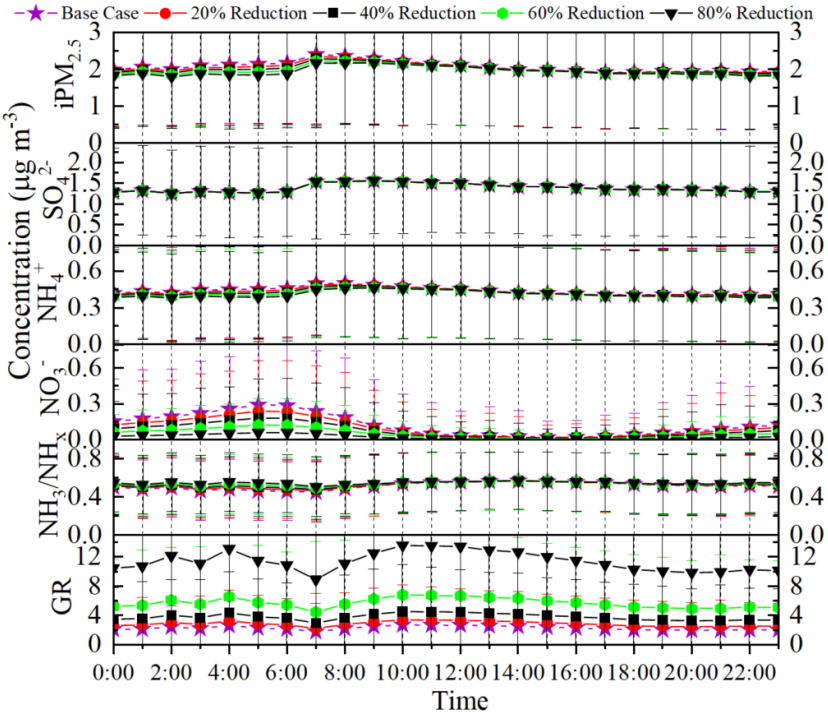

Figure 5.15. Responses of $iPM_{2.5}$, SO_4^{2-}, NH_4^+, NO_3^-, NH_3/NH_x, and GR to the reductions in $THNO_3$ at the CTR site in 2012-2016

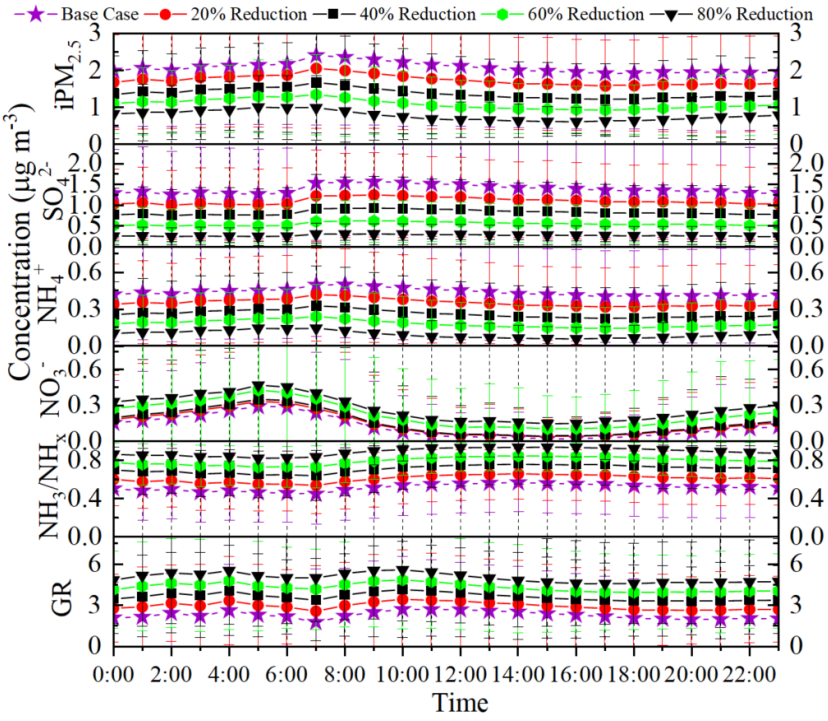

Figure 5.16. Responses of $iPM_{2.5}$, SO_4^{2-}, NH_4^+, NO_3^-, NH_3/NH_x, and GR to the reductions in TH_2SO_4 at the CTR site in 2012-2016

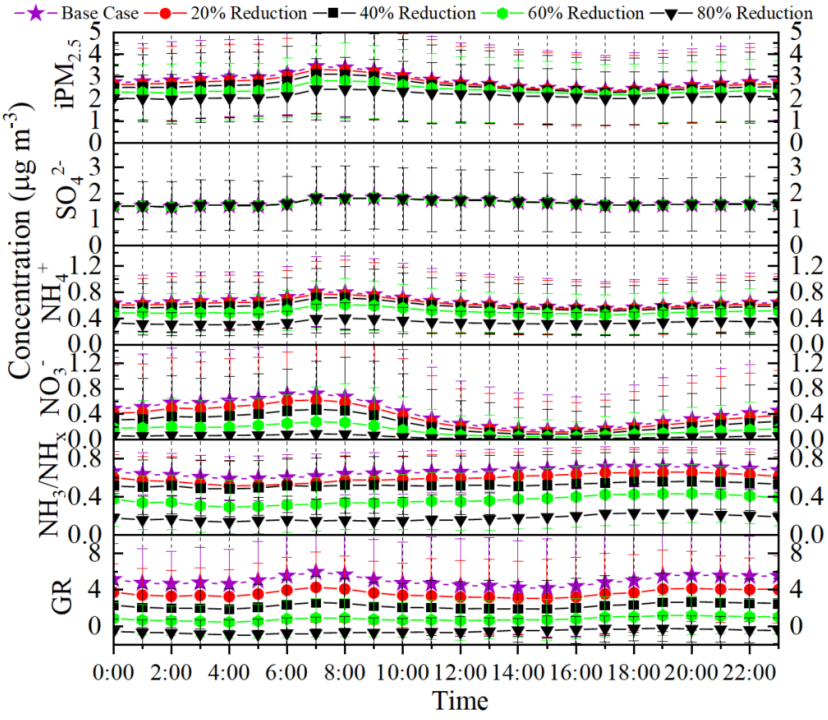

Figure 5.17. Responses of $iPM_{2.5}$, SO_4^{2-}, NH_4^+, NO_3^-, NH_3/NH_x, and GR to the reductions in TNH_3 at the JST site in 2012-2016

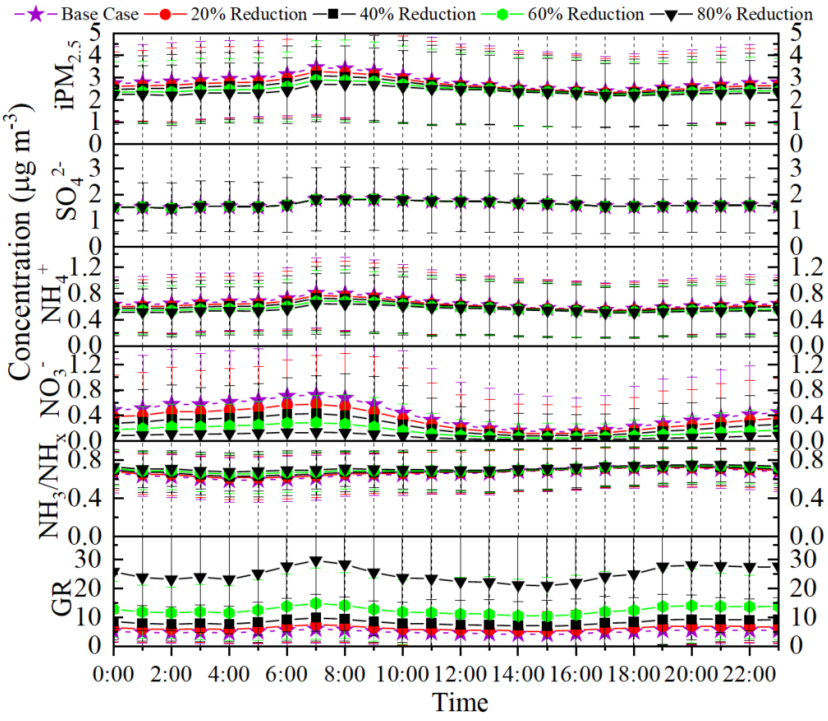

Figure 5.18. Responses of $iPM_{2.5}$, SO_4^{2-}, NH_4^+, NO_3^-, NH_3/NH_x, and GR to the reductions in $THNO_3$ at the JST site in 2012-2016

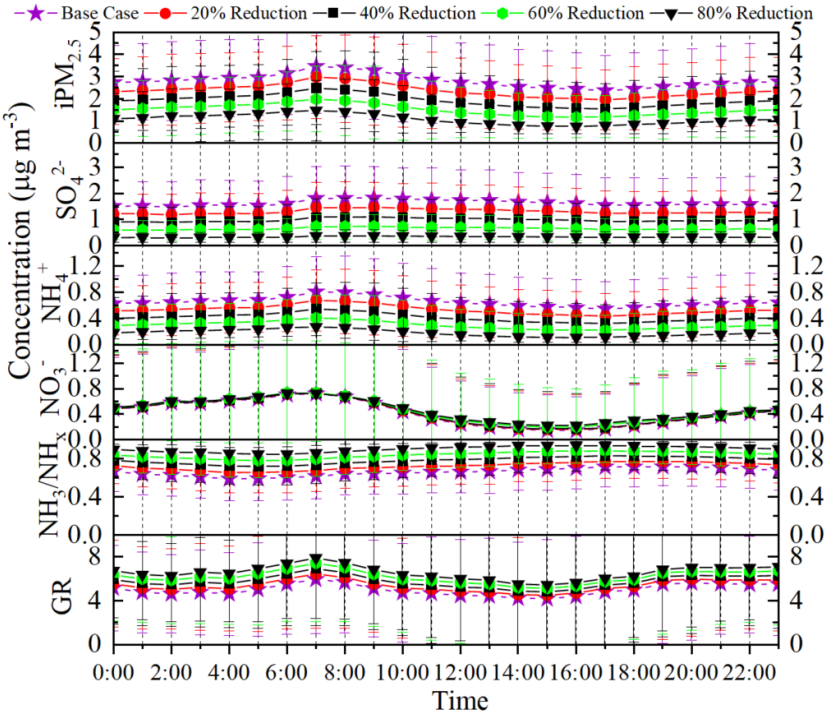

Figure 5.19. Responses of $iPM_{2.5}$, SO_4^{2-}, NH_4^+, NO_3^-, NH_3/NH_x, and GR to the reductions in TH_2SO_4 at the JST site in 2012-2016

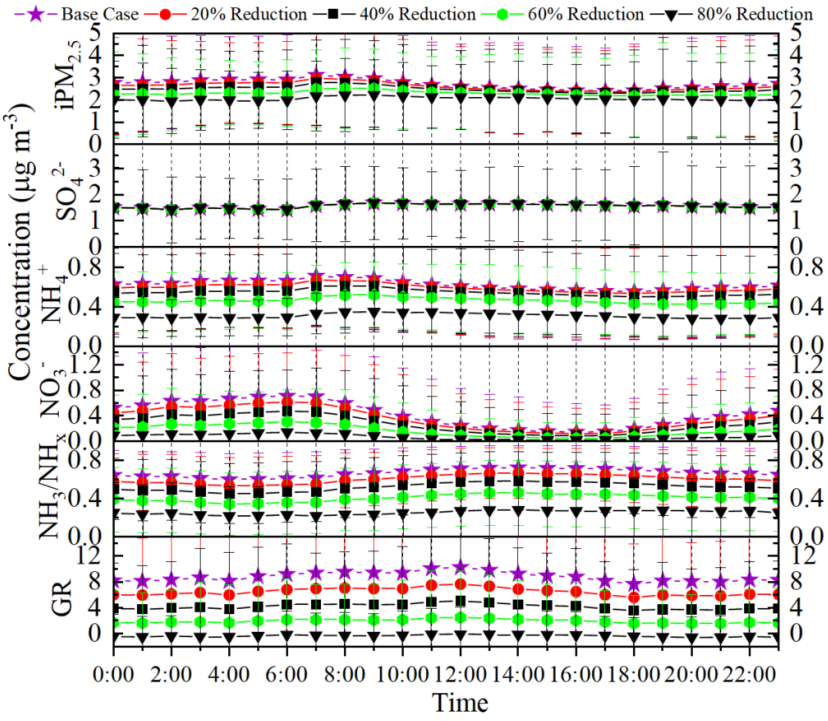

Figure 5.20. Responses of $iPM_{2.5}$, SO_4^{2-}, NH_4^+, NO_3^-, NH_3/NH_x, and GR to the reductions in TNH_3 at the YRK site in 2012-2016

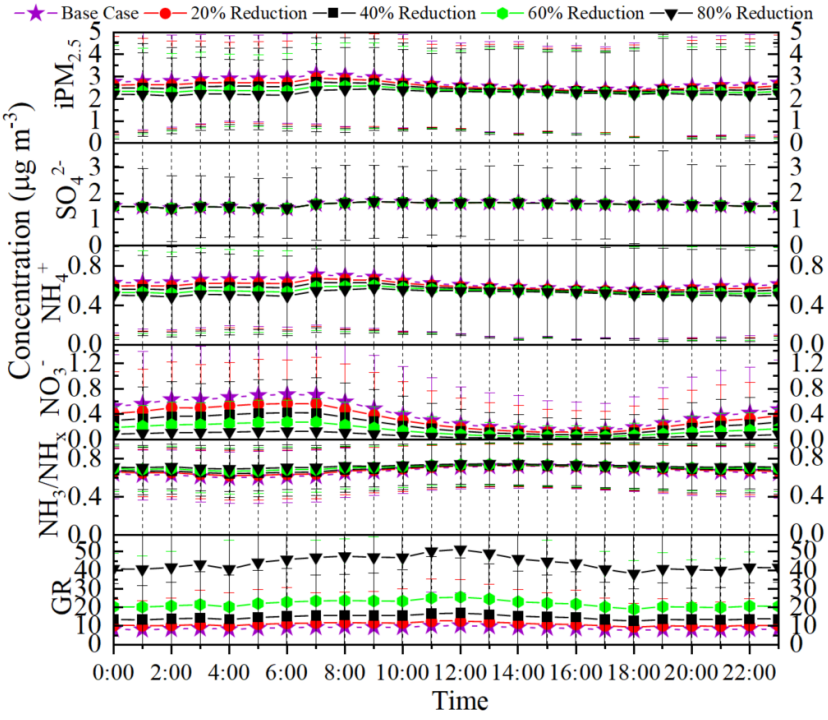

Figure 5.21. Responses of $iPM_{2.5}$, SO_4^{2-}, NH_4^+, NO_3^-, NH_3/NH_x, and GR to the reductions in $THNO_3$ at the YRK site in 2012-2016

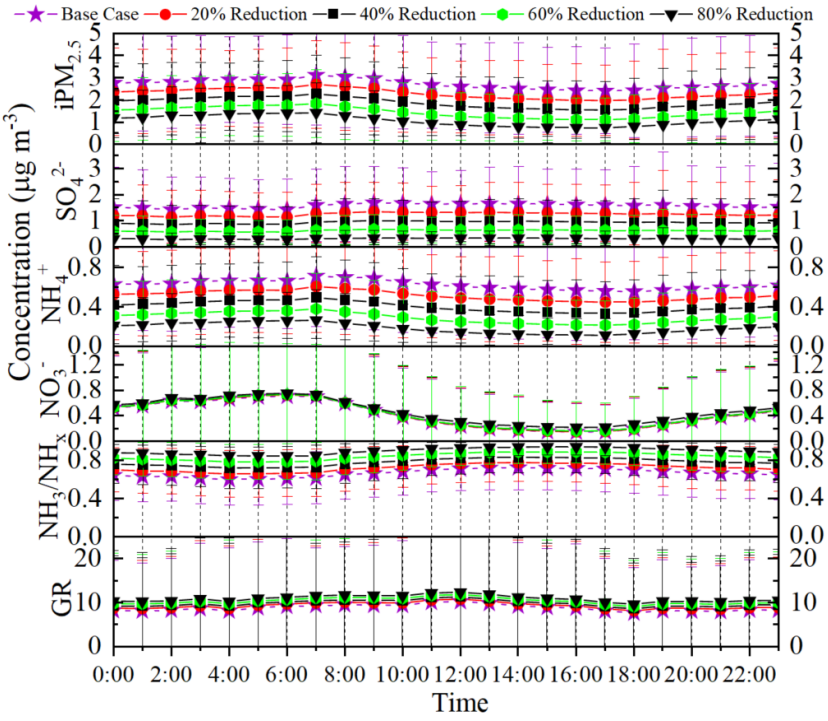

Figure 5.22. Responses of $iPM_{2.5}$, SO_4^{2-}, NH_4^+, NO_3^-, NH_3/NH_x, and GR to the reductions in TH_2SO_4 at the YRK site in 2012-2016

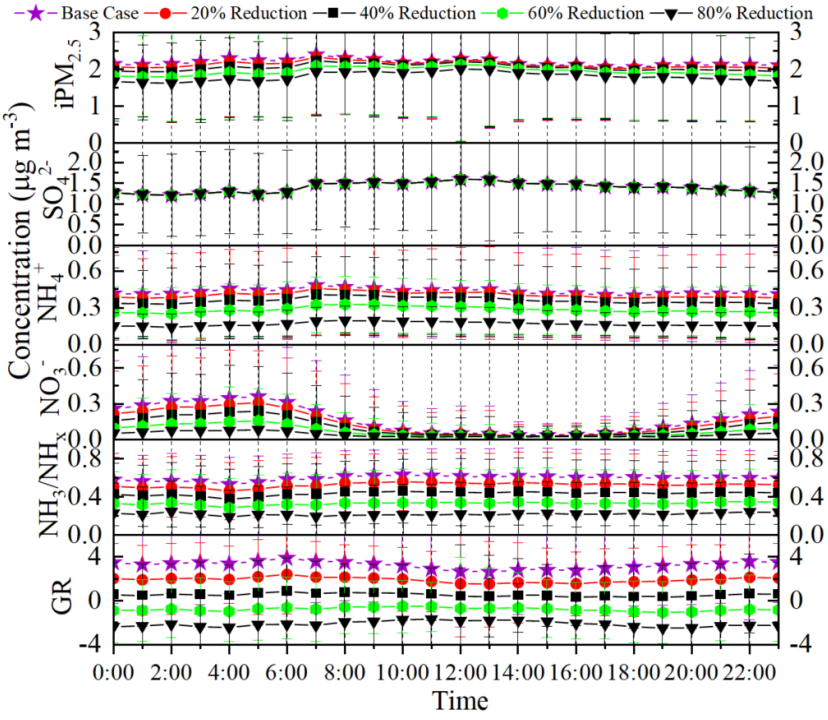

Figure 5.23. Responses of $iPM_{2.5}$, SO_4^{2-}, NH_4^+, NO_3^-, NH_3/NH_x, and GR to the reductions in TNH_3 at the OLF site in 2013-2016

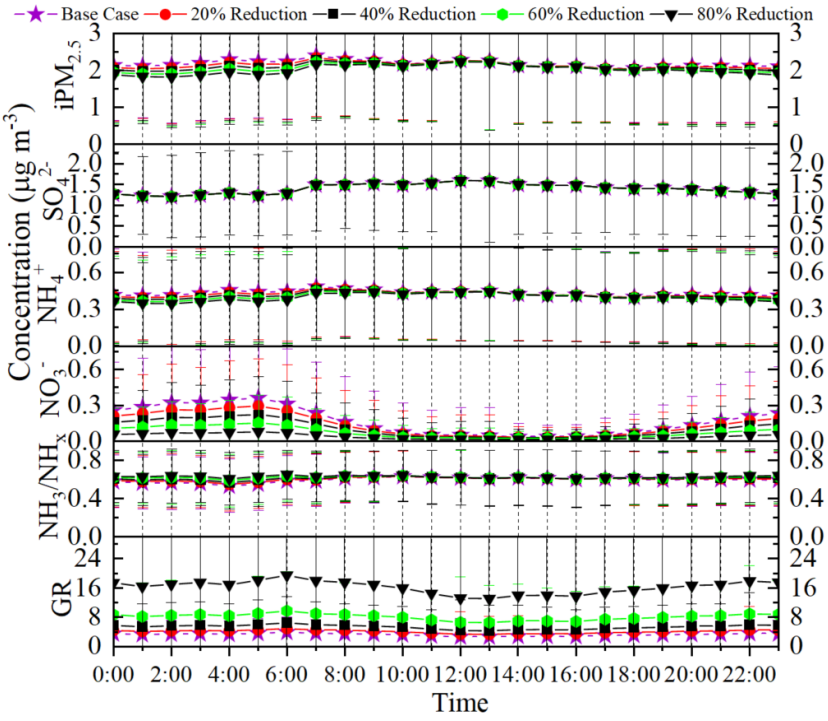

Figure 5.24. Responses of $iPM_{2.5}$, SO_4^{2-}, NH_4^+, NO_3^-, NH_3/NH_x, and GR to the reductions in $THNO_3$ at the OLF site in 2013-2016

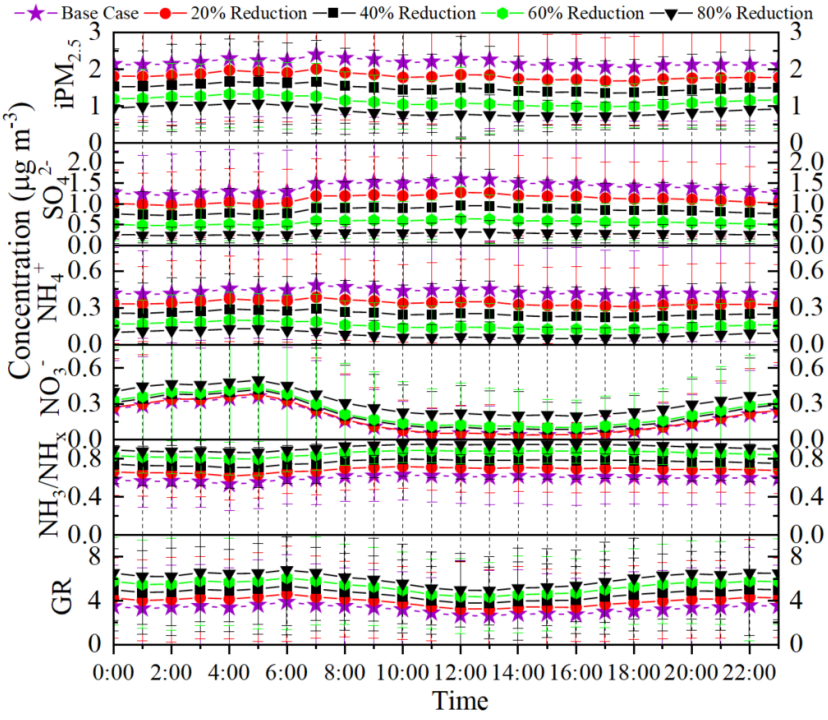

Figure 5.25. Responses of $iPM_{2.5}$, SO_4^{2-}, NH_4^+, NO_3^-, NH_3/NH_x, and GR to the reductions in TH_2SO_4 at the OLF site in 2013-2016

As it can be seen from Figures 5.11-5.25, the reduction of total NH_3 and total HNO_3 may not be effective to reduce the concentration of $iPM_{2.5}$ unless 60% to 80% of reduction can be achieved. In addition, the reduction of total NH_3 and total HNO_3 can only lead to the decrease of NH_4NO_3, while the SO_4^{2-} concentration remains approximately the same level. The reduction of total NH_3 concentration decreases both NH_3/NH_x and GR, and the NH_3 tends to stay in particle phase instead of gas phase. On the contrary, the reduction of total HNO_3 leads to the increase of both NH_3/NH_x and GR, and the NH_3 tends to stay in gas phase instead of particle phase. Thus, reductions of total NH_3 and total HNO_3 pose reverse influence on the atmospheric chemical condition.

The reduction of total H_2SO_4 is more effective to reduce the concentrations of $iPM_{2.5}$; however, the reduction of total H_2SO_4 may sometimes lead to the increase of NO_3^- concentration, especially at the CTR and OLF sites. The YRK, JST, and BHM sites are all in NH_3–rich area and the NH_3 gas is in excess to fully neutralize both HNO_3 and H_2SO_4 at these three sites. The reduction of total H_2SO_4 may free some NH_3 tied up with H_2SO_4, however, the increase of gas–phase NH_3 isn't able to transform more HNO_3 into particle phase at NH_3–rich sites. While at the CTR and OLF sites, the increase of gas–phase NH_3 may change the partitioning of HNO_3– NO_3^- toward particle phase when the NH_3 isn't in excess to neutralize both HNO_3 and H_2SO_4. The reduction of total H_2SO_4 can also increase both NH_3/NH_x and GR, which indicates that the NH_3 tends to stay in gas phase instead of particle phase in this process.

Reduction of total H_2SO_4 concentration may lead to significant reduction of $iPM_{2.5}$, thus, it is more effective than reducing total HNO_3 and total NH_3 concentrations to reduce $iPM_{2.5}$ concentration. However, the reduction of total H_2SO_4 concentration may also increase the

concentration NO_3^- at some sites. Therefore, the future reduction of $iPM_{2.5}$ may necessitate the coordinated reduction of both H_2SO_4 and HNO_3 in the Southeastern U.S.

The YRK site is located in rural area impacted by the NH_3 emissions from AFOs, while BHM and JST sites are located in the area impacted by industrial emission sources. The CTR site is located in a forest area and the OLF site is located in suburban area. The spatial variation of the responses of the partitioning of $NH_3 - NH_4^+$ to the reductions of precursor gases implicates the important impact of AFOs NH_3 emissions. At the agricultural rural site–YRK site, the NH_3 emissions from AFOs lead to elevated NH_3 concentration, which is in excess to fully neutralize acidic gases, and the formation of NH_4NO_3 is not affected by the reduction of total H_2SO_4.

5.4. Conclusion

In this research, the effects of changes in precursor gases on the formation of $iPM_{2.5}$ as well as the partitioning of $NH_3 - NH_4^+$ were investigated using ISORROPIA II based on field measurements of gas–phase and particle–phase pollutants and meteorological data in SEARCH Network. The results indicate that the reduction of total H_2SO_4 is more effective to decrease the formation of $iPM_{2.5}$ especially under NH_3–rich condition. In addition, the reduction of total H_2SO_4 may change the partitioning of $NH_3 - NH_4^+$ towards gas phase. Moreover, the reduction of total H_2SO_4 may lead to the increase of NO_3^- when NH_3 is not in excess to fully neutralize the acidic gases. Thus, the future reduction of $iPM_{2.5}$ may necessitate the coordinated reduction of both H_2SO_4 and HNO_3 in the Southeastern U.S. It is discovered that the response of $iPM_{2.5}$ to the change of total H_2SO_4 is more sensitive in summer than winter. The dominance of SO_4^{2-} salts of $iPM_{2.5}$ and high T in summer don't favor the formation of NH_4NO_3, the decrease in SO_4^{2-} salts caused by the reduction in total H_2SO_4 won't be offset by the increase in the NO_3^- salts. The

significant NH_3 emissions from AFOs in the agricultural rural area have great impact on the partitioning of $NH_3 - NH_4^+$ and the NH_3 emissions from AFOs leads to the elevated NH_3 concentration, which is in excess to fully neutralize acidic gases. The formation of NH_4NO_3 is not affected by the reduction of total H_2SO_4 in agricultural rural area. The ISORROPIA II model simulation integrated the previous findings in environmental research and provided projected prediction, thus serves as a powerful tool for us to get a deeper understanding about the partitioning of $NH_3 - NH_4^+$.

CHAPTER 6: FUTURE WORK

While this research advanced our understanding of impacts of AFOs NH_3 emissions on the partitioning of NH_3–NH_4^+ in the Southeastern U.S., more work is needed to further investigate the applicability of ISORROPIA II for predicting $iPM_{2.5}$ and NH_3 deposition pattern.

1. High time–resolution (e.g., 5 min) measurements of gas–phase and particle–phase pollutants including NH_3, HNO_3, HCl, NH_4^+, SO_4^{2-}, NO_3^-, Cl^-, Na^+, K^+, Mg^{2+}, and Ca^{2+} are required to further evaluate the applicability of ISORROPIA II model in simulation inorgarnic aerosols under different atmospheric chemical conditions.
2. The impact of organic gases and/or organic aerosols on the equilibrium process of inorganic aerosols is not determined. Thus, future studies should be performed to investigate the linkage between organic and inorganic $PM_{2.5}$.
3. The time scale to reach equilibrium state varies for different sizes of aerosols. Thus, the size–resolved measurements of $PM_{2.5}$ chemical compositions may be needed to determine the applicability of thermodynamic equilibrium model for simulation of different sizes of inorganic aerosols.
4. As the acidic gas concentrations were significantly reduced in the past decade, the deposition pattern will change for NH_3 correspondingly, the NH_3 tends to stay in gas phase instead of particle phase. Future study may be needed to investigate the deposition pattern change of NH_3 under urban and rural conditions.

REFERENCES

Abbatt, J. P. D., Benz, S., Cziczo, D. J., Kanji, Z., Lohmann, U., Mohler, O. (2006). Solid ammonium sulfate aerosols as ice nuclei: a pathway for cirrus cloud formation. *Science, 313*(5794), 1770-1773.

Abdeen, Z., Qasrawi, R., Heo, J., Wu, B., Shpund, J., Vanger, A., Sharf, G., Moise, T., Brenner, S., Nassar, K., Saleh, R., Al-Mahasneh, Q. M., Sarnat, J. A. & Schauer. J. J. (2014). Spatial and temporal variation in fine particulate matter mass and chemical composition: The Middle East consortium for aerosol research study. *Scientific World J., 2014*, 1-16. http://dx.doi.org/10.1155/2014/878704.

Allen, A. G., Harrison, R. M., & Wake, M. T. (1988). A meso-scale study of the behavior of atmospheric ammonia and ammonium. *Atmos. Environ., 22*(7), 1347-1353.

Allen, A. G., & Harrison, R. M. (1989). Field measurements of the dissociation of ammonium nitrate and ammonium chloride aerosols. *Atmos. Environ., 23*(7), 1591-1599.

Andrews, E., Saxena, P., Musarra, S., Hildemann, L. M., Koutrakis, P., McMurry, P. H., Olmez I. & White, W. H. (2000). Concentration and Composition of Atmospheric Aerosols from the 1995 SEAVS Experiment and a Review of the Closure between Chemical and Gravimetric Measurements. *J. Air & Waste Manage. Assoc., 50*(5), 648-664.

Aneja, V. P., Chauhan, J. P., & Walker, J. T. (2000). Characterization of atmospheric ammonia emissions from swine waste storage and treatment lagoons. *J. Geophy. Res., 105*(D9), 11535-11545.

Aneja, V. P., Nelson, D. R., Roelle, P. A., Walker, J. T., & Battye, W. (2003). Agricultural ammonia emissions and ammonium concentrations associated with aerosols and precipitation in the southeast United States. *J. Geophys. Res., 108*(D4), 4152.

Ansari, A. S., & Pandis, S. N. (1998). Response of inorganic PM to precursor concentrations. *Environ. Sci. Technol., 32*(18), 2706-2714.

Ansari A. S., & Pandis, S. N. (1999a). Prediction of multicomponent inorganic atmospheric aerosol behavior. *Atmos. Environ., 33*, 745-757.

Ansari A. S., & Pandis, S. N. (1999b), An analysis of four models predicting the partitioning of semivolatile inorganic aerosol components. *Aeros. Sci. Tech., 31*, 129-153.

Ansari A. S., & Pandis, S. N. (2000). The effect of metastable equilibrium states on the partitioning of nitrate between the gas and aerosol phases. *Atmos. Environ., 34*(2000), 157-168.

Arogo, J., Westerman, P. W., Heber, A. J., Robarge, W. P. & Classen, J. J. (2006). Ammonia emissions from animal feeding operations. Available at http://citeseerx.ist.psu.edu/viewdoc/download?doi=10.1.1.484.8060&rep=rep1&type=pdf.

Asman, W. A. H., & van Jaarsveld, H. A. (1992). A variable-resolution transport model applied for NH_x for Europe. *Atmos. Environ., 26A*, 445-464.

Asman, W. A. H. (1998). Factors influencing local dry deposition of gases with special reference to ammonia. *Atmo. Environ., 32*, 415–421.

Asman, W. A. H., Sutton, M. A. & Schjoerring, J. K. (1998). Ammonia: Emission, atmospheric transport and deposition. *New Phytologist, 139*(1), 27-48.

Bell, M. L., Dominici, F., Ebisu, K., Zeger, S. L. & Samet, J. M. (2007). Spatial and temporal variation in $PM_{2.5}$ chemical composition in the United States for health effects studies. *Environ. Health Perspect., 115*(7), 989-995.

Bittman, S. & Mikkelsen, R. (2009). Ammonia Emissions from Agricultural Operations: Live Stock. Better Crops. Available at https://pdfs.semanticscholar.org/ba25/d10cd0ca0cad97ca3cc0ab759d82e7deb75b.pdf.

Blanchard, C. L., Tanenbaum, S., Hidy, G. M. (2012). Source contributions to atmospheric gases and particulate matter in the Southeastern United States. *Environ. Sci. Technol., 46,* 5479-5488.

Blanchard, C. L., Hidy, G. M., Tanenbaum, S., Edgerton, E. S., & Hartsell, B. E. (2013a). The Southeastern Aerosol Research and Characterization (SEARCH) study: Spatial variations and chemical climatology, 1999–2010, *J. Air Waste Manage. Assoc., 63*(3), 260-275.

Blanchard, C. L., Roth, P. M., Tanenbaum, S. J., Ziman, S. D., & Seinfeld, J. H. (2000). The use of ambient measurements to identify which precursor species limit aerosol nitrate formation. *J. Air Waste Manage. Assoc., 50*(12), 2073-2084.

Blanchard, C. L., & Hidy, G. M. (2003). Effects of Changes in Sulfate, Ammonia, and Nitric Acid on Particulate Nitrate Concentrations in the Southeastern United States, *J. Air Waste Manage. Assoc., 53*(3), 283-290.

Blanchard, C. L. & Hidy, G. M. (2005). Effects of SO_2 and NO_x Emission Reductions on $PM_{2.5}$ Mass Concentrations in the Southeastern United States, *J. Air Waste Manage. Assoc., 55*(3), 265-272.

Blanchard, C. L., Tanenbaum, S., & Hidy, G. M. (2007). Effects of Sulfur Dioxide and Oxides of Nitrogen Emission Reductions on Fine Particulate Matter Mass Concentrations: Regional Comparisons, *J. Air Waste Manage. Assoc., 57*(11), 1337-1350.

Blanchard, C. L., Hidy, G. M., Tanenbaum, S., Edgerton, E. S., & Hartsell, B. E. (2013b). The Southeastern Aerosol Research and Characterization (SEARCH) study: Temporal trends in gas and PM concentrations and compositions, 1999–2010, *J. Air Waste Manage. Assoc.*, 63(3), 247-259.

Cambra-Lopez, M., Aarnink, A. J. A., Zhao, Y., Calvet, S., & Torres, A. G. (2010). Airborne particulate matter from livestock production systems: a review of an air pollution problem. *Environ. Pollut., 158*(1), 1-17.

Cambra-Lopez, M., Toores, A. G., Aarnink, A. J. A., & Ognik, N. W. M. (2011a). Source analysis of fine and coarse particulate matter from livestock houses. *Atmos. Environ., 45*(3), 694-707.

Cambra-Lopez, M., Hermosilla, T., Lai, H. T., Aarnink, A. J. A., & Ognik, N. W. M. (2011b). Particulate matter emitted from poultry and pig houses: source identification and quantification. *Transactions of the ASABE, 54*(2), 629-642.

Cambra-Lopez, M., Hermosilla, T., Lai, H. T., Aarnink, A. J. A., & Ognik, N. W. M. (2011c). Selection of particle characteristics to distinguish amongst potential sources of particulate matter in poulty and pigs. ASABE Paper No. 1111225. Louisville, Kentucky: ASABE.

Cohen, M. A., & Ryan, P. B. (1989). Observations less than the analytical limit of Detection: A new approach. *JAPCA, 39*(3), 328-329.

Capaldo, K. P., Pilinis, C., & Pandis, S. N. (2000). A computationally efficient hybrid approach for dynamic gas/aerosol transfer in air quality models. *Atmos. Environ., 34*, 3617-3627.

Cassel, T., Ashbaugh, L., Meyer, D., & Flocchini, R. (2005). Ammonia flux from open–lot dairies: development of measurement methodology and emission factors, *J. Air Waste Manage. Assoc., 55*(6), 816-825.

Cassel,T., Ashbaugh, L., Flocchini, R. & Meyer, D. (2005). Ammonia emission factors for open–lot dairies: direct measurements and estimation by nitrogen intake, *J. Air Waste Manage. Assoc., 55*(6), 826-833

Chang, J. C., & Hanna, S. R. (2004). Air Quality Model Performance Evaluation. *Meteo. Atmos. Phys., 87*(1-3), 167-196.

Dawson, J. P., Adam, P. J., & Pandis, S. N. (2007). Sensitivity of $PM_{2.5}$ to climate in the Eastern U.S.: a modeling case study. *Atmos. Chem. Phys., 7*, 4295-4309.

Donham, K. J., Reynolds, S. J., Whitten, P., Merchant, J. A., Burmeister, L., & Popendorf, W. J. (1995). Respiratory dysfunction in swine production facility workers: dose-response

relationships of environmental exposures and pulmonary-function. *Am. J. Ind. Med., 27*(3), 405-418.

Doorn, M. R. J., Natschke, D. F., Thorneloe, S. A., & Southerland, J. (2002). Development of an emission factor for ammonia emissions from US swine farms based on field tests and application of a mass balance method. *Atmos. Environ., 36*, 5619-5625.

Duyzer, J. (1994). Dry deposition of ammonia and ammonium aerosols over heathland. *J. Geophy. Res., 99*(D9), 18757.

Edgerton, E.S., B.E. Hartsell, R.D. Saylor, J.J. Jansen, D.A. Hansen, and G.M. Hidy. (2005). The Southeastern Aerosol Research and Characterization Study: Part 2: Filter-based measurements of $PM_{2.5}$ and PM_{coarse} mass and composition. *J. Air Waste Manage. Assoc., 55*, 1527-1542.

Edgerton, E.S., B.E. Hartsell, R.D. Saylor, J.J. Jansen, D.A. Hansen, and G.M. Hidy. (2006). The Southeastern Aerosol Research and Characterization Study: Part 3: Continuous measurements of fine particulate matter mass and composition. *J. Air Waste Manage. Assoc., 56*, 1325-1341.

Edgerton, E.S., R.D. Saylor, B.E. Hartsell, J.J. Jansen, and D.A. Hansen. (2007). Ammonia and ammonium measurements from the southeastern United States. *Atmos. Environ.,* 41, 3339–3351.

Electric power research institute (EPRI). 2008. Available at https://yosemite.epa.gov/sab%5CSABPRODUCT.NSF/B99E5E7B1FC13632852575B50069AAC2/$File/EPRI-SEARCH+for+EPA+SAB+INC+May+14-15+2009+Meeting.pdf.

Faulkner, W. B., & Shaw, B. W. (2008). Review of ammonia emission factors for United States animal agriculture. *Atmos. Environ., 42*(27), 6567-6574.

Finlayson-Pitts, B. J., Pitts, J. N., 2000. Chemistry of the upper and lower atmosphere: theory, experiments, and applications. Academic Press.

Flesch, T. K., Wilson, J. D., Harper, L. A., & Crenna, B. P. (2005). Estimating gas emissions from a farm with an inverse-dispersion technique. *Atmos. Environ., 39*(2005) 4863–4874.

Flesch, T. K., Wilson, J. D., Harper, L. A., Todd, R.W., & Cole, N. A. (2007). Determining ammonia emissions from a cattle feedlot with an inverse dispersion technique. *Agri. For. Meteorol., 144*(2007), 139-155.

Flesch, T. K., Harper, L. A., Powell, J. M., & Wilson, J. D. (2009). Inverse-dispersion calculation of ammonia emissions from Wisconsin dairy farms. *Transactions of ASABE.* 52(1), 253–265.

Fountoukis, C., & Nenes, A. (2007). ISORROPIA II: A computationally efficient thermodynamic equilibrium model for K^+-Ca^{2+}-Mg^{2+}-NH_4^+-Na^+-SO_4^{2-}-NO_3^--Cl^--H_2O aerosols. *Atmos. Chem. Phys. Discuss., 7*, 1893-1939.

Fountoukis, C., Nenes, A., Pandis, S., & Pilinis, C. (2009). ISSOROPIA v2.1 reference manual.

Fountoukis, C., Nenes, A., Sullivan, A., Weber, R., Van Reken, T., Fischer, M., Matias, E., Moya, M., Farmer, D., & Cohen, R. C. (2009). Thermodynamic characterization of Mexico City aerosol during MILAGRO 2006. *Atmos. Chem. Phys., 9*, 2141-2156.

Fowler, D., Pitcairn, C. E. R., Sutton, M.A., Flechard, C., Loubet, B., Coyle, M., & Munro, R. C. (1998). The mass budget of atmospheric ammonia in woodland within 1 km of livestock buildings. *Environ. Pollut., 102*(Sl), 343-348.

Franklin, M., Koutrakis, P., & Schwartz, J. (2008). The role of particle composition on the association between $PM_{2.5}$ and mortality. *Epidemiology*, *19*(5), 680-689.

Frank, N. H. (2006). Retained nitrate, hydrated sulfates, and carbonaceous mass in federal reference method fine particulate matter for six eastern U.S. cities. *J. Air & Waste Manage Assoc., 56*(4), 500–511.

Gates, R. S., Casey, K. D., Wheeler, E. F., Xin, H., Pescatore, A. J. (2008). U.S. broiler housing ammonia emissions inventory. *Atmos. Environ., 42, 3342-3350.*

Gill, P. S., Graedel, T. E., & Weschler, C. J. (1983). Organic films on atmospheric aerosol particles, fog droplets, cloud droplets, raindrops, and snowflakes. *Rev. Geophys., 21*(4), 903-920.

Gilland, B. (2002). World population and food supply Can food production keep pace with population growth in the next half-century? *Food Policy*, *27*, 47–63.

Goetz, S., Aneja, V. P., & Zhang, Y. (2008) Measurement, analysis, and modeling of fine particulate matter in Eastern North Carolina. *J. Air Waste Manage. Assoc., 58*, 1208–1214.

Gong, L., Lewicki, R., Griffin, R. J., Tittel, F. K., Lonsdale, C. R., Stevens, R. G., Pierce, J. R., Malloy, Q. G. J., Travis, S. A., Bobmanuel, L. M., Lefer, B. L., & Flynn, J. H. (2013). Role of

atmospheric ammonia in particulate matter formation in Houston during summertime. *Atmos. Environ., 77*(2013) 893–900.

Guo, H., Nenes, A., & Weber, R. J. (2017). The underappreciated role of nonvolatile cations on aerosol ammonium-sulfate molar ratios. *Atmos. Chem. Phys. Discuss.* Under review.

Hand, J. L., Schichtel, B. A., Pitchford, M., Malm, W. C., & Frank, N. H. (2012). Seasonal composition of remote and urban fine particulate matter in the United States. *J. Geophys. Res., 117,* D05209.

Hansen, D. A., Edgerton, E. S., Hartsell, B. E., Jansen, J. J., Kandasamy, N., Hidy, G. M., & Blanchard, C. L. (2003). The Southeastern Aerosol Research and Characterization Study: Part 1–Overview; *J. Air & Waste Manage. Assoc.*, *53,* 1460–1471.

Harper, L. A., Weaver, K. H., & Dotson, R. A. (2006). Ammonia emissions from swine waste lagoons in the Utah Great Basin. *J. Environ. Qual.,* 35:224–230.

Harper, L. A., Flesch, T. K., Powell, J. M., Coblentz, W. K., Jokela, W. E., Martin, N. P. (2009). Ammonia emissions from dairy production in Wisconsin. *J. Dairy Sci., 92*, 2326-2337.

Harper, L. A., Flesch, T. K., & Wilson, J. D. (2010). Ammonia emissions from broiler production in the San Joaquin Valley. *Poultry Science, 89*, 1802-1814.

Haywood, J. and Boucher, O. (2000). Estimates of the direct and indirect radiative forcing due to tropospheric aerosols: A review, *Rev. Geophys., 38*, 513-543.

Heederik, D., Sigsgaard, T., Thorne, P. S., Kline, J. N., Avery, R., Bonlokke, J. H., Chrischilles, E. A., Dosman J. A., Duchaine, C., Kirkhorn, S. R., Kulhankova, K., Merchant, J. A., 2007.

Health effects of airborne exposures from concentrated animal feeding operations. *Environ. Health Perspect., 115,* 298-302.

Hidy, G. M., Blanchar, C. L., Baumann, K., Edgerton, E., Tanenbaum, S., Shaw., S., Knipping, E., Tombach, I., Jansen, J., & Walters, J. (2014). Chemical climatology of the Southeastern United States, 1999–2013. *Atmos. Chem. Phys., 14* (2014), 11893–11914.

Hildemann, L. M., Russell, A. G., & Cass, G. R. (1984). Ammonia and nitric acid concentration in equilibrium with atmospheric aerosols: Experiment *vs.* theory. *Atmos. Environ., 18*(9), 1737-1750.

Hinds, W. C. (1998). Aerosol Technology; Properties, Behavior and Measurement of Airborne Particles, 2nd edition. New York, NY: John Wiley& Sons.

Holt, J., Selin, N. E., Solomon, S., 2015. Changes in inorganic fine particulate matter sensitivities to precursors due to large-scale US emissions reductions. *Environ. Sci. Tech., 49,* 4834-4841.

Huntzicker, J. J., Robert, A. C. & Ling, C. (1980). Neutralization of sulfuric acid aerosol by ammonia. *Environ. Sci. Tech., 14*(7), 819–824.

IPCC: Climate Change 2013: The Physical Science Basis. Contribution of Working Group I to the Fifth Assessment Report of the Intergovernmental Panel on Climate Change, 5th Edition.

Jacobson, M. Z., 2005. Fundamentals of Atmospheric Modeling. Cambridge University Press.

Kampa, M., & Castanas, E. (2008). Human health effects of air pollution. *Environ. Pollution. 151*(2008), 362-367.

Kim, E., Hopke, P. K., and Edgerton, E. S. (2003). Source identification of Atlanta aerosol by Positive Matrix Factorization. *J. Air Waste Manage. Assoc., 53*, 731-739.

Koo, B., Gaydos, T. M., & Pandis, S. N. (2003). Evaluation of the equilibrium, dynamic, and hybrid aerosol modeling approaches. *Aerosol Sci. Technol., 37*(1), 53-64.

Kumar, A., Dixit, S., Varadarajan, C., Vijayan, A., & Masuraha, A. (2006). Evaluation of the AERMOD dispersion model as a function of atmospheric stability for an urban area. *Environ. Prog.,* 25(2), 141-151.

Lefer, B. L., Talbot, R. W., & Munger, J. W. (1999). Nitric acid and ammonia at a rural northeastern U.S. site. *J. Geophys. Res.,* 104 (D1), 1645-1661.

Li, Q-F., Wang-Li, L., Liu, Z., Beasley, D. B., (2009). Chemical characterization of particulate matter emitted from animal feeding operations. ASABE paper No. 095948. Presented at 2009 ASABE Annual International Meeting. Reno, Nevada. June 21-24, 2009.

Li, Q-F. (2012). Particulate matter from an egg production facility: emission, chemistry and local dispersion. PhD diss. Raleigh, NC: North Carolina State University, Department of Biological and Agricultural Engineering.

Li, Q-F., Wang-Li, L., Shah, S. B., Jayanty, R. K. M., & Bloomfield, P. (2014a). Ammonia concentrations and modeling of inorganic particulate matter in the vicinity of an egg production facility in Southeastern USA. *Environ. Sci. Pollut. Res., 21*(6), 4675–4685.

Li, Q-F., Wang-Li, L., Liu, Z., Jayanty, R. K. M., Shah, S. B., & Bloomfield, P. (2014b). Major ionic composition of fine particulate matter in an animal feeding operation facility and its vicinity. *J. Air Waste Manage. Assoc., 64*(11), 1279-1287.

Li, Q-F., Wang-Li, L., Liu, Z., Beasley, D. B. (2009). Chemical characterization of particulate matter emitted from animal feeding operations. ASABE paper No. 095948. Presented at 2009 ASABE Annual International Meeting. Reno, Nevada. June 21-24, 2009.

Li, Q.-F. (2012). Particulate matter from an egg production facility: emission, chemistry and local dispersion. Ph. D. Dissertation, Department of Biological and Agricultural Engineering, North Carolina State University: Raleigh, NC.

Li, Y., Schwandner, F. M., Sewell, H. J., Zivkovich, A., Tigges, M., Raja, S., Holcomb, S., Molenar, J. V., Sherman, L., Archuleta, C., Lee, T., & Collett, J. L. Jr. (2014). Observations of ammonia, nitric acid, and fine particles in a rural gas production region. *Atmos. Environ., 83*, 80-89.

Li, Y. (2015). Characterizing ammonia concentrations and deposition in the United States. Dissertation. Department of Atmospheric Science, Colorado State University.

Liang, Y., Xin, H., Wheeler, E. F., Gates, R. S., Li, H., Zajaczkowski, J. S., Topper, P. A., Casey, K. D., Behrends, B. R., Burnham, D. J., & Zajaczkowski, F. J. (2005). Ammonia Emissions from U.S. laying hen houses in Iowa and Pennsylvania. *Transactions of the ASAE. 48*(5), 1927-1941.

Liggio, J., Li, S.-M., Vlasenko, A., Stroud, C., & Makar, P. (2011). Depression of ammonia uptake to sulfuric acid aerosols by competing uptake of ambient organic gases. *Environ. Sci. Technol.,* 45, 2790-2796,

Lin, X. J., Cortus, E. L., Zhang, R., Jiang, S., & Heber, A. J. (2012a). Ammonia, hydrogen sulfide, carbon dioxide and particulate matter emissions from California high-rise layer houses. *Atmos. Environ., 46*(2012), 81-91.

Lin, X. J., Cortus, E. L., Zhang, R., Jiang, S., & Heber, A. J. (2012b). Air emissions from broiler houses in California. *Transactions of the ASABE. 55*(5), 1895–1908.

Liu, Z., Wang-Li, L., Li, Q., & Beasley, D. B. (2009). Response of PM characteristics to NH_3 and other gaseous emissions at a southeaster layer operation. ASABE paper No. 096416. Reno, Nevada: ASABE.

Luke, W. T., Kelley, P., Lefer, B. L., Flynn, J., Rappenglück, B., Leuchner, M., Dibb, J. E., Ziemba, L. D., Anderson, C. H., Buhr, M. (2010). Measurements of primary trace gases and NO_y composition in Houston, Texas. *Atmos. Environ., 44*, 4068-4080.

Ma, Y., Chen, R., Pan, G., Xu, X., Song, W., & Chen, B. (2011). Fine particulate air pollution and daily mortality in Shenyang, China. *Sci. Total Environ. 409*(13), 2473-2477.

MacDonald, J. M., & McBride, W. D. (2009). The transformation of U.S. livestock agriculture: Scale, efficiency, and risks. Available at http://www.ers.usda.gov/media/184977/eib43.pdf.

Makar, P. A., Moran, M. D., Zheng, Q., Cousineau, S., Sassi, M., Duhamel, A., Besner, M., Davignon, D., Crevier, L. P., & Bouchet, V. S. (2009). Modelling the impacts of ammonia

emissions reductions on North American air quality. *Atmos. Chem. Phys. Discuss., 9*(2), 5371-5422.

Malm, W., Sisler J. F., Huffman, D., Eldred, R. A., & Cahill, T. A. (1994). Spatial and seasonal trends in particle concentration and optical extinction in the United States. *J. Geophys. Res., 99*(D1), 1347-1370.

Meng, Z., & Seinfeld, J. H. (1996). Time scale to achieve atmospheric gas-aerosol equilibrium for volatile species. *Atmos. Environ., 30*(16), 2889-2900.

Meng, Z., Dabdub, D., & Seinfeld, J. H. (1998). Size-resolved and chemically resolved model of atmospheric aerosol dynamics. *J. Geophys. Res. 103*, 3419-3435.

Metzger, S., Mihalopoulos, N., & Levieveld, J. (2006). Importance of mineral cations and organics in gas-aerosol partitioning of reactive nitrogen compounds: case study based on MINOS results. *Atmos. Chem. Phys., 6*, 2549-2567.

Montgomery, D. C., Peck, E. A., & Vining, G. G. (2012). *Introduction to linear regression analysis. Fifth edition*. John Wiley& Sons.

Moya, M., Ansari, A. S., & Pandis, S. N. (2001). Partitioning of nitrate and ammonium between the gas and particulate phases during the 1997 IMADA-AVER study in Mexico City. *Atmos. Environ., 35*(2001). 1791-1804.

Moya, M., Ansari, A. S., & Pandis, S. N. (2001). Partitioning of nitrate and ammonium between the gas and particulate phases during the 1997 IMADA-AVER study in Mexico City. *Atmos. Environ., 35*(2001), 1791-1804.

Moya, M., Pandis, S. N., Jacobson, M. Z. (2002). Is the size distribution of urban aerosols determined by thermodynamic equilibrium? An application to Southern California. *Atmos. Environ., 36*(2002), 2349-2365.

Mukhtar, S., Mutlu, A., Capareda, S. C., & Parnell, C. B. (2008). Seasonal and spatial variations of ammonia emissions from an open–lot dairy operation, *J. Air Waste Manage. Assoc., 58*(3), 369-376

Mwaniki, G. R., Rosenkrance, C., Wallace, H. W., Jobson, B. T., Erickson, M. H., Lamb, B. K., Hardy, R. J., Zalakeviciute, R., & VanReken, T. M. (2014). Factors contributing to elevated concentrations of $PM_{2.5}$ during wintertime near Boise, Idaho. *Atmos. Pollut. Res., 5*(2014), 96-103.

Nenes, A., Pilinis, C., & Pandis, S. N. (1998). ISORROPIA: a new thermodynamic equilibrium model for multiphase multicomponent inorganic aerosols. *Aqua. Geochem., 4*(1), 123-152.

Nenes A., Pilinis, C., & Pandis, S. N. (1999). Continued Development and Testing of a New Thermodynamic Aerosol Module for Urban and Regional Air Quality Models. *Atmos. Env., 33*, 1553-1560.

NRC. (2003). Air emissions from animal feeding operations: Current knowledge, future needs. Retrieved from http://www.epa.gov/ttnchie1/ap42/ch09/related/nrcanimalfeed_dec2002.pdf.

Olszyna, K. J., Bairai, S. T., & Tanner, R. L. (2005). Effect of ambient NH_3 levels on $PM_{2.5}$ compositions in the Great Smoky Mountains National Park. *Atmos. Environ., 39*(25), 4593-4606.

Paulot, F., & Jacob, D. J. (2014). Hidden cost of U.S. agricultural exports: particulate matter from ammonia emissions. *Environ. Sci. Tech., 48*(2), 903-908.

Pay, M. T., Jiménez-Guerrero, P., & Baldasano, J. M. (2012). Assessing sensitivity regimes of secondary inorganic aerosol formation in Europe with the CALIOPE-EU modeling system. *Atmos. Environ., 51*, 146-164.

Pimentel, D., & Pimentel, M. (2006). Global environmental resources versus world population growth. Ecological Economics, 59, 195-198. doi:10.1016/ j.ecolecon.2005. 11.034.

Pinder, R. W., Strader, R., Davidson, C. I., & Adam, P. J. (2004). A temporally and spatially resolved ammonia emission inventory for dairy cows in the United States. *Atmos. Environ., 38*, 3747-3756.

Pope III, C. A. & Dockery, D.W. (2006). Health effects of fine particulate air pollution: Lines that connect. *J. Air Waste Manage. Assoc., 56*, 709-742.

Pope, C. III, Ezzati, M., & Dockery, D. W. (2009). Fine-particulate air pollution and life expectancy in the United States. *The New England J. Med., 360*(4), 376-386.

Pui, D. Y. H., Chen, S., & Zuo, Z. (2014). $PM_{2.5}$ in China: Measurements, sources, visibility and health effects, and mitigation. *Particuology, 13*, 1-26.

Pun, B. K., Seigneur, C., 2001. Sensitivity of particulate matter nitrate formation to precursor emissions in the California San Joaquin Valley. *Environ. Sci. Tech., 35*, 2979-2987.

Ramanathan, V., Crutzen, P. J., Kiehl, J. T., & Rosenfeld, D. (2001). Aerosols, climate, and the hydrological cycle, *Science, 294*, 2119-2124.

Ravishankara, A. R. (1997). Heterogeneous and multiphase chemistry in the troposphere. *Science, 276*(5315), 1058-1065.

Redwine, J. S., Lacey, R. E., Mukhtar, S., & Carey, J. B. (2002). Concentration and emissions of ammonia and particulate matter in tunnel-ventilate broiler houses under summer conditions in Texas. *Transactions of the ASAE, 45*(4), 1101-1109.

Robarge, W. P., Walker, J. T., McCulloch, R. B., & Murray, G. (2002). Atmospheric concentrations of ammonia and ammonium at an agricultural site in the southeast United States. *Atmos. Environ., 36*, 1661-1674.

Rumburg, B., Mount, G. H., Yonge, D., Lamb, B., Westberg, H., Filipy, J., Bays, J., Kincaid, R., & Johnson, K. (2006). Atmospheric flux of ammonia from sprinkler application of dairy waste. *Atmos. Environ., 40*, 7246-7258.

Rumburg, B., Mount, G. H., Filipy, J., Lamb, B., Westberg, H., Yonge, D., Kincaid, R., & Johnson, K. (2008a). Measurement and modeling of atmospheric flux of ammonia from dairy milking cow housing. *Atmos. Environ.,* 42, 3364-3379.

Rumburg, B., Mount, G. H., Yonge, D., Lamb, B., Westberg, H., Neger, M., Filipy, J., Kincaid, R., & Johnson, K. (2008b). Measurements and modeling of atmospheric flux of ammonia from an anaerobic dairy waste lagoon. *Atmos. Environ., 42*, 3380-3393.

Saxena, P., Hudischewskyj, A. B., & Seigneur, C. (1986). A comparative study of equilibrium approaches to the chemical characterization of secondary aerosols. *Atmos. Environ., 20*(7), 1471-1483.

Saylor, R. D., Edgerton, E. S., Hartsell, B. E., Baumann, K., & Hansen D. A. (2010). Continuous gaseous and total ammonia measurements from the southeastern aerosol research and characterization (SEARCH) study. *Atmos. Environ., 44*, 4994-5004.

Saylor, R. D., Myles, L., Sibble, D., Caldwell, J., & Xing, X. (2015). Recent trends in gas-phase ammonia and $PM_{2.5}$ ammonium in the Southeast United States. *J. Air & Waste Manage Assoc., 65*(3), 347-357.

Schwartz, J., Dockery, D. W., & Neas, L.M. (1996). Is daily mortality associated specifically with fine particles? *J. Air & Waste Manag. Assoc.*, 46, 927-939.

Seinfeld, J. H. & Pandis, S. N. (2006). Atmospheric chemistry and physics: From Air Pollution to Climate Change. New York, NY: John Wiley& Sons.

Shiraiwa, M., Zuend, A., Bertram, A. K., & Seinfeld, J. H. (2013). Gas-particle partitioning of atmospheric aerosols: interplay of physical state, non-ideal mixing and morphology. *Phy. Chem. Chem. Phy., 2013*(15), 11441.

Siefert, R. L., & Scudlark, J. R. (2008). Determination of ammonia emission rates from a tunnel ventilated chicken house using passive samplers and a Gaussian dispersion model. *J. Atmos. Chem., 59*, 99-115.

Silvern, R. F., Jacob, D. J., Kim, P. S., Marais, E. A. & Turner, J. R. (2017). Inconsistency of ammonium-sulfate aerosol ratios with thermodynamic models in the eastern U.S.: a possible role of organic aerosol. *Atmos. Chem. Phys., 17*, 5107-5118.

Snider, G., Weagle, C. L., Murdymootoo, K. K., Ring, A., Ritchie, Y., Stone, E., & Martin, R. V. (2016). Variation in global chemical composition of $PM_{2.5}$: emerging results from SPARTAN. *Atmos. Chem. Phys., 16*(15), 9629-9653.

Stelson, A. W., & Seinfeld, J. H. (1982). Relative humidity and temperature dependence of the ammonium nitrate dissociation constant. *Atmos. Environ., 16*(5), 983-992.

Sutton, M. A., Asman, W. A. H., & Schjorring, J. K. (1994). Dry deposition of reduced nitrogen. *Tellus, 46B,* 255-273.

Takahama, S., Wittig, A. E., Vayenas, V., Davidson, C. I., Pandis, S. N. (2004). Modeling the diurnal variation of nitrate during the Pittsburgh Air Quality Study. *J. Geophys. Res., 109*(D16S06).

Tanner, R. L., Marlow, W. H., & Newman, L. (1979). Chemical composition correlations of size-fractionated sulfate in New York City. *Am. Chem. Soc., 13*(1), 75-78.

Tanner, R. L., Leaderer, B. P., Spengler, J. D., 1981. Acidity of atmospheric aerosols. *Environ. Sci. Technol., 15,* 1150-1153.

Tolocka, M. P., Solomon, P. A., Mitchell, W., Norris, G. A., Gemmill, D. B., Wiener, R. W., Vanderpool, R. W., Homolya, J. B., & Rice, J. (2001). East versus west in the US: Chemical characteristics of $PM_{2.5}$ during the winter of 1999. *Aerosol Sci. Technol.,* 34, 88-96.

Topper, P. A., Wheeler, E. F., Zajaczkowski, J. S., Gates, R. S., Xin, H., Liang, Y., & Casey, K. D. (2008). Ammonia emissions from two empty broiler houses with built-up litter. *Transactions of the ASABE., 51*(1), 219-225.

USEPA. (2000). Guidance for data quality assessment. Available at https://www.epa.gov/sites/production/files/2015-06/documents/g9-final.pdf.

USEPA. (2004). Estimating ammonia emissions from anthropogenic nonagricultural sources-draft final report. Available at https://www.epa.gov/sites/production/files/2015-08/documents/eiip_areasourcesnh3.pdf.

USEPA. (2011). National Emission Inventory. Available at https://www.epa.gov/air-emissions-inventories/2011-national-emissions-inventory-nei-data.

USGS. (2016). Global change monitoring portal. Available at https://my.usgs.gov/gcmp/program/show/943855.

USEPA. (2010). Agriculture-Air Monitoring, Data from Sites Monitored. Retrieved from http://www.epa.gov/airquality/agmonitoring/data.html.

USEPA. (2013). 2013 Program Progress: Clean air interstate rule, acid rain program, and former NO_x budget trading program. Available at https://www.epa.gov/sites/production/files/2016-10/documents/2013_full_report_0.pdf.

USEPA, (2015a). Glossary. http://www.epa.gov/airquality/airdata/ad_glossary.html.

USEPA, (2015b). Estimating ammonia emissions from anthropogenic nonagricultural sources-draft final report. http://www.epa.gov/ttn/chief/eiip/techreport/volume03/eiip_areasourcesnh3.pdf.

USEPA. (2016a). Basic information about NO_2. Available at https://www.epa.gov/no2-pollution/basic-information-about-no2#What is NO_2.

USEPA. (2016b). Sulfur dioxide basics. Available at https://www.epa.gov/so2-pollution/sulfur-dioxide-basics#what is so2.

USEPA. (2018a). NAAQS table. Available at https://www.epa.gov/criteria-air-pollutants/naaqs-table.

USEPA. (2018b). Clean Air Interstate Rule. Available at https://www.tceq.texas.gov/airquality/sip/caircamr.html.

USEPA. (2018c). Cross-State Air Pollution Rule. Available at https://www.epa.gov/csapr.

USEPA, (2018d). Health and environmental effects of particulate matter. Available at https://www.epa.gov/pm-pollution/health-and-environmental-effects-particulate-matter-pm.

Walker, J. T., Nelson, D., & Aneja, V. P. (2000a). Trends in ammonium concentration in precipitation and atmospheric ammonia emissions at a Coastal Plain site in North Carolina, USA. *Environ. Sci. Technol., 34*(17), 3527-3534.

Walker, J. T., Aneja, V. P., & Dickey, D. (2000b). Atmospheric transport and wet deposition of ammonium in North Carolina, USA. *Atmos. Environ., 34*, 3407-3418.

Walker, J. T., Whitall, D. R., Robarge, W., & Paerl, H. W. (2004). Ambient ammonia and ammonium aerosol across a region of variable ammonia emission density. *Atmos. Environ., 38*(9), 1235-1246.

Walker, J. T., Robarge, W. P., Shendrikar, A., & Kimball, H. (2006). Inorganic $PM_{2.5}$ at a U.S. agricultural site. *Environ. Pollut., 139*(2), 258-271.

Wang, K., Zhang, Y., Nenes, A., Fountoukis, C. (2012). Implementation of dust emission and chemistry into the Community Multiscale Air Quality modeling system and initial application to an Asian dust storm episode. *Atmos. Chem. Phys., 12*, 10209-10237.

Wang-Li, L. (2013). Techniques for characterization of particulate matter emitted from animal feeding operations. Peer-reviewed book chapter of "Evaluating Veterinary Pharmaceutical Behavior in the Environments". Chapter 2, pp15-39. *American Chemical Society (ACS).* doi**:** 10.1021/bk-2013-1126.ch002.5-1246.

Wang-Li, L. (2015). Insights to the formation of secondary inorganic $PM_{2.5}$: Current knowledge and future needs. *IJABE,* 8, 1-13.

Warner, J. X., Dickerson, R. R., Wei, Z., Strow, L. L., Wang,Y., & Liang, Q., (2017). Increased atmospheric ammonia over the world's major agricultural areas detected from space. *Geophys. Res. Lett., 44*, 2875-2884

Wexler, A. S. & Seinfeld, J. H. (1992) Analysis of Aerosol Ammonium Nitrate: Departures from Equilibrium during SCAQS. *Atmos. Environ., 26A,* 579-591.

Wheeler, E. F., Casey, K. D., Gates, R. S., Xin, H., Zajaczkowski, J. L., Topper, P. A., Liang, Y., & Pescatore, A. J. (2006). Ammonia emissions from twelve U.S.A. broiler chicken houses. *Transactions of the ASABE, 49*(5), 1495-1512.

Xing, J., Pleim, J., Mathur, R., Pouliot, G., Hogrefe, C., Gan, C. M., & Wei, C. (2013). Historical gaseous and primary aerosol emissions in the United States from 1990 to 2010. *Atmos. Chem. Phys. 13*, 7531-7549.

Xing, Y., Xu, Y., & Lian Y. (2016). The impact of $PM_{2.5}$ on the human respiratory system. *J. Thorac. Dis.*, *8*(1), E69–E74.

Yang, X., Wang, X., Zhang, Y., Lee, J., Su, J., Gates, R. S. (2011). Characterization of trace elements and ions in PM_{10} and $PM_{2.5}$ emitted from animal confinement buildings. *J. Atmos. Environ.*, *45* (2011), 7096-7104.

Yu, S., Dennis, R., Roselle, S., Nenes, A., Walker, J., Eder, B., Schere, K., Swall, J., Robarge, W. (2005). An assessment of the ability of three-dimensional air quality models with current thermodynamic equilibrium models to predict aerosol NO_3^-. *J. Geophys. Res.*, *110*, 1-22.

Zhang, Y., Seigneur, C., Seinfeld, J. H., Jacobson, M., Clegg, S. L., & Binkowski, F. S. (2000). A comparative review of inorganic aerosol thermodynamic equilibrium modules: similarities, differences, and their likely causes. *Atmos. Environ.*, *34*, 117-137.

Zhang, J., Chameides, W. L., Weber, R., Cass, G., Orsini, D., Edgerton, E. S., Jongejan, P., & Slanina, J. (2003). An evaluation of the thermodynamic equilibrium assumption for fine particulate composition: Nitrate and ammonium during the 1999 Atlanta Supersite Experiment. *J. Geophys. Res.*, *107*(D7), 8414.

Zhang, Y., Wu, S-Y, Krishnan, S., Wang, K., Queen, A., Aneja, V. P. & Arya, S. P. (2008). Modeling agricultural air quality: current status, major challenges and outlook. *Atmos. Environ., 42*(14), 3218-3237.

Zhang, L., Jacob, D. J., Knipping, E. M., Kumar, N., Munger, J. W., Carouge, C. C., van Donkelaar, A., Wang, Y. X. & Chen, D. (2012). Nitrogen deposition to the United States: distribution, sources, and processes. *Atmos. Chem. Phys.*, *12*, 4539-4554.

Zhao, L. (2007). Understanding air emissions from animal feeding operations. Available at http://citeseerx.ist.psu.edu/viewdoc/download?doi=10.1.1.184.934&rep=rep1&type=pdf.

APPENDICES

Appendix A

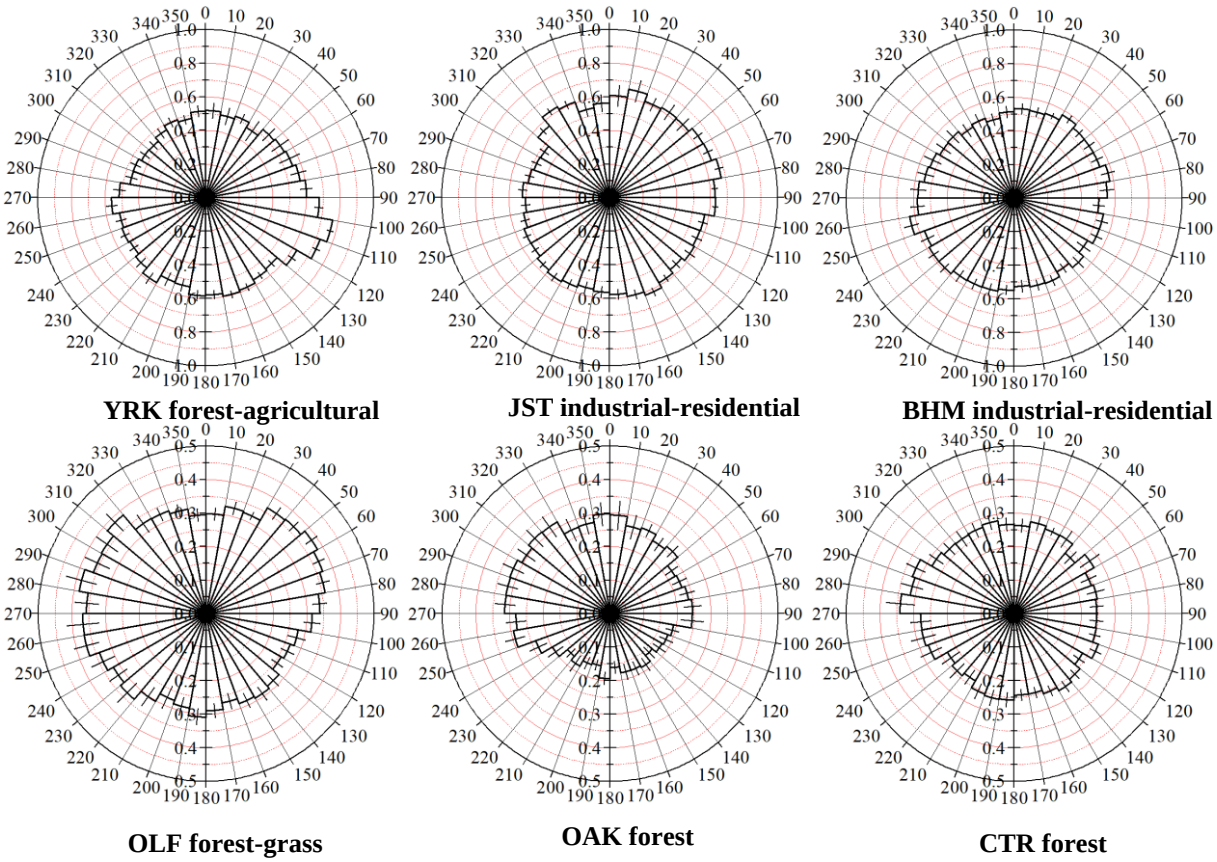

Figure S1. The NH_3/NH_x under various wind direction at the YRK, JST, CTR, BHM, and OLF sites in 2013 and OAK in 2010. Note different scales on figures.

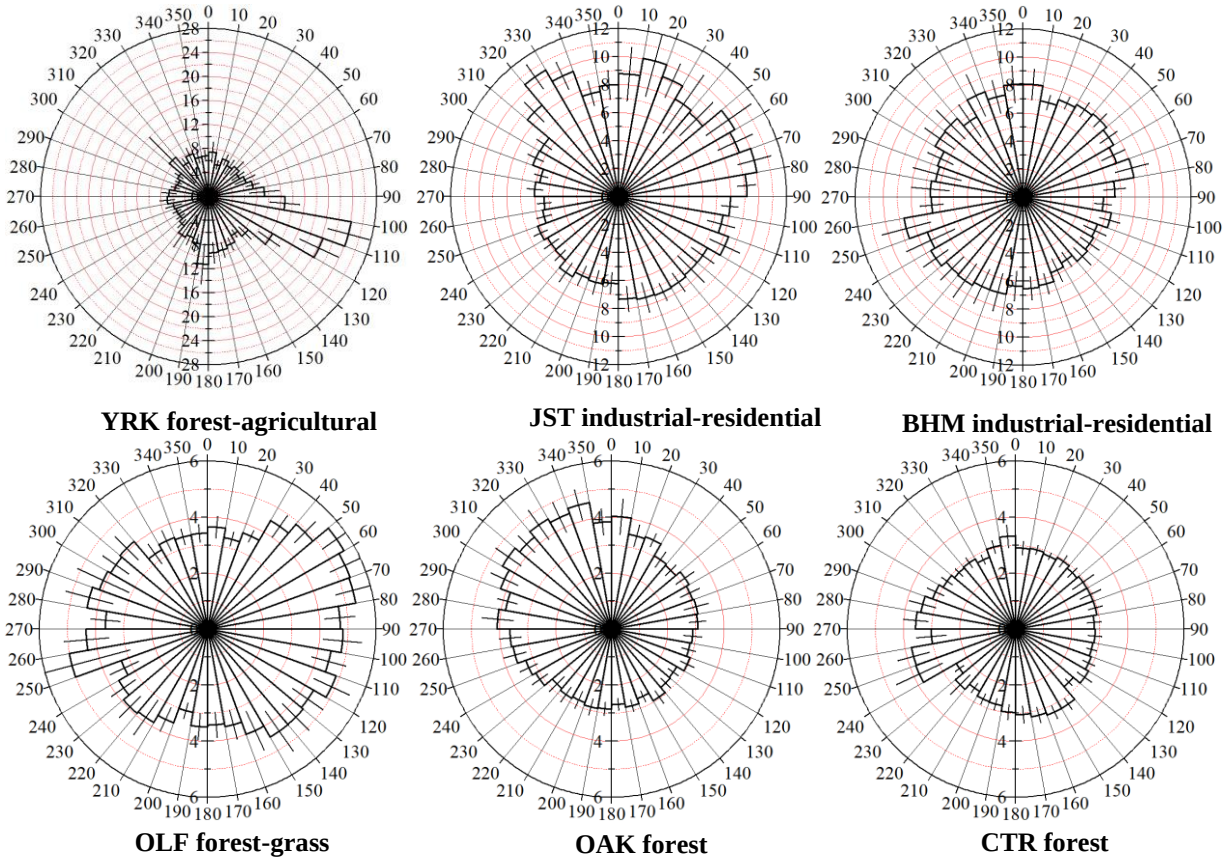

Figure S2. The TA/TS under different wind direction at the YRK, JST, CTR, BHM, and OLF sites in 2013 and OAK in 2010. Note different scales on figures.

Appendix B

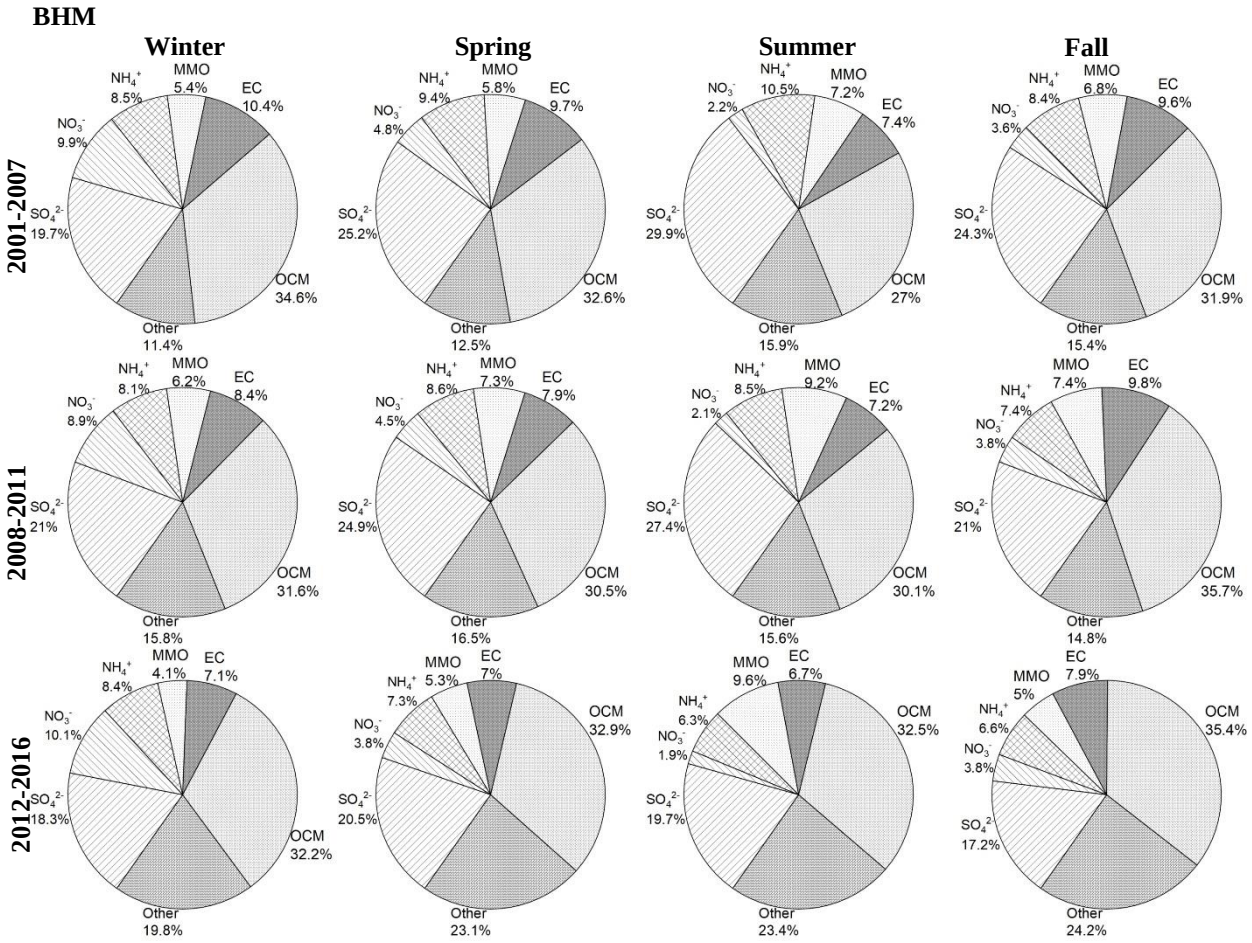

Figure S3. Seasonal variation of mass closure in three periods at the BHM site

CTR

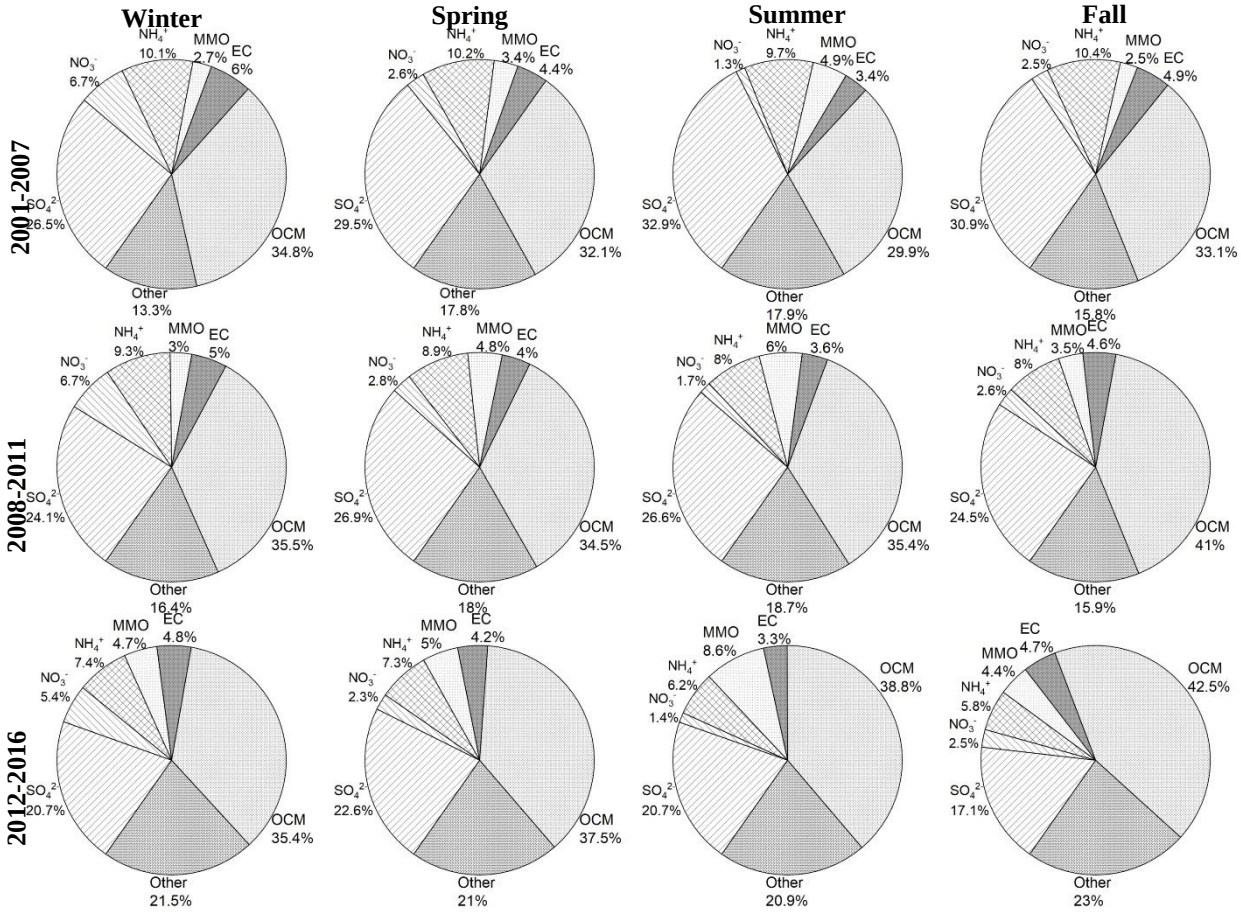

Figure S4. Seasonal variation of mass closure in three periods at the CTR site

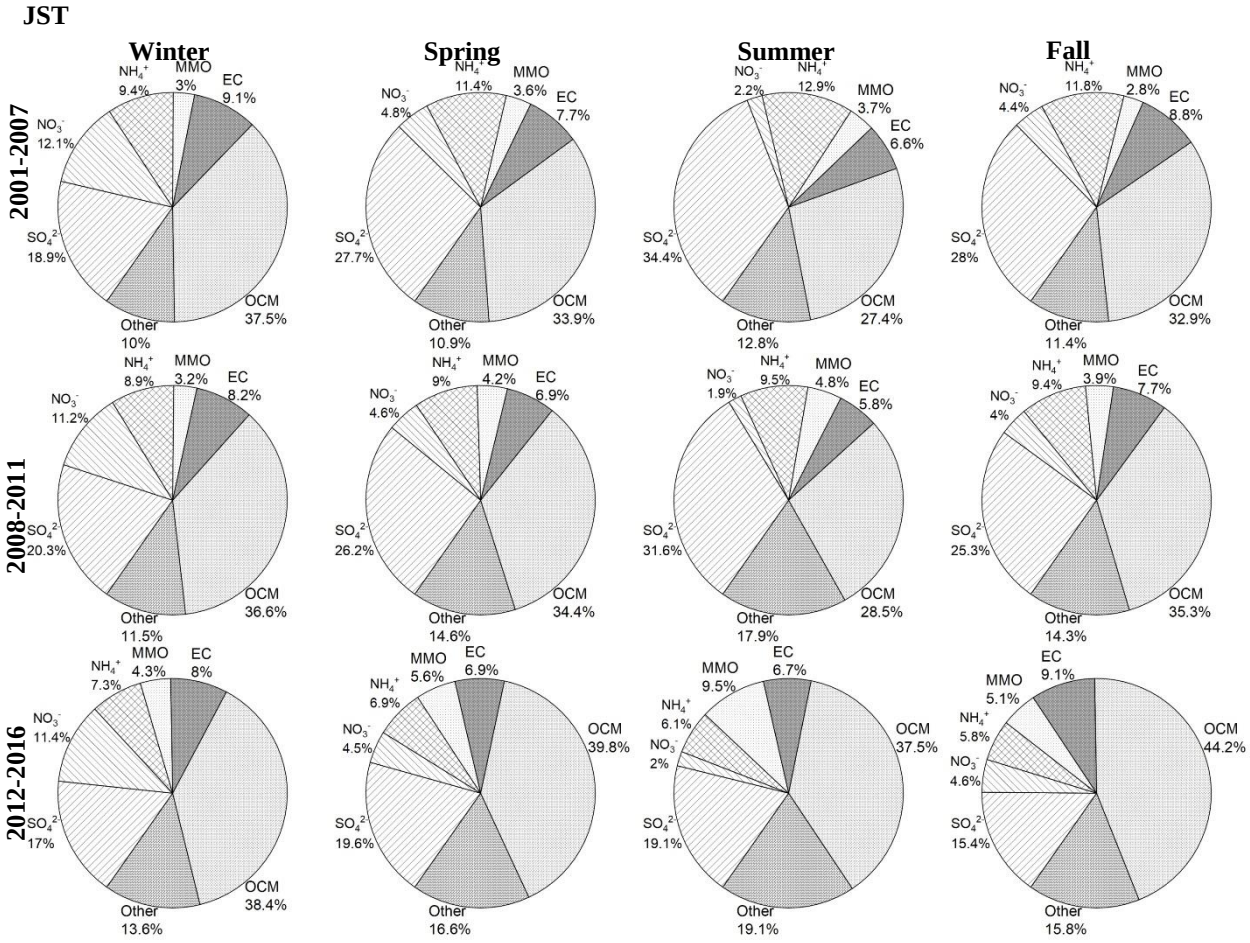

Figure S5. Seasonal variation of mass closure in three periods at the JST site

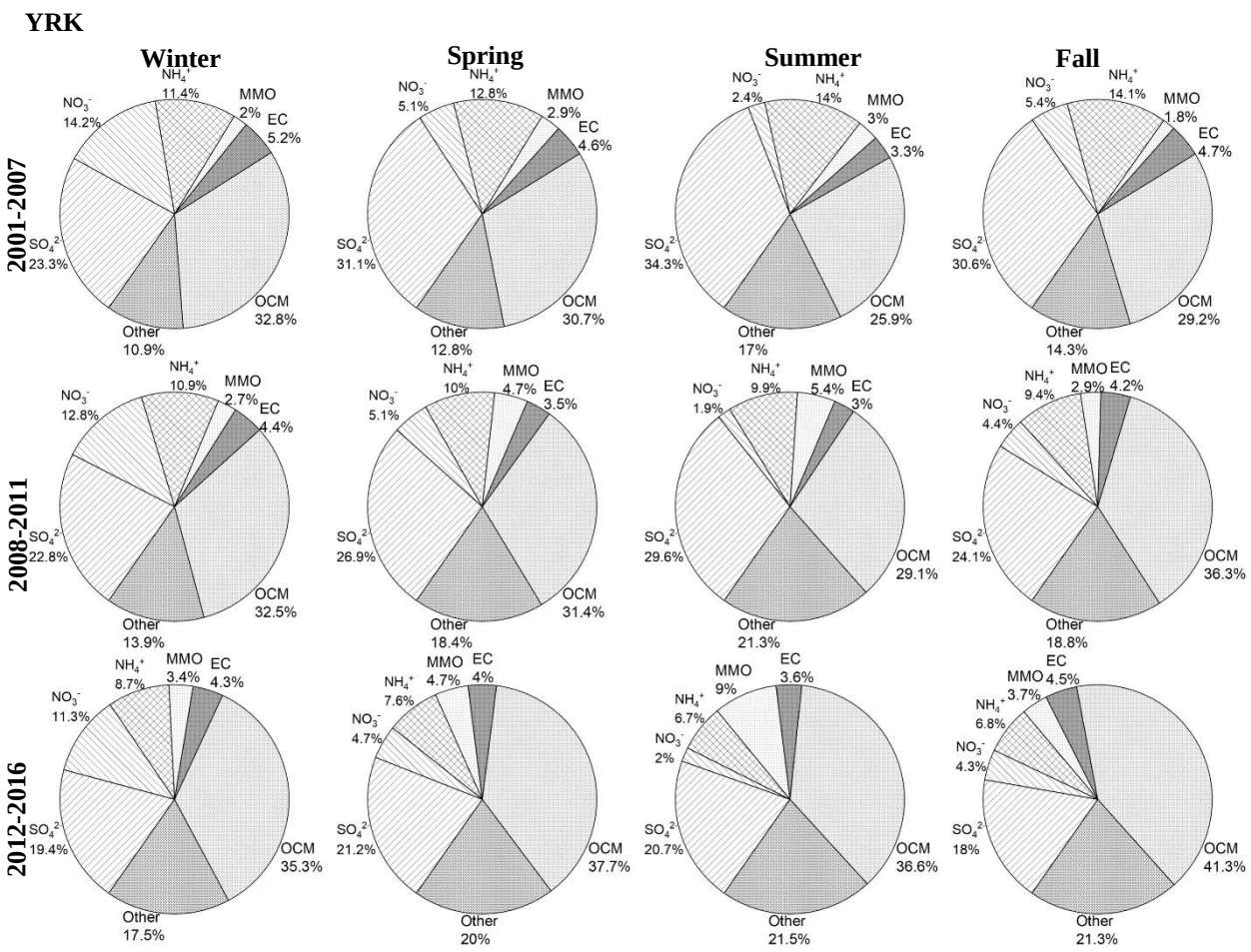

Figure S6. Seasonal variation of mass closure in three periods at the YRK site

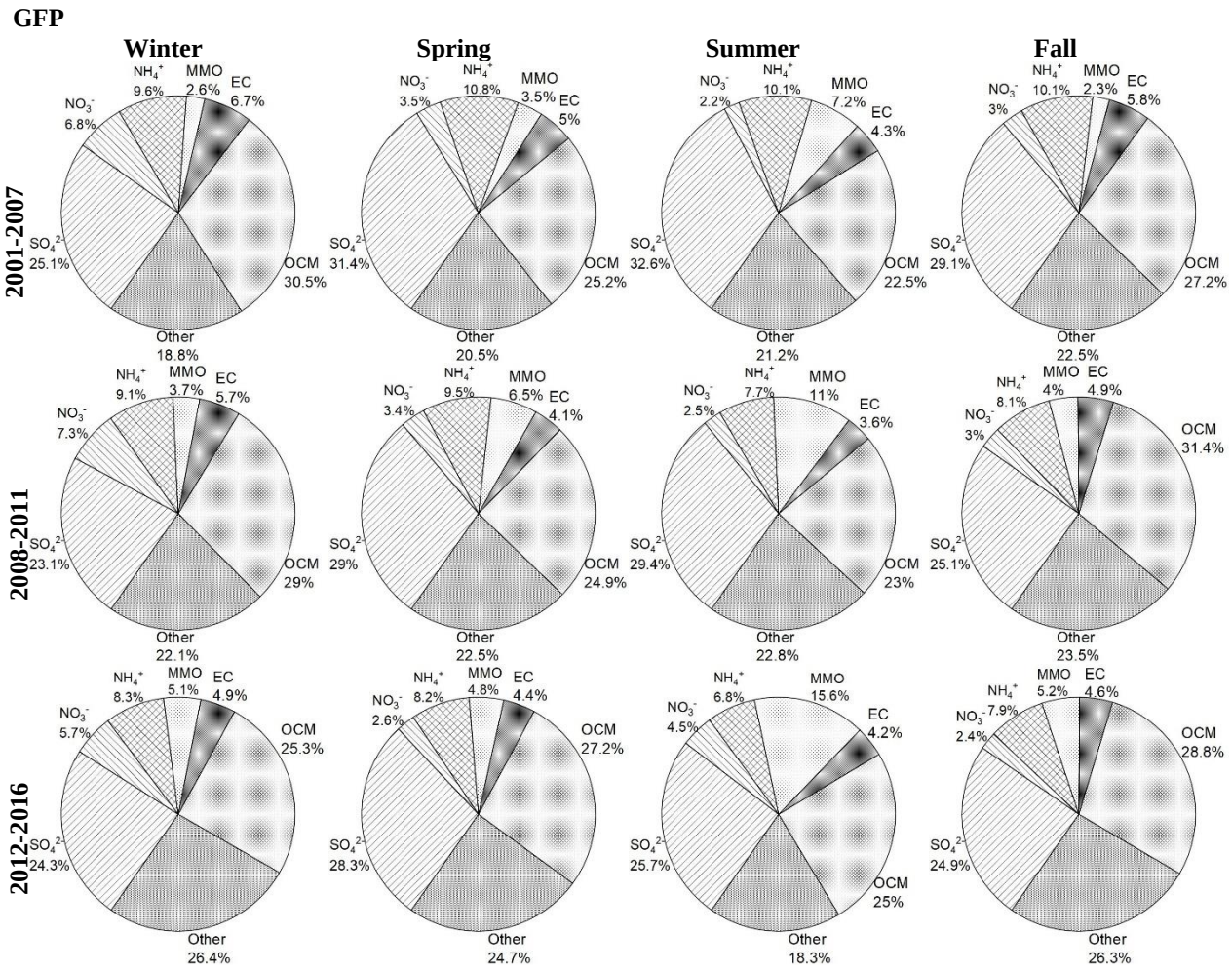

Figure S7. Seasonal variation of mass closure in three periods at the GFP site

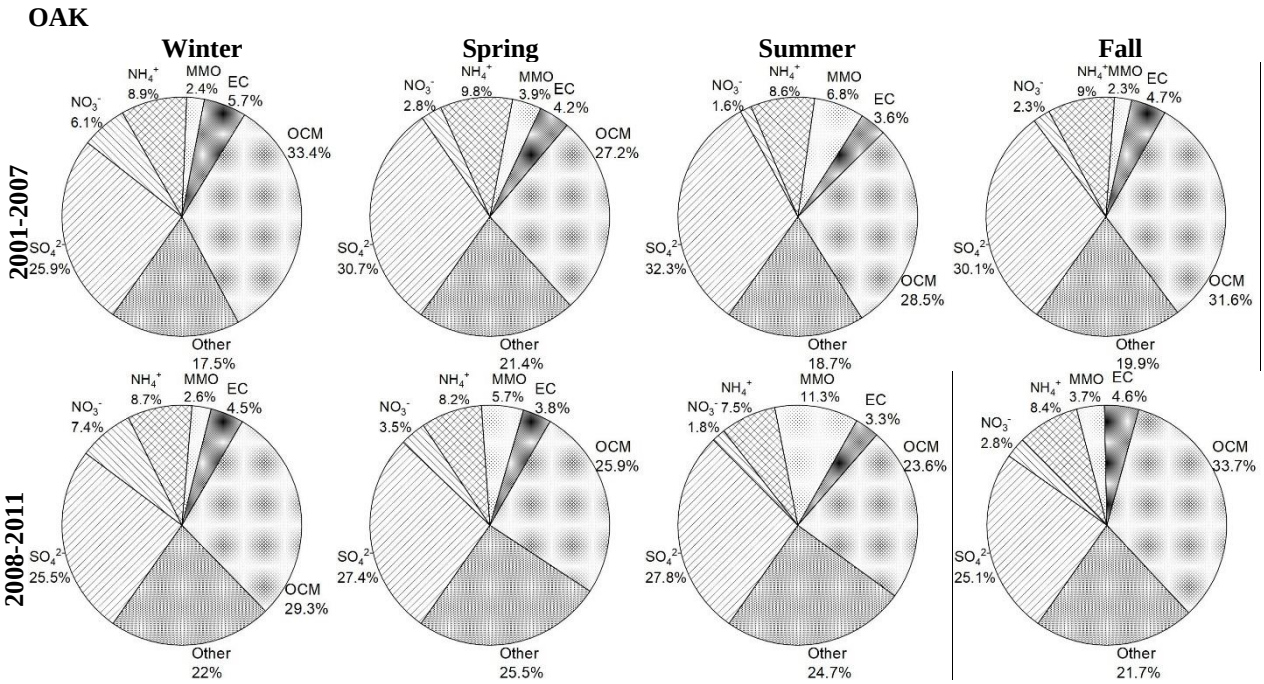

Figure S8. Seasonal variation of mass closure in three periods at the OAK site

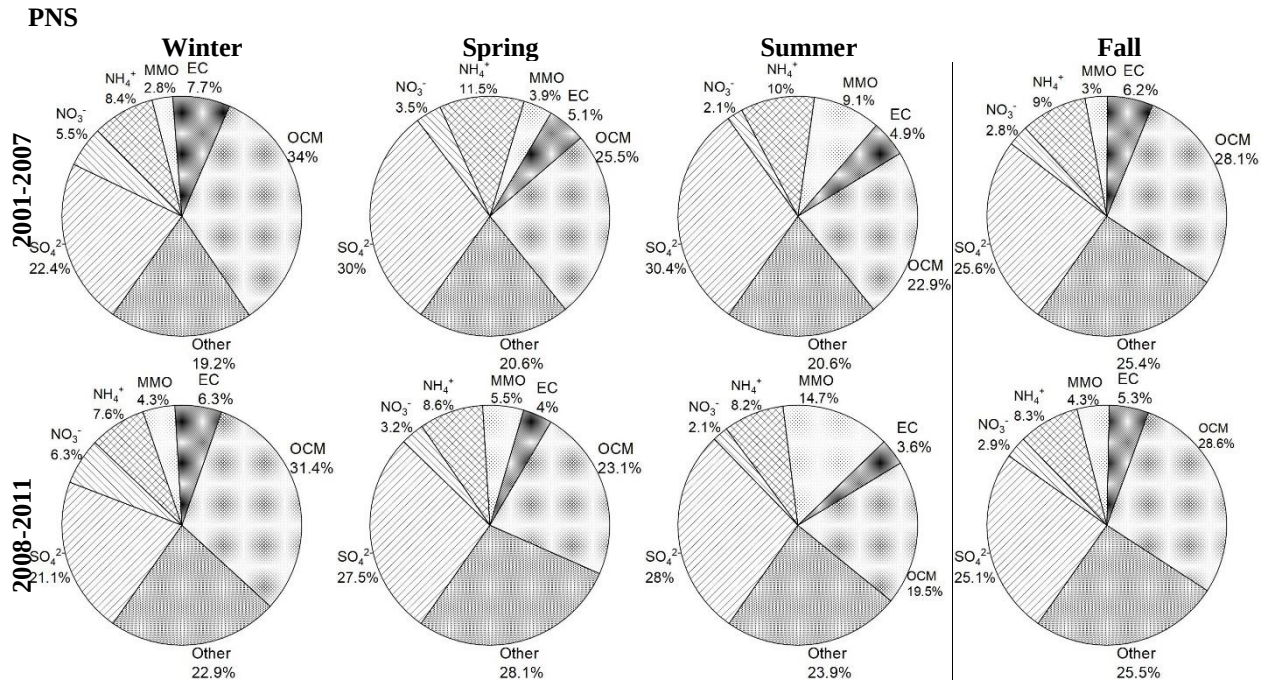

Figure S9. Seasonal variation of mass closure in three periods at the PNS site

OLF

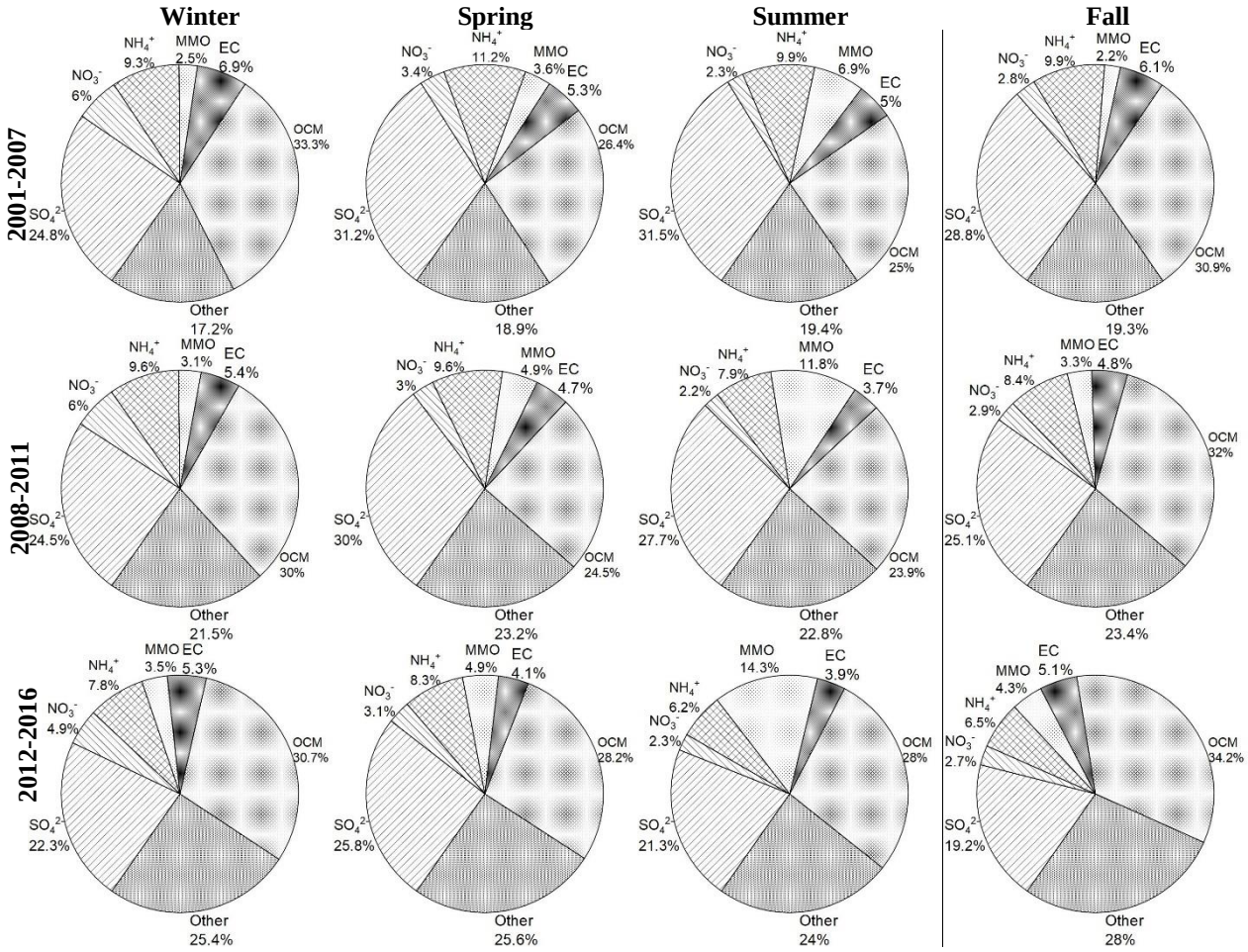

Figure S10. Seasonal variation of mass closure in three periods at the OLF site

Table S1. Seasonal variations of OCM concentration (μg/m^3) in 3 monitoring periods

Sites	Periods	Winter	Spring	Summer	Fall
JST	2001-2007	5.64 ± 3.68	5.64 ± 3.55	5.56 ± 2.08	5.79 ± 3.40
	2008-2011	4.21 ± 2.52	4.37 ± 2.27	4.28 ± 1.57	3.97 ± 1.86
	2012-2016	3.34 ± 1.71	3.69 ± 1.69	3.78 ± 1.51	4.31 ± 3.05
YRK	2001-2007	3.36 ± 1.66	4.34 ± 3.74	4.99 ± 1.96	4.03 ± 1.84
	2008-2011	3.04 ± 1.58	3.43 ± 1.99	4.01 ± 1.73	3.47 ± 1.51
	2012-2016	2.55 ± 1.27	3.15 ± 1.46	3.50 ± 1.32	3.24 ± 1.38
BHM	2001-2007	5.39 ± 3.55	6.26 ± 5.00	5.91 ± 3.11	5.44 ± 3.28
	2008-2011	3.57 ± 2.42	3.73 ± 2.28	4.45 ± 2.03	5.14 ± 2.87
	2012-2016	2.85 ± 1.73	3.26 ± 1.85	3.77 ± 1.73	3.80 ± 2.01
CTR	2001-2007	3.45 ± 2.97	4.17 ± 3.05	4.26 ± 2.08	4.11 ± 2.12
	2008-2011	3.08 ± 2.39	3.27 ± 2.02	4.48 ± 2.51	3.72 ± 1.73
	2012-2016	2.28 ± 1.38	3.13 ± 1.78	3.59 ± 1.52	3.45 ± 1.49
GFP	2001-2007	2.97 ± 1.95	2.85 ± 1.79	2.81 ± 1.63	3.38 ± 2.12
	2008-2011	2.41 ± 1.59	2.36 ± 1.23	2.55 ± 1.54	3.04 ± 1.56
	2012	1.83 ± 1.21	2.55 ± 1.88	2.12 ± 1.43	2.57 ± 1.30
OAK	2001-2007	3.22 ± 3.29	3.32 ± 2.38	3.63 ± 2.16	3.52 ± 1.87
	2008-2011	2.53 ± 1.83	2.53 ± 1.33	2.43 ± 1.00	2.90 ± 1.28
	2012-2016	N/A	N/A	N/A	N/A
PNS	2001-2007	4.28 ± 3.33	3.33 ± 2.68	2.86 ± 1.65	3.74 ± 2.12
	2008-2009	3.27 ± 2.69	2.72 ± 1.90	2.33 ± 1.25	3.25 ± 1.86
	2012-2016	N/A	N/A	N/A	N/A
OLF	2001-2007	3.09 ± 1.96	3.02 ± 1.86	3.23 ± 1.81	3.69 ± 1.85
	2008-2011	2.36 ± 1.55	2.29 ± 1.30	2.96 ± 2.25	2.82 ± 1.36
	2012-2016	2.22 ± 1.68	2.29 ± 1.54	2.32 ± 1.44	2.63 ± 1.24

Table S2. Seasonal variations of EC concentration (μg/m^3) in 3 monitoring periods

Sites	Periods	Winter	Spring	Summer	Fall
JST	2001-2007	1.40 ± 1.08	1.27 ± 0.69	1.35 ± 0.67	1.62 ± 1.19
	2008-2011	0.99 ± 0.79	0.89 ± 0.56	0.88 ± 0.40	0.87 ± 0.48
	2012-2016	0.72 ± 0.48	0.64 ± 0.32	0.65 ± 0.28	0.88 ± 0.56
YRK	2001-2007	0.54 ± 0.31	0.60 ± 0.34	0.64 ± 0.34	0.63 ± 0.31
	2008-2011	0.42 ± 0.24	0.38 ± 0.21	0.40 ± 0.19	0.40 ± 0.17
	2012-2016	0.31 ± 0.17	0.34 ± 0.19	0.34 ± 0.15	0.37 ± 0.17
BHM	2001-2007	1.68 ± 1.28	1.80 ± 1.34	1.61 ± 1.15	1.72 ± 1.21
	2008-2011	0.98 ± 0.79	1.01 ± 0.85	1.09 ± 0.71	1.45 ± 0.97
	2012-2016	0.67 ± 0.57	0.71 ± 0.59	0.79 ± 0.45	0.88 ± 0.59
CTR	2001-2007	0.58 ± 0.43	0.55 ± 0.38	0.50 ± 0.30	0.60 ± 0.31
	2008-2011	0.44 ± 0.34	0.39 ± 0.26	0.46 ± 0.27	0.43 ± 0.21
	2012-2016	0.32 ± 0.21	0.35 ± 0.24	0.31 ± 0.16	0.39 ± 0.22
GFP	2001-2007	0.66 ± 0.47	0.56 ± 0.38	0.51 ± 0.28	0.71 ± 0.48
	2008-2011	0.48 ± 0.33	0.39 ± 0.21	0.40 ± 0.23	0.48 ± 0.30
	2012	0.36 ± 0.26	0.36 ± 0.16	0.33 ± 0.13	0.41 ± 0.20
OAK	2001-2007	0.57 ± 0.58	0.51 ± 0.36	0.44 ± 0.24	0.53 ± 0.34
	2008-2011	0.40 ± 0.29	0.39 ± 0.34	0.33 ± 0.21	0.39 ± 0.25
	2012-2016	N/A	N/A	N/A	N/A
PNS	2001-2007	0.97 ± 0.74	0.64 ± 0.39	0.57 ± 0.34	0.80 ± 0.52
	2008-2009	0.68 ± 0.61	0.49 ± 0.42	0.43 ± 0.24	0.62 ± 0.45
	2012-2016	N/A	N/A	N/A	N/A
OLF	2001-2007	0.63 ± 0.37	0.59 ± 0.32	0.59 ± 0.32	0.71 ± 0.38
	2008-2011	0.42 ± 0.28	0.43 ± 0.32	0.42 ± 0.22	0.44 ± 0.25
	2012-2016	0.38 ± 0.27	0.34 ± 0.24	0.31 ± 0.15	0.40 ± 0.19

Table S3. Seasonal variations of MMO concentration (μg/m^3) in 3 monitoring periods

Sites	Periods	Winter	Spring	Summer	Fall
JST	2001-2007	0.41 ± 0.33	0.56 ± 0.38	0.68 ± 0.67	0.47 ± 0.27
	2008-2011	0.35 ± 0.22	0.56 ± 0.66	0.68 ± 0.50	0.42 ± 0.24
	2012-2016	0.36 ± 0.21	0.50 ± 0.25	1.04 ± 1.69	0.47 ± 0.30
YRK	2001-2007	0.19 ± 0.10	0.36 ± 0.29	0.50 ± 0.70	0.23 ± 0.23
	2008-2011	0.23 ± 0.11	0.55 ± 0.99	0.61 ± 0.59	0.27 ± 0.15
	2012-2016	0.22 ± 0.15	0.38 ± 0.22	0.97 ± 1.71	0.28 ± 0.13
BHM	2001-2007	0.85 ± 0.67	1.04 ± 0.77	1.37 ± 1.05	1.16 ± 0.90
	2008-2011	0.69 ± 0.65	0.87 ± 0.73	1.30 ± 0.99	1.12 ± 0.96
	2012-2016	0.34 ± 0.18	0.48 ± 0.27	1.10 ± 1.36	0.50 ± 0.31
CTR	2001-2007	0.23 ± 0.12	0.40 ± 0.37	0.55 ± 0.81	0.29 ± 0.24
	2008-2011	0.23 ± 0.10	0.43 ± 0.45	0.64 ± 0.69	0.31 ± 0.17
	2012-2016	0.27 ± 0.21	0.38 ± 0.19	0.84 ± 1.34	0.35 ± 0.27
GFP	2001-2007	0.23 ± 0.20	0.36 ± 0.29	0.72 ± 0.91	0.26 ± 0.20
	2008-2011	0.28 ± 0.20	0.63 ± 0.95	1.11 ± 1.11	0.38 ± 0.21
	2012	0.31 ± 0.33	0.38 ± 0.14	1.28 ± 1.25	0.45 ± 0.68
OAK	2001-2007	0.19 ± 0.13	0.45 ± 0.58	0.68 ± 0.84	0.25 ± 0.20
	2008-2011	0.21 ± 0.12	0.52 ± 0.32	1.28 ± 2.12	0.33 ± 0.35
	2012-2016	N/A	N/A	N/A	N/A
PNS	2001-2007	0.31 ± 0.22	0.46 ± 0.49	0.99 ± 1.43	0.38 ± 0.49
	2008-2009	0.37 ± 0.25	0.55 ± 0.27	1.57 ± 1.69	0.43 ± 0.24
	2012-2016	N/A	N/A	N/A	N/A
OLF	2001-2007	0.21 ± 0.16	0.40 ± 0.51	0.72 ± 1.05	0.25 ± 0.15
	2008-2011	0.22 ± 0.15	0.52 ± 1.09	1.11 ± 1.32	0.29 ± 0.14
	2012-2016	0.21 ± 0.16	0.38 ± 0.56	1.20 ± 1.45	0.31 ± 0.31

Appendix C

Table S4. Model performance assessment for NH_3 prediction with stable & metastable setups at the YRK site

Stable setup: Fractional bias

Temperature	Relative humidity							
	20-30%	30-40%	40-50%	50-60%	60-70%	70-80%	80-90%	90-100%
30-35 ºC	-0.10$^{\mathbf{M}}$	-0.18$^{\mathbf{M}}$	-0.13$^{\mathbf{M}}$	-0.06$^{\mathbf{M}}$	-0.02$^{\mathbf{M}}$	NA	NA	NA
25-30 ºC	-0.08$^{\mathbf{S}}$	-0.04$^{\mathbf{S}}$	-0.07$^{\mathbf{S}}$	-0.07$^{\mathbf{S}}$	-0.05$^{\mathbf{S}}$	-0.03$^{\mathbf{S}}$	0.01$^{\mathbf{S=M}}$	NA
20-25 ºC	0.00$^{\mathbf{S}}$	0.01$^{\mathbf{M}}$	-0.02$^{\mathbf{S}}$	-0.01$^{\mathbf{S}}$	-0.05$^{\mathbf{S}}$	-0.05$^{\mathbf{S}}$	-0.03$^{\mathbf{S}}$	-0.03$^{\mathbf{S=M}}$
15-20 ºC	0.03$^{\mathbf{M}}$	0.02$^{\mathbf{M}}$	0.00$^{\mathbf{S}}$	0.00$^{\mathbf{S}}$	-0.02$^{\mathbf{S}}$	-0.03$^{\mathbf{S}}$	-0.03$^{\mathbf{S}}$	-0.04$^{\mathbf{S=M}}$
10-15 ºC	0.04$^{\mathbf{M}}$	0.02$^{\mathbf{M}}$	0.01$^{\mathbf{S}}$	0.01$^{\mathbf{S}}$	-0.03$^{\mathbf{S}}$	-0.07$^{\mathbf{S}}$	-0.03$^{\mathbf{S}}$	-0.03$^{\mathbf{S=M}}$
5-10 ºC	0.03$^{\mathbf{M}}$	-0.01$^{\mathbf{S}}$	-0.04$^{\mathbf{S}}$	-0.05$^{\mathbf{S}}$	-0.05$^{\mathbf{S}}$	-0.12$^{\mathbf{S}}$	-0.09$^{\mathbf{S}}$	-0.12$^{\mathbf{S=M}}$
0-5 ºC	-0.09$^{\mathbf{S}}$	-0.09$^{\mathbf{S}}$	-0.14$^{\mathbf{S}}$	-0.13$^{\mathbf{S}}$	-0.14$^{\mathbf{S}}$	-0.15$^{\mathbf{S}}$	-0.24$^{\mathbf{S}}$	-0.15$^{\mathbf{S=M}}$
-5-0 ºC	NA	-0.21$^{\mathbf{S}}$	-0.30$^{\mathbf{S}}$	-0.21$^{\mathbf{S}}$	-0.20$^{\mathbf{S}}$	-0.15$^{\mathbf{S}}$	-0.23$^{\mathbf{S}}$	-0.12$^{\mathbf{S=M}}$
-10 - -5 ºC	NA	NA	NA	-0.44$^{\mathbf{S}}$	-0.47$^{\mathbf{S}}$	-0.39$^{\mathbf{S}}$	-0.26$^{\mathbf{S}}$	NA

Metastable setup: Fractional bias

Temperature	Relative humidity							
	20-30%	30-40%	40-50%	50-60%	60-70%	70-80%	80-90%	90-100%
30-35 ºC	-0.09$^{\mathbf{M}}$	-0.17$^{\mathbf{M}}$	-0.12$^{\mathbf{M}}$	-0.05$^{\mathbf{M}}$	0.01$^{\mathbf{M}}$	NA	NA	NA
25-30 ºC	-0.08$^{\mathbf{S}}$	-0.04$^{\mathbf{S}}$	-0.07$^{\mathbf{S}}$	-0.07$^{\mathbf{S}}$	-0.05$^{\mathbf{S}}$	-0.03$^{\mathbf{S}}$	0.01$^{\mathbf{S=M}}$	NA
20-25 ºC	-0.01$^{\mathbf{S}}$	0.00$^{\mathbf{M}}$	-0.03$^{\mathbf{S}}$	-0.03$^{\mathbf{S}}$	-0.06$^{\mathbf{S}}$	-0.05$^{\mathbf{S}}$	-0.03$^{\mathbf{S}}$	-0.03$^{\mathbf{S=M}}$
15-20 ºC	0.02$^{\mathbf{M}}$	0.00$^{\mathbf{M}}$	-0.03$^{\mathbf{S}}$	-0.05$^{\mathbf{S}}$	-0.03$^{\mathbf{S}}$	-0.03$^{\mathbf{S}}$	-0.03$^{\mathbf{S}}$	-0.04$^{\mathbf{S=M}}$
10-15 ºC	0.02$^{\mathbf{M}}$	-0.01$^{\mathbf{M}}$	-0.03$^{\mathbf{S}}$	-0.05$^{\mathbf{S}}$	-0.07$^{\mathbf{S}}$	-0.07$^{\mathbf{S}}$	-0.03$^{\mathbf{S}}$	-0.03$^{\mathbf{S=M}}$
5-10 ºC	0.01$^{\mathbf{M}}$	-0.03$^{\mathbf{S}}$	-0.08$^{\mathbf{S}}$	-0.11$^{\mathbf{S}}$	-0.12$^{\mathbf{S}}$	-0.12$^{\mathbf{S}}$	-0.09$^{\mathbf{S}}$	-0.12$^{\mathbf{S=M}}$
0-5 ºC	-0.12$^{\mathbf{S}}$	-0.09$^{\mathbf{S}}$	-0.15$^{\mathbf{S}}$	-0.15$^{\mathbf{S}}$	-0.18$^{\mathbf{S}}$	-0.17$^{\mathbf{S}}$	-0.24$^{\mathbf{S}}$	-0.15$^{\mathbf{S=M}}$
-5-0 ºC	NA	-0.22$^{\mathbf{S}}$	-0.30$^{\mathbf{S}}$	-0.22$^{\mathbf{S}}$	-0.23$^{\mathbf{S}}$	-0.16$^{\mathbf{S}}$	-0.23$^{\mathbf{S}}$	-0.12$^{\mathbf{S=M}}$
-10 - -5 ºC	NA	NA	NA	-0.45$^{\mathbf{S}}$	-0.48$^{\mathbf{S}}$	-0.40$^{\mathbf{S}}$	-0.26$^{\mathbf{S}}$	NA

[1] The unacceptable FB values (< -0.5 or > 0.5) are labeled as bold

[2] NA: not applicable

[3] The FB values closer to 0 indicates the better model performance. The S superscript indicates the stable setup performs better , the M superscript indicates the metastable setup performs better, and the S=M superscript indicates the same model performance

Table S5. Model performance assessment for HNO_3 prediction with stable & metastable setups at YRK site

Stable setup: Fractional bias

Temperature	Relative humidity							
	20-30%	30-40%	40-50%	50-60%	60-70%	70-80%	80-90%	90-100%
30-35 ºC	0.03$^{\mathbf{M}}$	0.03$^{\mathbf{M}}$	0.04$^{\mathbf{M}}$	0.06$^{\mathbf{M}}$	0.07$^{\mathbf{M}}$	NA	NA	NA
25-30 ºC	0.03$^{\mathbf{M}}$	0.05$^{\mathbf{M}}$	0.07$^{\mathbf{M}}$	0.08$^{\mathbf{M}}$	0.11$^{\mathbf{M}}$	0.10$^{\mathbf{M}}$	0.10$^{\mathbf{S=M}}$	NA
20-25 ºC	0.06$^{\mathbf{M}}$	0.07$^{\mathbf{M}}$	0.09$^{\mathbf{M}}$	0.14$^{\mathbf{M}}$	0.15$^{\mathbf{M}}$	0.08$^{\mathbf{M}}$	0.04$^{\mathbf{M}}$	-0.27$^{\mathbf{S=M}}$
15-20 ºC	0.10$^{\mathbf{M}}$	0.10$^{\mathbf{M}}$	0.14$^{\mathbf{M}}$	0.19$^{\mathbf{M}}$	0.08$^{\mathbf{M}}$	-0.03$^{\mathbf{S}}$	-0.08$^{\mathbf{S}}$	**-0.57**$^{\mathbf{S=M}}$
10-15 ºC	0.21$^{\mathbf{M}}$	0.18$^{\mathbf{M}}$	0.15$^{\mathbf{M}}$	0.18$^{\mathbf{M}}$	0.01$^{\mathbf{S}}$	-0.32$^{\mathbf{S}}$	-0.39$^{\mathbf{S}}$	**-1.02**$^{\mathbf{S=M}}$
5-10 ºC	0.22$^{\mathbf{M}}$	-0.01$^{\mathbf{S}}$	-0.08$^{\mathbf{S}}$	-0.02$^{\mathbf{S}}$	-0.09$^{\mathbf{S}}$	-0.37$^{\mathbf{S}}$	-0.38$^{\mathbf{S}}$	**-0.68**$^{\mathbf{S=M}}$
0-5 ºC	-0.36$^{\mathbf{S}}$	**-0.51**$^{\mathbf{S}}$	-0.48$^{\mathbf{S}}$	-0.44$^{\mathbf{S}}$	-0.25$^{\mathbf{S}}$	-0.21$^{\mathbf{S}}$	-0.26$^{\mathbf{S}}$	**-0.92**$^{\mathbf{S=M}}$
-5-0 ºC	NA	**-1.01**$^{\mathbf{S}}$	**-0.93**$^{\mathbf{S}}$	**-0.72**$^{\mathbf{S}}$	-0.43$^{\mathbf{S}}$	-0.32$^{\mathbf{S}}$	-0.27$^{\mathbf{S}}$	**-0.78**$^{\mathbf{S=M}}$
-10 - -5 ºC	NA	NA	NA	**-0.95**$^{\mathbf{S}}$	**-0.65**$^{\mathbf{S}}$	-0.22$^{\mathbf{S}}$	-0.12$^{\mathbf{S}}$	NA

Metastable setup: Fractional bias

Temperature	Relative humidity							
	20-30%	30-40%	40-50%	50-60%	60-70%	70-80%	80-90%	90-100%
30-35 ºC	0.02$^{\mathbf{M}}$	0.02$^{\mathbf{M}}$	0.03$^{\mathbf{M}}$	0.04$^{\mathbf{M}}$	0.05$^{\mathbf{M}}$	NA	NA	NA
25-30 ºC	0.03$^{\mathbf{M}}$	0.04$^{\mathbf{M}}$	0.04$^{\mathbf{M}}$	0.05$^{\mathbf{M}}$	0.07$^{\mathbf{M}}$	0.09$^{\mathbf{M}}$	0.10$^{\mathbf{S=M}}$	NA
20-25 ºC	0.04$^{\mathbf{M}}$	0.03$^{\mathbf{M}}$	0.03$^{\mathbf{M}}$	0.05$^{\mathbf{M}}$	0.09$^{\mathbf{M}}$	0.08$^{\mathbf{M}}$	0.04$^{\mathbf{M}}$	-0.27$^{\mathbf{S=M}}$
15-20 ºC	0.04$^{\mathbf{M}}$	0.00$^{\mathbf{M}}$	0.00$^{\mathbf{M}}$	-0.01$^{\mathbf{M}}$	-0.02$^{\mathbf{M}}$	-0.03$^{\mathbf{S}}$	-0.08$^{\mathbf{S}}$	**-0.57**$^{\mathbf{S=M}}$
10-15 ºC	0.05$^{\mathbf{M}}$	0.04$^{\mathbf{M}}$	-0.07$^{\mathbf{M}}$	-0.17$^{\mathbf{M}}$	-0.28$^{\mathbf{S}}$	-0.32$^{\mathbf{S}}$	-0.39$^{\mathbf{S}}$	**-1.02**$^{\mathbf{S=M}}$
5-10 ºC	0.04$^{\mathbf{M}}$	-0.15$^{\mathbf{S}}$	-0.28$^{\mathbf{S}}$	-0.33$^{\mathbf{S}}$	-0.43$^{\mathbf{S}}$	-0.42$^{\mathbf{S}}$	-0.38$^{\mathbf{S}}$	**-0.68**$^{\mathbf{S=M}}$
0-5 ºC	**-0.64**$^{\mathbf{S}}$	**-0.58**$^{\mathbf{S}}$	**-0.60**$^{\mathbf{S}}$	**-0.62**$^{\mathbf{S}}$	-0.50$^{\mathbf{S}}$	-0.33$^{\mathbf{S}}$	-0.26$^{\mathbf{S}}$	**-0.92**$^{\mathbf{S=M}}$
-5-0 ºC	NA	**-1.04**$^{\mathbf{S}}$	**-0.96**$^{\mathbf{S}}$	**-0.79**$^{\mathbf{S}}$	**-0.58**$^{\mathbf{S}}$	-0.42$^{\mathbf{S}}$	-0.28$^{\mathbf{S}}$	**-0.78**$^{\mathbf{S=M}}$
-10 - -5 ºC	NA	NA	NA	**-0.97**$^{\mathbf{S}}$	**-0.69**$^{\mathbf{S}}$	-0.26$^{\mathbf{S}}$	-0.13$^{\mathbf{S}}$	NA

[1] The unacceptable FB values (< -0.5 or > 0.5) are labeled as bold values

[2] NA: not applicable

[3] The FB values closer to 0 indicates the better model performance. The S superscript indicates the stable setup performs better, the M superscript indicates the metastable setup performs better, and the S=M superscript indicates the same model performance

Table S6. Model performance assessment for NH_4^+ prediction with stable & metastable setups at YRK site

Stable setup: Fractional bias

Temperature	Relative humidity							
	20-30%	30-40%	40-50%	50-60%	60-70%	70-80%	80-90%	90-100%
30-35 ºC	0.14**M**	0.17**M**	0.12**M**	0.06**M**	0.02**M**	NA	NA	NA
25-30 ºC	0.16**S**	0.07**S**	0.08**S**	0.09**S**	0.05**S**	0.03**S**	-0.01**S=M**	NA
20-25 ºC	0.01**S**	-0.01**M**	0.04**S**	0.02**S**	0.06**S**	0.08**S**	0.05**S**	0.04**S=M**
15-20 ºC	-0.16**M**	-0.07**M**	0.00**S**	0.01**S**	0.04**S**	0.06**S**	0.05**S**	0.06**S=M**
10-15 ºC	-0.19**M**	-0.06**M**	-0.02**S**	-0.02**S**	0.07**S**	0.12**S**	0.04**S**	0.04**S=M**
5-10 ºC	-0.10**M**	0.02**S**	0.09**S**	0.08**S**	0.07**S**	0.14**S**	0.08**S**	0.09**S=M**
0-5 ºC	0.23**S**	0.20**S**	0.21**S**	0.18**S**	0.11**S**	0.09**S**	0.12**S**	0.07**S=M**
-5-0 ºC	NA	0.38**S**	0.33**S**	0.23**S**	0.12**S**	0.07**S**	0.06**S**	0.04**S=M**
-10 - -5 ºC	NA	NA	NA	0.29**S**	0.21**S**	0.15**S**	0.06**S**	NA

Metastable setup: Fractional bias

Temperature	Relative humidity							
	20-30%	30-40%	40-50%	50-60%	60-70%	70-80%	80-90%	90-100%
30-35 ºC	0.12**M**	0.16**M**	0.11**M**	0.05**M**	-0.01**M**	NA	NA	NA
25-30 ºC	0.16**S**	0.07**S**	0.09**S**	0.09**S**	0.06**S**	0.03**S**	-0.01**S=M**	NA
20-25 ºC	0.02**S**	0.01**M**	0.07**S**	0.05**S**	0.08**S**	0.08**S**	0.05**S**	0.04**S=M**
15-20 ºC	-0.11**M**	-0.01**M**	0.06**S**	0.10**S**	0.07**S**	0.06**S**	0.05**S**	0.06**S=M**
10-15 ºC	-0.08**M**	0.02**M**	0.08**S**	0.11**S**	0.14**S**	0.12**S**	0.04**S**	0.04**S=M**
5-10 ºC	-0.02**M**	0.07**S**	0.15**S**	0.17**S**	0.14**S**	0.15**S**	0.08**S**	0.09**S=M**
0-5 ºC	0.27**S**	0.21**S**	0.23**S**	0.21**S**	0.15**S**	0.11**S**	0.12**S**	0.07**S=M**
-5-0 ºC	NA	0.39**S**	0.34**S**	0.24**S**	0.14**S**	0.08**S**	0.06**S**	0.04**S=M**
-10 - -5 ºC	NA	NA	NA	0.29**S**	0.22**S**	0.15**S**	0.06**S**	NA

[1] The unacceptable FB values (< -0.5 or > 0.5) are labeled as bold values

[2] NA: not applicable

[3] The FB values closer to 0 indicates the better model performance. The S superscript indicates the stable setup performs better, the M superscript indicates the metastable setup performs better, and the S=M superscript indicates the same model performance

Table S7. Model performance assessment for NO_3^- prediction with metastable setups at the YRK site

Metastable setup: Fractional bias

Temperature	Relative humidity							
	20-30%	30-40%	40-50%	50-60%	60-70%	70-80%	80-90%	90-100%
30-35 ºC	**-1.82^{M}**	**-1.47^{M}**	**-1.34^{M}**	**-1.26^{M}**	**-1.00^{M}**	NA	NA	NA
25-30 ºC	**-1.29^{M}**	**-1.05^{M}**	**-1.00^{M}**	**-0.91^{M}**	**-0.81^{M}**	**-0.64^{M}**	-0.48$^{S=M}$	NA
20-25 ºC	**-0.89^{M}**	-0.49^{M}	-0.31^{M}	-0.45^{M}	**-0.51^{M}**	-0.26^{M}	-0.09^{M}	0.25$^{S=M}$
15-20 ºC	-0.22^{M}	-0.03^{M}	-0.02^{M}	0.06^{M}	0.05^{M}	0.06^{S}	0.12^{S}	0.36$^{S=M}$
10-15 ºC	-0.12^{M}	-0.10^{M}	0.14^{S}	0.27^{M}	0.34^{S}	0.31^{S}	0.29^{S}	0.41$^{S=M}$
5-10 ºC	-0.04^{M}	0.14^{S}	0.26^{S}	0.30^{S}	0.31^{S}	0.23^{S}	0.17^{S}	0.17$^{S=M}$
0-5 ºC	0.27^{S}	0.33^{S}	0.34^{S}	0.32^{S}	0.21^{S}	0.12^{S}	0.07^{S}	0.17$^{S=M}$
-5-0 ºC	NA	0.41^{S}	0.44^{S}	0.32^{S}	0.20^{S}	0.10^{S}	0.06^{S}	0.13$^{S=M}$
-10 - -5 ºC	NA	NA	NA	0.38^{S}	0.21^{S}	0.06^{S}	0.02^{S}	NA

[1] The unacceptable FB values (< -0.5 or > 0.5) are labeled as bold values

[2] NA: not applicable

[3] The FB values closer to 0 indicates the better model performance. The S superscript indicates the stable setup performs better, the M superscript indicates the metastable setup performs better, and the S=M superscript indicates the same model performance

Table S8. Model performance assessment for $iPM_{2.5}$ prediction with stable & metastable setups at YRK site

Stable setup: Fractional bias

Temperature	Relative humidity							
	20-30%	30-40%	40-50%	50-60%	60-70%	70-80%	80-90%	90-100%
30-35 ºC	0.02**M**	0.03**M**	0.02**S**	0.00**M**	-0.01**S**	NA	NA	NA
25-30 ºC	0.02**S**	0.00**M**	0.00**S**	0.00**S**	-0.01**M**	-0.01**M**	-0.01**S=M**	NA
20-25 ºC	-0.04**M**	-0.04**M**	-0.03**M**	-0.04**M**	-0.02**M**	0.01**S**	0.01**S=M**	0.03**S=M**
15-20 ºC	-0.11**M**	-0.08**M**	-0.06**M**	-0.07**M**	-0.01**S**	0.02**S**	0.02**S=M**	0.06**S=M**
10-15 ºC	-0.17**M**	-0.10**M**	-0.07**M**	-0.07**S**	0.01**S**	0.08**S**	0.06**S**	0.10**S=M**
5-10 ºC	-0.11**M**	0.01**S**	0.05**S**	0.03**S**	0.04**S**	0.08**S**	0.06**S**	0.07**S=M**
0-5 ºC	0.13**S**	0.17**S**	0.16**S**	0.13**S**	0.06**S**	0.04**S**	0.04**S**	0.08**S=M**
-5-0 ºC	NA	0.28**S**	0.27**S**	0.18**S**	0.09**S**	0.04**S**	0.03**S**	0.05**S=M**
-10 - -5 ºC	NA	NA	NA	0.24**S**	0.14**S**	0.06**S**	0.02**S**	NA

Metastable setup: Fractional bias

Temperature	Relative humidity							
	20-30%	30-40%	40-50%	50-60%	60-70%	70-80%	80-90%	90-100%
30-35 ºC	0.02**M**	0.03**M**	0.02**S**	0.00**M**	-0.01**S**	NA	NA	NA
25-30 ºC	0.03**S**	0.00**M**	0.01**S**	0.01**S**	0.00**M**	-0.01**M**	-0.01**S=M**	NA
20-25 ºC	-0.02**M**	-0.01**M**	0.01**M**	0.00**M**	0.00**M**	0.01**S**	0.01**S=M**	0.03**S=M**
15-20 ºC	-0.05**M**	0.00**M**	0.01**M**	0.03**M**	0.02**S**	0.02**S**	0.02**S=M**	0.06**S=M**
10-15 ºC	-0.05**M**	-0.01**M**	0.05**M**	0.08**S**	0.10**S**	0.09**S**	0.06**S**	0.10**S=M**
5-10 ºC	-0.02**M**	0.06**S**	0.12**S**	0.13**S**	0.11**S**	0.09**S**	0.06**S**	0.07**S=M**
0-5 ºC	0.18**S**	0.19**S**	0.18**S**	0.17**S**	0.10**S**	0.06**S**	0.04**S**	0.08**S=M**
-5-0 ºC	NA	0.29**S**	0.28**S**	0.19**S**	0.10**S**	0.05**S**	0.03**S**	0.05**S=M**
-10 - -5 ºC	NA	NA	NA	0.24**S**	0.14**S**	0.06**S**	0.02**S**	NA

[1] The unacceptable FB values (< -0.5 or > 0.5) are labeled as bold values

[2] NA: not applicable

[3] The FB values closer to 0 indicates the better model performance. The S superscript indicates the stable setup performs better, the M superscript indicates the metastable setup performs better, and the S=M superscript indicates the same model performance

Appendix D

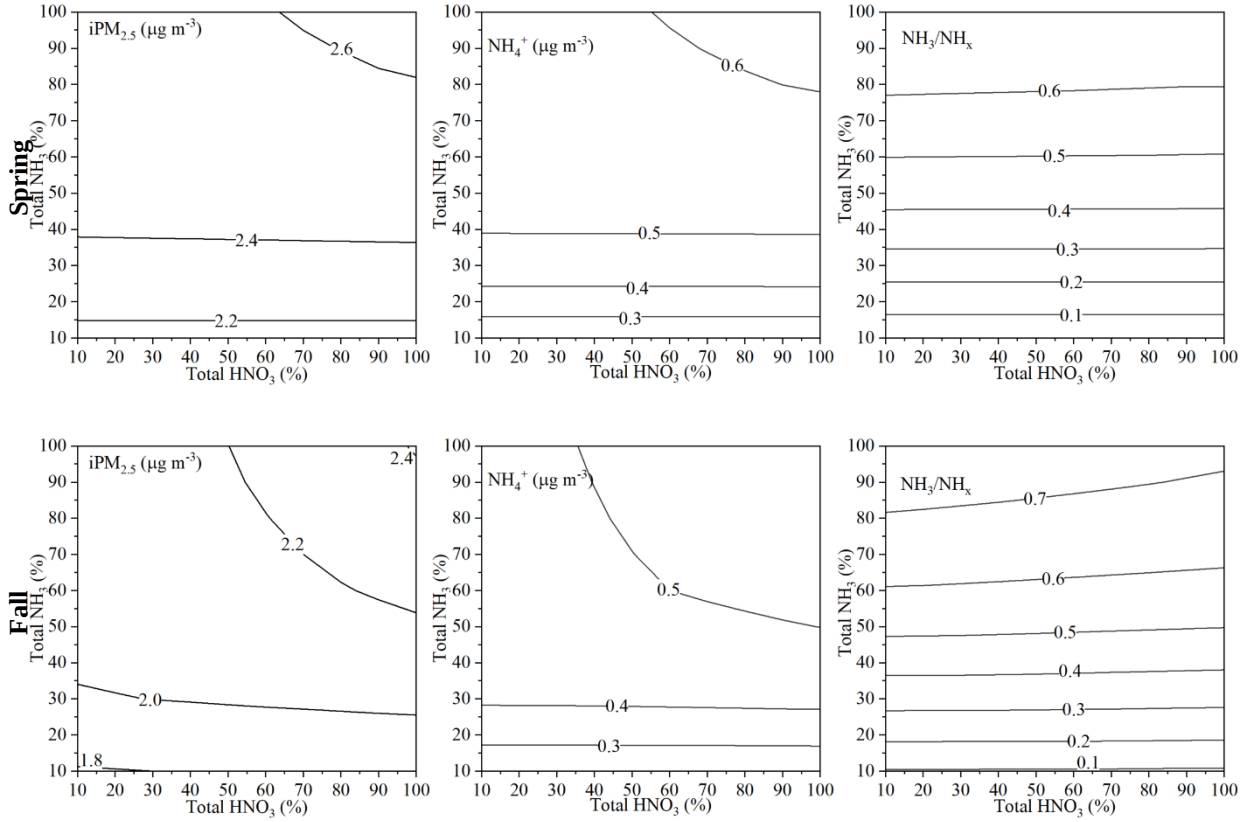

Figure S11. Responses of $iPM_{2.5}$, NH_4^+, and NH_3/NH_x to the changes of TNH_3 and $THNO_3$ at the YRK site in 2012-2016

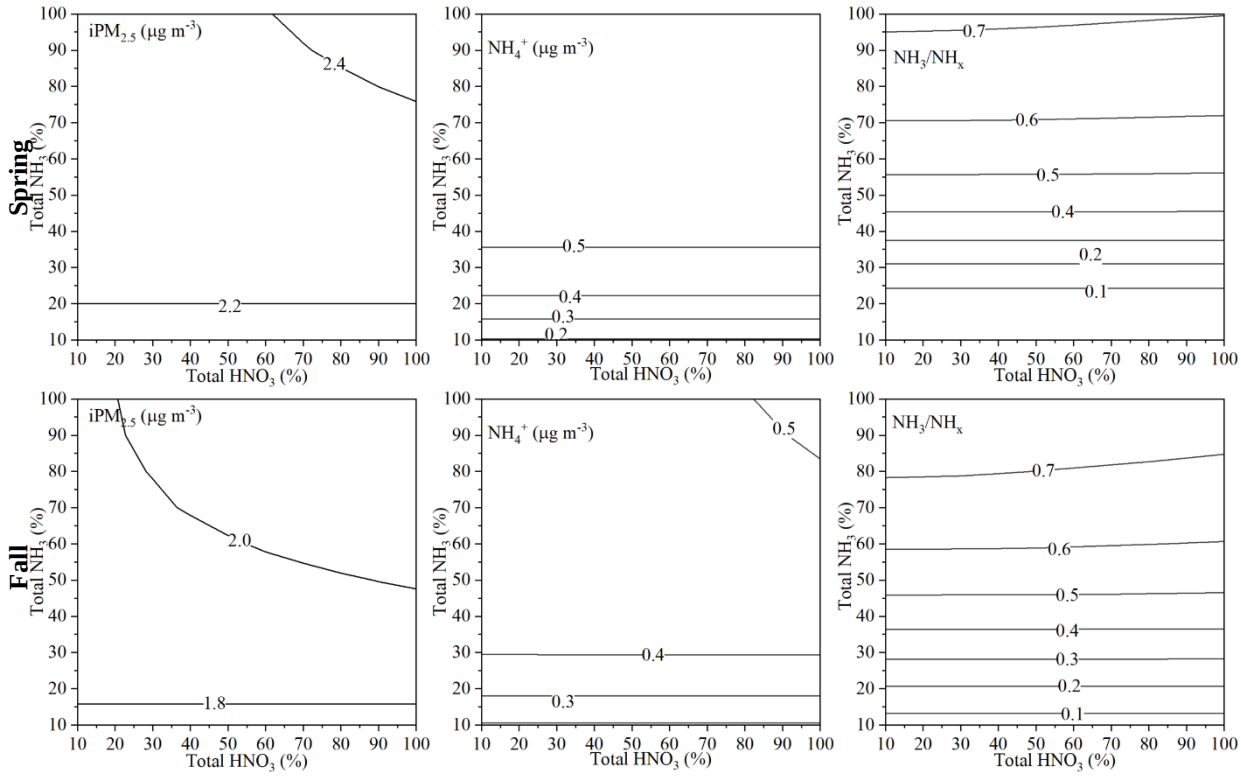

Figure S12. Responses of $iPM_{2.5}$, NH_4^+, and NH_3/NH_x to the changes of TNH_3 and $THNO_3$ at the JST site in 2012-2016

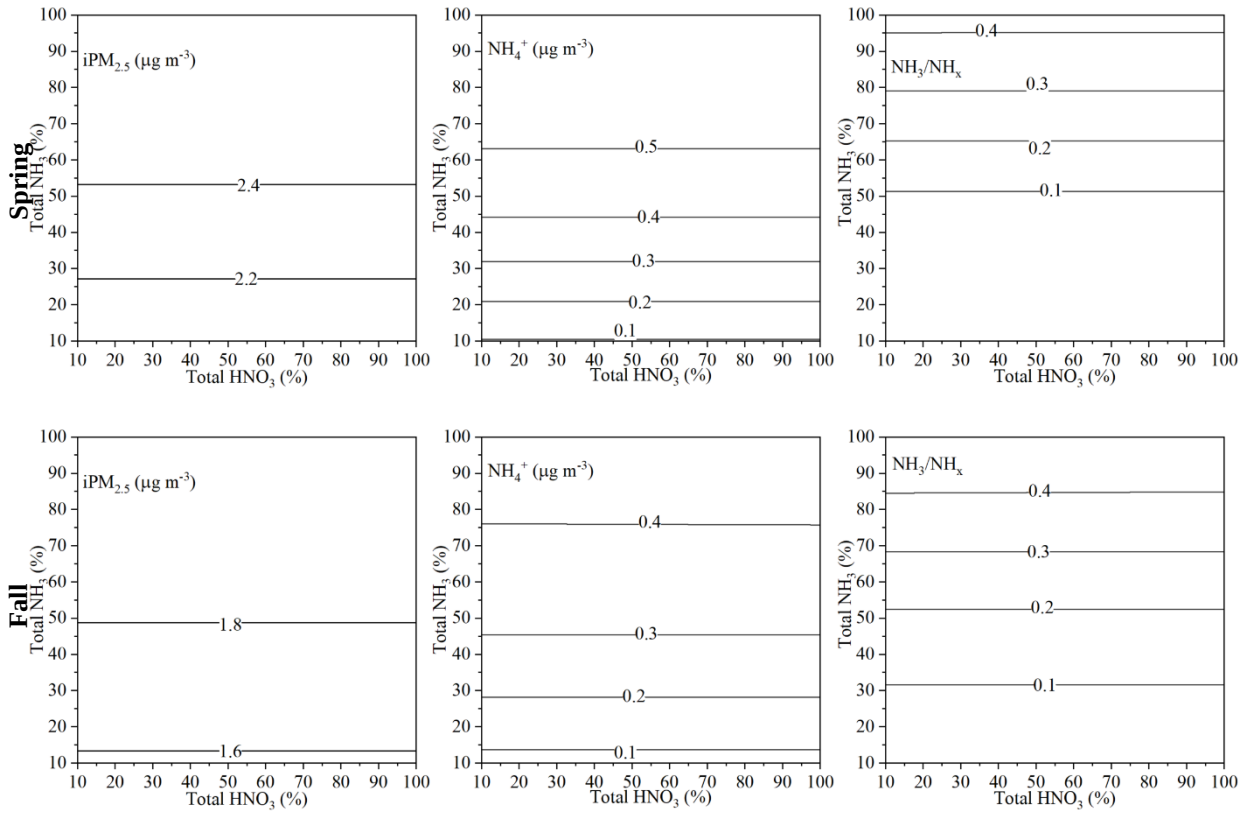

Figure S13. Responses of $iPM_{2.5}$, NH_4^+, and NH_3/NH_x to the changes of TNH_3 and $THNO_3$ at the CTR site in 2012-2016

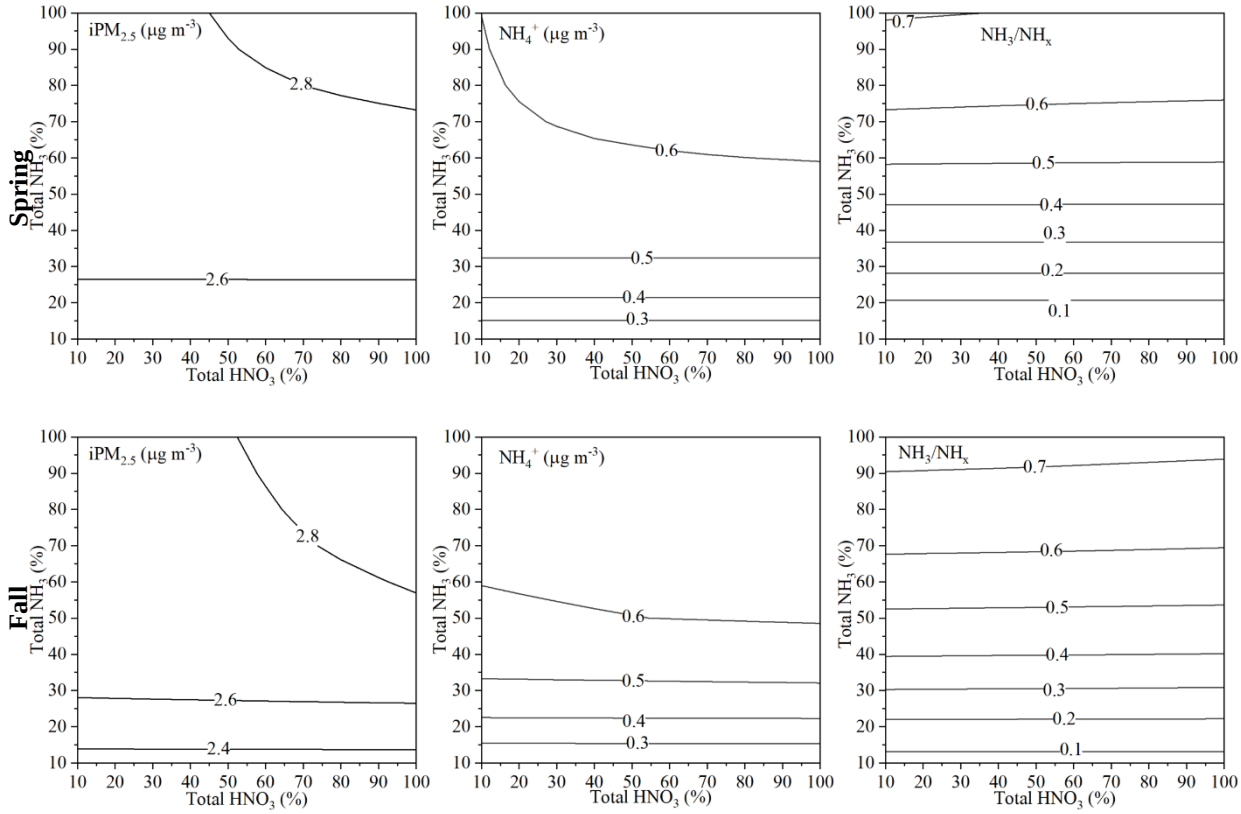

Figure S14. Responses of $iPM_{2.5}$, NH_4^+, and NH_3/NH_x to the changes of TNH_3 and $THNO_3$ at the BHM site in 2012-2016

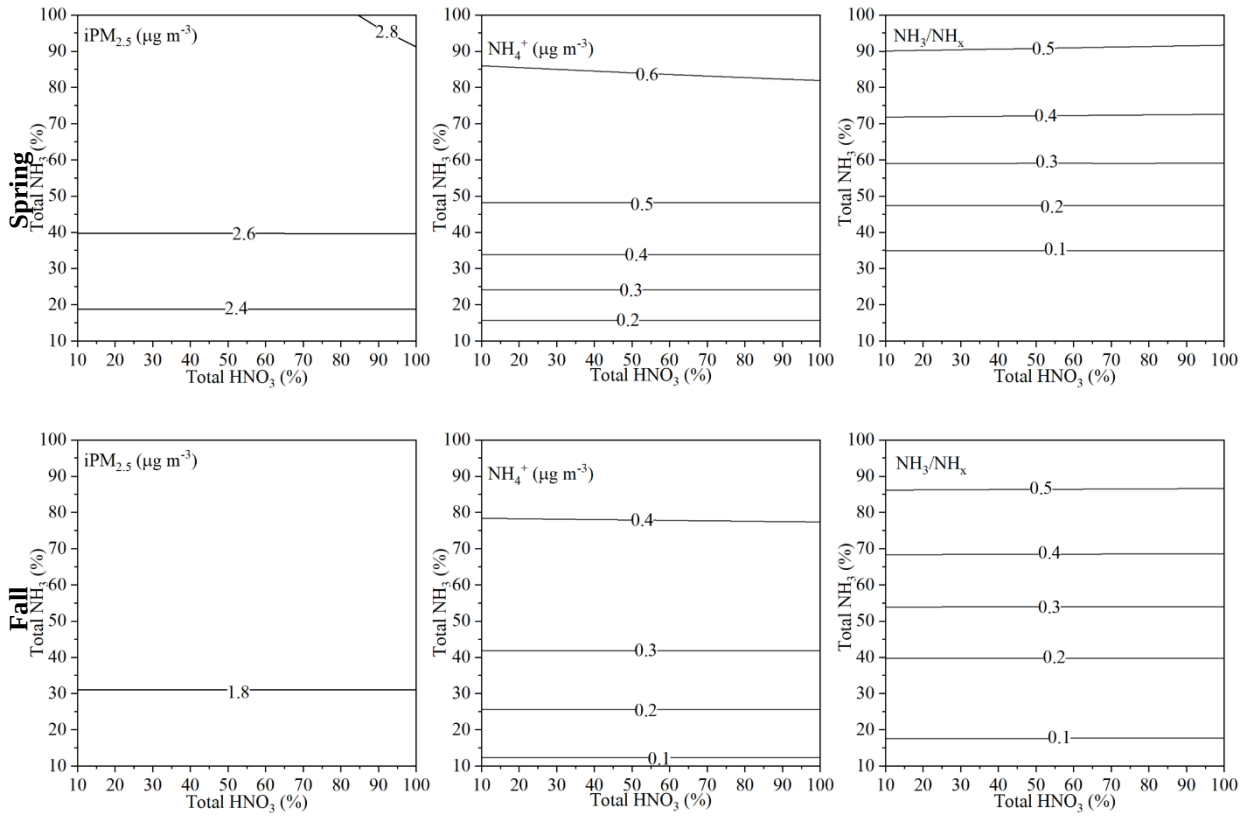

Figure S15. Responses of $iPM_{2.5}$, NH_4^+, and NH_3/NH_x to the changes of TNH_3 and $THNO_3$ at the OLF site in 2013-2016

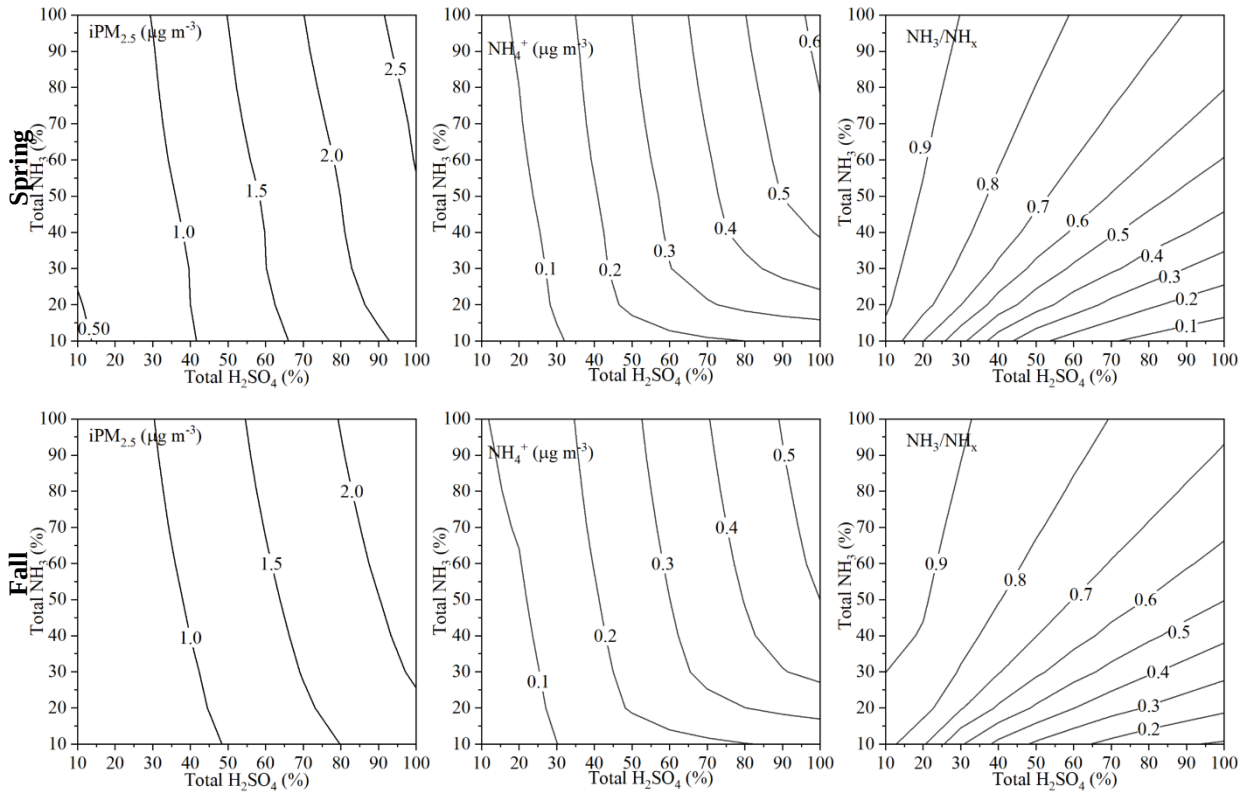

Figure S16. Responses of $iPM_{2.5}$, NH_4^+, and NH_3/NH_x to the changes of TNH_3 and TH_2SO_4 at the YRK site in 2012-2016

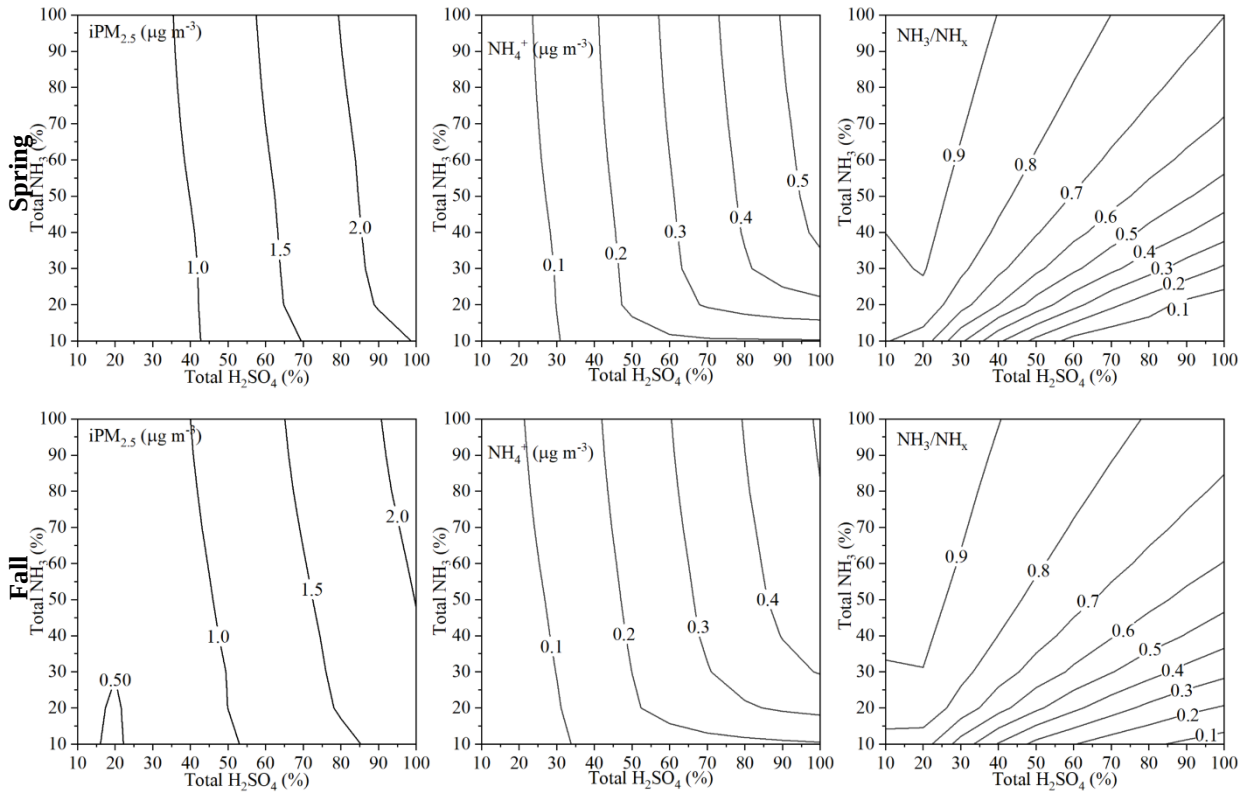

Figure S17. Responses of $iPM_{2.5}$, NH_4^+, and NH_3/NH_x to the changes of TNH_3 and TH_2SO_4 at the JST site in 2012-2016

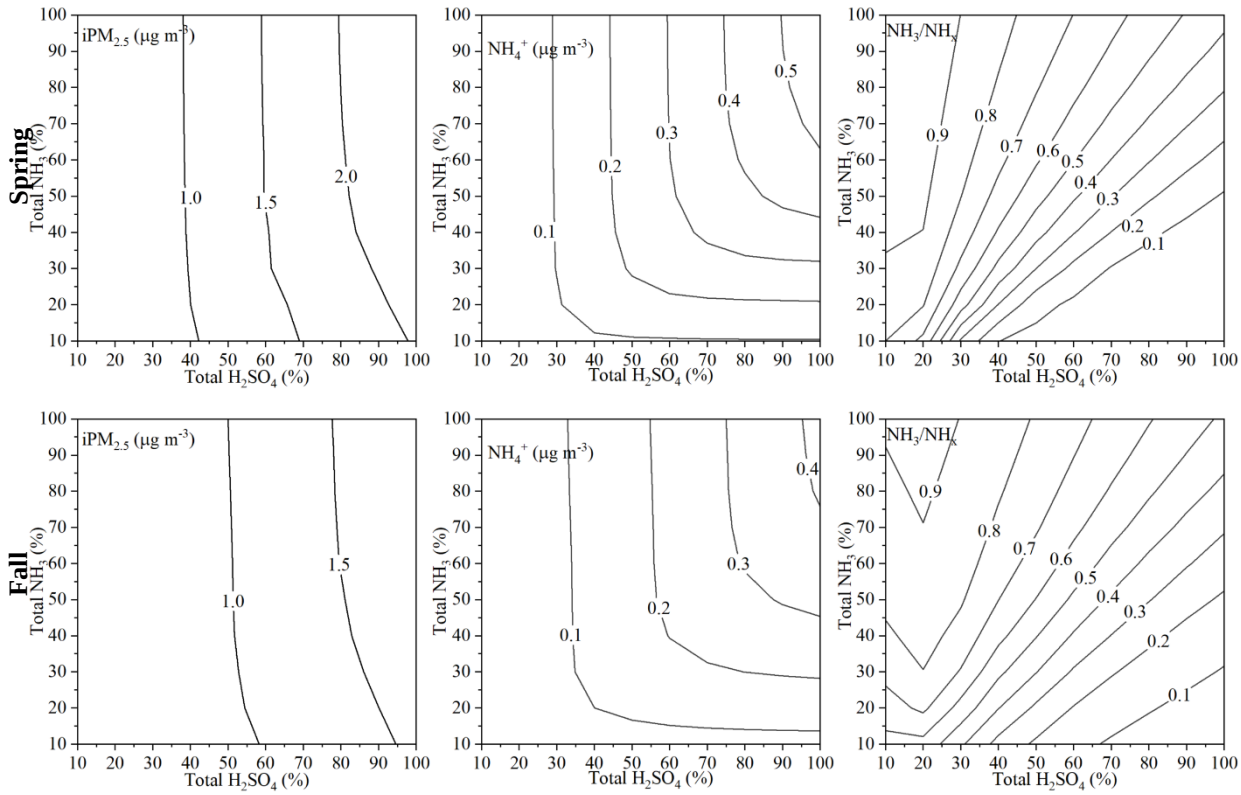

Figure S18. Responses of $iPM_{2.5}$, NH_4^+, and NH_3/NH_x to the changes of TNH_3 and TH_2SO_4 at the CTR site in 2012-2016

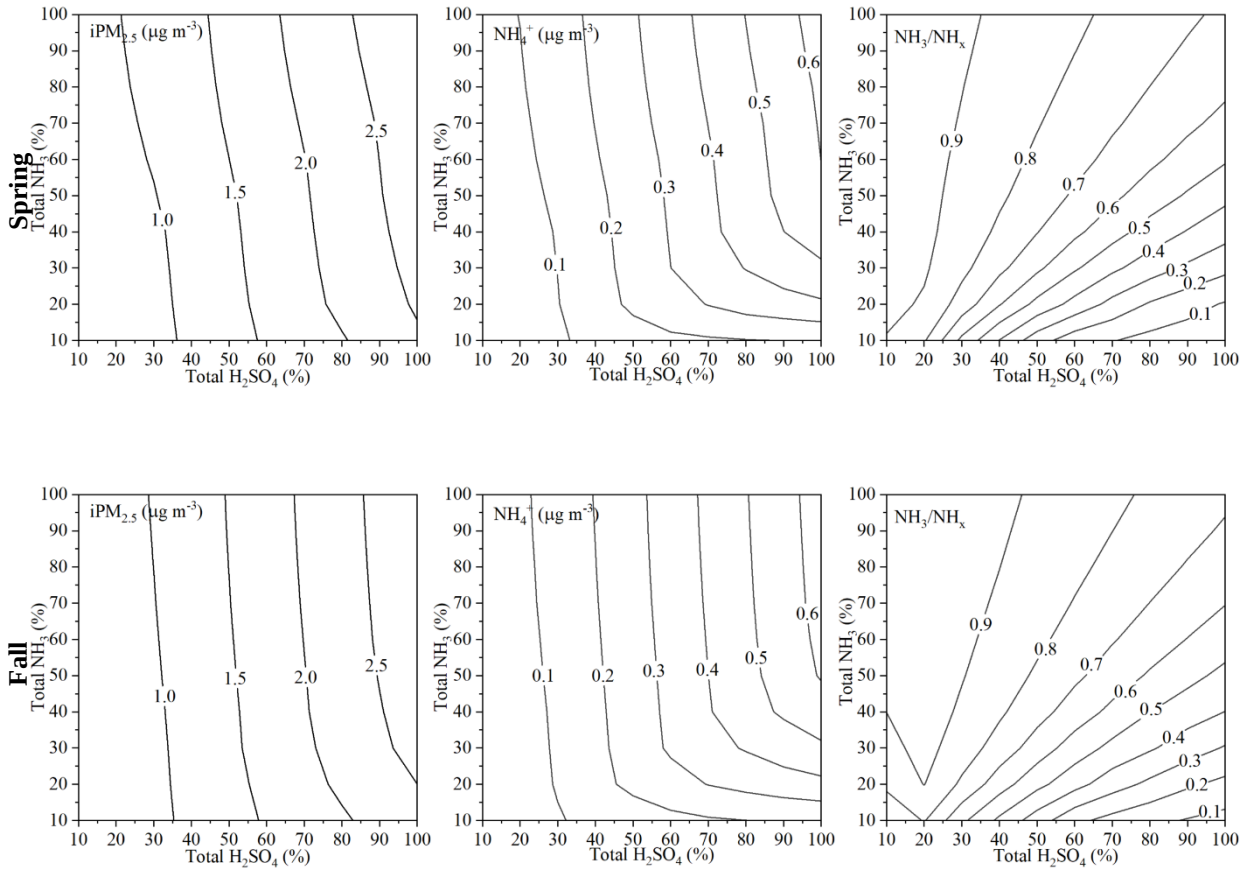

Figure S19. Responses of $iPM_{2.5}$, NH_4^+, and NH_3/NH_x to the changes of TNH_3 and TH_2SO_4 at the BHM site in 2012-2016

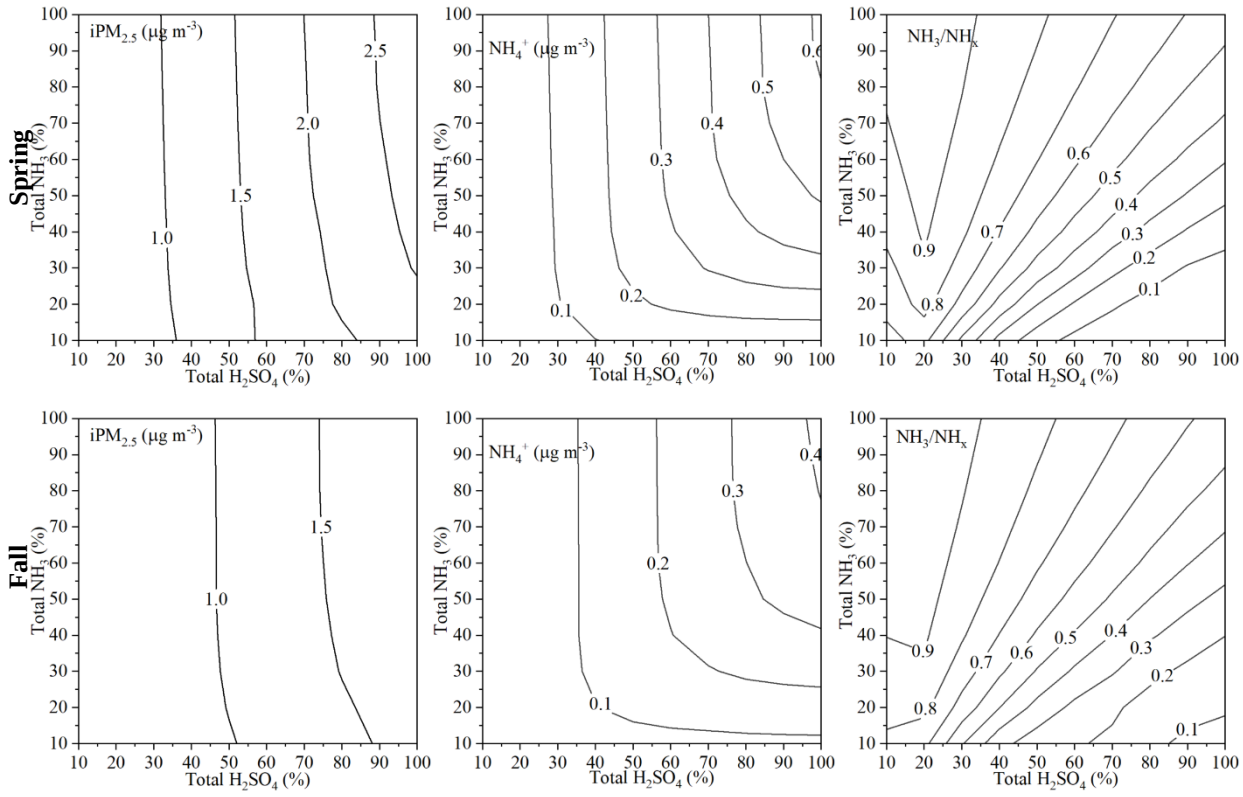

Figure S20. Responses of $iPM_{2.5}$, NH_4^+, and NH_3/NH_x to the changes of TNH_3 and TH_2SO_4 at the OLF site in 2013-2016

Appendix E

Table S9. The statistics of different precursor gases of iPM$_{2.5}$ by season at the YRK site in 2008-2011

Season		Na^+	TH_2SO_4	TNH_3	$THNO_3$	THCl	Ca^{2+}	K^+	Mg^{2+}	RH	T (K)
Winter	min	0.00	0.63	0.83	0.47	0.02	0.00	0.01	0.00	0.37	264.93
	median	0.02	2.19	1.84	1.99	0.04	0.02	0.02	0.00	0.61	277.18
	max	0.28	5.12	5.00	8.01	0.21	0.15	0.11	0.03	0.91	290.62
	mean	0.05	2.22	2.15	2.49	0.05	0.03	0.03	0.01	0.62	277.61
	SD	0.06	1.01	1.05	1.50	0.05	0.03	0.03	0.01	0.14	5.70
	N	30	30	30	30	30	30	30	30	30	30
Spring	min	0.01	0.80	0.87	0.23	0.01	0.01	0.01	0.00	0.35	272.68
	median	0.03	3.36	2.71	1.62	0.04	0.03	0.03	0.01	0.64	291.29
	max	0.47	12.09	9.26	3.86	0.18	0.26	0.11	0.03	0.93	299.32
	mean	0.07	3.42	2.91	1.68	0.04	0.06	0.04	0.01	0.64	289.45
	SD	0.09	2.04	1.52	0.70	0.04	0.07	0.02	0.01	0.14	6.12
	N	34	34	34	34	34	34	34	34	34	34
Summer	min	0.00	1.57	1.06	0.35	0.01	0.01	0.00	0.00	0.47	294.27
	median	0.02	3.98	2.87	1.34	0.03	0.03	0.02	0.01	0.71	298.60
	max	0.21	13.66	7.81	3.82	0.13	0.06	0.35	0.07	0.96	301.90
	mean	0.04	4.51	3.07	1.51	0.03	0.03	0.03	0.01	0.70	298.42
	SD	0.04	2.60	1.27	0.64	0.02	0.01	0.05	0.01	0.11	1.82
	N	62	62	62	62	62	62	62	62	62	62
Fall	min	0.00	0.71	0.88	0.49	0.01	0.01	0.01	0.00	0.40	277.96
	median	0.02	2.04	1.67	1.25	0.03	0.02	0.02	0.00	0.62	290.19
	max	0.53	7.15	8.31	3.17	0.20	0.08	0.07	0.03	1.00	299.58
	mean	0.04	2.37	2.24	1.52	0.04	0.03	0.02	0.01	0.65	289.05
	SD	0.09	1.45	1.40	0.75	0.04	0.02	0.01	0.01	0.14	5.39
	N	40	40	40	40	40	40	40	40	40	40

[1] All the concentration values are expressed in μg m^{-3}.

[2] $TNH_3 = NH_3 + NH_4^+$; $THNO_3 = HNO_3 + NO_3^-$; $TH_2SO_4 = SO_4^{2-}$; TNH_3, $THNO_3$, TH_2SO_4 are all expressed as the equivalent concentration; T is temperature; RH is relative humidity; SD is standard deviation; N is the number of observations.

Table S10. The statistics of different precursor gases of $iPM_{2.5}$ by season at the YRK site in 2012-2016

Season		Na^+	TH_2SO_4	TNH_3	$THNO_3$	THCl	Ca^{2+}	K^+	Mg^{2+}	RH	T (K)
Winter	min	0.00	0.33	0.74	0.61	0.01	0.00	0.01	0.00	0.31	265.13
	median	0.01	1.31	1.40	1.22	0.02	0.02	0.02	0.00	0.62	279.18
	max	0.35	3.78	4.23	2.50	0.04	0.03	0.04	0.01	0.85	287.25
	mean	0.04	1.56	1.53	1.41	0.02	0.01	0.02	0.00	0.61	278.22
	SD	0.07	0.97	0.69	0.55	0.01	0.01	0.01	0.00	0.15	4.83
	N	27	27	27	27	27	27	27	27	27	27
Spring	min	0.00	0.59	0.91	0.30	0.01	0.00	0.00	0.00	0.31	273.66
	median	0.02	1.58	2.06	1.13	0.02	0.02	0.02	0.01	0.66	291.94
	max	0.26	3.81	4.55	2.15	0.10	0.06	0.05	0.02	0.88	299.26
	mean	0.05	1.82	2.11	1.13	0.03	0.03	0.03	0.01	0.62	289.63
	SD	0.06	0.81	0.89	0.47	0.02	0.01	0.02	0.01	0.14	6.42
	N	30	30	30	30	30	30	30	30	30	30
Summer	min	0.01	0.70	1.10	0.39	0.01	0.00	0.00	0.00	0.44	290.01
	median	0.02	1.93	2.32	1.01	0.02	0.02	0.03	0.01	0.73	297.58
	max	0.20	4.15	10.69	2.15	0.07	0.09	0.07	0.03	0.87	303.83
	mean	0.03	2.05	2.66	1.11	0.03	0.03	0.03	0.01	0.71	297.56
	SD	0.04	0.92	1.62	0.49	0.01	0.02	0.02	0.01	0.11	2.27
	N	37	37	37	37	37	37	37	37	37	37
Fall	min	0.00	0.10	0.24	0.16	0.01	0.01	0.00	0.00	0.44	273.19
	median	0.02	1.29	1.91	0.97	0.02	0.02	0.02	0.00	0.66	290.73
	max	0.64	3.11	10.33	3.37	0.07	0.05	0.08	0.02	0.93	298.62
	mean	0.04	1.49	2.45	1.10	0.02	0.02	0.03	0.00	0.68	289.40
	SD	0.10	0.76	1.93	0.65	0.01	0.01	0.02	0.00	0.13	6.58
	N	39	39	39	39	39	39	39	39	39	39

[1] All the concentration values are expressed in $\mu g\ m^{-3}$.

[2] $TNH_3 = NH_3 + NH_4^+$; $THNO_3 = HNO_3 + NO_3^-$; $TH_2SO_4 = SO_4^{2-}$; TNH_3, $THNO_3$, TH_2SO_4 are all expressed as the equivalent concentration; T is temperature; RH is relative humidity; SD is standard deviation; N is the number of observations.

Table S11. The statistics of different precursor gases of $iPM_{2.5}$ by season at the JST site in 2010-2011

Season		Na^+	TH_2SO_4	TNH_3	$THNO_3$	THCl	Ca^{2+}	K^+	Mg^{2+}	RH	T (K)
Winter	min	0.00	1.09	0.97	0.76	0.02	0.00	0.00	0.00	0.48	268.09
	median	0.03	1.86	1.82	1.29	0.03	0.03	0.02	0.00	0.61	276.09
	max	0.18	4.94	4.01	6.50	0.19	0.05	0.08	0.02	0.97	289.73
	mean	0.04	2.26	1.89	1.84	0.06	0.02	0.02	0.01	0.66	276.74
	SD	0.05	1.06	0.70	1.40	0.05	0.01	0.02	0.00	0.15	5.98
	N	17	17	17	17	17	17	17	17	17	17
Spring	min	0.01	1.00	1.50	0.87	0.01	0.01	0.01	0.00	0.39	275.99
	median	0.05	2.98	2.34	2.24	0.03	0.02	0.02	0.01	0.61	293.16
	max	0.14	7.65	3.89	3.72	0.15	0.03	0.11	0.02	0.80	300.87
	mean	0.06	3.30	2.44	2.14	0.04	0.02	0.04	0.01	0.61	289.56
	SD	0.05	1.62	0.69	0.84	0.03	0.01	0.03	0.00	0.09	7.17
	N	19	19	19	19	19	19	19	19	19	19
Summer	min	0.01	1.98	1.70	1.58	0.02	0.01	0.01	0.00	0.55	297.73
	median	0.02	3.77	2.60	2.25	0.03	0.03	0.03	0.01	0.64	300.86
	max	0.09	5.88	3.78	3.40	0.04	0.06	0.10	0.02	0.75	302.93
	mean	0.03	4.01	2.59	2.28	0.03	0.03	0.03	0.01	0.65	300.80
	SD	0.02	1.35	0.57	0.65	0.01	0.01	0.03	0.01	0.07	1.29
	N	17	17	17	17	17	17	17	17	17	17
Fall	min	0.01	0.88	1.18	0.66	0.02	0.01	0.01	0.00	0.47	283.32
	median	0.02	2.04	2.18	1.14	0.03	0.03	0.03	0.01	0.54	292.56
	max	0.05	4.48	3.92	2.77	0.05	0.05	0.11	0.01	0.70	300.74
	mean	0.02	2.15	2.31	1.42	0.03	0.03	0.04	0.01	0.55	292.20
	SD	0.01	1.09	0.78	0.70	0.01	0.01	0.03	0.00	0.07	5.83
	N	14	14	14	14	14	14	14	14	14	14

[1] All the concentration values are expressed in $\mu g\ m^{-3}$.

[2] $TNH_3 = NH_3 + NH_4^+$; $THNO_3 = HNO_3 + NO_3^-$; $TH_2SO_4 = SO_4^{2-}$; TNH_3, $THNO_3$, TH_2SO_4 are all expressed as the equivalent concentration; T is temperature; RH is relative humidity; SD is standard deviation; N is the number of observations.

Table S12. The statistics of different precursor gases of $iPM_{2.5}$ by season at the JST site in 2012-2016

Season		Na^+	TH_2SO_4	TNH_3	$THNO_3$	THCl	Ca^{2+}	K^+	Mg^{2+}	RH	T (K)
Winter	min	0.01	0.57	0.95	0.58	0.02	0.01	0.01	0.00	0.37	271.33
	median	0.02	1.32	1.54	1.45	0.03	0.02	0.02	0.00	0.52	278.25
	max	0.13	3.38	2.85	3.92	0.39	0.05	0.07	0.02	0.95	290.89
	mean	0.04	1.65	1.69	1.73	0.07	0.02	0.03	0.01	0.58	279.74
	SD	0.03	0.85	0.58	0.96	0.09	0.01	0.02	0.00	0.18	5.37
	N	17	17	17	17	17	17	17	17	17	17
Spring	min	0.00	0.54	0.82	0.37	0.01	0.01	0.01	0.00	0.29	275.26
	median	0.03	1.67	1.96	1.08	0.02	0.02	0.03	0.01	0.57	290.19
	max	0.18	3.21	3.25	2.27	0.15	0.06	0.06	0.02	0.75	299.37
	mean	0.05	1.72	1.84	1.16	0.03	0.03	0.03	0.01	0.56	290.31
	SD	0.05	0.67	0.61	0.53	0.03	0.01	0.02	0.01	0.12	6.47
	N	29	29	29	29	29	29	29	29	29	29
Summer	min	0.01	0.69	0.86	0.73	0.01	0.01	0.01	0.00	0.42	296.19
	median	0.02	1.77	1.92	1.53	0.02	0.02	0.03	0.01	0.63	298.97
	max	0.11	3.99	2.87	3.71	0.05	0.07	0.23	0.02	0.85	305.40
	mean	0.03	2.02	1.96	1.70	0.02	0.03	0.05	0.01	0.63	299.53
	SD	0.02	0.94	0.58	0.67	0.01	0.01	0.05	0.01	0.10	2.27
	N	35	35	35	35	35	35	35	35	35	35
Fall	min	0.00	0.41	1.02	0.34	0.01	0.01	0.00	0.00	0.41	276.27
	median	0.02	1.30	1.86	1.00	0.02	0.03	0.03	0.01	0.63	293.00
	max	0.12	3.33	3.12	2.33	0.06	0.07	0.07	0.02	0.77	300.46
	mean	0.03	1.45	1.96	1.16	0.02	0.03	0.03	0.01	0.61	291.56
	SD	0.03	0.76	0.53	0.50	0.01	0.02	0.02	0.00	0.10	6.26
	N	36	36	36	36	36	36	36	36	36	36

[1] All the concentration values are expressed in $\mu g\ m^{-3}$.

[2] $TNH_3 = NH_3 + NH_4^+$; $THNO_3 = HNO_3 + NO_3^-$; $TH_2SO_4 = SO_4^{2-}$; TNH_3, $THNO_3$, TH_2SO_4 are all expressed as the equivalent concentration; T is temperature; RH is relative humidity; SD is standard deviation; N is the number of observations.

Table S13. The statistics of different precursor gases of $iPM_{2.5}$ by season at the CTR site in 2012-2016

Season		Na^+	TH_2SO_4	TNH_3	$THNO_3$	THCl	Ca^{2+}	K^+	Mg^{2+}	RH	T (K)
Winter	min	0.01	0.36	0.21	0.19	0.01	0.01	0.00	0.00	0.37	271.98
	median	0.02	0.97	0.59	0.70	0.02	0.02	0.03	0.00	0.60	280.59
	max	0.42	4.40	1.48	2.22	0.09	0.06	0.08	0.02	0.94	290.03
	mean	0.05	1.41	0.65	0.99	0.02	0.02	0.03	0.01	0.61	279.95
	SD	0.08	1.02	0.32	0.61	0.02	0.01	0.02	0.00	0.15	4.47
	N	31	31	31	31	31	31	31	31	31	31
Spring	min	0.00	0.69	0.47	0.22	0.01	0.01	0.01	0.00	0.35	280.90
	median	0.02	1.69	0.84	0.66	0.02	0.02	0.04	0.01	0.58	291.83
	max	0.19	4.48	1.59	1.25	0.13	0.06	0.10	0.02	0.89	299.51
	mean	0.05	1.82	0.91	0.67	0.03	0.03	0.04	0.01	0.60	291.70
	SD	0.05	0.83	0.27	0.24	0.03	0.02	0.02	0.01	0.16	4.71
	N	34	34	34	34	34	34	34	34	34	34
Summer	min	0.00	0.69	0.24	0.29	0.01	0.00	0.01	0.00	0.51	296.19
	median	0.03	1.77	0.79	0.69	0.02	0.03	0.03	0.01	0.73	299.43
	max	0.19	3.95	1.48	1.60	0.58	0.21	0.08	0.05	0.87	303.32
	mean	0.04	1.93	0.82	0.70	0.04	0.04	0.04	0.01	0.72	299.62
	SD	0.04	0.77	0.31	0.28	0.08	0.04	0.02	0.01	0.09	1.56
	N	47	47	47	47	47	47	47	47	47	47
Fall	min	0.00	0.28	0.19	0.17	0.01	0.01	0.00	0.00	0.35	276.48
	median	0.02	1.26	0.71	0.72	0.02	0.03	0.03	0.01	0.67	292.91
	max	0.19	4.40	1.44	1.79	0.09	0.09	0.14	0.03	0.95	301.75
	mean	0.04	1.38	0.72	0.71	0.02	0.03	0.04	0.01	0.66	291.33
	SD	0.04	0.81	0.26	0.32	0.01	0.02	0.03	0.01	0.13	6.52
	N	62	62	62	62	62	62	62	62	62	62

[1] All the concentration values are expressed in $\mu g\ m^{-3}$.

[2] $TNH_3 = NH_3 + NH_4^+$; $THNO_3 = HNO_3 + NO_3^-$; $TH_2SO_4 = SO_4^{2-}$; TNH_3, $THNO_3$, TH_2SO_4 are all expressed as the equivalent concentration; T is temperature; RH is relative humidity; SD is standard deviation; N is the number of observations.

Table S14. The statistics of different precursor gases of $iPM_{2.5}$ by season at the BHM site in 2011

Season		Na^+	TH_2SO_4	TNH_3	$THNO_3$	THCl	Ca^{2+}	K^+	Mg^{2+}	RH	T (K)
Winter	min	0.00	1.63	1.33	0.91	0.01	0.01	0.01	0.00	0.53	272.70
	median	0.04	2.47	3.21	2.31	0.33	0.05	0.05	0.01	0.61	279.40
	max	0.40	3.42	3.97	4.36	0.56	0.12	0.11	0.03	0.91	288.52
	mean	0.11	2.43	2.65	2.30	0.26	0.05	0.05	0.01	0.65	279.60
	SD	0.14	0.66	1.07	0.98	0.23	0.05	0.03	0.01	0.13	5.61
	N	9	9	9	9	9	9	9	9	9	9
Spring	min	0.01	1.35	1.61	0.94	0.02	0.02	0.02	0.00	0.45	288.03
	median	0.02	3.68	2.41	1.83	0.11	0.06	0.03	0.01	0.59	294.88
	max	0.22	5.38	5.20	2.60	0.50	0.08	0.15	0.03	0.72	301.94
	mean	0.08	3.55	2.77	1.80	0.15	0.05	0.06	0.02	0.58	295.16
	SD	0.09	1.64	1.16	0.65	0.15	0.02	0.05	0.01	0.08	4.78
	N	9	9	9	9	9	9	9	9	9	9
Summer	min	0.01	2.07	1.85	1.20	0.04	0.02	0.01	0.00	0.52	298.14
	median	0.03	4.05	3.23	1.95	0.08	0.04	0.05	0.01	0.70	301.47
	max	0.55	5.88	4.55	2.78	0.17	0.06	0.14	0.02	0.77	303.04
	mean	0.11	3.96	3.12	2.01	0.09	0.04	0.06	0.01	0.67	301.02
	SD	0.17	1.20	1.05	0.49	0.04	0.01	0.04	0.01	0.09	1.69
	N	9	9	9	9	9	9	9	9	9	9
Fall	min	0.00	1.65	1.43	0.72	0.03	0.02	0.01	0.00	0.46	285.59
	median	0.02	2.45	2.44	1.25	0.12	0.04	0.02	0.02	0.74	287.77
	max	0.13	4.49	2.89	1.93	0.16	0.16	0.13	0.03	0.87	291.71
	mean	0.05	2.77	2.29	1.31	0.11	0.06	0.04	0.02	0.70	288.42
	SD	0.05	1.08	0.61	0.59	0.05	0.06	0.05	0.01	0.16	3.00
	N	5	5	5	5	5	5	5	5	5	5

[1] All the concentration values are expressed in $\mu g\ m^{-3}$.

[2] $TNH_3 = NH_3 + NH_4^+$; $THNO_3 = HNO_3 + NO_3^-$; $TH_2SO_4 = SO_4^{2-}$; TNH_3, $THNO_3$, TH_2SO_4 are all expressed as the equivalent concentration; T is temperature; RH is relative humidity; SD is standard deviation; N is the number of observations.

Table S15. The statistics of different precursor gases of $iPM_{2.5}$ by season at the BHM site in 2012-2016

Season		Na^+	TH_2SO_4	TNH_3	$THNO_3$	THCl	Ca^{2+}	K^+	Mg^{2+}	RH	T (K)
Winter	min	0.01	0.61	1.35	0.92	0.03	0.01	0.01	0.00	0.44	274.65
	median	0.02	1.26	1.61	1.27	0.10	0.02	0.02	0.01	0.62	281.76
	max	0.08	4.57	2.96	4.07	0.53	0.05	0.07	0.02	0.91	290.62
	mean	0.03	1.92	1.79	1.60	0.15	0.03	0.03	0.01	0.61	282.85
	SD	0.03	1.28	0.52	0.92	0.14	0.01	0.02	0.00	0.13	4.19
	N	11	11	11	11	11	11	11	11	11	11
Spring	min	0.01	1.05	1.20	0.55	0.02	0.01	0.01	0.00	0.44	282.14
	median	0.06	1.76	1.95	1.15	0.10	0.04	0.04	0.02	0.65	294.59
	max	0.18	3.95	3.19	2.13	0.52	0.18	0.07	0.03	0.88	298.40
	mean	0.07	2.00	2.01	1.22	0.14	0.05	0.04	0.02	0.63	292.62
	SD	0.05	0.89	0.61	0.46	0.13	0.05	0.02	0.01	0.13	5.09
	N	13	13	13	13	13	13	13	13	13	13
Summer	min	0.00	0.59	0.66	0.34	0.01	0.01	0.00	0.00	0.42	293.39
	median	0.03	2.26	2.17	1.20	0.04	0.03	0.04	0.01	0.63	299.67
	max	0.11	4.62	3.65	2.35	0.08	0.17	0.17	0.04	0.88	303.38
	mean	0.04	2.41	2.09	1.23	0.04	0.05	0.04	0.02	0.67	299.72
	SD	0.03	1.16	0.79	0.48	0.02	0.04	0.04	0.01	0.11	2.85
	N	25	25	25	25	25	25	25	25	25	25
Fall	min	0.01	0.40	0.83	0.44	0.02	0.03	0.02	0.00	0.42	280.01
	median	0.03	1.35	1.90	0.96	0.08	0.04	0.04	0.01	0.67	295.22
	max	0.15	4.63	4.27	2.10	0.64	0.15	0.10	0.07	0.73	301.70
	mean	0.05	1.98	2.17	1.02	0.13	0.05	0.05	0.02	0.63	293.08
	SD	0.04	1.27	0.97	0.39	0.16	0.03	0.02	0.01	0.10	6.58
	N	20	20	20	20	20	20	20	20	20	20

[1] All the concentration values are expressed in $\mu g\ m^{-3}$.

[2] $TNH_3 = NH_3 + NH_4^+$; $THNO_3 = HNO_3 + NO_3^-$; $TH_2SO_4 = SO_4^{2-}$; TNH_3, $THNO_3$, TH_2SO_4 are all expressed as the equivalent concentration; T is temperature; RH is relative humidity; SD is standard deviation; N is the number of observations.

Table S16. The statistics of different precursor gases of iPM$_{2.5}$ by season at the OLF site in 2013-2016

Season		Na^+	TH_2SO_4	TNH_3	$THNO_3$	THCl	Ca^{2+}	K^+	Mg^{2+}	RH	T (K)
Winter	min	0.00	0.22	0.43	0.30	0.01	0.01	0.01	0.00	0.38	268.30
	median	0.03	1.32	0.88	0.77	0.03	0.02	0.05	0.00	0.66	282.15
	max	0.41	4.16	2.52	1.96	0.48	0.04	0.15	0.05	0.96	295.25
	mean	0.07	1.50	1.02	0.85	0.06	0.02	0.06	0.01	0.68	282.58
	SD	0.10	0.95	0.57	0.47	0.10	0.01	0.04	0.01	0.15	5.77
	N	22	22	22	22	22	22	22	22	22	22
Spring	min	0.01	0.62	0.70	0.54	0.01	0.01	0.01	0.00	0.47	282.67
	median	0.06	1.52	1.18	0.93	0.04	0.03	0.04	0.01	0.72	294.65
	max	0.27	4.46	2.17	2.17	0.27	0.14	0.12	0.05	0.96	298.84
	mean	0.08	2.01	1.24	1.01	0.06	0.03	0.05	0.01	0.70	293.68
	SD	0.08	1.05	0.35	0.37	0.06	0.02	0.03	0.01	0.13	4.49
	N	23	23	23	23	23	23	23	23	23	23
Summer	min	0.02	0.86	0.43	0.38	0.02	0.01	0.01	0.00	0.69	297.99
	median	0.08	1.98	1.04	0.79	0.04	0.04	0.03	0.01	0.80	300.78
	max	0.27	4.20	1.78	2.31	0.16	0.12	0.11	0.05	0.87	302.99
	mean	0.09	2.14	1.00	0.88	0.06	0.05	0.04	0.02	0.79	300.94
	SD	0.06	0.97	0.36	0.40	0.04	0.03	0.02	0.01	0.05	1.18
	N	28	28	28	28	28	28	28	28	28	28
Fall	min	0.00	0.33	0.40	0.16	0.01	0.01	0.00	0.00	0.44	281.68
	median	0.05	1.30	0.79	0.51	0.02	0.02	0.04	0.01	0.73	295.37
	max	0.37	4.27	1.54	1.46	0.48	0.05	0.10	0.04	0.88	300.49
	mean	0.07	1.43	0.81	0.59	0.05	0.03	0.04	0.01	0.71	293.28
	SD	0.08	0.86	0.30	0.34	0.10	0.01	0.03	0.01	0.13	5.69
	N	23	23	23	23	23	23	23	23	23	23

[1] All the concentration values are expressed in μg m^{-3}.

[2] $TNH_3 = NH_3 + NH_4^+$; $THNO_3 = HNO_3 + NO_3^-$; $TH_2SO_4 = SO_4^{2-}$; TNH_3, $THNO_3$, TH_2SO_4 are all expressed as the equivalent concentration; T is temperature; RH is relative humidity; SD is standard deviation; N is the number of observations.